Investigating the ultra-violet bright stars in star clusters

A thesis
submitted for the degree of

Doctor of Philosophy

in

The Department of Physics,
Pondicherry University,
Puducherry - 605 014, India

by

Sharmila Rani
Indian Institute of Astrophysics,
Bangalore - 560 034, India

February 2023

Investigating the ultra-violet bright stars in star clusters

Sharmila Rani
Indian Institute of Astrophysics

Indian Institute of Astrophysics
Bangalore - 560 034, India

Title of the thesis	:	**Investigating the ultra-violet bright stars in star clusters**
Name of the author	:	**Sharmila Rani**
Address	:	Indian Institute of Astrophysics II Block, Koramangala Bangalore - 560 034, India
Email	:	sharmila.rani@iiap.res.in
Name of the supervisor	:	**Prof. Gajendra Pandey**
Name of the co-supervisor	:	**Prof. Annapurni Subramaniam**
Address	:	Indian Institute of Astrophysics II Block, Koramangala Bangalore - 560 034, India
Email	:	pandey@iiap.res.in
	:	purni@iiap.res.in

Declaration of Authorship

I hereby declare that the matter contained in this thesis is the result of the investigations carried out by me at the Indian Institute of Astrophysics, Bangalore, under the supervision of Gajendra Pandey and Annapurni Subramaniam. This work has not been submitted for the award of any other degree, diploma, associateship, fellowship, etc., of any other university or institute.

Signed: Sharmila Rani

Date: 02-02-2023

Certificate

This is to certify that the thesis entitled **'Investigating the ultra-violet bright stars in star clusters'** submitted to Pondicherry University by Ms Sharmila Rani for the award of the degree of Doctor of Philosophy is based on the results of the investigations carried out by her under my supervision and guidance, at the Indian Institute of Astrophysics. This thesis has not been submitted for the award of any other degree, diploma, associateship, fellowship, etc., of any other university or institute.

Signed: 

Date: 02-02-2023

List of Publications

1. **Rani, Sharmila**; Pandey, Gajendra; Subramaniam, Annapurni; Sahu, Snehalata; Kameswara Rao, N., 2020, "The horizontal branch morphology of the globular cluster NGC 1261 using *AstroSat*", *Journal of Astrophysics and Astronomy*, 41, 35 *

2. **Rani, Sharmila**; Pandey, Gajendra; Subramaniam, Annapurni; Sahu, Snehalata; Kameswara Rao, N., 2021, "Study of UV-bright stellar populations in the globular cluster NGC 1261 using *AstroSat*", *MNRAS*, 501, 2140 †

3. **Rani, Sharmila**; Pandey, Gajendra; Subramaniam, Annapurni; Chung Chul; Sahu, Snehalata; Kameswara Rao, N., 2021, "*AstroSat* Study of the Globular Cluster NGC 2298: Probable Evolutionary Scenarios of Hot Horizontal Branch Stars", *The Astrophysical Journal*, 923, 162 ‡

4. **Rani, Sharmila.**; Subramaniam, Annapurni; Pandey, Sindhu; Sahu, Snehalata; Mondal, Chayan; Pandey, Gajendra, 2021, "UOCS. V. UV study of the old open cluster NGC 188 using *AstroSat*", *Journal of Astrophysics and Astronomy* , 42, 47 §

5. Sahu, Snehalata; Subramaniam, Annapurni; Singh, Gaurav; Yadav, Ramakant; Valcarce, Aldo R.; Choudhury, Samyaday; **Rani, Sharmila**; Prabhu, Deepthi S.; Chung, Chul; Côté, Patrick; Leigh, Nathan; Geller, Aaron M.; Chatterjee, Sourav; Kameswara Rao, N.; Bandyopadhyay, Avrajit; Shara, Michael; Dalessandro, Emanuele; Pandey, Gajendra; Postma, Joesph E.; Hutchings, John; Simunovic, Mirko; Stetson, Peter B.; Thirupathi, Sivarani; Puzia, Thomas; Sohn, Young-Jong, 2022, "Globular Cluster UVIT Legacy Survey (GlobULeS) - I. FUV-optical colour-magnitude diagrams for eight globular clusters", *MNRAS*, 514, 1122

6. Prabhu, Deepthi S.; Subramaniam, Annapurni; Sahu, Snehalata; Chung, Chul; Leigh, Nathan W. C.; Dalessandro, Emanuele; Chatterjee, Sourav;

*presented in Chapter 3
†presented in Chapter 3
‡presented in Chapter 4
§presented in Chapter 5

Kameswara Rao, N.; Shara, Michael; Côté, Patrick; Choudhury, Samyaday; Pandey, Gajendra; Valcarce, Aldo A. R.; Singh, Gaurav; Postma, Joesph E.; **Rani, Sharmila**; Bandyopadhyay, Avrajit; Geller, Aaron M.; Hutchings, John; Puzia, Thomas; Simunovic, Mirko; Sohn, Young-Jong; Thirupathi, Sivarani; Yadav, Ramakant Singh, 2022, "Globular Cluster UVIT Legacy Survey (GlobULeS). III. Omega Centauri in Far-ultraviolet", *ApJ Letters*, 939, 20

7. **Rani, Sharmila**; Pandey, Gajendra; Subramaniam, Annapurni; Kameswara Rao, N., 2023, "UOCS-IX. *AstroSat*/UVIT study of the open cluster NGC 2818: Blue Stragglers, Yellow Stragglers, Planetary Nebula, and their membership.", *The Astrophysical Journal*, 945, 11 ¶

8. Dattatrey, Arvind K.; Yadav, Ramakant Singh; **Rani, Sharmila**; Subramaniam, Annapurni; Singh, Gaurav; Sahu, Snehalata; Singh, Ravi Shankar, 2023, "GlobULeS-IV. UVIT/*AstroSat* detection of extremely low mass white dwarf companions to blue straggler stars in NGC 362", *The Astrophysical Journal*, 943, 130

9. Dattatrey, Arvind K.; Yadav, Ramakant Singh; Kumawat, Gourav; **Rani, Sharmila**; Singh, Gaurav; Subramaniam, Annapurni; Singh, Ravi Shankar, 2023, "GlobULeS-V. UVIT/*AstroSat* studies of stellar populations in NGC 362: Detection of Blue Lurkers in a Globular Cluster", *MNRAS Letters*, 523, 58

10. Panthi, Anju; Subramaniam, Annapurni; Vaidya, Kaushar; Jadhav, Vikrant; **Rani, Sharmila**; Thirupathi, Sivarani; Pandey, Sindhu, 2023, "Field blue straggler stars: discovery of white dwarf companions to blue metal-poor stars using UVIT/*AstroSat*", *MNRAS*, 525, 1311

¶presented in Chapter 6

Presentations

1. Presented a talk titled "**Study of GC NGC 1261: Exploring the formation mechanisms of extreme horizontal branch stars**" in *Chemical elements in the Universe: origin and evolution*, December 16-19, 2019, IIA Campus, Bangalore, India.

2. Presented a talk titled "**A UV study of GC NGC 1261: Insight into the formation scenario of extreme horizontal branch stars**" in *MODEST 20*, 2-7 February 2020, TIFR, Mumbai, India.

3. Presented a poster titled "**Study of UV bright stellar populations in Galactic Globular Cluster NGC 1261**" at *38th Meeting of the Astronomical Society of India (ASI:2020)*, 13-17 February 2020, IISER Tirupati, Tirupati, India.

4. Presented a talk titled "**UV study of the old open cluster NGC 188 using** *AstroSat*" in *UVIT: 5 years of Operation meeting*, 1-3 December 2020, IIA, Bangalore, India.

5. Presented a talk titled "**Investigation of the horizontal branch stellar populations in the globular cluster NGC 2298 with UVIT**" in *International Conference on 5 years of AstroSat*, 19-21 January 2021, ISRO, India, Online.

6. Presented a poster titled "**Hot horizontal branch stars in NGC 2298: Clues about their origin from** *AstroSat*/**UVIT study**" *21st National Space Science Symposium*, January 31 – February 4, 2022, Online.

7. Presented a poster titled "*AstroSat*/**UVIT Study of the Globular Cluster NGC 2298: Probable Evolutionary Scenarios of Hot Horizontal Branch Stars**" in *40th Meeting of the Astronomical Society of India (ASI:2022)*, 25-29 March 2022, IIT Roorkee, Roorkee, India.

8. Presented a poster titled "**Hot horizontal branch stars in globular clusters NGC 1261 and NGC 2298: Insights from UV observations**" in *44th COSPAR Scientific Assembly*, 16-24 July 2022, Athens, Greece.

9. Presented a poster titled "*AstroSat*/**UVIT study of the open cluster NGC 2818: Blue Stragglers, Yellow Stragglers, Planetary Nebula and their membership**" in *7 years of AstroSat meeting*, 28-29 September 2022, ISRO Headquarters, Bangalore, India.

10. Presented a poster titled "*AstroSat*/**UVIT study of the open cluster NGC 2818: Membership, Blue Stragglers, Yellow Stragglers, and Planetary Nebula**" in *The Impact of Binaries on Stellar Evolution (ImBaSE) meeting*, 14–18 November 2022, Garching, Germany.

Acknowledgements

I sincerely want to acknowledge and express my heartfelt gratitude and regards towards my supervisors, Prof. Gajendra Pandey and Prof. Annapurni Subramaniam, Indian Institute of Astrophysics (IIA), Bangalore, for their invaluable guidance, support, and encouragement throughout my PhD life. I would like to appreciate the fruitful discussions with them that enhanced my understanding of the field of stellar astrophysics. I consider it an immense privilege to work under her guidance, who, with her inspiring brilliance, profound knowledge and admirable dedication to the subject, provide an academic direction to this thesis. Each day spent here was an opportunity for growth and learning, for which I am truly grateful.

I am grateful to the Director, Dean, and the Board of Graduate Studies (BGS) for providing me with the opportunity to work at this institute and for the resources needed for my research. I would also like to extend my sincere thanks to my Doctoral committee members, Prof. Sujan Sengupta and Dr KVP. Latha, for their constant support and valuable suggestions. I also thank IIA for providing me with their facilities.

I extend my heartfelt thanks to the library staff and Data Center team, including Ashok, Fayaz, Anish, and other employees, for their help in locating books and journals and resolving computer and internet issues, respectively. My appreciation goes to the Bhaskara staff for their care and attention, which always made me feel at home. My sincere thanks to Mr Shankaranarayanan and the administrative team, including the administrative officer, personnel officer, accounts officer, and other members, for their quick assistance in administrative tasks.

I am extremely grateful to be a part of an excellent and supportive research group and appreciate the numerous valuable discussions that happened during our weekly

meetings. I extend my sincere gratitude to Snehalata Sahu and Sindhu Pandey, my seniors, for their advice and support during the early phases of my PhD. I would like to thank my groupmates, Snehalata Sahu, Sindhu Pandey, Chayan Mondal, Prasanta Nayak, Gaurav Singh, Deepthi S. Prabhu, Vikrant Jadhav, Dhanush S. R., and Sipra Hota for their support and the productive discussions we had during my PhD journey. Their contributions have been invaluable and greatly appreciated. I also thank Prof. N. K. Rao and Prof. Ram Sagar for their invaluable insights and constructive feedback on my work.

My heartfelt thanks go to my M.Sc. Prof. Sandeep Sahijpal for introducing me to the captivating and exciting field of stellar astrophysics and for his exceptional teaching method, which inspired me to pursue it as my area of research. I express my sincere gratitude to all my teachers and mentors throughout my academic journey.

I am thankful to my fellow batchmates, Partha, Bibhuti, Athira, Satabdwa, Manika, Suman, and Soumya, for their love and support. I sincerely appreciate the company of my close friends, Partha, Satabdwa, Bibhuti, Shubham, Bharat, Athira and Manika, for making my PhD life full of cherishable memories. I owe a special thanks to my best friends cum brothers, Partha and Satabdwa, for their constant motivation, care and love. They have always been a great source of inspiration to me, and I have learnt so much from them.

I want to thank my roommates, Piyali, Pavana, Jyoti, and Lupamudra, for their love and care. I especially thank my dearest friends, Bharti and Parwinder, who always encouraged and supported me during this beautiful journey. Their belief in me and my abilities was a constant inspiration, and their contributions have been invaluable. I want to convey thanks to seniors as well as juniors, Priya, Bhoomika, Deepa, Raghu, Deepthi, Sonith, Anirban, Indrani, Jyoti, Fazlu, Swastik, Sioree, Shubham, Manju, Raveena, Khushbu, Chandan, Rupesh, Saili, Renu, Shubhangi,

Shivani, Annu, Lupamudra, Abhishek, Shashank, Satakshi, Ayushi for making my stay enjoyable and memorable at Bhaskara.

I am deeply grateful to my sisters, Gurinder, Parveen, Mani, Minku, Sapandeep, and Amandeep, who make themselves available whenever I need their help and support. I am blessed to have such loving and supportive sisters. I would like to express a special thanks to my brothers, Kulwinder Singh and Amandeep Singh, for their encouragement and motivation in pursuing this field and for always being by my side throughout the journey.

It has always been my dream to pursue higher studies, and now, at the end of this journey, I feel like worth chasing this dream. I am indebted to my parents for their constant support and belief in me throughout this journey; without their love and blessings, it would not have been possible.

Finally, I would take this opportunity to thank the Almighty for being with me every step of the way during this wonderful journey.

With this, I look forward to an exciting and joyful journey ahead of my PhD.

Sharmila

Data and software usage

I have made use of telescopic data from various space and ground-based facilities in several studies presented in this thesis. I duly acknowledge the data usage. I wish to express my gratitude to the members and associates of these facilities for providing data.

In this thesis work, we majorly used data from the UVIT instrument on *AstroSat* mission of the Indian Space Research Organisation (ISRO), archived at the Indian Space Science Data Centre (ISSDC). UVIT project is a result of collaboration between IIA, Bengaluru, IUCAA, Pune, TIFR, Mumbai, several centres of ISRO, and the Canadian Space Agency (CSA). Several groups from ISAC (ISRO), Bengaluru, and IISU (ISRO), Trivandrum have contributed to the design, fabrication, and testing of the payload. The Mission Group and ISTRAC at ISAC have continued to support the project through the process of making observations, receiving data, and initial data processing. We would like to thank all individuals involved in the various teams who have supported the project, from the initial design phase to the launch and in-orbit observations.

Apart from the UVIT, we have also used other space-based data for our work, such as *GALEX*, *HST* and *Gaia*. We have used the *GALEX* archival data available from various programs/surveys that have been made available by the Multi-Mission archive at the Space Telescope Science Institute (MAST)[‖]. GALEX is operated for NASA by the California Institute of Technology under NASA contract NAS5-98034. The UV-optical photometric data from the *HST* UV Globular Cluster Survey (HUGS) catalogue provided by Nardiello *et al.* (2018) have been used for combining with the UVIT data of the clusters and is available at https://archive.stsci.edu/prepds/hugs/.

[‖] http://galex.stsci.edu/GR6/

We have used the Gaia DR2 and EDR3 catalogue of the cluster members provided by Gaia Collaboration *et al.* (2018, 2021), which is obtained from the European Space Agency (ESA) mission Gaia[**]and processed by the Gaia Data Processing and Analysis Consortium (DPAC, https://www.cosmos.esa.int/web/gaia/dpac/consortium). The DPAC has received financial support from various national institutions, particularly those that are members of the Gaia Multilateral Agreement.

We also have used archival data from several ground-based observations, such as SDSS and Pan-STARRS. Funding for the SDSS, SDSS-II and SDSS-III has been provided by the Alfred P. Sloan Foundation, the Participating Institutions, the National Science Foundation, the U.S. Department of Energy, the National Aeronautics and Space Administration, the Japanese Monbukagakusho, the Max Planck Society, and the Higher Education Funding Council for England. This data can be accessed on the SDSS website at http://www.sdss.org/.

We have used IRAF for the data reductions. IRAF is distributed by the National Optical Astronomy Observatory (NOAO), which is operated by the Association of Universities for Research in Astronomy (AURA) under a cooperative agreement with the National Science Foundation. For proper motion membership estimation in clusters, we have used the available python script GaiaTools developed by Vasiliev (2019). For the data analysis, we have used VOSA, developed under the Spanish Virtual Observatory project supported by the Spanish MINECO through grant AyA2017-84089. We also made use of the Aladin sky atlas developed at CDS, Strasbourg Observatory, France. This work also made use of TOPCAT, Matplotlib, NumPy, Scipy, Pandas, and Astropy, a community-developed core Python package for Astronomy.

[**]https://www.cosmos.esa.int/gaia

Dedicated to

my

family

Abstract

Star clusters are gravitationally bound systems composed of a large number of stars, ranging from thousands to millions. As the dynamic age of the cluster is less than the age of the universe, dynamical interactions happening among stars within clusters result in stellar exotica such as blue straggler stars (BSSs), cataclysmic variables, etc. Globular clusters (GCs), being old and dense, host low-mass stars in various stages of evolution, making them ideal for investigating the end stages of low-mass star evolution and the origins of exotic stellar populations, which are not yet fully understood. Ultraviolet (UV) studies conducted so far using *HST* and *GALEX* data have revealed the presence of intriguing stars such as extreme horizontal branch (EHB) stars and blue hook (BHk) stars in GCs, making them enigmatic systems. Furthermore, the discovery of multiple stellar populations (MSPs) in both types of clusters through UV observations has provided new perspectives on their formation and evolution.

In this thesis, we examined the properties of late-stage, UV-bright stellar populations and the exotic BS and yellow straggler (YS) stars in targeted star clusters. We primarily have employed the UV data from the Ultraviolet Imaging Telescope (UVIT) onboard *AstroSat*, India's first multi-wavelength observatory in both far-UV (FUV) and near-UV (NUV) bands. We have conducted an in-depth analysis of four clusters, consisting of two intermediate-mass GCs (NGC 1261 and NGC 2298) and two open clusters (OCs) (NGC 188 and NGC 2818). We performed the PSF photometry on the UV images obtained from UVIT and further combined the UVIT-detected sources with the other available archival data. In the case of GCs, we utilised the *HST* data to find the optical counterparts of the UV detected sources for the central region ($\sim$2.′7 square) of the cluster, and *Gaia* DR2 and EDR3 catalogue for the outer region of the cluster not covered with *HST*. To obtain the proper-motion (PM) members of the clusters, we used *Gaia* DR2 and EDR3 catalogues for all the clusters.

In the case of GCs, NGC 1261 and NGC 2298, we explored their horizontal branch (HB) morphology. In NGC 1261, we constructed UV colour-magnitude diagrams (CMDs) in combination with *HST*, *Gaia* DR2, and ground-based optical photometry for member stars. We detected the full HB in NUV, and blue HB (BHB) in the FUV and identified two EHB stars. HB stars have a tight sequence in UV-optical CMDs well fitted with isochrones generated (12.6 Gyr age, [Fe/H] = -1.27 dex metallicity) using updated BaSTI-IAC models. Effective temperatures (T_{eff}), luminosities and radii of bright HB stars were estimated using spectral energy distribution (SED). As we detect the complete sample of UV bright HB stars, the hot end of the HB distribution is found to terminate at the G-jump (T_{eff} $\sim$11,500 K). The two EHB stars, fitted well with single spectra, have T_{eff} = 31,000 K and a mass = 0.495 $M_{\odot}$ and follow the same $T_{eff}-$Radius relation of the BHB stars. We constrain the formation pathways of these EHB stars to extreme mass loss in the RGB phase (either due to rotation or enhanced Helium) OR early hot-flash scenario.

In NGC 2298, UV-optical CMDs are constructed for member stars in combination with *HST* UV Globular Cluster Survey (HUGS) data for the central region and *Gaia* EDR3 and ground-based photometric data for the outer region. BHB sequence with a spread and four hot HB stars are detected in all FUV-optical CMDs. They are compared with theoretical updated BaSTI isochrones and synthetic HB models with a range in helium abundance, suggesting that the hot HB stars are helium enhanced when compared to the BHB. The estimated T_{eff}, radius, and luminosity of HB stars, using best SED fits, were compared with various HB models. BHB stars span a temperature range from 7,500-12,250 K. The three hot HB stars have 35,000-40,000 K. In contrast; one star has around $\sim$100,000 K. We suggest the following evolutionary scenarios: two stars are likely to be the progeny of EHB stars formed through an early hot-flasher scenario; one is likely to be an EHB star with probable helium enrichment, the hottest HB star is about to enter the white dwarf (WD) cooling phase, could have evolved from BHB phase. Nevertheless, these are interesting spectroscopic targets to understand the late stages of evolution.

In the old OC NGC 188, UVIT data is utilised in combination with optical photometric data to construct the optical and UV CMDs. In the FUV images, we detect only hot and bright BSSs, one hot subdwarf, and one WD candidate. In the NUV images, we detect members up to a faintness limit of $\sim$22 mag, including 21 BSSs, 2 YSSs, and one WD candidate. This study presents the first NUV-optical CMDs, which are overlaid with updated BaSTI-IAC isochrones and WD cooling sequences, which are found to fit well with the observed CMDs. We use SED fitting to estimate the T_{eff} radii, and luminosities of the UV-bright stars. We find the cluster to have an HB population with three stars (T_{eff} = 4,750$-$21,000 K). We also detect two YSSs, with one of them with UV excess connected to its binarity and X-ray emission.

In the intermediate-age OC NGC 2818 that has a Planetary nebula (PN) within the field, we present the first FUV imaging results. We explore whether the PN is a member of the cluster using images taken from the UVIT. We detect four bright and hot BSSs and two YSSs based on their location in the optical and FUV-optical CMDs. The theoretical isochrones more or less fit the observed distribution of detected stars in all the CMDs. Based on the parameters estimated using SED, we infer that the BSSs are either collisional products or might have undetectable WD companions. Our photometric analysis of YSSs confirms their binarity, consistent with the spectroscopic results. We find the YSSs to be formed through a mass-transfer scenario and the hot components are likely to be A-type subdwarfs. A comparison of the radial velocity (RV), *Gaia* EDR3 PM of the PN with the cluster members, and reddening towards the PN and the cluster does not rule out the membership of the PN. Using SED, the estimated stellar parameters of the PN's central star match well with the previous estimations. Comparing the central star's position with theoretical post-AGB (pAGB) models suggest that it has already entered the WD cooling phase, and its mass is deduced to be $\sim$0.66 $M_{\odot}$. The corresponding progenitor mass turns out to be $\sim$2.1 $M_{\odot}$, comparable to the turn-off mass of the cluster, implying that the progenitor could have formed in the cluster. We suggest that the NGC 2818 might be one of the few known clusters to host a PN, providing a unique opportunity to test stellar evolution

models.

Overall, our study showcases the effectiveness of UVIT in resolving stars in GCs, such as NGC 1261 and NGC 2298 in FUV, and identifying the hot companions to BSSs and YSSs in OCs, providing more insight into their formation pathways. Additionally, its multiple filters facilitate in constructing the multi-wavelength SEDs and estimating parameters of the hot stellar populations.

Contents

List of Figures

List of Tables

Abbreviations

1G	**F**irst **G**eneration
2G	**S**econd **G**eneration
ACS	**A**dvanced **C**amera for **S**urveys
AGB	**A**symptotic **G**iant **B**ranch
AGBM	**A**symptotic **G**iant **B**ranch **M**anqué
ACS	**A**dvanced **C**amera for **S**urveys
AIS	**A**ll sky **I**maging **S**urvey
BaSTI	**Ba**gs of **S**tellar **T**racks and **I**sochrones
BHB	**B**lue **H**orizontal **B**ranch
BHk	**B**lue **H**ook
BSS	**B**lue **S**traggler **S**tar
CCD	**C**harge **C**oupled **D**evices
CMD	**C**olour-**M**agnitude **D**iagram
CMOS	**C**omplementary **M**etal **O**xide **S**emiconductor
cog	**c**urve **o**f **g**rowth
COS	**C**osmic **O**rigins **S**pectrograph
CPS	**C**ounts **P**er **S**econd
CSPNe	**C**entral **S**tar of **P**lanetary **Ne**bulae
CV	**C**ataclysmic **V**ariables
CZTI	**C**admium **Z**inc **T**elluride **I**mager
Dec	**Dec**lination
DIS	**D**eep **I**maging **S**urvey

DR	**D**ata **R**elease
EDR	**E**arly **D**ata **R**elease
EHB	**E**xtreme **H**orizontal **B**ranch
EHF	**E**arly **H**ot **F**lasher
ELM	**E**xtremely **L**ow **M**ass
ESA	**E**uropean **S**pace **A**gency
ESO	**E**uropean **S**outhern **O**bservatory
FGS	**F**ine **G**uidance **S**ensor
FOV	**F**ield **O**f **V**iew
FRMS	**F**ast **R**otating **M**assive **S**tars
FSPS	**F**lexible **S**tellar **P**opulation **S**ynthesis
FUV	**F**ar **U**ltra-**V**iolet
FWHM	**F**ull **W**idth **H**alf **M**aximum
GALEX	**G**alaxy **E**volution **E**xplorer
GC	**G**lobular **C**luster
GGC	**G**alactic **G**lobular **C**luster
GI	**G**uest **I**nvestigator
GlobULeS	**U**VIT **Le**gacy **S**urvey of **Glob**ular clusters
GMM	**G**aussian **M**ixture **M**odel
H-R	**H**ertzsprung-**R**ussell
HB	**H**orizontal **B**ranch
HCT	**H**imalayan **C**handra **T**elescope
HEFM	**He**lium **F**lash **M**ixing
HESP	**H**anle **E**chelle **Sp**ectrograph
HRC	**H**igh **R**esolution **C**hannel
HST	**H**ubble **S**pace **T**elescope
HUGS	**H**ST **U**V **G**lobular Cluster **S**urvey
HUT	**H**opkins **U**ltra-Violet **T**elescope
IFMR	**I**nitial–**F**inal **M**ass **R**elation
IR	**I**nfra**r**ed

IRAF	**I**mage **R**eduction and **A**nalysis **F**acility
ISRO	**I**ndian **S**pace **R**esearch **O**rganisation
IUE	**I**nternational **U**ltraviolet **E**xplorer
KPNO	**K**itt **P**eak **N**ational **O**bservatory
L1	**L**evel **1**
LAXPC	**L**arge **A**rea **X**-ray **P**roportional **C**ounter
LHF	**L**ate **H**ot **F**lasher
LTE	**L**ocal **T**hermodynamic **E**quilibrium
MAST	**M**ikulski **A**rchive for **S**pace **T**elescopes
MCP	**M**icro **C**hannel **P**late
MESA	**M**odules for **E**xperiments in **S**tellar **A**strophysics
MIS	**M**edium **I**maging **S**urvey
MIST	**M**ESA **I**sochrones & **S**tellar **T**racks
MS	**M**ain **S**equence
MSP	**M**ultiple **S**tellar **P**opulation
MSTO	**M**ain **S**equence **T**urn **O**ff
MT	**M**ass **T**ransfer
MW	**M**ilky **W**ay
NASA	**N**ational **A**eronautics and **S**pace **A**dministration
NGC	**N**ew **G**eneral **C**atalogue
NGS	**N**earby **G**alaxy **S**urvey
NICMOS	**N**ear **I**nfrared **C**amera and **M**ulti-**O**bject **S**pectrometer
NIR	**N**ear **I**nfra**r**ed
NLTE	**N**on-**L**ocal **T**hermodynamic **E**quilibrium
NOAO	**N**ational **O**ptical **A**stronomy **O**bservatory
NUV	**N**ear **U**ltra-**V**iolet
OC	**O**pen **C**luster
OGLE	**O**ptical **G**ravitational **L**ensing **E**xperiment
pAGB	**P**ost **A**symptotic **G**iant **B**ranch
peAGB	**p**ost-**e**arly-**AGB**

pHB	**p**ost **HB**
Pan-STARRS	**Pan**oramic **S**urvey **T**elescope **A**nd **R**apid **R**esponse **S**ystem
PC	**P**hoton **C**ounting
PM	**P**roper **M**otion
PMS	**P**re-**M**ain **S**equence
PSF	**P**oint **S**pread **F**unction
RA	**R**ight **A**scension
RGB	**R**ed **G**iant **B**ranch
RHB	**R**ed **H**orizontal **B**ranch
RRL	**RR L**yrae
RUWE	**R**enormalized **U**nit **W**eight **E**rror
SB	**S**pectroscopic **B**inary
SBC	**S**olar **B**lind **C**hannel
sdA	**A**-type **S**ub**d**warf
sdB	**B**-type **S**ub**d**warf
sdO	**O**-type **S**ub**d**warf
SDSS	**S**loan **D**igital **S**ky **S**urvey
SED	**S**pectral **E**nergy **D**istribution
SGB	**S**ub **G**iant **B**ranch
SSM	**S**canning **S**ky **M**onitor
SSP	**S**imple **S**tellar **P**opulation
STIS	**S**pace **T**elescope **I**maging **S**pectrograph
SVO	**S**panish **V**irtual **O**bservatory
SX Phe	**SX P**hoenicis
SXT	**S**oft **X**-ray **T**elescope
TAHB	**T**erminal **A**ge **H**orizontal **B**ranch
TMAP	**T**übingen NLTE **M**odel **A**tmosphere **P**ackage
TOPCAT	**T**ool for **OP**erations on **C**atalogues **A**nd **T**ables
2MASS	**Two M**icron **A**ll **S**ky **S**urvey
UDIS	**U**ltra-**d**eep **I**maging **S**urvey

UIT	**U**ltraviolet **I**maging **T**elescope
UOCS	**U**VIT **O**pen **C**luster **S**urvey
UV	**U**ltra-**V**iolet
UVIS	**U**ltraviolet-**Vis**ible
UVIT	**U**ltra-**V**iolet **I**maging **T**elescope
UVOT	**U**ltra**v**iolet **O**ptical **T**elescope
VPD	**V**ector **P**oint **D**iagram
VIS	**Vis**ible
VOSA	**V**irtual **O**bservatory **S**ED **A**nalyzer
WCS	**W**orld **C**oordinate **S**olution
WD	**W**hite **D**warf
WFC	**W**ide **F**ield **C**hannel
WFC3	**W**ide **F**ield **C**amera **3**
WISE	**W**ide-field **I**nfrared **S**urvey **E**xplorer
YEPS	**Y**onsei **E**volutionary **P**opulation **S**ynthesis
YSS	**Y**ellow **S**traggler **S**tar
ZAHB	**Z**ero **A**ge**H**orizontal **B**ranch
ZAMS	**Z**ero-**A**ge **M**ain **S**equence
ZP	**Z**ero **P**oint

Chapter 1

Introduction

The night sky, decorated with a variety of stars and other cosmic objects, has always captivated the attention of humans and led us to constantly seek a deeper understanding of its nature to uncover its secrets. Our own galaxy, the Milky Way, is home to an intriguing group of stars bound by gravity called star clusters found in different locations. Their detailed study provides an insightful understanding of how our Galaxy was formed and its evolution with time.

1.1 Star Clusters

Star clusters consist of a large group of stars bound through gravity that are traditionally considered to be formed out of the same molecular cloud at the same time (Portegies Zwart *et al.* 2010). They are considered one of the best laboratories to test stellar evolution theory as they provide a sample of stars with similar ages and chemical compositions located at the same distance from us. This makes it possible to study the properties of stars of different masses and compare them with

FIGURE 1.1: HST optical images of the GC M3 (left panel, credits: Karel Teuwen) and an OC M44 (right panel, credits: Stuart Heggie).

theoretical predictions, which is not possible with field stars. Clusters, because they are easier to estimate their age and distance compared to individual field stars, have been utilised as a tool to trace the structure and history of its host galaxy (Moffat and Vogt 1973; Janes and Adler 1982; Friel 1995; Moitinho 2010; Moraux 2016). In addition to their importance in understanding the evolution of galaxies and the history of the universe, star clusters are also interesting to astronomers because they provide a unique laboratory for studying the properties of stars and the dynamics of their interactions. In the Milky Way, they are typically classified into two types: Globular Clusters (GCs) and Open Clusters (OCs). Figure 1.1 shows examples of these two types of clusters, with M3 being a GC and M44 being an OC. These images are taken by the Hubble Space Telescope (*HST*).

Globular Clusters

GCs are large, spherical collections of stars that orbit around the centre of a galaxy. They are composed of hundreds of thousands to millions of stars and are held together by mutual gravitational attraction. GCs are found in the halo of a galaxy, and they are one of the oldest known structures in the universe, with ages estimated to be between 10 and 13 billion years, and hence, provide an important constraint for the age of the Universe. They are made up of mostly old, metal-poor, low-mass stars and are thought to have formed during the early stages of a galaxy's evolution. The stars in GCs are tightly packed together, with distances

between stars ranging from a few hundredths to a few tenths of a light year. The high concentration of stars in a GC leads to a high probability of interactions between the stars, such as close encounters and binary star formation (Baumgardt and Makino 2003; Krumholz *et al.* 2019; Krause *et al.* 2020).

Open Clusters

OCs are groups of stars found in the disk of a Galaxy that are bound together by gravitational forces. They usually have a few hundred to a few thousand stars and are relatively young, with ages ranging from a few million to a few billion years. OCs within a galaxy's spiral arms typically have a high percentage of blue, hot, and bright stars with relatively short lifetimes. These clusters can be used to study the structure and evolution of a galaxy and the formation and evolution of stars. OCs are generally less massive and less densely packed than GCs (Krumholz *et al.* 2019; Krause *et al.* 2020).

1.2 Stellar Evolution

GCs, being one of the oldest objects in our Galaxy, are composed of stars that are, in fact, less massive than $< 1M_{\odot}$ (except those that gained mass) as stars heavier than $1M_{\odot}$ are already in the advanced stages of evolution. On the contrary, OCs, being younger compared to GCs, contain more massive stars. The ultimate fate of a star is largely determined by its initial mass, with stars less massive than 8 $M_{\odot}$ eventually becoming white dwarfs (WDs), while more massive stars will undergo a supernova explosion and leave behind a neutron star or black hole. The different phases of stellar evolution of a low-mass star ($M \leq 2.3M_{\odot}$) beginning from protostar to its end-stage, i.e., WD, are illustrated in Figure 1.2. The colour-magnitude diagram (CMD) and H-R diagram are powerful tools to derive basic parameters such as age, metallicity, and reddening of star clusters. Figure 1.3

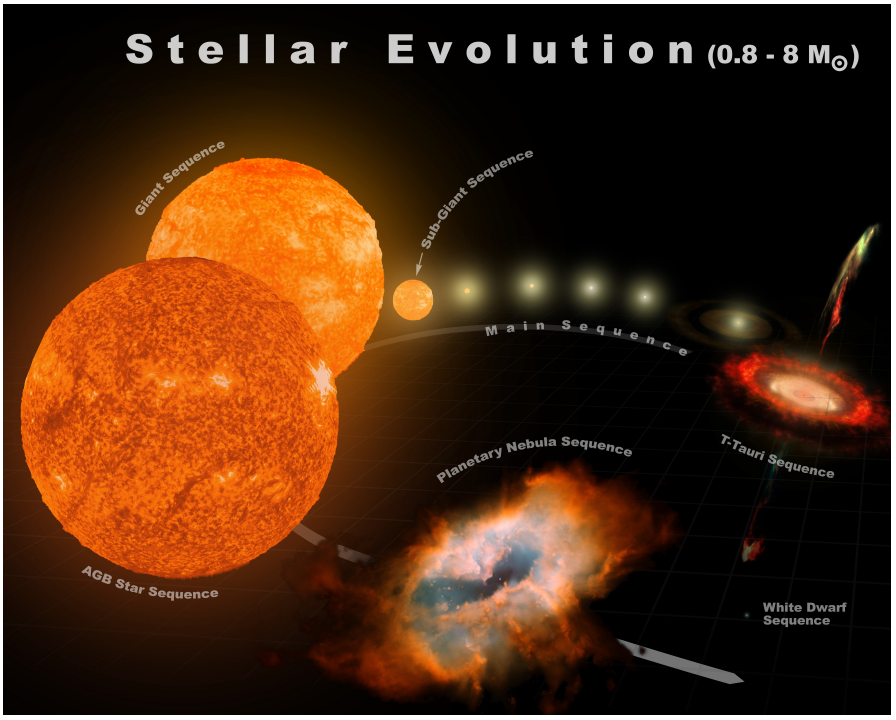

FIGURE 1.2: A schematic representation of the various stages of stellar evolution. (Credits: Antonio Ciccolella)

presents the evolutionary track of a 1 $M_{\odot}$ star and its structure during various stages of post-MS evolution. Here, we briefly discuss the main evolutionary phases of low-mass stars that pertain to both GCs as well as OCs (Iben 1991).

All stars are born from a dense cloud of gas and dust, which collapses under the force of gravity (Myers and Benson 1983). As the material falls inwards, it heats up due to the increasing pressure, eventually forming a protostar. During the protostar evolutionary phase (Hayashi 1966; Walker 1994), the primary source of energy will be gravitational potential energy resulting from the contraction of the star. As the protostar continues to contract, the temperature and pressure at its core increases. However, the role of magnetic fields, radiation from other stars and unknown sources, and other factors are not considered (Wurster and Li 2018; Tsukamoto *et al.* 2022).

The contraction will continue till the core of the star becomes dense and hot enough

to ignite the nuclear fusion of hydrogen. Generally, the minimum core temperature and density required to fuse hydrogen are $\sim 10^7$ K and 100 kg/m^3, respectively. Stars in this stage of evolution are known as main-sequence (MS) stars. Low as well as intermediate mass ($2.5M_\odot \leq M_* \leq 8M_\odot$) stars spend most of their lifetime in the MS phase, accounting for ∼70% of their total lifetime. As the core runs out of hydrogen fuel, hydrogen burning ceases referring to the MS turn-off (MSTO) point, and the core, mainly consisting of helium, again begins contracting gravitationally. As the core contracts, it heats itself up, as well as the layers just above it. Eventually, the hydrogen shell surrounding the hydrogen-exhausted core becomes hot enough to begin hydrogen fusion. The helium produced in the shell falls onto the core and increases the core mass. The core of a star shrinks as more mass is added to it, which makes the gravity at the border of the core stronger. This increased gravity affects the hydrogen-burning shell, causing the rate of hydrogen burning to increase. The envelope of the star is radiative, so some of the luminosity generated in the shell is used to heat the intermediate layers, causing them to expand and increasing the total radius of the star. As the radius increases, the effective temperature decreases for a given, nearly constant surface luminosity (Prialnik 2009; Kippenhahn *et al.* 2013).

After a star leaves the MS, its position on the H-R diagram moves to the right, turning it into a subgiant (Catelan 2007). The star's surface expands and cools, appearing red in colour. Keeping the surface temperature almost constant, it begins ascending the red giant branch (RGB) (Iben 1967; Boehm-Vitense 1992). In this phase, the envelope is no longer radiative; it has become convective, an efficient energy transport from the shell region to the surface. This, in turn, increases its radius as well as surface luminosity. Meanwhile, the core continues to contract, and the high electron density in the core leads to degeneracy, especially in the case of low-mass stars. At RGB star's tip, the temperature in the core with a mass of $\sim 0.45-0.5M_\odot$ rises to about 10^8 K, which is high enough to ignite helium and burn it into carbon via the triple-alpha process. In the case of low-mass stars

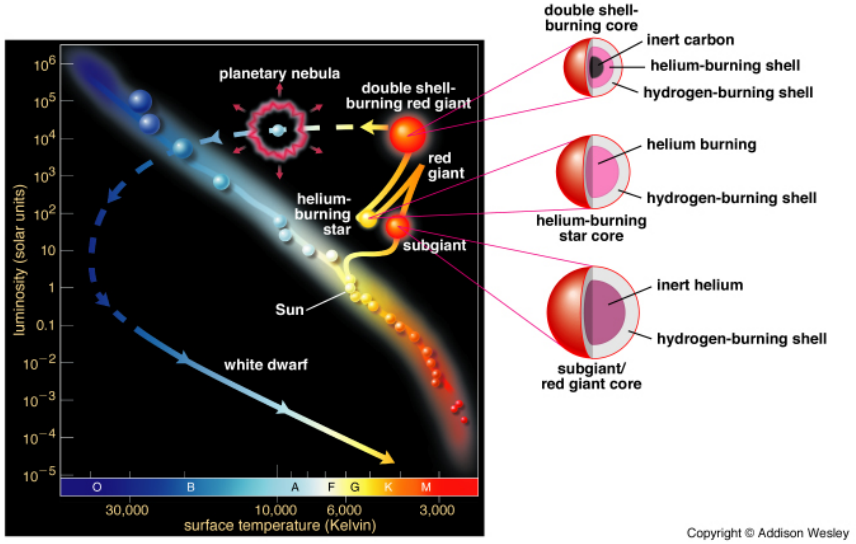

FIGURE 1.3: The H-R diagram illustrates the evolution of a low-mass star, with a corresponding diagram on the right side showing the internal structure of the star at different stages in its evolution. (Image Credit: Pearson Addison Wesley)

with masses less than 2 $M_{\odot}$, helium ignition in the core occurs under degenerate conditions. In a degenerate core, the pressure is independent of temperature. If the temperature of the degenerate core increases, it will produce more nuclear energy without a corresponding increase in pressure or expansion. This results in an explosive release of energy called a helium flash (Schwarzschild and Härm 1962; Boehm-Vitense 1992). The energy released in a flash is so great that it raises the temperature of the core enough to remove the degeneracy, causing the core to expand. This expansion decreases the gravity at the core's border, reducing the shell's hydrogen burning rate and lowering the star's overall luminosity of the star (Iben 1974).

It then settles on the horizontal branch (HB), where the helium-burning core with a mass of $\sim$0.5 $M_{\odot}$ is surrounded by a hydrogen-burning shell (Hoyle and Schwarzschild 1955; Iben and Rood 1970). The location of an HB star in the H-R diagram depends on many factors, including its initial mass, chemical composition, and mass loss along the RGB stage. The low gravity at the distended surface of the RGB causes the outer layers to shed due to their difficulty in being held.

For the same mass star on the RGB, more mass loss makes it end up on the blue side of the HB, and vice-versa. Stars on the HB have a range of masses due to the varying hydrogen envelope masses, while their core mass remains nearly constant. When the helium in the core of a star is exhausted, the carbon-oxygen core begins to contract, increasing the pressure and temperature of the surrounding layers. This causes helium to ignite in a shell just outside the core while hydrogen begins to fuse in an outer shell. The star is now in a stage of double shell burning called the asymptotic giant branch (AGB) (Iben and Renzini 1983; Habing and Olofsson 2004; Herwig 2005). As the core continues to shrink, the temperatures and luminosities of the hydrogen-burning and helium-burning shells increase. Along this phase, again, the whole hydrogen envelope strips off as the radius and luminosity of a star become too high. Thus, it takes a right turn in the H-R diagram, known as post-AGB (pAGB) phase. As the central star is extremely hot, its UV radiation ionizes the material it has ejected. This absorbed UV light energizes the shell of gas surrounding the central star, causing it to appear as a brightly coloured planetary nebula (PN) (Iben 1995; Kwok 2000). This phase is relatively short-lived, lasting approximately 10,000 to 100,000 years, compared to the longer stages of stellar evolution. Ultimately, the star will end up as a CO WD (Weidemann 1990; de Boer and Seggewiss 2008). The WDs observed in GCs have the mean mass of $\sim$0.5-0.6 $M_{\odot}$ (Moehler *et al.* 2004a; Cummings *et al.* 2018).

In this thesis, I have mainly explored the stars present in their late stages of evolution, such as HB, post-HB (pHB), etc., and UV bright as well. Apart from them, I have also focused on the exotic stars, which are believed to be the result of binary evolution. Standard single-star evolution fails to explain their origin. The details of them are discussed in the following section.

1.3 Exotic Stellar Populations

The interactions between stars within a cluster can lead to the formation of binary systems and exotic types of stars, such as blue straggler stars (BSSs), yellow straggler stars (YSSs), and cataclysmic variables. Below we describe their characteristics and what makes them so intriguing to study.

1.3.1 Blue Straggler stars

BSSs are one of the intriguing byproducts of stellar interactions, and the mechanisms behind their formation and evolution are still not fully understood (Boffin *et al.* 2015). BSSs were first discovered in one of the largest and brightest Galactic GC (GGC) M3 by Allan Sandage in 1953 (Sandage 1953). These stars appear in a region of the CMD of star clusters where one would expect to find evolved stars that already have used up their nuclear fuel and moved on to advanced stages of evolution or become WDs. However, BSSs have not yet exhausted their nuclear fuel and are still actively burning hydrogen in the core, which is not explained through canonical stellar evolution theory. At first, they were considered as non-members of the clusters, but later with the improvement in the observational facilities, especially observations with *HST* in the inner region of GCs, confirmed that they are lying all over the cluster, and hence might be their members. Moreover, several studies involving the proper motion (PM) and radial velocity (RV) of stars within clusters have found that these stars are indeed members of the cluster. Compared to the MSTO stars within the cluster, these stars are generally brighter and bluer in colour, suggesting that they are more massive. BSSs are marked with blue colour-filled symbols in the optical CMD of OC M67 as shown in Figure 1.4.

Several theories are put forth to explain these objects' mass gain and rejuvenation.

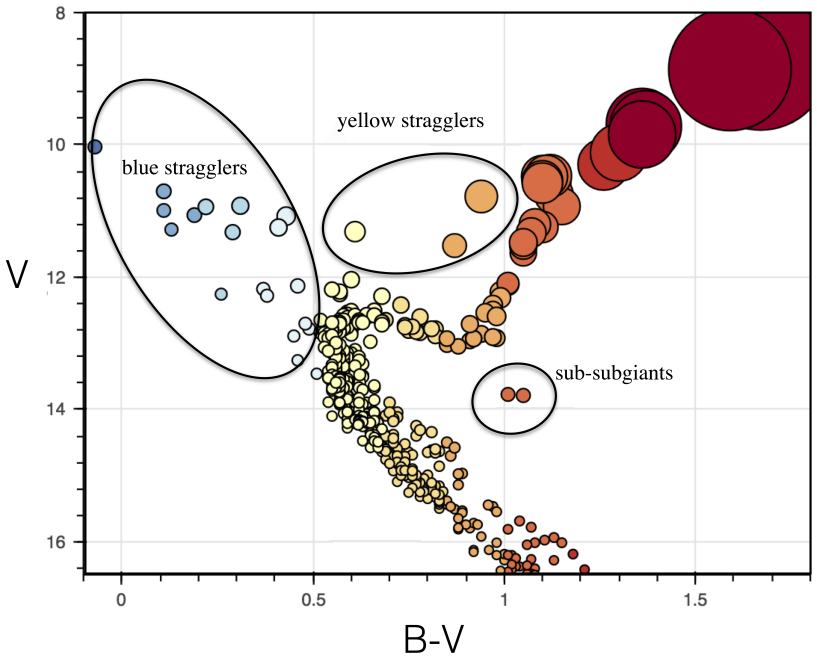

FIGURE 1.4: Optical CMD of OC M67 showing the location of non-standard stars including BSSs, and YSSs. Image Courtesy: Emily Leiner

Two primary formation pathways proposed to explain their origin are either formed through direct collisions or mergers of binary stars (Hills and Day 1976), or mass-transfer in close-binary systems (McCrea 1964). The schematic in Figure 1.5 presents the two primary mechanisms by which BSSs form. Another possibility is that they might result from the dynamical evolution of hierarchical triple systems, in which the merger of an inner binary is facilitated by the Kozai mechanism (Iben and Tutukov 1999; Perets and Fabrycky 2009; Naoz and Fabrycky 2014). As BSSs can form through multiple channels, the prevalence of these channels may vary depending on the environment. These environments include OCs (de Marchi *et al.* 2006; Ahumada and Lapasset 2007), GCs (Ferraro *et al.* 2012), the Galactic field (Santucci *et al.* 2015), and dwarf galaxies (Santana *et al.* 2012). It is believed that all of the formation scenarios may contribute to the overall population of BSSs in these various environments. Despite the support for the above-stated mechanisms

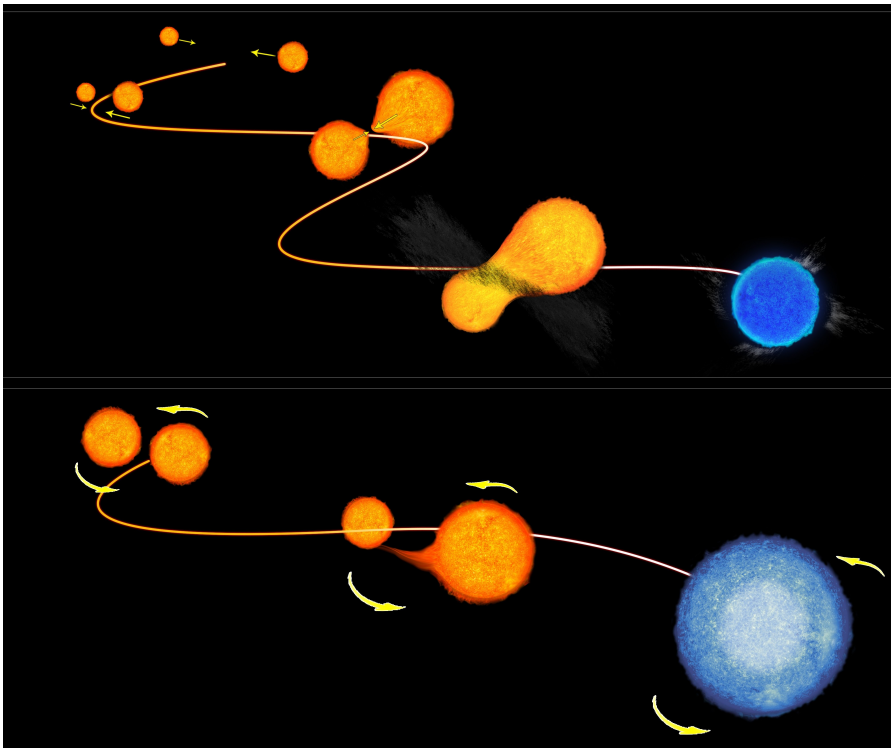

FIGURE 1.5: The diagram illustrates the two leading mechanisms for forming BSSs or "rejuvenated" stars in clusters: (Upper) collision and (Lower) "vampire" or mass-transfer models. The collision model shows two low-mass stars merging due to a head-on collision in a dense environment. The vampire model depicts a low-mass star accreting material from a larger companion to fuel its rejuvenation. Credits: NASA/ESA

through various studies, there are some BSSs that these models are unable to explain (Cannon 2015). Thus, studying binary star systems such as BSSs can give insight into the impact of dynamics on binary evolution, the frequency of binary systems, and their contribution to cluster evolution.

The instability strip where the variables are supposed to lie passes through the BSSs region. The BSSs which lie in this region are called SX Phoenicis (SX Phe) variables. They have a short period ranging from 0.03-0.08 days (0.7-1.9 hours).

1.3.2 Yellow Straggler stars

In optical CMDs of OCs and GCs, member stars occupy the position above the sub-giant branch (SGB), between BSSs and RGB, referred to as YSSs (Leiner *et al.* 2016; Sindhu *et al.* 2018). These stars might be the result of the evolution of BSSs (Mathieu *et al.* 1990). These stars are labelled and indicated with light yellow colour symbols in the optical CMD of M67 as displayed in Figure 1.4. These systems are generally identified in OCs but are likely to be present in GCs as well. These, like the BSSs, may have multiple formation pathways.

1.4 Horizontal Branch Morphology

The distribution of stars along the HB in an optical CMD based on their colour is referred to as the HB morphology. Depending on their temperatures (colour), HB is mainly classified into three categories: the red HB (RHB), the blue HB (BHB), and the extreme HB (EHB). Figure 1.6 (left panel) shows different parts of HB in the UV CMD of one of the massive and dense GC NGC 2808. The RR Lyrae instability strip separates the RHB from the BHB, where the former is cooler than the latter. RHB and BHB stars have effective temperatures ranging from about $\sim 5,000 - 6,200$ K and $\sim 8,000 - 20,000$ K, respectively. EHB stars have a very thin envelope of $M_{env} \leq 0.02 M_{\odot}$, which is not enough to support shell hydrogen burning (Caloi 1972). They have a T_{eff} of more than ∼20,000 K and are usually located at the end of the blue part of the HB in the optical CMD. Greenstein (1971) explored subluminous stars and showed that EHB stars were found to be analogous to B-type subdwarfs (sdB) stars in the field. Besides these hot HB stars, there is a subclass of EHB stars, called Blue Hook (BHk) stars, that are particularly sub-luminous and have a $T_{eff} > 32,000$ K. BHk stars can be identified by their hook-like shape in the UV CMDs, and are located at the hot

end of the canonical EHB (D'Cruz *et al.* 2000; Brown *et al.* 2001, 2010). During the pHB evolution, unlike more massive BHB stars, both EHB and BHk stars with less envelope mass bypass the AGB stage and evolve directly into WDs (Sweigart *et al.* 1974; Gingold 1976). Hence, they are known as AGB manqué (AGBM) stars (Greggio and Renzini 1990).

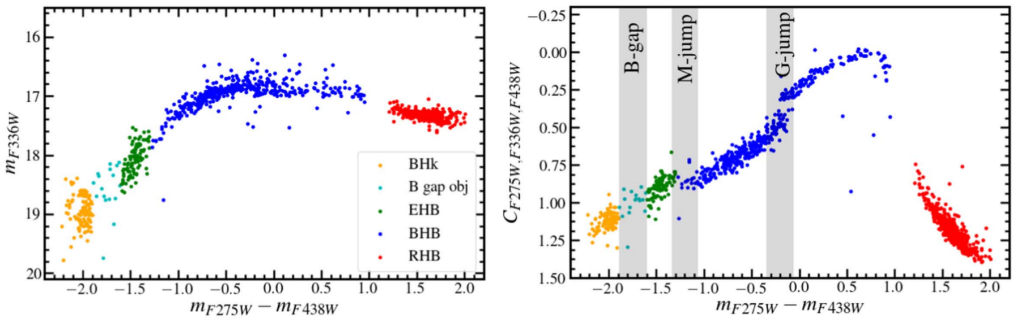

FIGURE 1.6: Left Panel: UV CMD of GC NGC 2808 where different sub-populations of HB are labelled and shown. Right Panel: Colour-Colour diagram, created using *HST* data in three filters, F275W, F336W, and F438W, displaying the positions of prominent photometric discontinuities observed along the HB distribution. Credits: Prabhu *et al.* (2021)

The HB is of particular interest because it exhibits different morphologies in different clusters. This is a well-known problem in GCs referred to as the second parameter problem, first mentioned by Sandage & Wallerstein (Sandage and Wallerstein 1960; van den Bergh 1967; Sandage and Wildey 1967). It is influenced by a number of factors, including the metallicity and age of the cluster, mass-loss along the RGB, rotation, and chemical composition. It was originally thought that the metallicity of GGCs plays a key role in determining their HB's shape. In general, metal-poor GCs tend to have bluer HBs; on the contrary, metal-rich GCs likely to have redder HBs. This is due to the fact that metal-poor stars have fewer heavy elements, hence less opacity in their envelope, which makes them more efficient at shedding their outer layers, resulting in a higher surface temperature and a bluer colour and vice-versa (Moehler 2001; Catelan 2009). Later, it was found observational that despite having similar metallicities, some GCs exhibit diverse HB morphologies. For instance, the GC pairs M3-M13, or NGC 288-NGC 362, have

different HB shapes even though they have similar metal content. Even metal-rich clusters like NGC 6441 and NGC 6388 feature blue HBs, as well (Rich *et al.* 1997; Busso *et al.* 2007; Dalessandro *et al.* 2008). These exceptions have indicated the need for a second and possibly a third parameter to explain the HB distributions in GCs. Other potential parameters that could play a role include age, helium abundance, mass loss during the RGB phase, and rotation. However, it is not clear which, if any, of these parameters are the most important as some of them are not well understood. The study, conducted by Milone *et al.* (2014) using *HST* data, has shown that the age and metallicity of GCs are the main global parameters influencing the shape and structure of their HB, while the abundance of helium within a GC is a key non-global parameter. A more recent study by Tailo *et al.* (2020) also found that both an increase in helium abundance and mass loss contribute to the HB morphology, as determined by comparing observations with theoretical models of stellar evolution. For more details, see the review papers Catelan (2009); Gratton *et al.* (2010) and references therein. However, none of the above-proposed explanations fully reproduce the observed HB morphology of GCs, and more investigation is required to fully comprehend this phenomenon through both observation and theory.

Detailed observational studies of GCs with HB encompassing a broad range of optical colours reveal additional distinctive features called jumps or discontinuities, or gaps (Brown *et al.* 2016a), although their visibility may vary based on the specific passbands employed in the analysis. Until now, three such prominent jumps or gaps have been discovered and named after the astronomer who first identified them. These include the "Grundahl jump" (G-jump) (Grundahl *et al.* 1999), which is found within the BHB at a temperature ∼11,500 K, "Momany jump" (M-jump) (Momany *et al.* 2004, 2002) found between BHB and EHB at ∼20,000 K and the gap separating EHB from BHk stars (Brown *et al.* 2001), covering a temperature range of ∼32,000-36,000 K. It is well illustrated in the right panel of Figure 1.6 that these jumps are more evident in clusters that comprise significant

numbers of both EHB and BHB stars. These jumps' colour is consistent across the distinct clusters (Ferraro *et al.* 1998; Brown *et al.* 2016a). These unexpected jumps in the HB distribution have not been explained by canonical evolutionary scenarios and have been attributed to a variety of non-canonical explanations, including evolutionary divergence, mass-loss, atmospheric processes, and differences in CNO or rotation rates (Moehler 2001). Other proposed explanations include dynamical interactions, helium mixing in RGB stars, and statistical fluctuations. It was later understood that atmospheric phenomena, including radiative levitation and gravitational settling, are primarily responsible for these HB features. BHB stars that lie blueward of the G-jump show an increase in metal content resulting from radiative levitation and a decrease in helium caused by gravitational settling (Moehler *et al.* 1999, 2000; Behr 2003; Pace *et al.* 2006). The reason for the sudden emergence of radiative levitation and diffusion patterns, which results in the jumps, is currently not fully understood. However, Sweigart (2002) pointed out that this phenomenon occurs near the temperature at which surface convection vanishes in HB stars, suggesting a possible connection between the disappearance of convection and the onset of radiative levitation and gravitational diffusion effects in these stars. Additionally, BHB stars with temperatures higher than the G-jump were found to have low rotational velocities, which might be caused by the spin-down of the surface layers by a faint stellar wind generated by the radiative levitation of iron.

The formation pathways of hot HB stars, including EHB and BHk stars in GCs, are still a matter of debate. A variety of theories have been proposed, including dynamical interactions among binary stars (Mengel *et al.* 1976; Tutukov and Iungelson 1987), helium-mixing (Sweigart 1997), early and late hot-flasher (Brown *et al.* 2001, 2010) and helium enhancement (Lei *et al.* 2015; Heber 2016), but the ultimate explanation for the existence of these stars remain elusive. Nonetheless, the population of such stars in clusters is largely affected by their mass and density (Rosenberg *et al.* 2004; Moehler *et al.* 2004b); denser, more massive clusters

(NGC 2808, ω Cen) tend to have a large number of hot HB stars.

1.5 Multiple Stellar Populations

For many years, it was thought that the stars within GCs were all created during a single burst of star formation, resulting in a population of monometallic and coeval stars known as a simple stellar population (SSP). But in the last two decades, extensive photometric as well as spectroscopic studies uncovered the presence of multiple stellar populations (MSPs) in GCs. MSPs correspond to different generations of stars that have formed through multiple star formation events or stellar populations with distinct light element abundances such as He, C, N, O, Na and Al. In general, stars that have a chemical composition similar to the typical composition of the Galactic field stars are referred to as the first generation (1G); on the contrary, the second generation (2G) of stars is defined by an enrichment of Al, Na, N, and He and depletion of O and C. The CMDs of most GCs contain multiple photometric sequences that can be followed throughout a range of evolutionary stages, as can be seen in the photometric diagrams illustrated in Figure 1.7 These sequences can be traced from the start of the MS (Piotto *et al.* 2007), through the SGB (Milone *et al.* 2008; Anderson *et al.* 2009; Piotto *et al.* 2012), RGB (Marino *et al.* 2008; Yong and Grundahl 2008; Lee *et al.* 2009; Piotto *et al.* 2015; Milone *et al.* 2017, 2018) and HB Dondoglio *et al.* (2021), and up to the AGB (Lagioia *et al.* 2021) and WD cooling sequence (Bellini *et al.* 2013). Even several photometric as well as spectroscopic studies of some clusters found variations in He abundances among different sequences such as MS, RGB, and HB of stellar populations (D'Antona *et al.* 2005; Piotto *et al.* 2005, 2007; Hema *et al.* 2020). In a recent study, Dondoglio *et al.* (2021) discovered the presence of MSPs in the RHB of 14 GCs for the first time by examining their distribution in UV-optical two-colour diagrams. Recently, different scenarios have been suggested

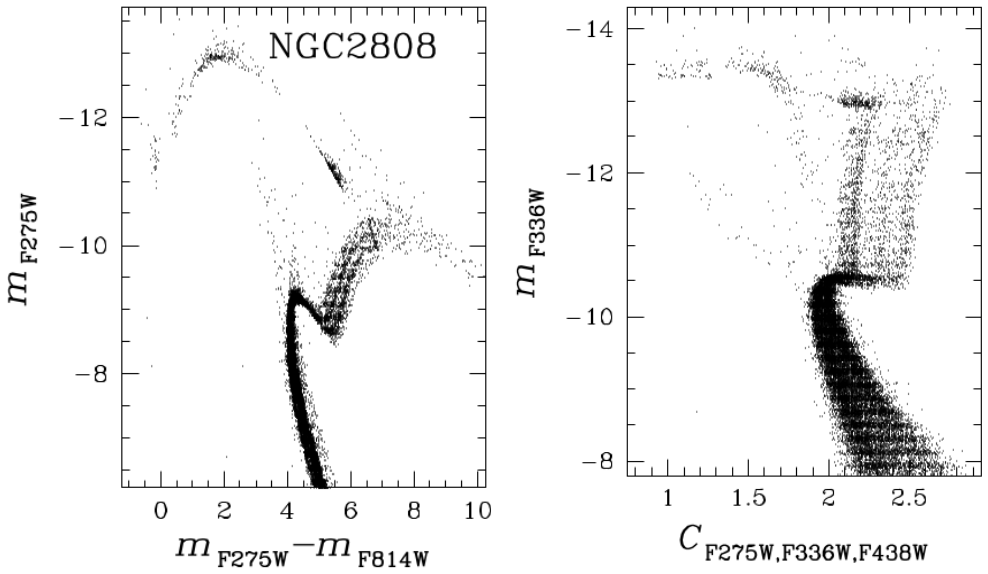

FIGURE 1.7: HST photometric diagrams showing the presence of spread and split along the different sequences in GC NGC 2808. Credits: Piotto *et al.* (2015)

to account for the origin and evolution of MSPs within GCs, and these include the AGB scenario, fast-rotating massive star (FRMS) scenario, massive interacting binaries, super-massive-star scenarios, stellar mergers, etc. The details of these formation channels are well described in the recent review paper merely dedicated to MSPs (Milone and Marino 2022). As of now, none of the above-mentioned theories properly explain the origin of MSPs in GCs. Therefore, more in-depth study and investigation are required to fully comprehend the multiple population phenomenon.

In contrast to GCs, even the CMDs of young star clusters (∼2 Gyr) are not reproduced with simple isochrones. In these star clusters, the MSP phenomenon is manifested as either a widening of the MSTO region, also known as extended MSTO (eMSTO) or splitting of the MS, which cannot be attributed to photometric uncertainties, crowding or binarity (Bertelli *et al.* 2003; Mackey and Broby Nielsen 2007; Milone *et al.* 2009). Till now, it has been observed among star clusters younger than ∼2 Gyr located both in our own Galaxy (OCs) (Bastian *et al.* 2018) and Large and small Magellanic-Clouds (LMC & SMC). The eMSTO, first

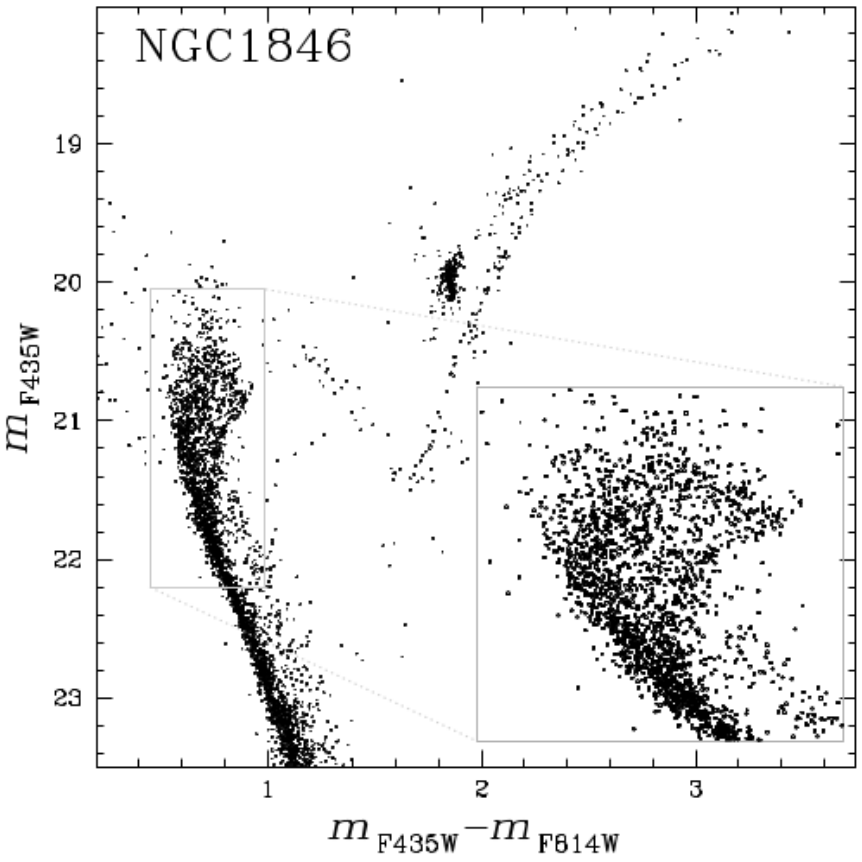

FIGURE 1.8: Optical *HST* CMD of the ∼1.7 Gyr old LMC cluster NGC 1846, where the inset panel shows a zoom of the CMD region around the eMSTO of it. Credits: Milone *et al.* (2009)

detected in star clusters NGC 1846 and NGC 2173 of LMC (Bertelli *et al.* 2003; Mackey and Broby Nielsen 2007) as shown in Figure 1.8, is observed in both optical and UV CMDs. On the contrary, other sequences, such as the MS, RGB, and AGB, are narrow and well-defined, indicating that the eMSTO is not caused by differential reddening or observational errors. Additionally, star clusters younger than ∼800 Myr exhibit a split in their MS, with the red MS hosting most of the stars (Milone *et al.* 2016). This split disappears for stars with masses below ∼1.5-1.6 $M_{\odot}$, which is the point at which they experience magnetic braking (Georgy *et al.* 2019).

The cause of the occurrence of the MSP phenomenon in GCs and young star clusters is not the same. Unlike older GCs with MSPs, young star clusters with

ages <2 Gyr are chemically homogeneous, as observed through both photometry (Milone *et al.* 2016; Martocchia *et al.* 2017; Li *et al.* 2020) and high-resolution spectroscopy (Mucciarelli *et al.* 2014). The eMSTO has originally been attributed to prolonged star formation (Keller *et al.* 2011; Goudfrooij *et al.* 2011), but recent studies have revealed that stellar rotation also plays a crucial role, as first suggested by Bastian and de Mink (2009). Similarly, the split in the MS can be explained by the presence of multiple populations of stars with different rotation rates, with the blue part of the MS being reproduced by a non-rotating model and the red part requiring the inclusion of fast rotations near the critical rotation rate (D'Antona *et al.* 2015). In a recent study by Wang *et al.* (2022), it was proposed that blue MS stars are formed through the merger of binary stars, which results in slow rotation, while red MS stars are formed through the accretion of material from a disk and have rapid rotation. Therefore, uncovering the origin of the MSP phenomenon poses a significant challenge, and further probing into areas like stellar evolution, stellar nucleosynthesis, and the mechanisms of star formation during the early universe is required to achieve this goal.

In this thesis work, we have explored the presence of MSPs along the HB in GC NGC 2298 and also probed the eMSTO in OC NGC 2818 by examining the response of UV colours to stellar rotation presented in Chapters 4 and 6, respectively.

1.6 UV bright stellar populations and importance of their UV study

Star clusters, mainly GCs, host hot stellar populations such as HB, pHB, pAGB, and WDs, which are particularly bright in the UV regime (Zinn *et al.* 1972; Harris *et al.* 1983). In addition, they are home to exotic populations, which deviate from

traditional single stellar evolution, including BSSs, cataclysmic variables, EHB, and BHk stars. These hot stars' spectral energy distribution (SED) peak lies in the short-wavelength region, specifically in the NUV or FUV. Thus, to identify and study them in detail, UV observations have been proven to be an efficient window. In the case of OCs, crowding does not affect the detection of such populations. On the contrary, it can be challenging to identify hot populations in optical images of GCs due to the high density of stars in the cluster cores, which are dominated by the MS and RGB stars. Additionally, many of the exotic stars that are hotter than other cluster members and emit much of their radiation in the UV are also optically faint and located in the dense inner regions of the GCs. However, in UV images, due to the fact that normal cluster stars (MS and RGB) are cooler than late A-type stars and faint at short wavelengths less than 2000 Å, crowding due to MS and RBG cluster members is generally not an issue in detecting hotter members. The recent studies on GCs (Ferraro *et al.* 2003; Dieball *et al.* 2010; Haurberg *et al.* 2010; Parada *et al.* 2016; Dieball *et al.* 2017; Raso *et al.* 2017) have uncovered the key role of using UV CMDs in identifying and understanding the properties of UV-bright stars. The observed optical and UV CMDs display the distribution of identified UV bright stars as stated above along different sequences as shown in Figure 1.9. In UV CMDs, it can be noted that HB stars no longer fall on the horizontal sequence and cover a wide range of over 3 magnitudes when compared to optical CMDs. BSSs also appear brighter and form a vertical sequence similar to HB stars, spanning more than 3 magnitudes. Even EHB and BHk stars follow a particular sequence in UV CMDs, separating them from BHB and hot BSSs. Thus, the most effective way to spot and analyse them in star clusters is by utilising a combination of both optical and UV magnitudes (Ferraro *et al.* 1998; Dieball *et al.* 2010; Dalessandro *et al.* 2011, 2013; Subramaniam *et al.* 2017; Sahu *et al.* 2019; Rani *et al.* 2020; Singh *et al.* 2020; Prabhu *et al.* 2021; Rani *et al.* 2021b).

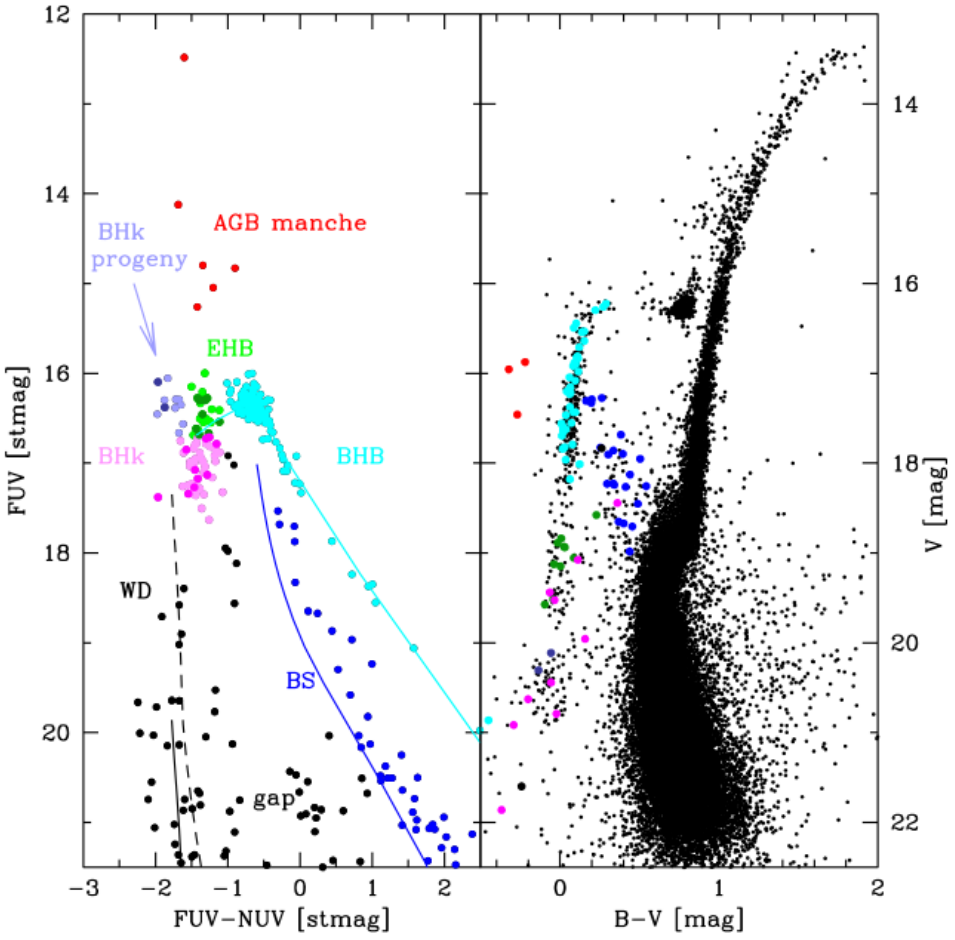

FIGURE 1.9: Observed UV (Left) and optical (Right) photometric diagrams showing the location of various stellar evolutionary sequences. Credits: Dieball *et al.* (2010)

Apart from the above-stated merits of UV observations, they can also be used to investigate the presence of MSPs in GCs and OCs. Piotto *et al.* (2015) analysed 54 GGCs to explore the existence of MSPs among them using three *HST* filters, namely, F275W, F336W and F435W, known as “magic trio". Combining these three filters with other optical filters is the optimal approach for identifying and determining the properties of multiple populations in GCs. The key benefit of utilising them to disentangle the distinct populations is that they span the wavelength range of 3000−4000 Å, which includes the OH, NH, CN, and CH absorption bands. Appropriate combinations of magnitudes in the F275W, F336W, F438W,

and F814W filters have been shown to be effective in identifying multiple populations along almost all sequences in GCs, as demonstrated in the study by Monty *et al.* (2018). In addition, the F275W−F814W colour covers a broad wavelength range. Hence, it is very sensitive to T_{eff} of stars, allowing for the identification of different stellar populations based on their He and metal content. This also revealed that the identification of MSPs within GCs is highly dependent on the filter used; specifically, the UV filters are very sensitive to variations in the abundances of C, N, O and He. These filters make it more apparent to discern the features of MSPs in CMDs by increasing the separation between sequences.

Code and Welch (1979) first discovered the UV upturn phenomenon in elliptical galaxies using the OAO-2 space telescope and found that their spectra show a rise in the flux below 2500 Åfalling near the FUV region. As old systems, Elliptical galaxies are normally expected to consist of old stellar populations, which mainly contribute their light in the visible regime and are not expected to emit UV flux. Later, various space missions, which include Hopkins Ultra-Violet Telescope (HUT), International Ultra-Violet Explorer (IUE), Galaxy Evolution Explorer (*GALEX*), etc., confirmed the UV upturn phenomenon in these galaxies (Bertola *et al.* 1982; Brown *et al.* 1997; Yi *et al.* 2011), but the cause of it was not known earlier. UV sources found in elliptical galaxies have temperatures around 20,000-30,000 K (Brown *et al.* 1997) and properties similar to the hot HB stars (Piotto *et al.* 1999) identified in GGCs, indicating their dominant contribution to the "UV upturn" seen in their spectra (Dorman *et al.* 1995; Brown *et al.* 2000, 2008; Chung *et al.* 2011; Bekki 2012). All the facts stated above clearly indicate the importance of locating and characterising these stars to shed more light on their formation pathways and evolution in star clusters.

1.7 Motivation and Aim

In literature, there have been a few UV imaging studies of GCs done using *HST* and *GALEX* data, but they have their own limitations. Schiavon *et al.* (2012) presented and discussed the main features of the UV CMDs (FUV−NUV vs FUV) in 44 GGCs by exploiting data from *GALEX*. They demonstrated that the HB stars fall along a diagonal sequence that spans greater than 4 mag in UV-optical colour, thereby removing the degeneracy in colour (B−V) from optical CMDs. They also identified the population of BSSs in UV CMDs, which is found to be located parallel to the HB sequence spanning ∼3 mag in UV colour, and 1-1.5 mag fainter than the HB. Along with these two populations, they detected and catalogued other UV bright stars such as pAGB, post-early-AGB (peAGB) and AGBM stars, which are in the pHB evolutionary phase and more luminous than the HB stars. Hence, they are easier to identify in UV CMDs, unlike optical CMDs. However, their study lacked membership information for the detected stellar sources. Additionally, the centre of the cluster could not be resolved by *GALEX* in both NUV (5-6″) and FUV (4-5″) images due to its poor resolution as given in the parentheses. They also didn't compare the UV CMDs with stellar evolutionary models.

Brown *et al.* (2016a) characterised the HB features in 53 GGCs, including NGC 1261, and NGC 2298, using three *HST* filters (F275W, F336W, F475W). They created colour-colour plots for all selected clusters. Their study found that UV CMDs are the most effective tools to examine the shape of the HB in GCs and detect gaps related to it. On the other hand, the GCs survey, HUGS, conducted by Piotto *et al.* (2015) detected MSPs in GCs, thanks to its high resolution (0.″05). Nonetheless, both studies mentioned above were restricted to only analyzing GC's core regions due to *HST*'s restricted FOV (∼ 3.′4 square) and was further constrained to observe only in NUV wavelengths. Note that the FUV filters on the *HST* have a flaw that causes them to let in too much red light. This leads to an inaccurate

measurement of the amount of FUV light coming from cool stars, making them appear brighter than they actually are. Thus, in GCs analysis, we mainly aim to examine not only the central regions but also the entire cluster and focus on the hot stellar populations using a combination of FUV and NUV wavelengths to get a more accurate picture.

In the old OCs, NGC 6791, NGC 188, and M67, hot stars have been detected and studied by Landsman *et al.* (1998) using Ultraviolet Imaging Telescope (*UIT*) data. De Martino *et al.* (2008) have obtained FUV and NUV images of the old OC NGC 2420 from *GALEX* and cross-matched with Sloan Digital Sky Survey (SDSS) u,g,r,i,z photometric data in search of WDs in the cluster. The wide field photometry for nearby clusters M79, NGC 2539, M67, and NGC 188 using Swift Ultraviolet Optical Telescope (*UVOT*) by Siegel *et al.* (2014) reveals that the UV CMDs can easily identify the unusual UV bright stars. Browne *et al.* (2009) used *GALEX* observations to check UV variability in OCs Hyades and the Pleiades and detected 16 UV variable sources. Gosnell *et al.* (2015) utilised *HST* data in FUV passbands to detect and identify hot companions to BSSs in old OC NGC 188. Therefore, UV imaging to study OCs offers a specific opportunity to identify and characterise hot stellar populations to further shed light on their formation and evolution.

There are only a few OCs in our Galaxy known to harbour Planetary nebulae (PNe). PNe are classically considered to represent the late stages in the stellar evolution of all the low as well as intermediate-mass stars with a mass range of 0.8−8 $M_{\odot}$ (Weidemann 2000). As the evolutionary lifetime of PNe are short (around $10^3 - 10^5$ years, depending on the mass of the progenitor) when compared to other evolutionary phases, especially when the number of evolved stars present in OCs are small, PNe as members of OCs are rare and are not expected in young OCs. Objects in this brief phase are essential to comprehend the physical processes and steps that transform stars into their remnants. They are crucial in

testing the theory of stellar evolution, including the nucleosynthesis physics and the correlation between a star's initial mass and its final WD remnant (Kwitter *et al.* 2014). Furthermore, the chemical composition of PNe can offer insight into the dredge-up of chemical elements, which is believed to be linked to the initial mass and composition of the star. Finding a PN as a member of an OC gives us an excellent opportunity to better characterise and constrain its crucial parameters, such as distance, reddening, and age.
This thesis's objectives are:

- to present the UV and UV-optical CMDs of GCs and OCs members covering the entire cluster region and interpret them using theoretical stellar evolution models.
- to classify and investigate the behaviour of stars that appear bright in the UV as we shift from optical to UV CMDs.
- to examine the morphology of HB in GCs and investigate the MSPs that can be present within them.
- to identify and determine the parameters of hot HB stars, including EHB, BHk, and pHB stars, in order to gain insight into their UV properties.
- to identify and study the properties of BSSs and YSSs in a variety of OCs and understand their formation and evolution in them.
- to characterise the central star of the PN (CSPN) to explore its physical association with the cluster and understand the late stages of evolution of low-mass stars.

In order to accomplish our objectives as stated above, we employed the Ultra-Violet Imaging Telescope (UVIT) on *Astrosat*, India's first multi-wavelength space observatory, and combined it with various other archival data as detailed in Chapter 2. The advantage of observing with UVIT over the other UV telescopes is

its good spatial resolution ($< 1\farcs5$), large FOV ($28'$ in diameter) and the multiple number of FUV (130-180 nm) and NUV (200-300 nm) filters with both narrow and broad passbands, which help in probing the properties of different stellar populations. The UVIT's wide FOV will allow us to detect UV stellar populations over a full cluster region with good resolution. By combining UV data with optical data from archives such as *HST* and *Gaia*, we can accurately identify cluster members and classify them in the UV. UVIT's multiple filters in the FUV and NUV will also enable more precise sampling of the UV wavelength range and detection of BSSs and other UV bright candidates showing UV excess.

1.8 Overview of the thesis

This thesis is organised in the following way:

- **Chapter 1:** We introduce star clusters and their UV stellar populations, including the properties and characteristics that are relevant to our study. We also outline the motivation and aim of our research. Our study focuses mainly on bright UV objects such as HB, pHB, BS stars and other objects that appear bright in UV.

- **Chapter 2:** We present the details of the observations and multi-wavelength data employed in this thesis. This chapter also describes the methods and tools used to analyse the data and characterise the UV-bright stellar population identified in the clusters under study.

- **Chapter 3:** We study the HB and BS stars, focusing mainly on the hot HB stars detected in GC NGC 1261 using UV observations, and present the important findings by comparing them with theoretical models.

- **Chapter 4:** We present the results obtained from the UVIT-*HST*-*Gaia* study of GC NGC 2298 to investigate its HB morphology and hot HB stars. In addition, we also examined the presence of the MSPs along HB in it by comparing observations with simulations.

- **Chapter 5:** We present the results obtained for identified UV-bright stars other than BSSs in one of the old OC NGC 188, and estimate their properties using UV photometry.

- **Chapter 6:** We present the results obtained from the UV study of intermediate-age OC NGC 2818, mainly focusing on the BSSs, YSSs, and PN. It also includes results from the membership analysis of the cluster and its associated PN using *Gaia* EDR3 PM data and UV photometry.

- **Chapter 7:** We present a summary of our findings, draw conclusions, and discuss future prospects.

Chapter 2

Observational Data and Methods

In the previous chapter, we discussed the details of stellar populations in star clusters and the motivation behind studying them in this thesis. As we are mainly interested in hot and bright stellar populations that emit the bulk of their energy in the UV part of the electromagnetic spectrum, most of the telescopes used to collect data in that region are space-based. In optical and IR regions, we have used imaging data from both space and ground-based facilities, as described in the following Sections. Apart from the observing facilities used, this chapter also includes details of the various methods and models adopted to analyse the data and accomplish the broad goals of the thesis.

2.1 Space Based Telescopes

Here we discuss about the space-based telescopes that are used for obtaining UV observations. It is not possible to observe the UV region from the ground as the atmosphere of our planet blocks UV radiation. Therefore, in order to collect the

UV radiation emitted by the stellar objects of interest, we must rely on space-based telescopes.

2.1.1 UVIT

AstroSat, the first multi-wavelength Indian Space Observatory, has the UVIT as one of its payloads (Singh *et al.* 2014; Singh 2022). On September 28, 2015, ISRO launched *AstroSat* into a 650 km, nearly equatorial orbit. It also carries four X-ray instruments in addition to the UVIT. These instruments include three LAXPCs, an SXT, a CZTI, and an SSM. A schematic of *AstroSat* is shown in Figure 2.1, where all the payloads are marked. There are three SSM onboard *AstroSat* to monitor bright transient X-ray sources. All telescopes are oriented in the same direction to allow for the simultaneous observation of astronomical sources across a wide spectrum of wavelengths, including X-rays, UV and visible regions.

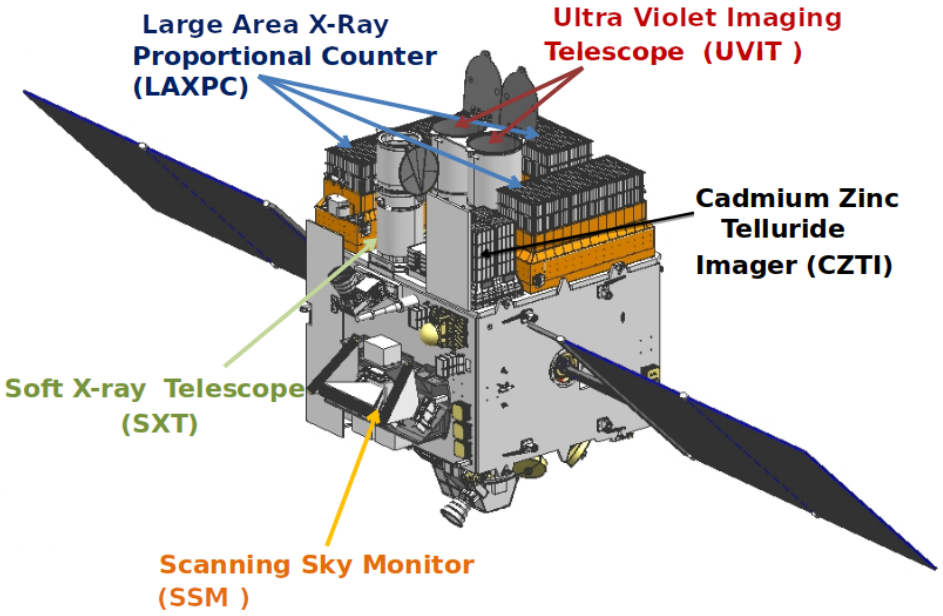

FIGURE 2.1: The Figure shows the *AstroSat* setup, with each instrument listed and labelled. Image Credits: ISRO

The UVIT instrument is primarily designed to observe in both the UV and optical bands. UVIT comprises two Ritchey-Chretien type telescopes with a primary mirror of $\sim$ 38 cm diameter. One of them takes observations in the FUV (130-180 nm) channel and the other one in NUV (200-300 nm) as well as VIS (320-550 nm) channels simultaneously. UVIT has a circular field of view (FOV) of diameter $\sim 28'$. The spatial resolution (FWHM) is better than $1''.5$ for the FUV and NUV channels. Each channel (FUV, NUV and VIS) consists of a set of selectable filters having different wavelength passbands. The details of all UVIT filters are provided in two calibration papers (Tandon *et al.* 2017b, 2020). Figure 2.2 depicts the UVIT's configuration. Further details about effective area curves, calibration results of UVIT, and instrumentation can be found in Kumar *et al.* (2012), and Tandon *et al.* (2017a, 2020). Note that observations of HZ4, a WD used as a spectrophotometric standard, were performed to carry out in-orbit calibration of the instrument in order to compute the zero point magnitudes, unit conversion, etc.((Tandon *et al.* 2017b)).

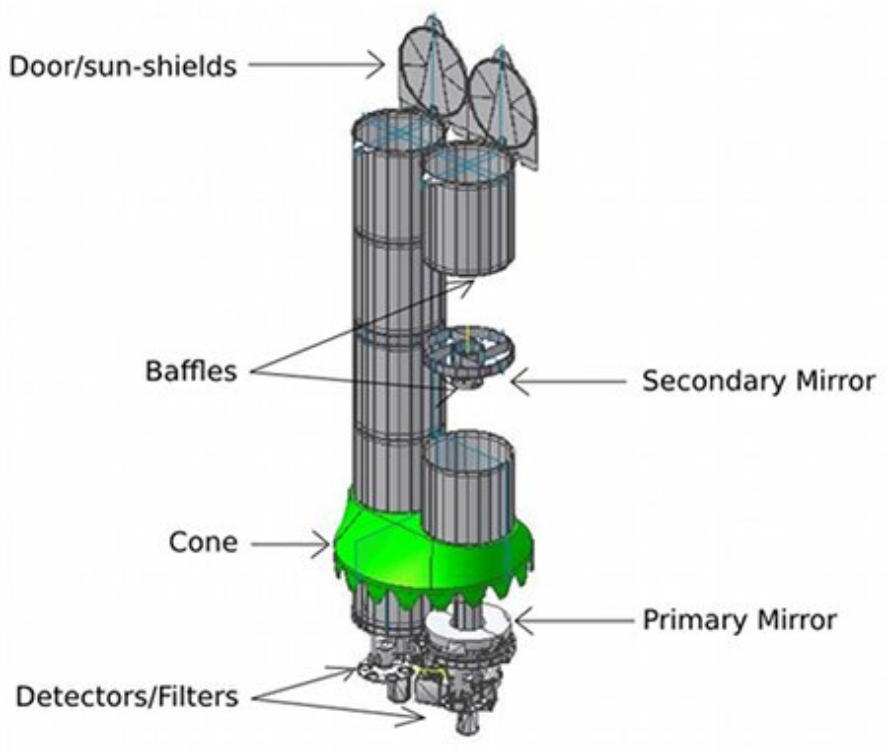

FIGURE 2.2: UVIT's schematic displaying its two telescopes (Tandon *et al.* 2017a).

As the photon counts at UV wavelengths are not high, intensified CMOS detectors are used in the photon-counting mode for the FUV and NUV channels. In contrast, in the optical channel, due to large photon counts, it is operated in integration mode. When a UV photon strikes the photocathode, it causes the release of a primary electron which is further accelerated to a microchannel plate (MCP) amplified by a factor of $\sim 10^7$. The subsequent electron shower illuminates a phosphor anode, and the light from it passes through a fibreglass taper to be detected by a CMOS chip (512×512-pixel array). The centroid of the incident photon is then determined using the photon event that spans a fraction of a CMOS pixel ($\frac{1}{8}$ pixel) using a centroiding algorithm (See for more details in Hutchings *et al.* (2007); Postma *et al.* (2011)). These centroid positions are eventually used to construct the science images. The final resolution of the UVIT images is determined by photoelectron spread on the detector ($\sim 1''$) and the tracking jitter ($\sim 0''.5$). The CMOS is generally read out at 29 frames per second for a full frame; however, this can be raised to roughly 200 frames per second for a subarray. Since optically bright sources are more easily available than those emitting UV light, the VIS channel is particularly employed to monitor and calculate spaceship drift.

AstroSat has a 90-minute orbit, and UVIT only observes the night part of that orbit. Therefore, the observations typically last for less than 25 minutes every orbit. To complete the required exposure time, the UVIT instrument makes observations over several orbits. The recorded UVIT data is provided in the Level1 (L1) format, which comprises a set of fits tables containing centroid data as well as additional spacecraft and observational metadata. A customised software package, CCDLAB, is used to process the L1 data to produce the scientific images (Postma and Leahy 2017). This software particularly takes care of the following corrections: geometric distortion, centroiding bias, flat-field illumination, and spacecraft drift. The final images obtained after correcting for drift are aligned and combined to create a science-ready image. For example, Figure 2.3 shows the UVIT FUV image without applying drift correction in the left panel and after drift correction

in the right panel.

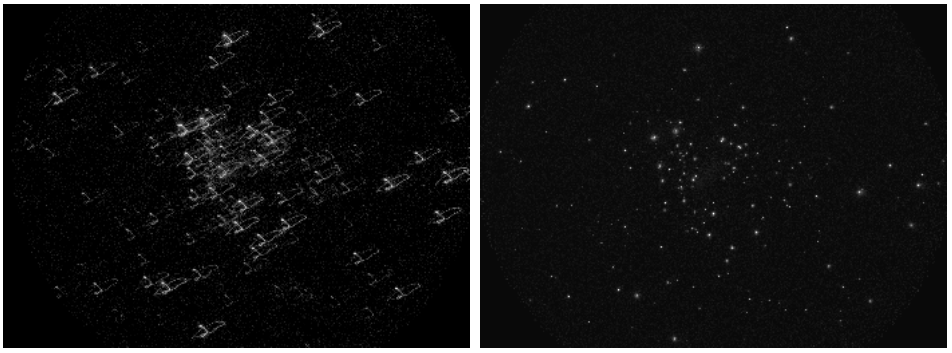

FIGURE 2.3: UVIT image of young OC NGC 663 in FUV F154W filter without (left panel) and with (right panel) drift correction (Postma and Leahy 2017).

Due to the VIS data being sampled at 1 Hz as compared to the UV data being sampled at 29 Hz, the combined images are still not perfect. Furthermore, a slight discrepancy in the pointing direction of the VIS and FUV telescopes can occur due to thermal stick-slip (Postma and Leahy 2021). To fix this, CCDLAB offers a point spread function (PSF) optimization feature that stacks images of bright sources with an exposure time of 20 seconds or less to get the optimal PSF and a minimal drift correction. The FWHM of PSF for point sources in various targets and filters typically varies from $\sim 1\farcs2 - 1\farcs5$.

We exploited *Gaia* and *GALEX* point source databases for performing astrometry on the UVIT images. For the UVIT data observed before 2018, we used the astrometric coordinates of the bright sources common in *GALEX* and UVIT images to get the astrometric solution using the CCMAP task of IRAF followed by the WCSTRAN task to register the UVIT images. As astrometry of *GALEX* is not as accurate as *Gaia*, we further used the *Gaia* catalogue to make astrometry more precise. We have applied the coordinate matching algorithm from the upgraded CCDLAB to do the astrometry on NGC 2818 images. Details of the algorithm can be found in Postma and Leahy (2020).

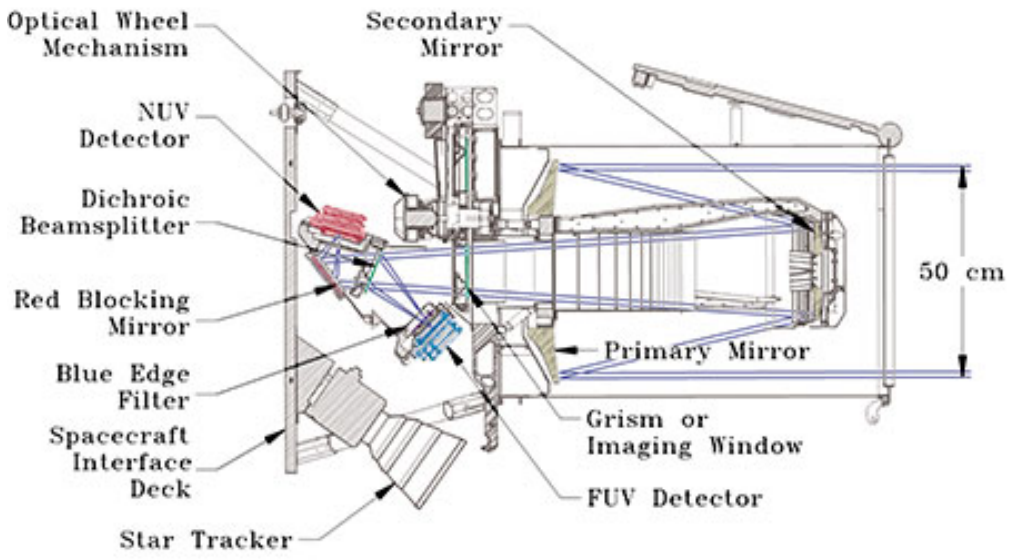

FIGURE 2.4: Overview of the *GALEX* instrument. Image Credits: NASA

2.1.2 *GALEX*

The Galaxy Evolution Explorer, *GALEX*, is a space-based telescope launched on April 28, 2003, by National Aeronautics and Space Administration (NASA), specifically designed to observe in UV wavelengths (Martin *et al.* 2003). The instrument consists of a 50 cm diameter modified Ritchey-Chrétien telescope with photon-counting mode detectors to obtain simultaneous images in two bands, NUV (1771–2831 Å) and FUV (1344–1786 Å). The FOV of the instrument is very large, with a circular shape of 1.2° and it offers a spatial resolution of 5.″3 and 4.″2 in the NUV and FUV channels, respectively. The plate scale of detectors is $1.''5 pixel^{-1}$. The *GALEX* schematic is shown in Figure 2.4. This mission's main goal was to analyse galaxies' UV properties to probe star formation and its evolution with time.

GALEX has conducted five imaging surveys in two bands to address the main science goals. These surveys include the All-sky imaging survey (AIS), Medium Imaging Survey (MIS), Deep Imaging Survey (DIS), Ultra-deep Imaging Survey

(UDIS), and Nearby Galaxy Survey (NGS). The instrument's detection limit depends on the imaging survey type, and in NUV, it is ∼20-21 ABmag in AIS, ∼23 ABmag in MIS, ∼25 ABmag in DIS, ∼26 ABmag in UDIS. *GALEX* data is publicly available at Multimission Archive at Space Telescope (MAST). We have used photometric data for all clusters studied in the thesis from the updated *GALEX* UV sources catalogue containing FUV and NUV images of ∼500 million sources (Bianchi *et al.* 2017).

2.1.3 *HST*

The Hubble Space Telescope, *HST*, is a space-based telescope that was launched on April 24, 1990, by NASA. It comprises five main instruments which capture images in wavelengths of light spanning from UV to near-infrared (NIR). The primary mirror of the telescope has a diameter of 2.4 m. The currently working instruments on board *HST* are Advanced Camera for Surveys (ACS), Wide Field Camera 3 (WFC3), Cosmic Origins Spectrograph (COS), Space Telescope Imaging Spectrograph (STIS), and Fine Guidance Sensor (FGS). One more instrument, namely, the Near Infrared Camera and Multi-Object Spectrometer (NICMOS), used for both imaging and spectroscopic observations, is currently inactive. The widely used third-generation imaging instrument ACS has three channels: Wide Field Channel (WFC), High-Resolution Channel (HRC) and Solar Blind Channel (SBC). WFC, the most utilised channel of ACS, has a plate scale of $0\farcs05$ per pixel and an effective FOV of $202'' \times 202''$. It features a number of filters that cover the 350–1100 nm spectral range. WFC3 is a fourth-generation instrument with two channels, the Ultraviolet-Visible (UVIS) and the NIR, providing images in three broad regions of the spectrum, UV-Visible-NIR (Quijada *et al.* 2006). The UVIS channel spans a spectral range from 200-1000 nm, and a NIR detector covers a wavelength range from 800-1700 nm. The UVIS channel has a plate scale of $0\farcs04$ per pixel with FOV $164'' \times 164''$, less than compared to the ACS camera. The

spatial resolution of ACS and WFC3 cameras are similar, allowing for a resolution of $\sim 0\farcs09$ for point sources with depths of AB $<\sim$26–27 mag (5-σ) (Windhorst *et al.* 2011).

We have used the catalogue provided under the *HST* UV Globular Cluster Survey (HUGS) (Nardiello *et al.* 2018) to identify common stellar sources between UVIT and *HST* and construct different CMDs to select stellar populations along distinct phases. The catalogues include details on high-precision stellar astrometry and photometry in three UV/blue WFC3/UVIS bands (F275W, F336W, F438W) and two optical ACS/WFC bands (F606W, and F814W) of every star detected in the cluster field. Additional information about their PM membership is also provided in the catalogue.

2.1.4 *Gaia*

The Global Astrometric Interferometer for Astrophysics, *Gaia*, is a space mission launched on 19 December 2013 by European Space Agency (ESA) dedicated to astrometry. *Gaia* has twin optical telescopes with a primary mirror of 1.45×0.5 square m pointing at two different portions of the sky, separated by a fixed wide angle of $106\fdg5$ as illustrated in Figure 2.5. Each telescope has a large primary mirror with a collecting area of about 0.7 m^2. Both *Gaia* telescopes have a common focal plane containing 106 charge-coupled devices (CCDs) of 4500×1966 pixels each (total ∼938 megapixels) as shown in Figure 2.6. The five distinct components of the focal plane are the wavefront sensor (2 CCDs) and the basic angle monitor (2 CCDs), sky mappers (14 CCDs), astrometric field (62 CCDs), blue and red photometer (14 CCDs), radial velocity spectrometer (12 CCDs). Its three major instruments are an astrometer, a photometer, and a spectrometer. A detailed description of the focal plane and instruments can be found in Gaia Collaboration *et al.* (2016). The three passbands in *Gaia* are G (330-1050 nm), GBP (330-680

nm), and GRP (640-1050 nm). *Gaia* has an spatial resolution of $\sim 0''.4$. The main objective of *Gaia* is to utilise global astrometry from space along with multi-colour, multi-epoch photometric measurements to produce a catalogue of about one billion stars, or roughly 1 % of the stars in the Milky Way. In terms of completeness, it will be complete for stars with magnitudes up to 20. Over a span of five years, *Gaia* will observe each of its target stars approximately 70 times. It will precisely map out their locations, distances, motions, and brightness variations.

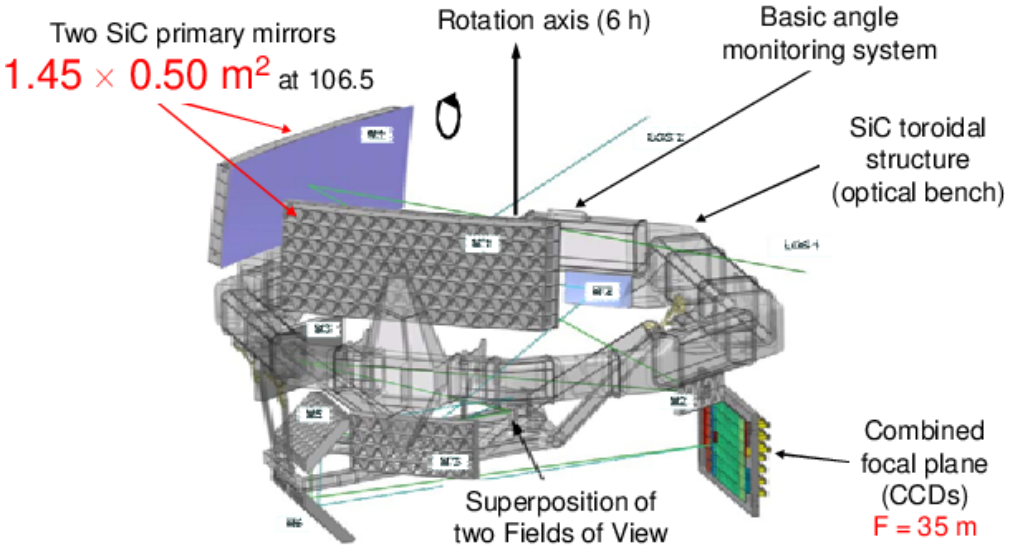

FIGURE 2.5: Diagram of *Gaia* Payload showing two mirrors and instruments mounted on the optical bench. Image Courtesy: EADS Astrium

Depending on the duration of observations, there have been three major releases of *Gaia* data to date. On September 14, 2016, the first data release, known as *Gaia* DR1, based on observations acquired over the course of the first 14 months, was made available. It contains locations and magnitudes for over 1.1 billion stars, albeit not all sources have PM data. The second DR, known as *Gaia* DR2, was made available on 25 April 2018, and it is based on 22 months of observations. It includes locations, parallaxes, and PMs for around 1.3 billion stars. Based on 34 months of observations, the third data release has been divided into two parts, allowing the first data set to be released earlier. *Gaia* Early Data Release 3 ("*Gaia* EDR3"), the first component, was made public on December 3, 2020. It included enhanced locations, parallaxes, and appropriate movements for over

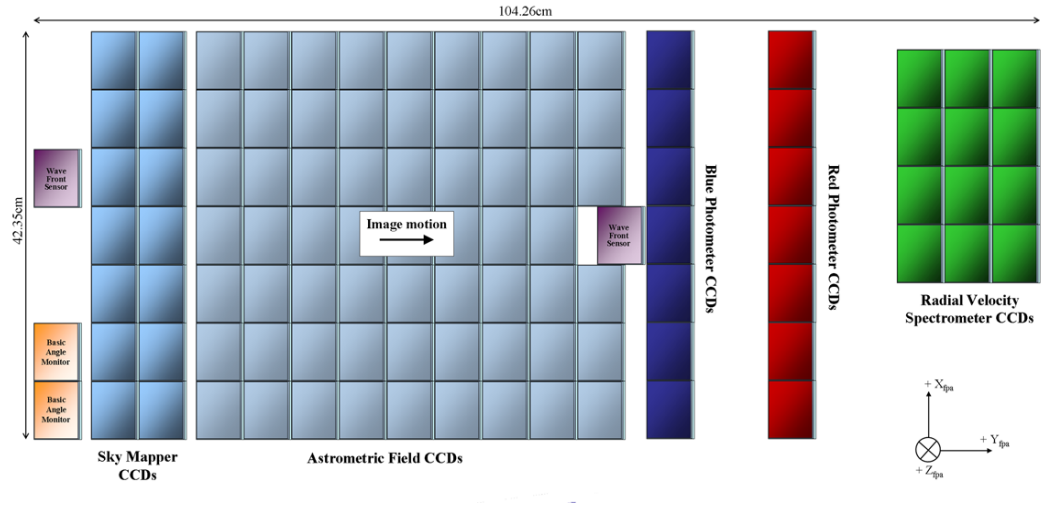

FIGURE 2.6: Schematic of the *Gaia* telescope's focal plane (Image courtesy: ESA)

two billion sources. *Gaia* DR3, which was made accessible on June 13, 2022, is the most current data release and comprises *Gaia* EDR3 data complemented with astrophysical parameters, variability data, and light curves. (Gaia Collaboration *et al.* 2022; Babusiaux *et al.* 2022). *Gaia*-released data can be accessed through *Gaia* Archive.

In this thesis, we have made use of *Gaia* DR2 and *Gaia* EDR3 catalogues to obtain the PM membership of UVIT-detected sources only in the outer region of the programme GCs and for the entire region of the programme OCs. In addition to that, we also used the photometric information in different wavelength bands to create the CMDs.

2.1.5 *WISE*

Wide-field Infrared Survey Explorer, *WISE* is a 40 cm IR space-based telescope launched on December 14, 2009, by NASA (Wright *et al.* 2010). *WISE*'s FOV is 47′ and consists of four passbands, W1(3.4μm), W2(4.6μm), W3(12μm), and

W4(22μm) with a spatial resolution of 6$''$.1, 6$''$.4, 6$''$.5, and 12$''$.0, respectively; the bands' central wavelengths are given in parentheses. The prime goal of this mission was to image the whole sky in the IR region of the electromagnetic spectrum. The *WISE* All-Sky (WISEA) data was made available on 14 March 2012 and can be found at the Infrared Science Archive. In this thesis work, we have utilised WISE data points to construct the SEDs for stars studied in-depth.

2.2 Ground Based Telescopes

Apart from the data from space telescopes, we also have used optical and IR photometric data from ground-based telescopes. Below I will briefly describe each telescope used in the thesis.

2.2.1 LCO

We have used archival photometric data of GC NGC 1261 (Kravtsov *et al.* 2010) from the 1.3 m Warsaw telescope, the main instrument of the Optical Gravitational Lensing Experiment (OGLE), situated at Las Campanas Observatory (LCO). It is a Ritchey-Chrètien telescope. Kravtsov *et al.* (2010) made observations of NGC 1261 in UBVRI filters using 2048×2048 CCD camera attached to telescope. The plate scale of this telescope is 0$''$.4 per pixel, and the corresponding FOV is $14' \times 14'$. Details of observations can be found in Kravtsov *et al.* (2010).

2.2.2 KPNO

We have utilised the archival photometric catalogue of NGC 188 (Sarajedini *et al.* 1999) from the 0.9 m Cassegrain telescope at Kitt Peak National Observatory (KPNO). Sarajedini *et al.* (1999) obtained observations of OC NGC 188 using 2048×2048 pixel Tektronix CCD (T2KA) camera in UBVRI filters. The image scale of this telescope is 0.″68 per pixel, giving a FOV of 23′×23′. The observational details can be found in (Sarajedini *et al.* 1999).

2.2.3 SDSS

The Sloan Digital Sky Survey (SDSS) telescope, specially designed for survey purposes, is a 2.5 m modified Ritchey-Chrètien optical telescope situated at Apache Point Observatory in New Mexico, United States (York *et al.* 2000; Gunn *et al.* 2006). It makes observations in spectroscopic and imaging modes. The photometric system of the SDSS telescope consists of five optical filters, namely, u, g, r, i and z, covering a wavelength range of 3500–9300 Å. The image camera is made up of 30 Tektronix 2048×2048 CCDs arranged in a six-column, five-row array for observations in several bandpasses. The plate scale of the telescope is 0.″4 per pixel, and a FOV is 3°. The observed photometric data of point sources with a typical seeing of 2.″0 is 95 % complete up to the magnitudes 22.0, 22.2, 22.2, 21.3, and 20.5, for the filters u, g, r, i, and z, respectively. In addition to the imaging camera, it has two fibre-fed double spectrographs with a spectral resolution of R ∼1500-2500 that can simultaneously obtain 640 spectra in a spectral range of 3800–9200 Å.

In our study of clusters, we used the SDSS DR9 imaging catalogue, which provides information on more than 1.2 billion objects dispersed over a 31.637 deg^2 area.

2.2.4 Pan-STARRS

Panoramic Survey Telescope and Rapid Response System (Pan-STARRS), primarily dedicated to imaging survey observations, is situated at Haleakala Observatory in Hawaii. It consists of two 1.8 m Ritchey-Chrètien telescopes equipped with a 1.4 Gpixel detector spanning a 3.°3 FOV. Its photometric system contains five broadband filters designated as g,r,i,z, and y, covering a wavelength range of 400-1000 nm. Further details about the instrument can be found in Tonry *et al.* (2012).

We have used a photometric catalogue from Pan-STARRS data release 1 (Pan-STARRS1) survey (Chambers *et al.* 2016) containing information about the positions and magnitudes of $\sim$ 2 billion objects. In the Pan-STARRS1 survey, each source was observed typically for 30-60 sec in five filters (grizy) with a sensitivity of 23.3, 23.2, 23.1, 22.3 and 21.4, respectively.

2.2.5 2MASS

The Two Micron All Sky Survey, 2MASS consists of two 1.3 m Cassegrain equatorial telescopes, one located at the Whipple Observatory at Mount Hopkins, Arizona, while another telescope site is at Cerro Tololo, Chile (Skrutskie *et al.* 2006). Each telescope has a camera containing three NIR detectors with dimensions 256×256 pixels used to simultaneously image the sky in three wave bands, J (1.25 μm), H (1.65 μm), and Ks (2.16 μm). The plate scale of each telescope is $2''\text{pixel}^{-1}$ with FOV $8'.5 \times 8'.5$. 2MASS conducted an astronomical survey from 1997 to 2001 covering 99.998 % of the sky in three bandpasses. The limiting magnitudes of the telescope are 15.8, 15.1, and 14.3 mag in the J, H, and Ks bands, respectively, for a 7.8-sec exposure. The 2MASS All-Sky Data Release, which contains 472 million sources, including both point and extended, was released in 2003.

2.3 Observations

We largely employed the UVIT observations to analyse the clusters presented in this thesis. Observations of the two GCs, NGC 1261 and NGC 2298, as well as the two OCs, NGC 188 and NGC 2818, were made between November 2015 and June 2020 in various UVIT filters. NGC 188 was selected as the initial target for UVIT observations on 30 November 2015. The cluster was monitored regularly over the first six months of UVIT's operation to track the changes in the sensitivity of the UVIT. The observations of NGC 188 used in thesis work were made from December 2015 to March 2016. The observations log of the clusters is provided in Table 2.1, together with information about the filters that were utilised and their individual exposure times. CCDLAB was used to create images of the clusters with dimensions 4096×4096 pixels and had a 1/8 pixel resolution.

TABLE 2.1: Details of UVIT observations of studied star clusters.

Cluster	Observation Date	Proposal ID	PI	Filters	T_{exp} (sec)
NGC 188	22 March 2016	T01_034	A. Subramaniam	F148W, F172M, N279N	3216, 4708, 9365
NGC 1261	26 August 2017	A03_112	G. Pandey	F169M, F172M, N219M, N245M, N263M, N279N	1746, 6662, 2847, 740, 1022, 3831
NGC 2298	13 December 2018	A05_025	G. Pandey	F148W, F154W, F169M	2300, 558, 1263
NGC 2818	21 December 2018	A05_196	N. K. Rao	F154W, F169M, F172M	1491, 1715, 1903
NGC 2818	11 June 2020	A09_047	N. K. Rao	F148W, F154W, F169M, F172M	1736, 2877, 1999, 2878

2.4 Research Methodology

We have used various methods, which are discussed in the following sections, in order to analyse the data obtained from the various telescopes mentioned above.

2.4.1 Photometry

Photometry is the method of measuring the flux emitted by an astronomical object. In astronomy, the brightness of a star is measured in terms of magnitude defined as:

$$m = -2.5 \log \left(\frac{f}{f_0} \right)$$

Where m is an apparent magnitude of the object, f corresponds to the flux of the object at a particular wavelength; f_0 represents flux giving the zero point (ZP) magnitude. In order to estimate the ZP, the Vega star is used by assuming it has a zero magnitude in that filter.

In our analysis of UVIT images of various clusters, we performed the photometry on them using the DAOPHOT package (Stetson 1987) in Image Reduction and Analysis Facility (IRAF) software provided by National Optical Astronomy Observatory (NOAO). There are two types of photometry techniques used to obtain magnitudes of point sources depending upon the crowding in the field, Aperture and PSF photometry. A brief description of both techniques is given below.

2.4.2 Aperture Photometry

The fundamental idea behind aperture photometry is to enclose the star within a radius, r, from its centre and sum up all the light that falls within that circle. The star's brightness is then determined by subtracting the total contribution of the sky background within the same region. Thus, this technique will allow for the absolute measurement of a star's emission flux, which can then be used to determine its instrumental magnitude. The following steps are used to do the aperture photometry.

- imexamine: To estimate the FWHM of the stars in the image and the standard deviation (σ) of the sky.
- daofind: To find and locate the stellar sources above a given threshold (generally 4σ).
- phot: To compute magnitudes for a list of stars identified by daofind.

The aperture radius of a star should be chosen in such a way that it will include its total flux and not include the background contribution. We made use of a curve of growth method to estimate the optimum aperture radius.

2.4.3 PSF Photometry

Aperture photometry does not work in the case of crowded fields as there are chances of finding more than one star in the neighbourhood of a target for a given aperture size. Hence, the flux will be overestimated for the target star. PSF photometry is utilised in such cases.

The fundamental concept behind PSF fitting is that all stars on an image have the same intrinsic profile shape, regardless of their brightness or amplitude. This is due to the fact that each star is simply a point source of light that has been distorted by the telescope's optics, and in the case of ground-based telescopes, by the Earth's atmosphere. Therefore, it is possible to create a "standard profile" for the stars on an image, which can then be scaled to fit the individual stars present in it.

The first few steps are identical for both aperture and PSF photometry. Further steps adopted to perform PSF photometry are given below.

- pstselect: To select the bright and isolated candidate psf stars in the image.
- psf: To construct a model PSF.
- allstar: To fit a model PSF to a group of stars simultaneously to obtain psf fitted magnitudes.
- ccmap: To compute world coordinate solution (WCS) using matched sources between UVIT and reference *GALEX* or *Gaia* images
- wcsctran: To apply the WCS solution to register the image.

PSF photometry gives relative magnitudes, unlike aperture photometry. In order to get the instrumental magnitude, we did the PSF correction. To estimate the PSF correction, we calculated the mean difference between the output from ALLSTAR and PHOT for common bright and isolated stars. Then, we added this mean difference to all the PSF-fitted magnitudes to convert them into instrumental magnitudes. Further, aperture correction is applied to instrumental magnitudes by computing the mean difference between the flux enclosed in the fiducial and small aperture radius to acquire the final magnitudes. The instrumental magnitudes of stellar sources detected in UVIT images are calibrated to the AB magnitude system utilising the ZPs reported in Tandon *et al.* (2017b, 2020). As the UVIT detector works in the photon counting mode for UV channels, saturation correction (to account for more than one photon per frame) was done to get the saturation corrected final magnitudes. The saturation correction mainly affects stars brighter than 17 magnitude. The details of the saturation correction are described in (Tandon *et al.* 2017b). The details of both types of photometry are given in the manual by W. E. Harris*.

After performing the photometry on all science images, we made use of the TOPCAT tool (Taylor 2011) to identify the common sources between UVIT and other

*https://physics.mcmaster.ca/~harris/daophot_irafmanual.txt

optical catalogues using the maximum separation $< 1.7''$ to create the CMDs as discussed in the introduction Section 1.2.

2.5 Spectral Energy Distribution

All astronomical objects radiate over a broad range of wavelengths of the electromagnetic spectrum. The light emitted by them helps in probing their nature and evolution. SED is one of the techniques to obtain the physical properties, for example, T_{eff}, L (in terms of $L_{\odot}$), and R (in terms of $R_{\odot}$) of astronomical sources using multi-wavelength imaging observations to put insights into their formation. A SED is a plot of flux emitted by an object as a function of wavelength/frequency. The shape of the continuum reveals information about the source. The other method to characterise the stellar sources is using spectroscopic observations by fitting the spectrum with a model template. But, acquiring spectroscopic observations over a wide wavelength range is challenging as well as time-consuming. In the case of faint sources, it is difficult to get spectroscopic observations. Each given data point in an observed SED refers to the integrated flux radiated by a star over a bandpass encompassing a certain wavelength range. Compared to spectroscopy, the SED technique is cheaper and equivalent to a low-resolution spectrum. Wide-field imaging surveys have been carried out in a variety of wavelength ranges over the past few years, yielding multiwavelength photometric (archival) data for a significant number of stellar sources. Hence, SEDs play a vital role in deriving the physical parameters of stars.

In order to construct and fit the observed SEDs with theoretical models, we have used the virtual observatory tool, VO SED analyser (VOSA[†]) (Bayo *et al.* 2008).

[†] http://svo2.cab.inta-csic.es/theory/vosa/index.php

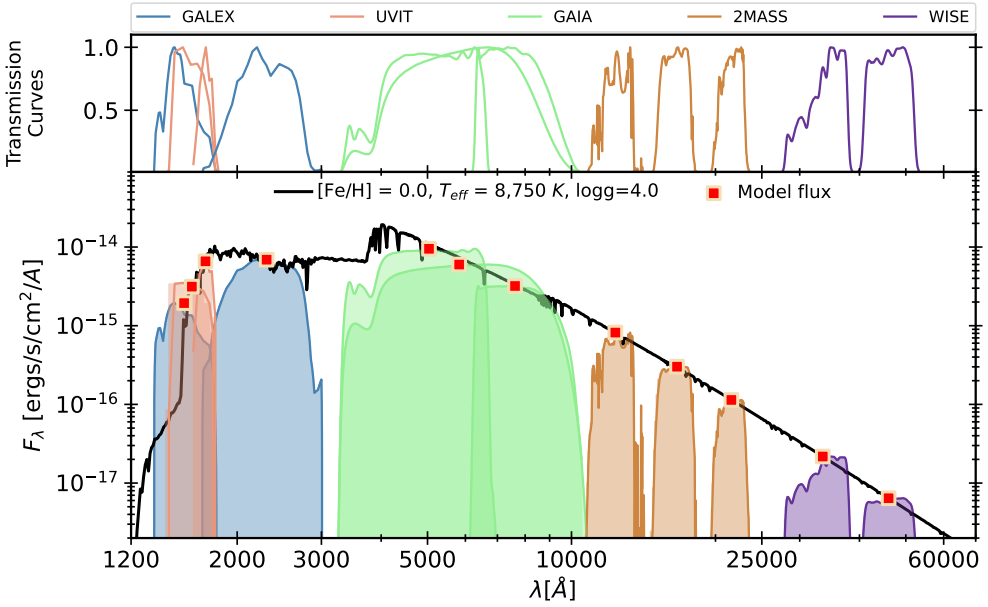

FIGURE 2.7: SED of the MS star with solar metallicity and effective temperature of 8,750 K. The theoretical Kurucz spectrum with the mentioned parameters in the legend is displayed with a solid black line overlaid with the corresponding model integrated flux in each filter. The transmission curves of used filters to obtain SED are shown in both panels.

VOSA, developed by the Spanish Virtual Observatory (SVO[‡]), encompasses spectral libraries and VO services. Moreover, the properties of the filters used by VO services are provided by the SVO Filter Profile Service.

In this thesis, we employed the photometric data from various telescopes spanning a wavelength range from FUV-to-IR to build the observed SEDs. We mainly have provided the UVIT photometry combined with *HST*, *Gaia*, LCO, and KPNO data to VOSA. The other available archival photometric data points such as *GALEX*, Pan-STARRS1, SDSS, 2MASS and *WISE* for the target sources are obtained using the VO services to increase the number of data points in the SEDs. After obtaining extinction corrected observed SED, VOSA computes the synthetic photometry by using the filter transmission curves for a selected theoretical spectral model. The next task VOSA performs is comparing the synthetic photometry obtained from model SEDs to the observed data using a χ^2 minimization test to estimate the

[‡]http://svo2.cab.inta-csic.es/theory/fps/

best fit stellar parameters. The reduced χ^2_{red} is calculated through the following expression:

$$\chi^2_{red} = \frac{1}{N - N_f} \sum_{i=1}^{N} \frac{(F_{o,i} - M_d F_{m,i})^2}{\sigma^2_{o,i}} \tag{2.1}$$

The number of photometric data points is represented by N, while the number of adjustable parameters in the model is represented by N_f. The observed flux is symbolized as $F_{o,i}$, and the flux of the star predicted by the model is represented as $M_d F_{m,i}$. The scaling factor for the star, which is determined by the ratio of the star's radius to its distance, is represented as $M_d = \left(\frac{R}{D}\right)^2$, and the uncertainty in the observed flux is represented as $\sigma_{o,i}$. Figure 2.9 illustrates the single SED fit of a star with solar metallicity and T_{eff} of 8,750 K. The solid line displayed with black colour represents the Kurucz model spectrum, and square symbols with red colour depict the model fluxes in each of the bandpasses used to generate the synthetic SED. In our study of four clusters, the number of photometric data points (N) for target stars varies from 9 to 20 depending upon their observations available in different filters. The scaling factor is used to calculate the radii of stars through the following expression:

$$R_* = \sqrt{M_d} \times D \tag{2.2}$$

The luminosity of a star can be measured by using the estimated values of effective temperature and radius in the following formula:

$$L_* = 4\pi R_*^2 \sigma_{SB} T_{eff}^4 \tag{2.3}$$

VOSA estimates the error in T_{eff} to be approximately half of the grid step size in the vicinity of the optimal fitting value. In order to get realistic errors in all estimated parameters, VOSA uses a statistical approach, i.e., the Markov Chain Monte Carlo (MCMC) technique using 100 best-fit SED iterations. If the error

estimated using the MCMC method exceeds half the grid spacing for a particular parameter, then that will be flagged as an error; otherwise, it will give half the grid step as uncertainty. To estimate the extinction in different bandpasses used to create SED, VOSA uses Fitzpatrick reddening law (Fitzpatrick 1999; Indebetouw *et al.* 2005).

2.5.1 Binary SED fitting

In some of the stars in our study, we could not fit their observed SEDs with a single model as they show significant UV excess. In general, UV excess can be attributed to chromospheric activity, the presence of a hot companion, or lower metallicity. SEDs can also be used to disentangle both components of a binary star, provided they have different T_{eff}. In the case of stars showing UV excess, we fitted the observed SED with two spectral SED models depending on the nature of the hot companion. We used the VOSA binary fit feature to fit the two-component SEDs. It will fit both components of the observed SED simultaneously by using the linear combination of two spectral models. A two-component SED fit of a binary star that was constructed and fitted using the VOSA binary function is shown in Figure 2.8. Apart from VOSA, we also have utilised a python script[§] to fit the double component SEDs. The details of how the script fits the double component SED and estimate their parameters are given in (Jadhav *et al.* 2021). In the latest version of this code, bootstrapping method is used to estimate uncertainties in all parameters.

[§]https://github.com/jikrant3/Binary_SED_Fitting

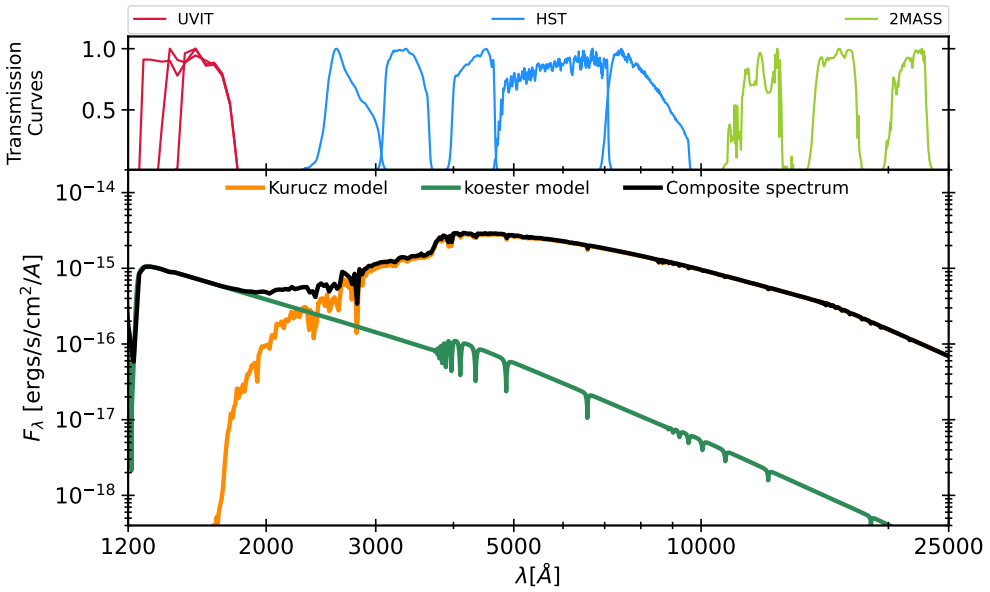

FIGURE 2.8: Example of the composite SED fit (Black spectrum) of the binary star consisting of an RHB (cool component) and sdB (hot component) star with T_{eff} of 5,750 K and 17,000 K, respectively. The Kurucz and Koester model spectra are displayed with orange and sea-green solid lines, respectively. The upper panel displays the scaled transmission curves of the passbands utilised to create the SED.

2.6 Theoretical Models

In this section, I will describe different stellar models employed to compare the distribution of stellar populations in observed CMDs with expected ones. It will also include a brief description of spectral models used to characterise hot stars identified in the analysed clusters.

2.6.1 Isochrones and Evolutionary Tracks

An isochrone defines the locus of a population of stars assumed to form at the same time with the same metallicity and different initial masses in the H-R diagram/CMD. As star clusters are home to stars with different masses lying in different evolutionary phases, their observed distribution in CMDs can be best

illustrated with theoretical isochrones. Isochrones are used to compute the basic parameters of star clusters, such as age, reddening/extinction, and metallicity, by comparing their location with the observed CMDs.

In our study, we have employed two types of theoretical isochrone models, namely, updated BaSTI Stellar Evolution Models and Isochrones (BaSTI-IAC) (Hidalgo *et al.* 2018; Pietrinferni *et al.* 2021), and MESA Isochrones and Stellar Tracks (MIST)[¶] (Choi *et al.* 2016). We obtained BaSTI-IAC isochrones for cluster metallicity and age with and without α enhancement from the updated BaSTI database[‖] for the UVIT, *HST*, and *Gaia* filters used in the analysis. The BaSTI-IAC models without α enrichment span a mass range from 0.1−15 $M_{\odot}$, metallicity ($\left[\mathrm{Fe/H}\right]$) from −3.20 to +0.45 dex, and age range from 20 Myr to 14.5 Gyr. Besides, these models also incorporate the effect of diffusion, overshooting, and mass loss efficiency parameter $\eta = 0.3$.

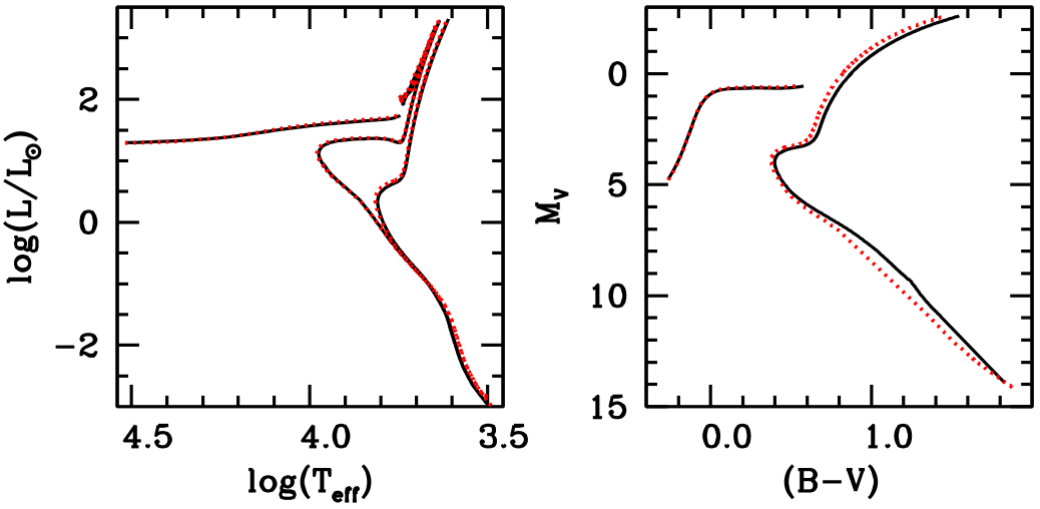

FIGURE 2.9: (Left panel) BaSTI-IAC isochrones with solar-scaled (solid lines) and α-enhanced (dotted lines) abundances of metallicity, $\left[\mathrm{M/H}\right] = -1.4$ dex, Y = 0.2478, with two distinct ages 2 and 12 Gyr, respectively. ZAHB track corresponds to the 12 Gyr isochrone. (Right panel) Optical CMD showing the 12 Gyr solar-scaled (solid lines) and α-enhanced (dotted lines) isochrones and ZAHBs with a metallicity of $\left[\mathrm{M/H}\right] = -1.4$ dex (Pietrinferni *et al.* 2021).

[¶] https://waps.cfa.harvard.edu/MIST/interp_isos.html
[‖] http://basti-iac.oa-abruzzo.inaf.it/

The modified version of BaSTI-IAC models computed for an α-enhanced heavy element distribution includes all improvements and updates in their previous models, have a mass range between 0.1 and 15 $M_{\odot}$, 18 metallicities between $\left[\mathrm{Fe/H}\right] = -3.20$ and $+0.06$ dex with $\left[\alpha/\mathrm{Fe}\right] = +0.4$ dex (Pietrinferni *et al.* 2021). In addition, they also have provided the helium-enhanced models for each metallicity for enhanced α abundances. The BaSTI-IAC model also offers the HB model, which consists of zero age HB (ZAHB), post-ZAHB tracks, and terminal age HB (TAHB) referring to the end of the core-helium-burning phase, with or without diffusion for a specific mass range. The updated BaSTI-IAC isochrones with solar-scaled and α enhanced abundances are illustrated in HRD and CMD in Figure 2.9. We created the ZAHB and TAHB tracks for a metallicity of $\left[\mathrm{Fe/H}\right] = 0, -1.3, -1.92$ dex corresponding to clusters NGC 188, NGC 1261, and NGC 2298, respectively, considering diffusion that occurs in these stars' sub-atmospheric regions. In the case of NGC 2298, we also have utilised α as well as helium-enhanced HB models to compare them with the observed distribution of HB stars in FUV CMDs. The hot flasher models, including early hot-flasher (EHF) and late hot-flasher (LHF), explaining the late evolutionary stages of low-mass stars (EHB and BHk) in GCs, are provided by Santi Cassisi (private comm.). We used these models, generated for UVIT and *Gaia* EDR3 filters, in NGC 2298 to probe the nature of hot HB populations.

MIST models provide isochrones and evolutionary tracks spanning a wide range in metallicities ($-4 \leq \left[Fe/H\right] \leq +0.5$), masses ($0.1\ M_{\odot} \leq M \leq 300 M_{\odot}$), ages ($5 \leq log\, t \leq 10.3$) and evolutionary stages. Depending on the initial stellar mass and metallicity, these models take into account the evolution starting from the pre-main sequence (PMS) phase to the end of hydrogen burning, the WD cooling sequence, or the end of carbon burning. These models also provide the isochrones incorporating the effect of rotation on different phases. Figure 2.10 shows the overplotted BaSTI-IAC and MIST isochrones in the optical CMDs of GCs NGC 6397 and Ruprecht 106, respectively.

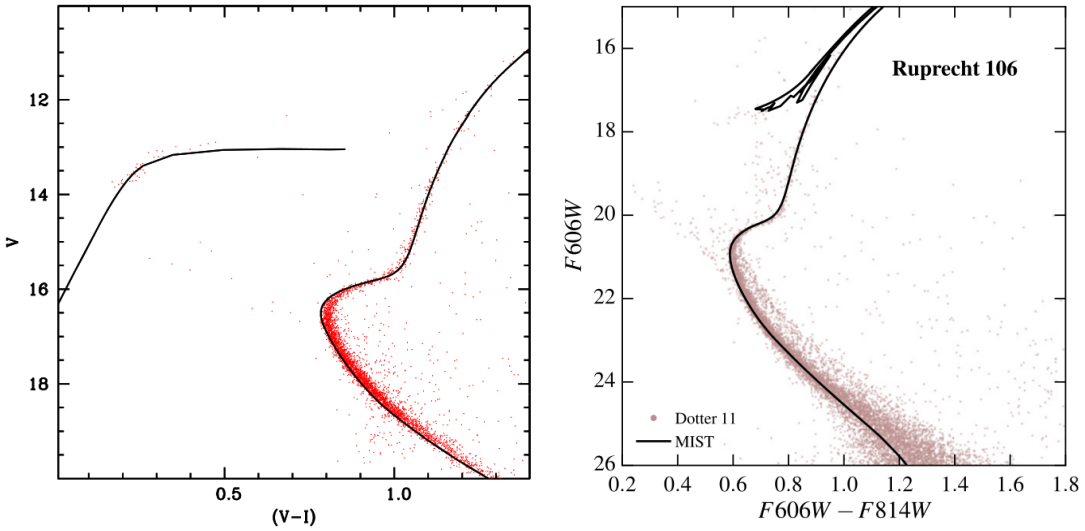

FIGURE 2.10: Left panel: Optical CMD of GC NGC 6397 (Stetson *et al.* 2019) overlaid with BaSTI-IAC isochrone of a metallicity −1.9 dex, age 13.5 Gyr and ZAHB with Y = 0.248 (Pietrinferni *et al.* 2021). Right panel: *HST* optical CMD of GC Ruprecht 106 (Dotter *et al.* 2011) overploted with a MIST isochrone of metallicity −1.50, age 12.0 Gyr (Choi *et al.* 2016).

In order to probe the state of central stars of planetary nebulae (CSPNe), pAGB stars in clusters, we have used the pAGB evolutionary tracks computed by Miller Bertolami (2016) for initial mass range 0.8-4 $M_{\odot}$, and a wide range of metallicities (Z = 0.02, 0.01, 0.001, 0.0001). All previous evolutionary stages, from the ZAMS through the WD phase, are incorporated into these pAGB models. Moehler *et al.* (2019) have calculated the theoretical evolutionary tracks for pHB stars by extending the pAGB models presented by Miller Bertolami (2016). These models include theoretical evolutionary tracks corresponding to different masses, beginning from the ZAHB and continuing through late pHB evolution or a point on the pAGB cooling track. We have used these pHB tracks obtained for metallicity close to the cluster metallicity in the study of HB and pHB populations in two GCs and one OC.

Apart from the above isochrones and evolutionary tracks, we made use of WD cooling models (Tremblay *et al.* 2011) with hydrogen-rich surfaces with a mass range of 0.2 − 1.3 $M_{\odot}$ provided by P. Bergeron (Private Comm.). The synthetic

UVIT magnitudes for these WD models were obtained by convolving them with all UVIT filters and then overplotted in the observed CMD to identify the location of WDs.

2.6.2 Spectral Models

The theoretical stellar model atmospheres are convolved with the given filter transmission curves to get the synthetic fluxes and construct the synthetic SED to derive the physical parameters of stars depending on their nature and stage of evolution. Below, I will briefly discuss the family of stellar model atmospheres used in this thesis.

textbfKurucz Models:

The Kurucz models are stellar atmospheric models used to predict the flux distribution of stars, which take into account various factors such as convection, rotation, and opacities in the atmosphere of the star (Castelli *et al.* 1997; Castelli and Kurucz 2003). These models are based on local thermodynamic equilibrium (LTE) and hydrostatic equilibrium and are computed using the ATLAS9 model atmospheres (Kurucz 1993). The models are arranged in a grid that have a wide range of parameters, including [Fe/H] values ranging from -2.5 to 0.5 dex, effective temperatures from 3,500 to 50,000 K and log g from 0 to 5 dex. Recently, new Kurucz models are computed for an extended metallicity range ($-4 \leq \left[Fe/H\right] \leq 0.5$) with enhanced α elements abundances (+0.4 dex) irrespective of any change in any other parameter range. These models cover a wide range of wavelengths, from UV to IR. We used both old and new Kurucz models in our analysis of MS, BS, and HB stars.

Koester WD Models:

(Koester 2010) computed models for DA-type WDs that have atmospheres rich in hydrogen. These models were computed by assuming that the layers of the WDs are homogeneous, arranged in a plane-parallel configuration, and have LTE. The

models also assume that the WDs are in hydrostatic, radiative, and convective equilibrium. The T_{eff} and surface gravity ($\log g$) of the WDs are the free parameters used in the model. The range of effective temperatures covered by Koester's models is 5,000-80,000 K, with step sizes that vary based on the value of T_{eff}: 250 K for T_{eff} values from 5,000 to 20,000 K, 1,000 K for T_{eff} values from 20,000 to 30,000 K, 2,000 K for T_{eff} values from 30,000 to 40,000 K, and 5,000 K for T_{eff} values from 40,000 to 80,000 K. The range of surface gravities covered by the models is 6.5 to 9.5, with a step size of 0.25.

Husfeld Models:

In the case of helium-enhanced hot HB and pHB stars, we utilised non-LTE helium-rich Husfeld models (Husfeld *et al.* 1989). These model atmospheres are calculated considering the basic assumptions that include plane-parallel geometry, non-LTE, hydrostatic equilibrium, radiative equilibrium and chemical composition of hydrogen and helium. The model grid spans the range of stellar parameters typical of extremely helium-rich O-type subdwarf (sdO) stars: 35,000 K $\leq T_{eff} \leq 80,000$ K, $4.0 \leq logg \leq 7.0$, and $0.01 \leq Y_{He} \leq 0.7$.

Tübingen NLTE Model Atmosphere Package (TMAP) Models:

For hot stars present in the pAGB and AGB-manqué stage of their evolution, we made use of available Tübingen NLTE Model Atmosphere Package (TMAP) Models depending on the available parameter space (Rauch and Deetjen 2003; Werner *et al.* 2003). The free parameters in this model are T_{eff}, $\log g$, and hydrogen mass fraction, X_H. The TMAP model grid consists of two sets of parameters: Grid3 and Grid4. The range of parameters covered by the Grid3 model includes T_{eff} from 50,000 K to 190,000 K, $\log g$ from 5.0 to 9.0, and X_H from 0 to 1, whereas Grid4 model covers a range of atmospheric parameters including $20,000K \leq T_{eff} \leq 150,000K$, $4.0 \leq logg \leq 9.0$, and $0 \leq X_H \leq 1$.

2.7 Summary

A summary of the data, observations, and methods used in this study is provided below:

- We described the specific details of various ground and space-based telescopes employed to study four clusters: NGC 1261, NGC 2298, NGC 188, and NGC 2818.
- We provide an overview and details of the UV observations of four programme clusters obtained from the UVIT telescope.
- We describe the methods of PSF and aperture photometry, including the utilisation of the IRAF/DAOPHOT package for its implementation.
- We discuss the brief details of the stellar models utilised to generate the theoretical isochrones used to analyse the observed CMDs of the programme clusters.
- We discuss the details of generating SEDs and fitting them with theoretical SED models using the χ^2 minimization test. We also provide brief information about the several spectral models used in our SED analysis of hot stellar populations.

Chapter 3

UVIT view of NGC 1261: HB morphology †

3.1 Introduction

In this chapter, we analyse the southern galactic GC NGC 1261 located in the constellation Horologium at a distance of 17.2 kpc (Arellano Ferro *et al.* 2019) and metallicity [Fe/H] = -1.27 dex (Carretta *et al.* 2009). Since this cluster is away from the Galactic disc (b = $-52^{\circ}.13$), it experiences almost negligible or no reddening. The age of this cluster is estimated to be 10.75 ± 0.25 Gyr (VandenBerg *et al.* 2013), 11.5 ± 0.5 Gyr (Dotter *et al.* 2010) and 12.6 ± 1 Gyr (Kharchenko *et al.* 2013). In this study, the adopted age of this cluster is 12.6 Gyr to generate the isochrones. Brown *et al.* (2016a) characterised HB features in 53 GCs, including NGC 1261. They created colour-colour plots for all selected clusters. They found less than four HB stars blue-ward of the G-jump in NGC 1261 (see Figure 5 in

†Results of this work are published in Rani *et al.* (2020, 2021b).

Brown *et al.* 2016a). Schiavon *et al.* (2012) constructed UV CMDs (FUV−NUV vs FUV) for 44 GGCs using *GALEX* data. They observed that the HB stars follow a diagonal sequence, unlike the horizontal distribution in optical, and its slope mainly depends on the bolometric correction effects.

The chapter presents the results of imaging analysis of NGC 1261 carried out with UVIT, using six filters, including two in FUV and four in NUV. In this chapter, we aim to focus on the following aspects of the cluster: a) identify and classify UV bright stars in comparison with theoretical isochrones in the optical and UV-optical CMDs, b) explore the HB morphology of the cluster in UV, c) determine the properties of hot HB stars to gain insights into their formation and evolution. This objective is accomplished by combining UVIT data with data obtained from the *HST* (Nardiello *et al.* 2018) and ground-based observations (Kravtsov *et al.* 2010). The cluster members detected by UVIT in both the inner and outer regions of the cluster were selected using PMs estimated from *HST* and *Gaia* DR2 data.

3.2 Data and Analysis

Observations of the cluster were obtained using UVIT's two FUV and four NUV filters. The science-ready images of the cluster were generated using CCDLAB in all filters. PSF photometry was performed on all images to determine the magnitudes of detected sources. The details of observations of NGC 1261 UVIT images are presented in Table 2.1 in Chapter 2. The UVIT image created using one NUV N279N, and one FUV F172M filter is depicted in Figure 3.1. In this figure, yellow and blue colours represent UVIT NUV and FUV detections, respectively. The FUV images show resolved stars in the cluster's centre, but the central regions of NUV images are affected by crowding. The FWHM of isolated sources in the

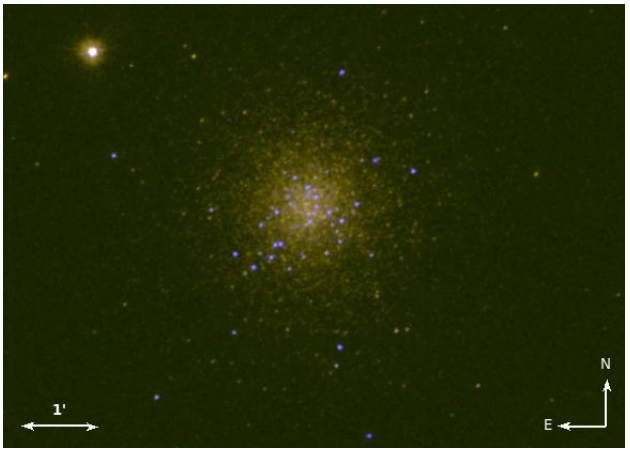

FIGURE 3.1: An image of NGC 1261 created from UVIT data by combining the FUV (F172M) and NUV (N279N) channel images.

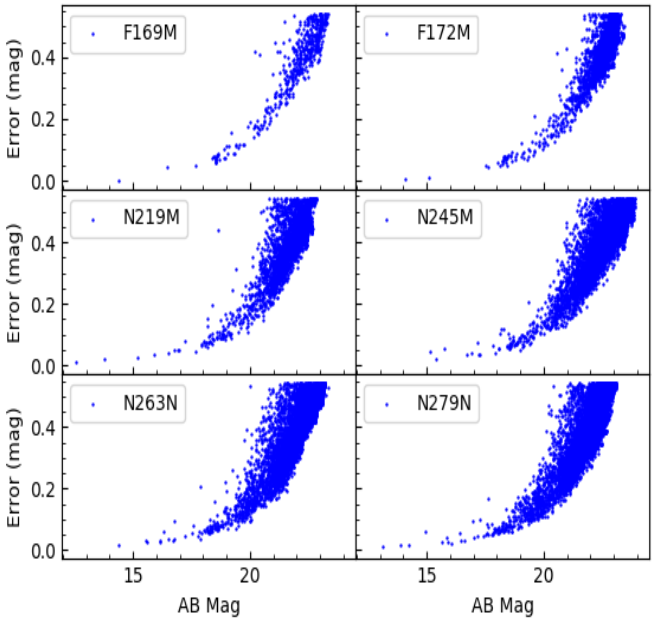

FIGURE 3.2: PSF fit errors as a function of magnitude for the UVIT observations of NGC 1261. The top two panels show the plot for two FUV filters, whereas the bottom 4 panels show for the NUV filters.

UVIT images is $\sim 1\farcs2$ in NUV and $\sim 1\farcs5$ in FUV. The PSF fit error plots, shown in Figure 3.2, are plotted against the magnitude for each filter. UVIT is able to detect stars down to 21 mag in NUV and 22 mag in FUV with typical errors of 0.2 mag and 0.3 mag, respectively.

3.3 Optical and UV-optical colour-magnitude diagrams

CMDs are a very important tool for identifying different evolutionary sequences in star clusters. As we have observed this cluster in 4 NUV and 2 FUV filters of UVIT, a large number of CMDs using various filter combinations are possible. To identify stars within a $\sim$ 3′.4 diameter in the inner region, we have used the HUGS catalogue (Nardiello *et al.* 2018) to cross-match with UVIT detected sources. Most likely, members of this cluster in the inner region have a proper motion probability of more than 90% as mentioned by Nardiello *et al.* (2018). In order to cross-match UVIT-detected sources with *HST* data, first, we selected stars with a proper motion membership probability of more than 90%. In *HST*, the filters F606W and F814W are proxy to the V and I bands. To cross-match HB stars and BSSs, we have used specific colour, and magnitude ranges in the optical *HST* CMD. In the F606W−F814W vs F814W *HST* CMD, we have used $-0.1<$F606W−F814W<0.7 and $15<$F814W<20.5 range for HB stars and $0<$F606W−F814W<0.4 and $17.3<$F814W<19.5 range for BSSs. In the optical CMD displayed in Figure 3.3, two stars appear near the faint end of the blue tail of the HB. These same stars are also present in the colour-colour plot of this cluster created by Brown *et al.* (2016a) (see their Figure 5). The Vega magnitude system used in *HST* is converted into the AB magnitude system in order to adopt the same magnitude system The magnitude system used to create optical CMDs in the inner and outer regions is the Vega magnitude system, but both photometric systems are different. Clement *et al.* (2001), Salinas *et al.* (2016) and Arellano Ferro *et al.* (2019) have studied the variability of stars in this cluster. To identify the variable stars such as RR Lyrae and Sx Phe, we have cross-matched UVIT data with variable star catalogue from Arellano Ferro *et al.* (2019). In NUV bands, our sample of HB stars is incomplete within the inner region as we are unable to resolve stars in the inner 1′ diameter region due to crowding, whereas, outside this region,

we detect about 90% stars in comparison to the *HST*. The number of BS, HB, and variable stars detected in each UVIT filter is tabulated in Table 3.1. Figures 3.4 and 3.3 present the UV-optical and optical CMDs, respectively. The photometric error bars shown in Figures 3.4 and 3.6 are the median of the photometric errors of stars at selected magnitude ranges. The HB stars in the UV-optical CMDs deviate from the horizontal distribution observed in the optical CMDs; instead, they follow a diagonal sequence with less spread (Busso *et al.* 2007; Dalessandro *et al.* 2008, 2011; Dieball *et al.* 2009, 2010; Sahu *et al.* 2019; Subramaniam *et al.* 2017; Raso *et al.* 2017). Nonetheless, note that the BSSs sequence, if diagonal, remains unaltered in both optical and UV-optical CMDs.

The optical and UV-optical CMDs are overlaid with updated BaSTI-IAC* isochrones (Hidalgo *et al.* 2018) obtained for an age 12.6 Gyr (Kharchenko *et al.* 2013), a distance modulus, $(\text{m-M})_V = 16.21$ mag (Arellano Ferro *et al.* 2019) and $\left[\text{Fe/H}\right] = -1.27$ dex (Carretta *et al.* 2009). These models are generated with normal helium abundance Y = 0.247 as expected for GCs, $\left[\alpha/\text{H}\right] = 0$, including diffusion, overshooting, and mass loss efficiency parameter $\eta = 0.3$. The BaSTI-IAC model also provides an HB model that encompasses ZAHB, post-ZAHB, and TAHB tracks with or without diffusion for a particular mass range. The ZAHB and TAHB tracks are obtained for a metallicity of $\left[\text{Fe/H}\right] = -1.27$ dex, including diffusion. The BaSTI-IAC model does not provide the BSS model line. In order to define the location of BSSs in CMDs, BaSTI isochrones (Pietrinferni *et al.* 2004) generated through the FSPS code by Conroy *et al.* (2009), Conroy and Gunn (2010) were utilised. We applied the reddening and extinction correction to the observed UVIT stellar magnitudes. For the Milky Way, we have adopted a reddening value of E(B−V) = 0.01 mag as reported in Kharchenko *et al.* (2013) and the total-to-selective extinction ratio of $R_v = 3.1$ from Whitford (1958). This resulted in an extinction coefficient in visible light of $A_V = 0.031$ mag. The A_V is utilised

*http://basti-iac.oa-abruzzo.inaf.it/

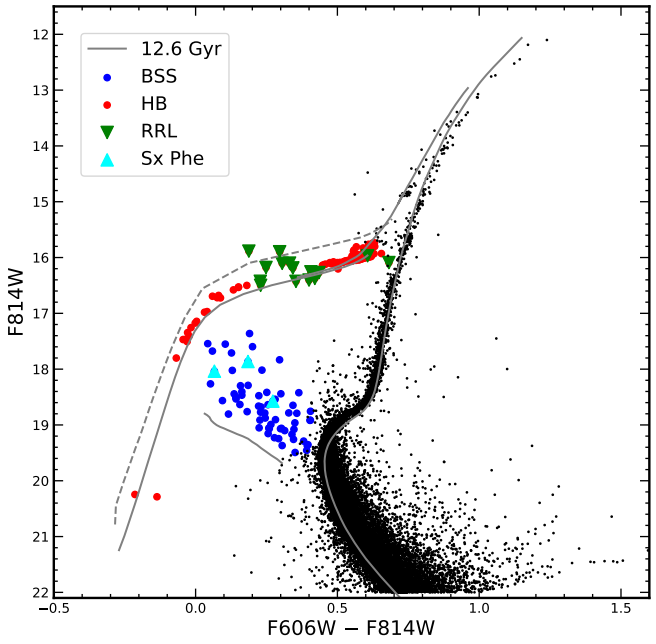

FIGURE 3.3: Optical CMD of NGC 1261 for the region covered by the *HST*. Black dots represent the *HST*-detected stars with a proper motion membership probability of more than 90%. only HB and BSS stars detected in the NUV N279N filter and cross-matched with the *HST* catalogue are shown in different colours, which are explained in the figure. The variable stars, such as RR Lyrae and SX Phe, are also marked in the plot. The solid grey line denotes the updated BaSTI-IAC model isochrone for an age of 12.6 Gyr and metallicity of $[Fe/H]$ = -1.27 dex. The solid grey line shown over the HB is the ZAHB, and the dotted one represents the TAHB. We also show the BSS model line, which is an extension of the ZAMS.

to calculate the extinction coefficients, A_λ, for each passband using the Cardelli *et al.* (1989) reddening relation. The BS sequence shown in optical as well as in UV CMDs is the extension of the zero-age MS (ZAMS). If BSSs are formed by the merging of two MS stars, their distribution should roughly follow the ZAMS until roughly twice the turn-off mass. The MSTO mass in NGC 1261 is estimated to be $\sim$0.8 $M_\odot$. The brightest and faintest part of the BS sequence shown in all CMDs corresponds to 1.6$M_\odot$ and 1.1$M_\odot$, respectively.

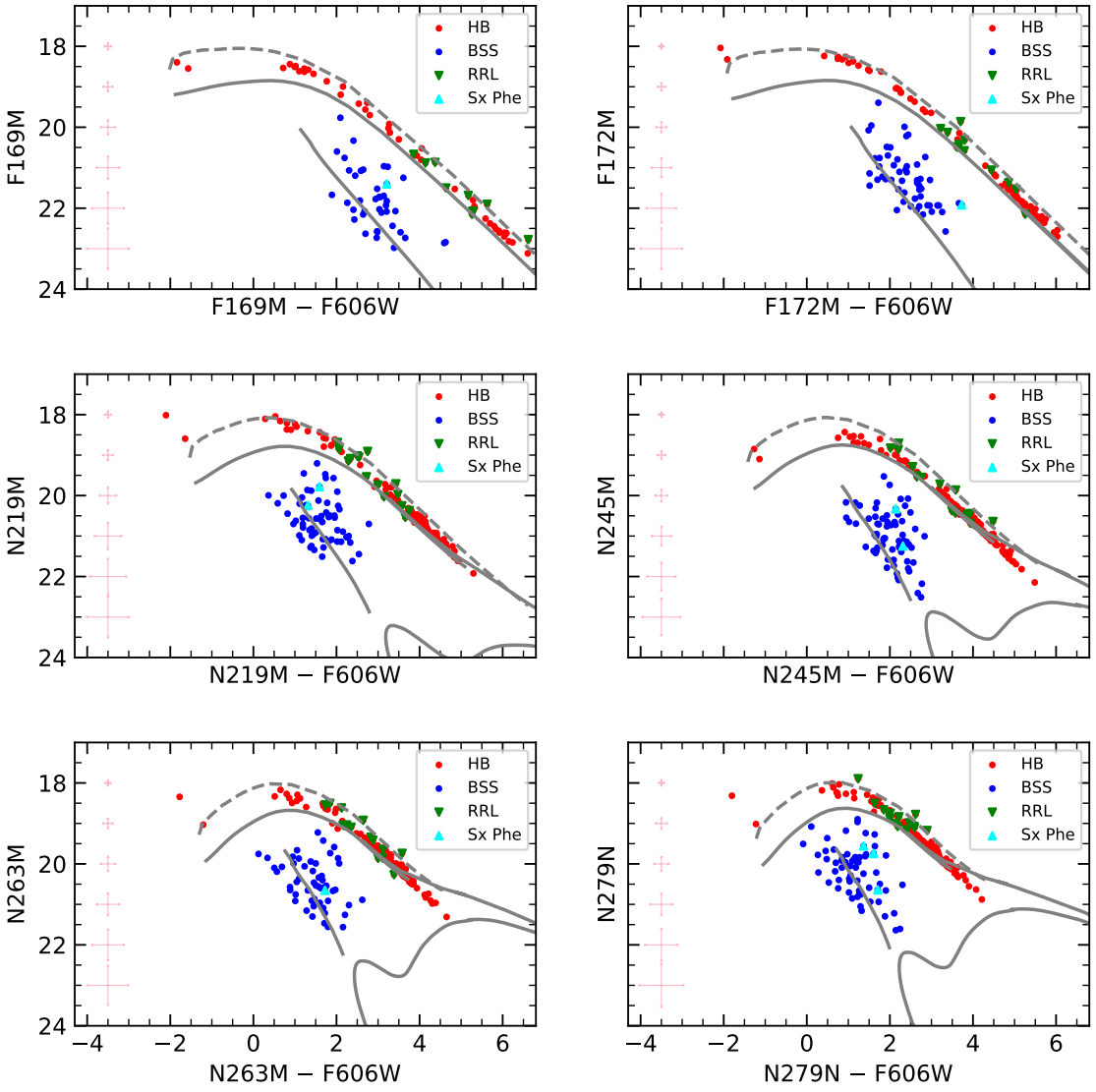

FIGURE 3.4: UV-optical CMDs of NGC 1261 members detected in the central region common with *HST* in 4 NUV and 2 FUV filters. The meaning of different colours and symbols is shown in the panels. The PSF-fit errors are also displayed in each panel. Grey lines denote the updated BaSTI-IAC model isochrone for generated for cluster parameters, i.e., the metallicity of $[\mathrm{Fe/H}] = -1.27$ dex, and age of 12.6 Gyr. Solid and dotted grey lines correspond to ZAHB and TAHB, respectively.

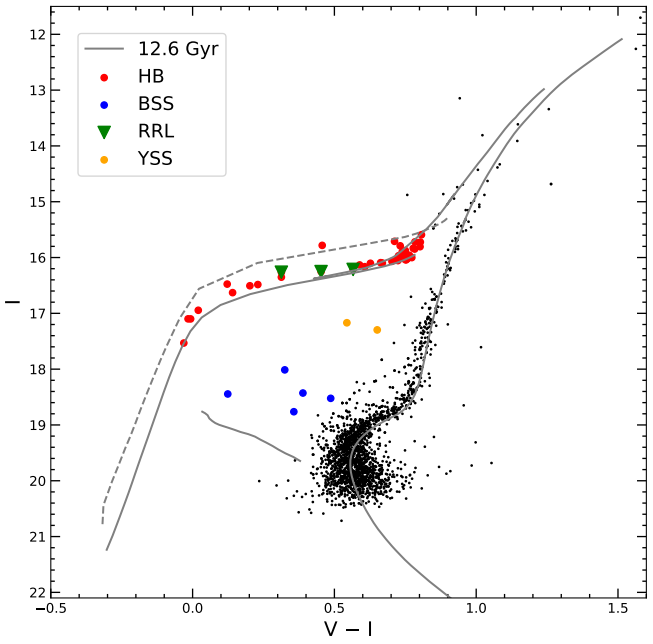

FIGURE 3.5: Optical CMD of NGC 1261 for the region outside the *HST* field. HB and BSS stars that are detected in the NUV N279M UVIT filter and cross-matched with ground-based photometric data (Kravtsov *et al.* 2010) and *Gaia* data are marked with different colours. The rest of the stars shown with black dots are cross-matched ground-based data with *Gaia* data. Other details are the same as in Figure 3.3.

In Figure 3.4, the top two panels display the FUV-optical CMDs, generated using the F169M and F172M filters. The overlaid isochrone helps in defining the location of HB stars and BSSs, which exhibit a large range in colour and magnitude in contrast to optical CMDs, suggesting FUV-optical CMDs have better resolution in colour at a given magnitude. The HB stars, redder and bluer than the RR Lyrae stars, are detected in the FUV, suggesting that both RHB and BHB stars are detected. The sequence of HB stars is well aligned with the isochrone suggesting that the predicted and observed FUV magnitudes match well. The BSSs in the FUV exhibit a wide range of magnitude for a given colour and vice versa. In NUV-optical CMDs, displayed in the rest of the four panels in Figure 3.4, we find that the BSSs are as hot as BHB stars covering a large range in colour and magnitude We have detected a full HB population in all NUV-optical CMDs. The HB

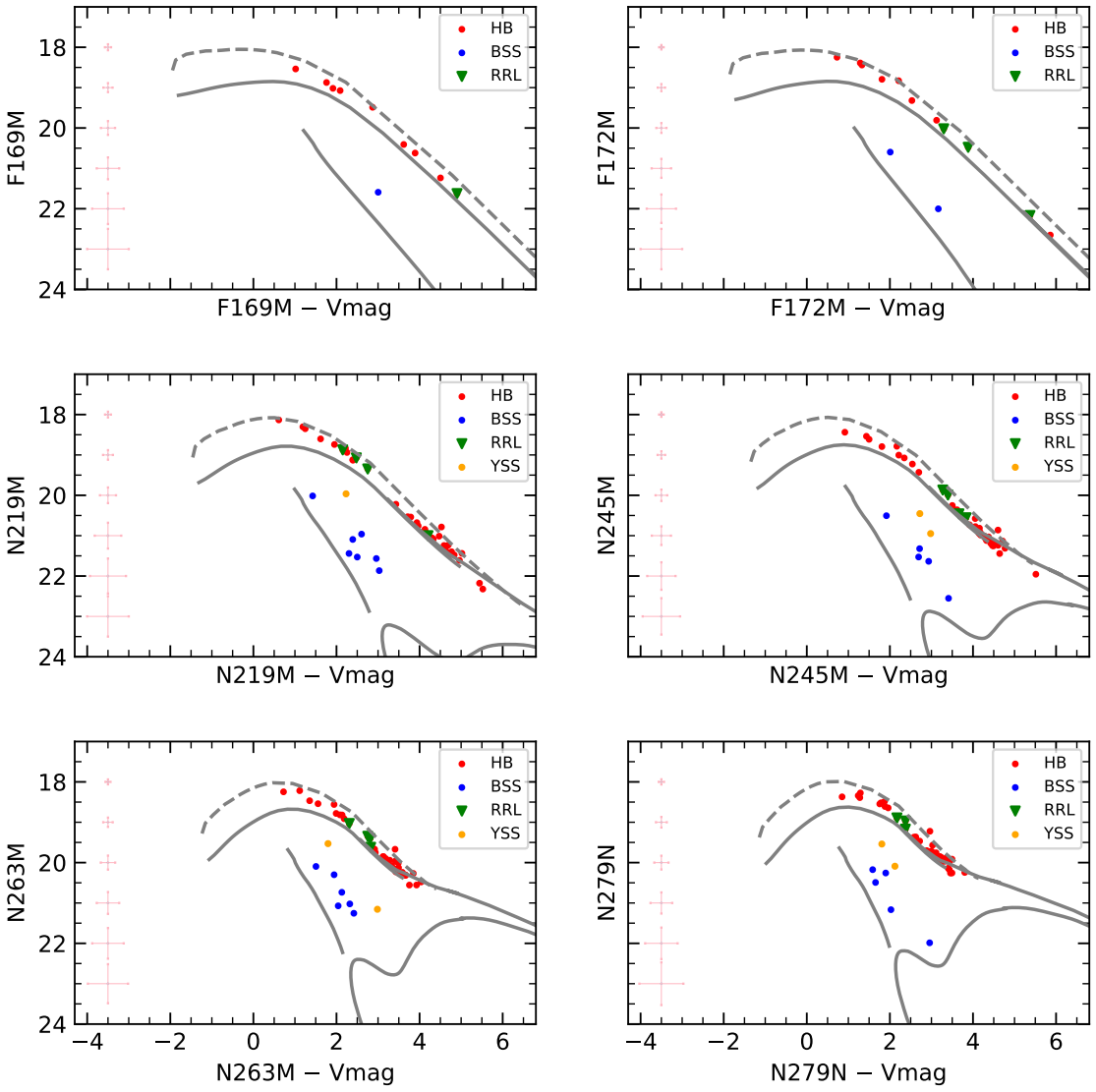

FIGURE 3.6: UV-optical CMDs of NGC 1261 after cross-matching ground-based photometric (Kravtsov *et al.* 2010) and *Gaia* data with UVIT data in 4 NUV and 2 FUV filters. The rest of the details are the same as in figure 3.4.

population appears as a tight sequence more-or-less aligned with the isochrone. In the case of CMDs created using N245M, N263M, and N279N filters, the redder part of the HB is fainter compared to the isochrone. As the photometric errors are also large at this limiting magnitude, our data is only suggestive. We also note that the same stars are fainter than the isochrone in both CMDs, where N263M and N279N magnitudes are shown. In all the CMDs, we have detected two stars located close to the blue extreme end of the HB. These stars are quite separated

TABLE 3.1: Number of detected HB stars and BSSs in different UVIT filters. Here N_{HB}, N_{BSS}, N_{RRL} and N_{SxPhe} represent the number of detected HB, BSS, RRL and Sx Phe stars, respectively. The number of stars detected in the outer region ($> 3'.4$ diameter) are shown in parentheses.

Filter	N_{HB}	N_{BSS}	N_{RRL}	N_{SxPhe}
F169M	59(9)	41(1)	10(1)	1
F172M	97(11)	55(2)	15(3)	1
N219M	196(40)	71(8)	19(4)	2
N245M	216(46)	75(7)	19(4)	2
N263M	222(47)	62(8)	19(4)	1
N279N	221(46)	70(7)	18(3)	3

from the observed HB sequence and are likely to be very hot HB stars, as suggested by their UV-optical colour.

To identify stars in a given cluster's outer region, UVIT-detected stars were first cross-matched with *Gaia* proper motion membership data provided by Bustos Fierro and Calderón (2019), followed by cross-match with the ground-based photometric data (Kravtsov *et al.* 2010). Here, the photometric system adopted to create optical CMD is the standard Johnson-Cousin photometric system. To generate UV-optical CMDs, we transformed the Vega magnitude system into the AB magnitude system using photometric calibration mentioned in Blanton and Roweis 2007. Our sample of UVIT-detected HB and BS stars is 90% complete in the outer region when compared to the number of stars detected with *Gaia*. The 10% of the stars, which are not detected, are fainter than the detection limit of the UVIT. Figures 3.5 and 3.6 present the optical and UV-optical CMDs, respectively. It can be clearly noticed that less number of HB and BS stars are detected in the cluster's outer region (outside $3'.4$ diameter) in contrast to the inner region. More stars are detected in the NUV images than in the FUV. Only BHB stars are detected in FUV passbands, and both BHB and RHB stars in all the NUV pass bands. We

have also detected YSSs, identified based on their location in the optical CMD (figure 3.5). The cluster's outer region has fewer BSSs than the inner region. It can be noticed that the detected BSSs are all redder than the predicted BSS line, though this could be an artefact due to the less number of their detections. The comparison of the HB and BS stars detected in the central and outer parts of the cluster suggests that they may be segregated towards the centre of the cluster.

3.4 SED analysis of the bright HB stars

The Kurucz stellar atmospheric models (Castelli *et al.* 1997; Castelli and Kurucz 2003) are utilised to generate SEDs for the bright HBs, which cover a wavelength range from UV to IR. We set the value of metallicity, $\left[\mathrm{Fe/H}\right] = -1.5$ dex, close to the cluster metallicity and had given the range of effective temperature from 5,000-50,000 K and corresponding log g from 3-5 dex for the adopted Kurucz models to fit the SED of HBs (see Figure 19 in Pandey *et al.* 2001). We have combined 6 UVIT photometric data points with 5 *HST* photometric data points from Nardiello *et al.* (2018) to generate SED for UV bright HB stars detected in the cluster's central region. For those detected in the outer region, the photometric data points of UVIT (6 passbands) were combined with *Gaia* (3 passbands) (Gaia Collaboration *et al.* 2018) and ground photometry (4 passbands) (Kravtsov *et al.* 2010). As errors in the *HST* measured flux are small, which blows up the χ^2 value for the *HST* data points, we assumed no error, which does not impact the fit parameters. In case there are photometric data points with a zero observational error, VOSA assumes the biggest relative error present in the SED. VOSA makes use of Fitzpatrick reddening relation (Fitzpatrick 1999; Indebetouw *et al.* 2005) to correct for extinction in observed data points. The extinction-corrected VOSA magnitudes match well with those described in Section 5.3.

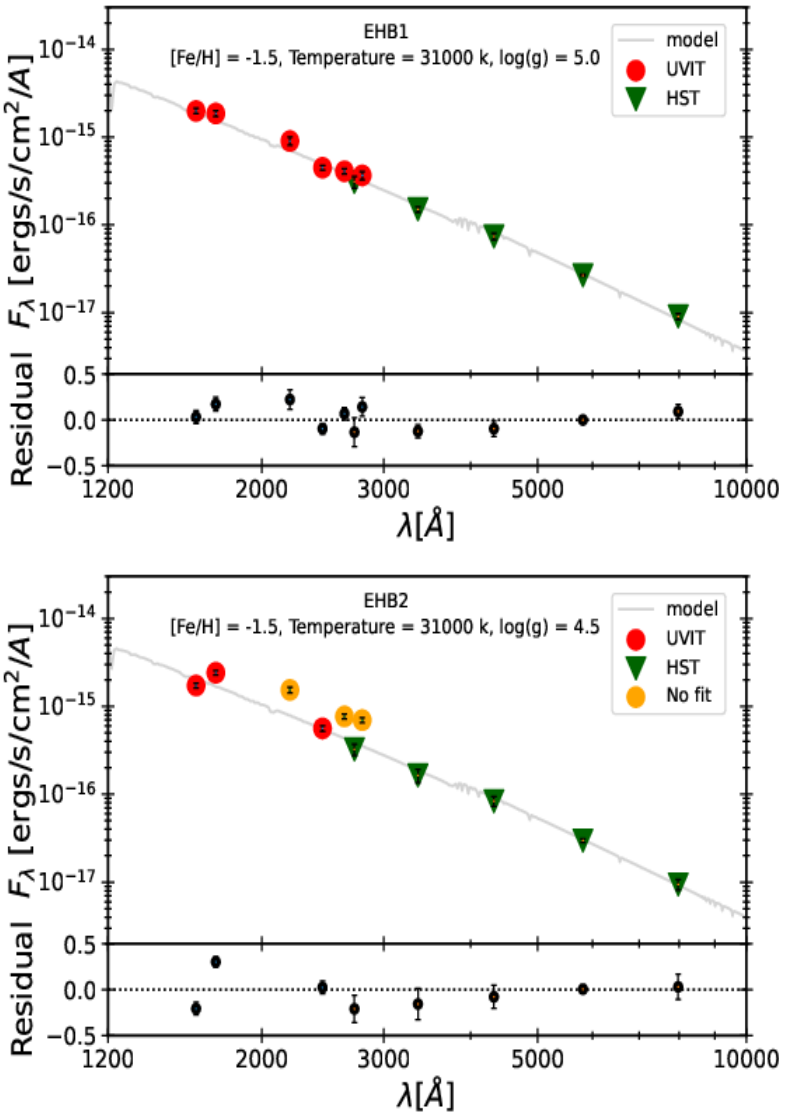

FIGURE 3.7: SEDs of EHB1 and EHB2 stars after applying the extinction correction. The fixed and estimated parameters are shown in the plots.

Best SED fits were obtained for 26 HB stars, out of which 2 are EHB stars and 24 are BHB stars. The SEDs of 2 EHB stars are shown in Figure 5. The estimated values of parameters T_{eff}, $\frac{R}{R_\odot}$ and $\frac{L}{L_\odot}$ corresponding to the best-fit Kurucz model along with the errors for 26 HB stars are listed in Table 3.2. In Figure 5 (left panel), note that the Kurucz model spectrum fits well to the observed data points, but in the case of the EHB2 star, three UVIT data points are not fitted with the model spectrum. There seems to be some amount of excess flux in these UVIT filters, as also reflected in figure 3.4. We excluded these three data points to

make a good fit of the observed data points to the Kurucz model spectrum. The high temperatures of EHB1 (31,000 K) and EHB2 (31,000 K) indicate that they belong to the category of EHB stars (Heber 1986). BHB stars have a range of temperature 8,000−12,750 K, with one star at 12,750 K. The SEDs of these stars are presented in Appendix-A.

We also note from Table 3.2 that the luminosity, $\frac{L}{L_\odot}$, is more or less constant for the HB stars (except for a few cases), whereas the T_{eff} is found to increase with a corresponding decrease in radius. We estimate this relation assuming a constant luminosity as we have a good number of BHB stars. Figure 3.8 depicts the variation of the T_{eff} of all bright HB stars with their corresponding radius. The best-fit relation to the observed points plotted in Figure 3.8 is :

$$T_{eff} = 0.5\sqrt{\frac{R}{R_\odot}} + 0.002$$

This relation corresponds to the well-known Stefan-Boltzmann law. Since the intrinsic luminosity of the BHB and EHB stars is not very different, so they should satisfy a quite similar T_{eff}-R relation. We, therefore, extended the plot to higher T_{eff} and included the EHB stars. This relation is found to fit the EHB stars quite well, as shown with a black line in Figure 3.8. The goodness of fit parameter value for this curve fit is determined to be 0.99, which is close to 1, indicating a very good fit. This fit validates the precision of the parameters obtained from the SED fit.

3.5 Evolutionary Status

To check the evolutionary stage of EHB stars identified with UVIT, we have plotted the theoretical evolutionary tracks using the models presented by Moehler *et al.* (2019). The models used in their paper were computed by the extension of the pAGB evolutionary models published by Miller Bertolami (2016). We have selected a model with metallicity close to the cluster metallicity. The theoretical evolutionary tracks corresponding to different masses starting from ZAHB through to a point late in pHB evolution or a point on the pAGB cooling track are shown in Figure 7. The TAHB is shown with a dash-dotted line in Figure 7. We can see in Figure 7 that all BHB stars are lying along the BHB tracks. Figure 7 also shows that two EHB stars are indeed found along EHB tracks lying below the TAHB. So, these two stars do not belong to any of the evolved class of stars, which lie on the hot pAGB cooling sequence. This suggests that the two EHB stars share the properties of the BHB stars and, therefore, can be considered as the extreme extension of the HB. They are, therefore, still in the HB evolutionary phase. From the model, the masses of these two stars turn out to be approximately $0.5 M_{\odot}$, which corresponds to the star's core mass on the HB.

3.6 Discussion

In this study, we used data from UVIT onboard the *AstroSat* satellite to create NUV and FUV CMDs and to investigate the morphology of HB stars. UVIT is not able to detect stars in the MS, RGB and SGB evolutionary phases since these stars are fainter than 22 mag in UV. To generate UV CMDs, UVIT-detected stars were cross-matched with *HST* catalogue for the inner region corresponding to $\sim 3'.4$ diameter and with ground-based data along with *Gaia* for the outer region as UVIT observes almost the entire cluster region. The UV and optical CMDs are

TABLE 3.2: Bright HB star's parameters derived using SED fitting method.

Star ID	RA (deg)	DEC (deg)	T_{eff} (K)	$\frac{L}{L_\odot}$	$\frac{R}{R_\odot}$	χ^2_{red}
EHB1	48.04181	-55.20597	31000 ± 500	38.92 ± 1.09	0.21 ± 0.01	2.7
EHB2	48.07732	-55.22445	31000 ± 500	41.28 ± 0.9	0.22 ± 0.01	8.6
BHB1	48.07928	-55.22457	12750 ± 125	44.26 ± 1.64	1.36 ± 0.03	4.6
BHB2	48.09452	-55.2267	11000 ± 125	43.46 ± 1.96	1.79 ± 0.04	6.9
BHB3	48.08742	-55.22956	11750 ± 125	48.75 ± 2.58	1.69 ± 0.04	2.9
BHB4	48.06405	-55.21413	11250 ± 125	42.77 ± 1.87	1.71 ± 0.04	3.6
BHB5	48.07904	-55.21753	11250 ± 125	45.97 ± 2.25	1.79 ± 0.04	4.3
BHB6	48.05424	-55.21919	11000 ± 125	46.91 ± 1.87	1.89 ± 0.04	4.5
BHB7	48.05896	-55.21738	10500 ± 125	49.12 ± 2.51	2.11 ± 0.05	7.3
BHB8	48.08082	-55.22729	10000 ± 125	46.70 ± 2.09	2.23 ± 0.05	6.3
BHB9	48.06626	-55.21944	9500 ± 125	47.28 ± 2.06	2.52 ± 0.06	6.8
BHB10	48.06391	-55.21627	9250 ± 125	44.54 ± 1.59	2.59 ± 0.06	5.9
BHB11	48.04864	-55.21555	9250 ± 125	56.64 ± 1.89	2.94 ± 0.07	4.2
BHB12	48.05479	-55.22369	8750 ± 125	48.88 ± 1.41	3.05 ± 0.07	3.6
BHB13	48.10376	-55.21723	8500 ± 125	49.55 ± 1.57	3.23 ± 0.08	5.0
BHB14	48.08487	-55.22036	8750 ± 125	49.63 ± 1.83	3.08 ± 0.07	2.1
BHB15	48.06478	-55.21766	8750 ± 125	49.42 ± 1.64	3.04 ± 0.07	5.5
BHB16	48.07389	-55.22981	8250 ± 125	49.79 ± 1.69	3.47 ± 0.08	4.1
BHB17	48.04274	-55.22656	8000 ± 125	51.07 ± 1.85	3.73 ± 0.09	3.4
BHB18	48.06466	-55.21258	8000 ± 125	50.06 ± 1.55	3.69 ± 0.09	5.0
BHB19	48.05484	-55.18698	11500 ± 125	46.69 ± 3.98	1.69 ± 0.04	5.7
BHB20	48.14102	-55.20569	10000 ± 125	47.64 ± 4.98	2.28 ± 0.05	4.6
BHB21	48.01035	-55.31072	9750 ± 125	47.85 ± 5.55	2.42 ± 0.06	3.9
BHB22	48.12378	-55.25798	9500 ± 125	48.24 ± 7.88	2.54 ± 0.06	1.8
BHB23	47.90097	-55.23117	8750 ± 125	59.04 ± 10.44	3.32 ± 0.07	1.5
BHB24	48.14307	-55.27254	8250 ± 125	51.27 ± 13.41	3.54 ± 0.08	1.8

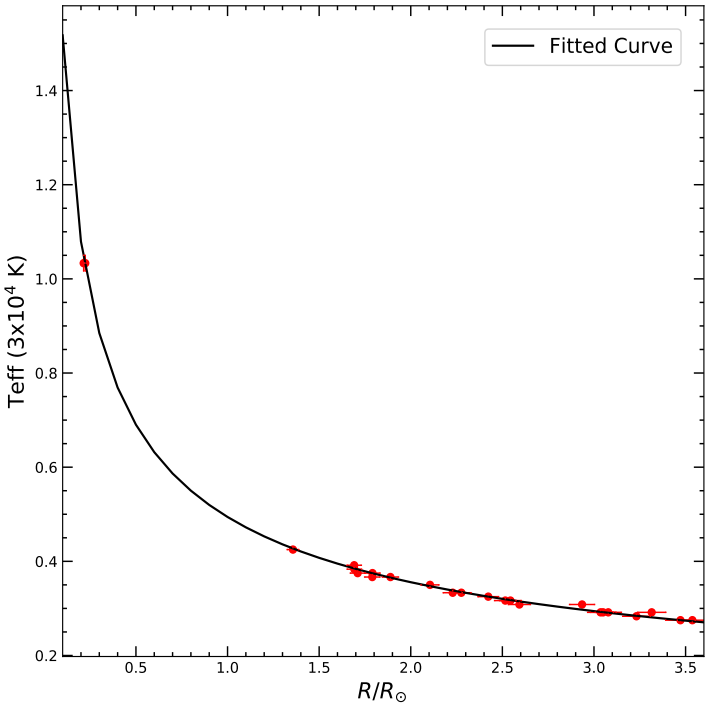

FIGURE 3.8: Variation of the radius of all bright HB stars with their effective temperatures, determined from SEDs. Red-filled circles represent bright HB stars, and the black curve representing the function $T_{eff} = \frac{0.5}{\sqrt{R}} + 0.002$ is the fitted curve to the observed distribution.

created for cluster PM members. In all UV-optical CMDs, we find that the HB stars do not show the horizontal distribution, as found in the optical CMDs. This is due to the fact that the HB stars have a range in temperature, and the flux in UV pass bands is more sensitive to temperature than in optical. The HB feature is therefore found to be slanting and is similar to that found in the *GALEX* UV CMDs obtained by Schiavon *et al.* (2012). They suggest that the slope of HB is mainly a result of bolometric correction effects. Dalessandro *et al.* 2013 investigated the HB morphology of three GCs, namely, M3, M13 and M79, using *HST* data in optical and UV bandpasses, and they also found a similar HB distribution in Far-UV CMDs (see their Fig. 2). The UV magnitude distribution of HB stars aligns well with the isochrones in all UV-optical CMDs, taking into account measurement errors. As we detect the entire stretch of the HB (RHB, RRL and BHB), we find a good match for the UV magnitudes between the observation and the updated BaSTI-IAC models.

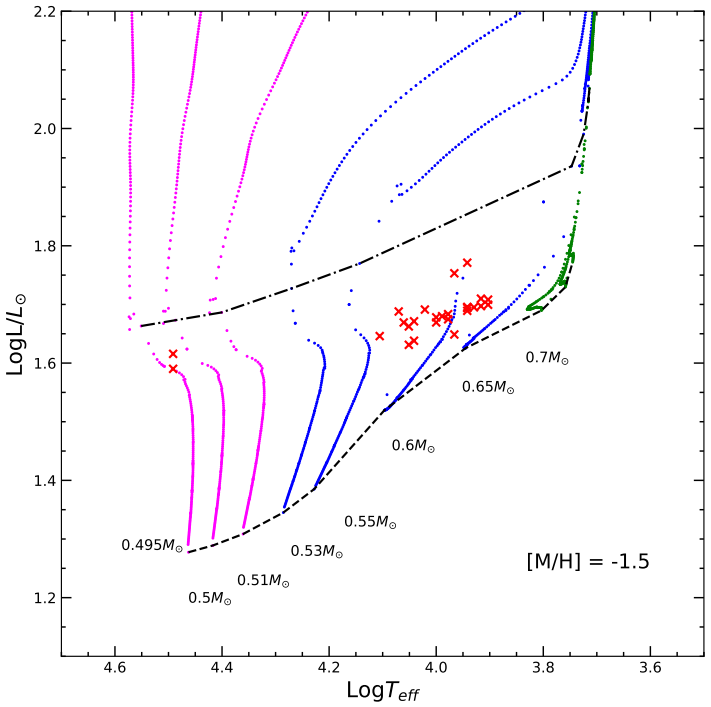

FIGURE 3.9: Evolutionary tracks corresponding to different masses with metallicity close to cluster metallicity. Evolution starting from the HB phase to the moment when the star has entered the pHB phase (Moehler *et al.* 2019) are shown. In the plot, magenta, blue and green colours represent the sequences populating the extreme, blue and red parts of the HB. The dashed and dash-dotted lines indicate the ZAHB and TAHB, respectively. Bright HB stars identified with UVIT are shown with red cross symbols.

A large gap is observed between EHBs and BHBs, and that needs to be explored. However, massive and dense GCs like NGC 6752, NGC 2808, and ω cen exhibit a substantial population of EHB stars that form a distinguishable sequence in their optical CMDs. Conversely, in less massive clusters, these stars are fewer in number and can be difficult to detect in optical CMDs at the faint end of the HB. In such cases, UV CMDs play an important role since EHB stars are bright in UV CMDs and also follow a separate sequence. The clusters with less number of stars hotter than the M-jump are NGC 2298, NGC 3201, NGC 5466, NGC 6981, etc. (see Figure 5 in Brown *et al.* 2016a). We have detected full HB in NUV and only hot HB stars in FUV. Two EHB stars are also identified in all UV-optical CMDs, which have bluer colours as compared to other hot HB stars. Vanderbeke *et al.* (2015) studied 48 galactic GCs to explore the radial distribution of multiple stellar

populations known to exist in clusters. They identified 6 EHB stars in NGC 1261, which may or may not be the members of the cluster. They also used different selection criteria to select different HB sub-populations. The HB stars identified by UVIT are PM members of the cluster, including the two EHB stars.
The bright HB stars span a T_{eff} range from 8,000 K to 12,750 K, with the hot end very close to G-jump (T_{eff} = 11,500 K) in the HB distribution. One star is found to have 12,750 K, along with the two hotter stars. The HB distribution's hot end, therefore, coincides with the G-jump in this cluster. There is only one star slightly hotter, and there is no further extension of the HB to the EHB beyond the G-jump. Therefore, we do not detect M-jump (Momany *et al.* 2002, 2004), expected at ∼23,000 K. Instead, we detect two stars with T_{eff} = 31,000 K, coinciding with the T_{eff} expected for the gap between EHB and the BHk stars. The cluster NGC 1261, therefore, has an HB distribution truncating at the G-jump at the hot end, including two EHB stars.

With the estimation of the surface parameters of the BHB stars, we are able to derive a relation between the temperature and radius, as the bolometric luminosity is found to be almost the same for these stars. We find that T_{eff} and radii of the two hot HB stars agree with the relation derived above, suggesting that they can be considered as part of the EHB population. Thus, the EHB stars in this cluster are still burning helium in their core, like other HB stars and are not in any different evolutionary phase. This is supported by their position in the HR diagram overlaid with isochrones. It must be noted that these two EHB stars may be starting to evolve off from the HB.

EHB stars, as described by Heber (1986), are a type of star that burns helium in their core and have a mass near 0.47 $M_{\odot}$. These stars are characterised by their thin hydrogen envelope, which makes up no more than 1% of their total mass.

Our estimation of mass for the detected EHB stars matches well with this definition. Although the EHB star's evolution after the exhaustion of Helium in the core is better comprehended, the formation pathways that lead to the EHB are much less understood. Many have explored the binary nature of EHB stars, and a wide variety of companions are found as the binary occurrence among EHB stars is observed to be remarkably higher than that of typical stars. The way in which the envelope is lost is mostly attributed to binary interactions, which are affected by the mass ratio of the binary system. According to Lei *et al.* (2015), the tidal enhancement of the stellar wind in binary evolution leads to increased mass loss during the RGB stage, which is necessary to explain the formation of BHk stars through the LHF mechanism. They have adopted different initial orbital periods for binaries to explore the formation of both canonical HB and BHk stars. As suggested by the SEDs, the EHB stars found in this cluster are most probably single stars. The SEDs are well-fitted by a single spectrum with minimum residual across the wavelength. It is proposed by Castellani and Castellani (1993) that the delayed helium flash (HEF) is a promising scenario to explain the existence of EHB stars. High mass loss during the RGB phase results in a significant reduction of the star's envelope mass, preventing it from igniting helium at the tip of the RGB. As a result, the star starts to evolve into a WD with an electron degenerate core. The location of the delayed helium flash, either at the bright end of the WD cooling sequence (EHF) or along the WD cooling sequence (LHF), depends on the residual envelope mass. These stars settle on a blue hook at the hot end of the HB, where they are much hotter than their counterparts on the canonical ZAHB due to their greatly reduced envelope mass. D'Cruz *et al.* (1996) also suggested a hot He-flash scenario to explain the origin of EHB stars in GCs. Cassisi *et al.* (2003) computed the models of low-mass Population II stars during the helium flash mixing (HEFM) phase, suggesting that the HEFM scenario may provide a viable explanation for the presence of BHk stars.

Here we summarise the possible scenarios accounting for the origin of single EHB populations. Webbink (1984) and Saio and Jeffery (2000) suggested the merger of two He-core WDs as a possible mechanism. Another scenario involves the ejection of a common envelope caused by a giant planet, which then evaporates (Soker 1998). The fraction of close binaries among the EHB stars in GCs is found to be very small (Moni Bidin *et al.* 2006, 2009, 2011). It is possible that in old systems like the GCs, the WD-WD merger may likely result in the formation of single EHB stars. If these two stars are the product of the merger of two He-core WDs, then they can be helium-rich, which will lead to higher T_{eff} compared to estimated using Kurucz stellar atmospheric models (Schonberner and Drilling 1984). Another model suggested for the EHB star formation is primordial enrichment in helium (D'Antona *et al.* 2002). EHB stars, in this scenario, are formed through the normal evolution of helium-rich sub-populations in GCs. These sub-populations might have formed out of the matter contaminated by the expelled material of massive AGB stars. Given a specific age and metallicity, He-enhanced stars have lower masses compared to He-normal stars, leading to a bluer HB morphology. A super-solar surface He abundance causes a huge mass loss on the RGB phase by increasing the RGB tip luminosity, but the phenomena responsible for a huge He enhancement invoke non-canonical mixing during the RGB stage and dredge-up induced by H-shell instabilities (Sweigart and Mengel 1979; von Rudloff *et al.* 1988; Sweigart 1997; Denissenkov and VandenBerg 2003). The finding of MSPs in GCs opened a new frontier, as one of the causes is the variation in Helium enrichment, with the blue HB stars produced by Helium rich stars (Bedin *et al.* 2004; Piotto *et al.* 2005, 2007, 2012, 2015). The models that consider populations with varying helium abundances have effectively reproduced both the MS splitting and the multi-modal HB observed in ω Cen (Lee *et al.* 2005) and NGC 2808 (D'Antona *et al.* 2005). As a result, helium enhancement presents itself as a promising and alternative explanation for the creation of EHB stars in GCs compared to the binary scenario. We find that both the EHB stars are single stars and estimate their masses to be 0.495 $M_{\odot}$, which is quite close to the theoretical estimate for

EHB stars. The possible formation mechanism for these stars is likely to be the enhanced mass loss during the RGB phase, caused by either rotation or increased helium content (primordial or mixing).

The comprehensive studies of EHB and BHk stars by Brown *et al.* (2001, 2010) suggest that these stars could be formed via delayed HEF after the RGB and are termed as early hot-flashers and late hot-flashers. In the case of an EHF scenario, helium ignition occurs while the star is evolving towards the WD cooling sequence. Flash mixing between the core and envelope is prevented by the high entropy barrier of a strong hydrogen-burning shell, leaving the envelope mass and composition unchanged. This results in a luminosity that is similar to that of canonical HB stars (See Figures 1 & 4 in Brown *et al.* 2010). In the case of an LHF, a helium flash occurs during the descent of the star along the WD cooling curve. This leads to mixing between the helium core and the hydrogen envelope, which in turn increases the helium and carbon content in the envelope. This mixing reduces the brightness of a star with respect to the canonical EHB star. The EHB stars of this cluster are not sub-luminous with respect to the BHB stars and hence are unlikely to be late hot-flashers. These stars, therefore, could be EHF objects which follow the properties of the normal HB stars. Follow-up spectroscopic observations are needed to probe their nature and confirm the formation scenarios described above. Since there is not enough mass for the hydrogen shell surrounding the core in EHB stars, these stars are likely to evolve directly to the white dwarf phase.

All the detected BSSs occupy a region parallel to HB sequence as well as span a wide range in both colour and magnitude in the UV-optical CMDs. In general, the temperature of BSSs ranges from 6,000-8,000K, but in this cluster, we notice that some of the BSSs have colours similar to the BHB stars, which in turn implies that BSSs may be as hot as the BHB stars. We detected a few BSSs in the cluster's

outer portion beyond the half-mass radius (r>r_h). These BSSs might be products of mass transfer in binaries, which dominate in a low-density environment. Mass-transfer models are required to confirm this. We also detect two YSSs in the outer part of the cluster. We plan to construct the SEDs of the BSSs as well as the YSSs to understand the properties of these stars.

3.7 Conclusions

In this chapter, we present the photometric results of NGC 1261 imaged using the UVIT on *AstroSat*. The advantage of using UVIT over *HST* is its large field of view covering the full cluster region, and over *GALEX* is its good spatial resolution and multiple filters. We have characterised the HB member stars for the first time in this cluster using UVIT, *HST*, ground-based and *Gaia* data. Below, we summarise the important findings of this study:

- We constructed UV-optical and optical CMDs of the cluster members and overlaid them with isochrones generated for respective filters. We detected only BHB and 2 EHB stars in the FUV CMDs, whereas the full HB is detected in NUV CMDs. We also detected BSSs which span a wide range in magnitude as well as in colour in NUV CMDs.

- The effective temperatures, luminosities and radii of 24 BHB and 2 EHB stars are estimated by generating SED using multi-wavelength data. The T_{eff} of BHB stars range from 8,000-12,750 K, whereas EHB stars have T_{eff} more than 30,000 K.

- Keeping the L constant, we fitted an R versus T_{eff} relation for the BHB stars, which is found to fit the EHB stars as well. Their location in the HR diagram overlaid with isochrones confirms that they are EHB stars with a mass of $\sim$0.5 $M_{\odot}$.

Based on findings from the UVIT study of this cluster, we conclude that:

- Most of the RHB stars are so faint that they can not be detected by UVIT in FUV filters. The stars of HB lie along a well-defined sequence in the UV-optical CMDs, largely fitted by the BaSTI-IAC isochrones.
- The EHB stars in this cluster are likely to be single stars. We suggest that single EHB stars are likely to have formed through intense mass loss during the RGB stage (either from rotation or helium enrichment) or through an early hot-flasher scenario.

3.8 Additional plots: SEDs of all BHB stars

The procedure of SED fitting for bright HB stars is presented in Section 3.4. The SED fits for 24 BHB stars are shown in Figure 12.

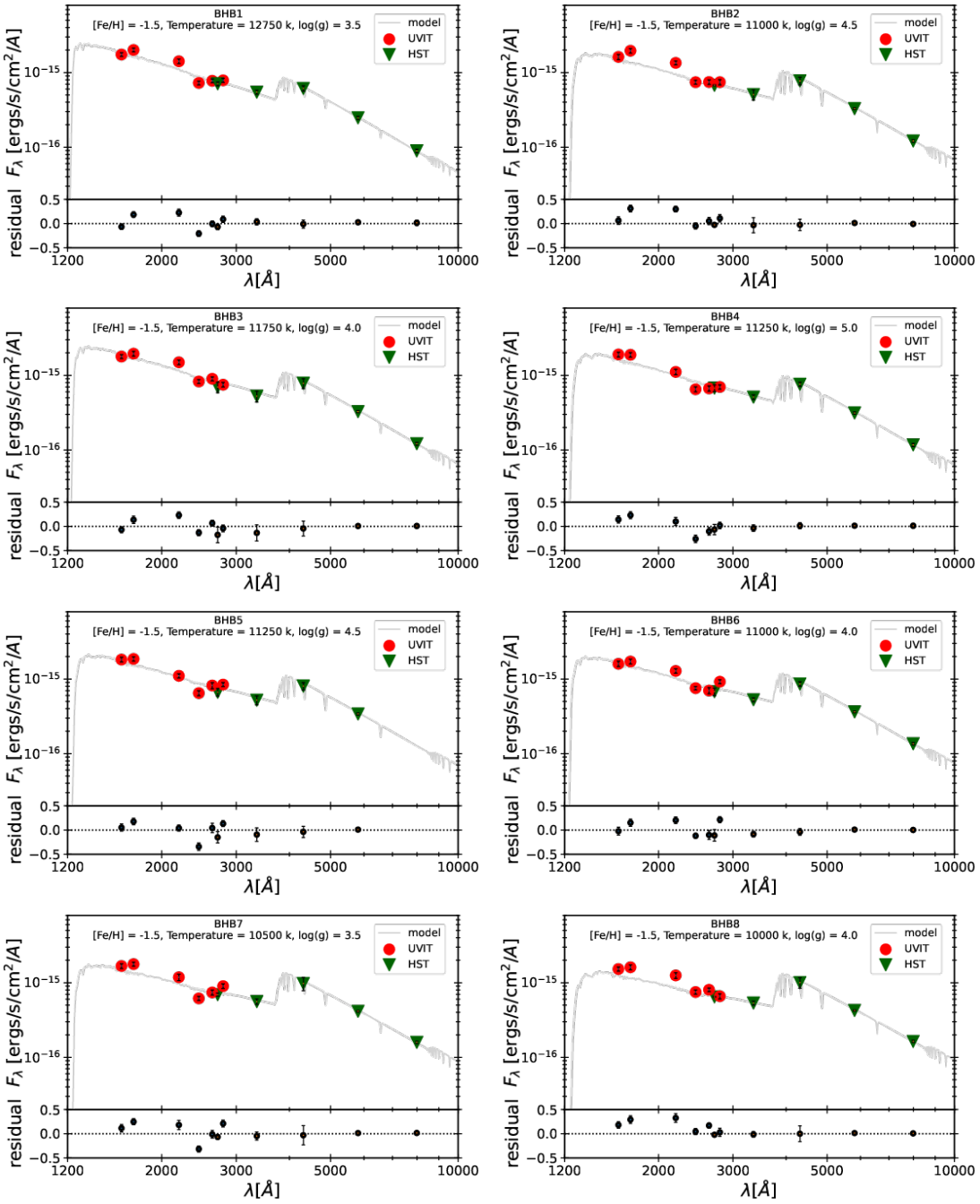

FIGURE 3.10: SEDs of all BHB stars after applying extinction correction. The optimal fit parameters are displayed within the plots. The UVIT and *HST* data points used to create SEDs for stars lying in the region covered with *HST* are represented with red circles and green triangles, respectively. For the stars lying in the outer region, UVIT, Ground-based photometric, and *Gaia* data points are shown with red circles, green triangles, and cyan squares, respectively.

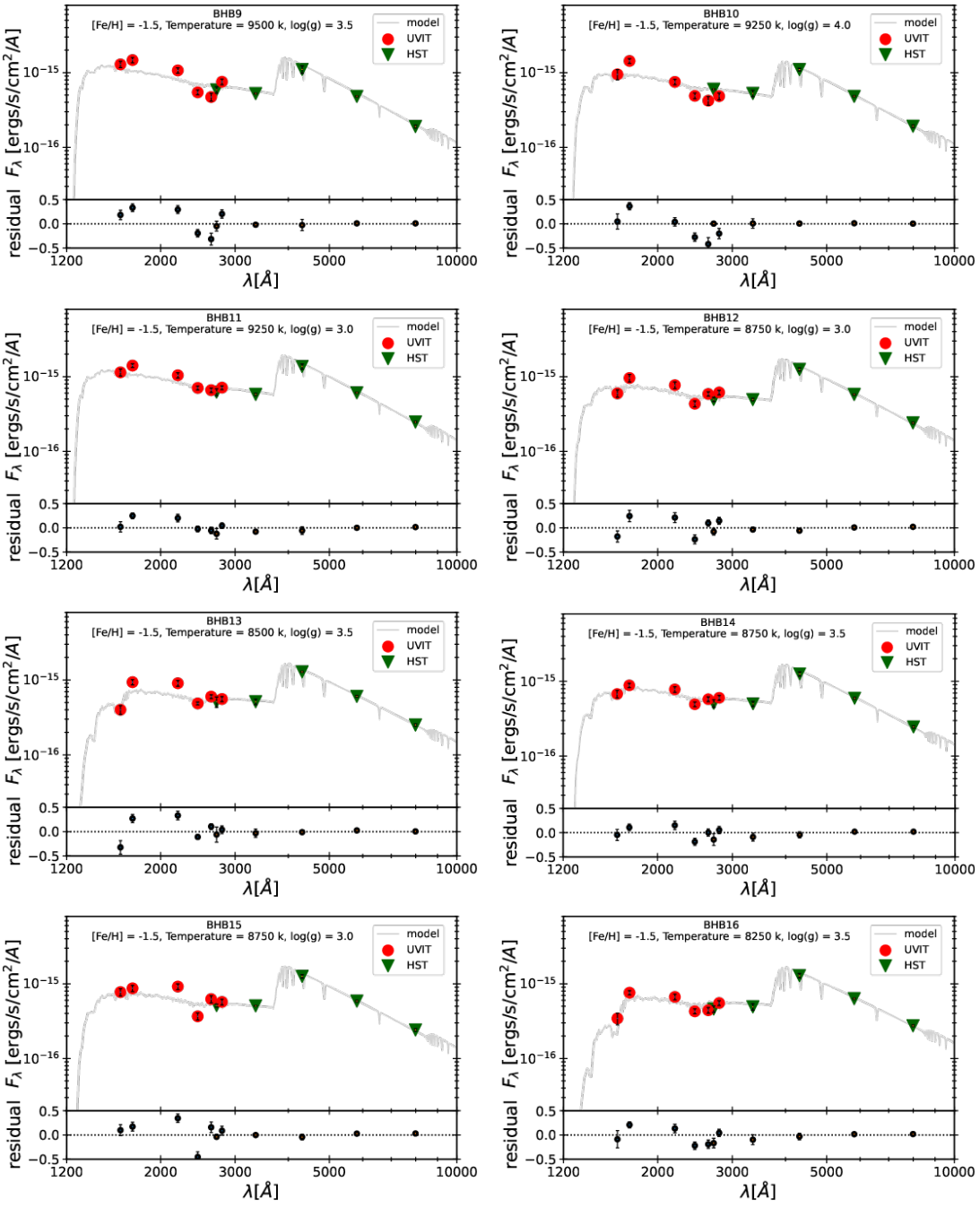

FIGURE A10: (Continued.)

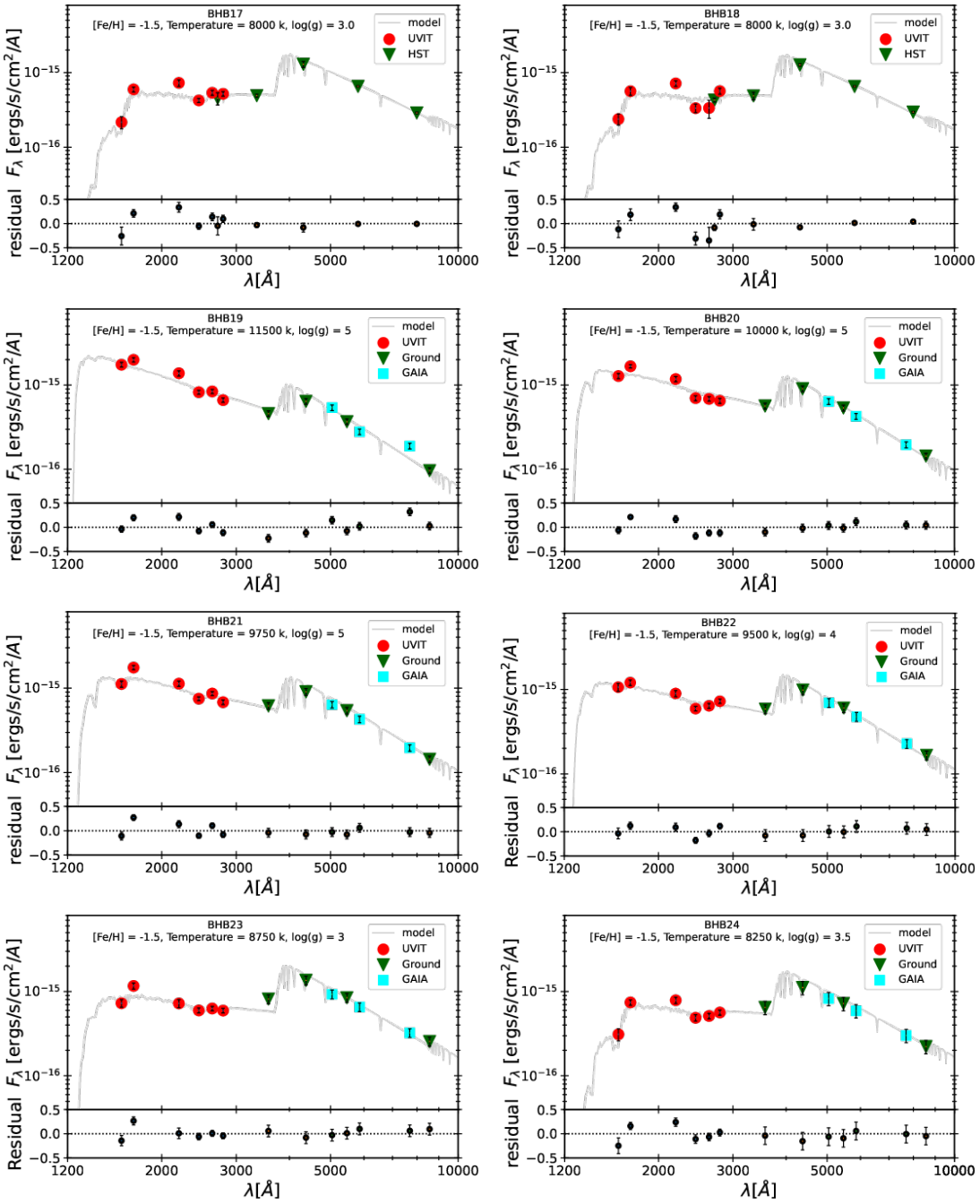

FIGURE A10: (Continued.)

Chapter 4

Hot HB stars in NGC 2298: Insights from UV observations[†]

4.1 Introduction

In this chapter, we study the southern GGC NGC 2298 located in the constellation Puppis at a distance of 10.6 kpc and has metallicity $\left[\mathrm{Fe/H}\right]$ = -1.92 dex (Carretta *et al.* 2009; Harris 2010; Monty *et al.* 2018). The adopted reddening value and age for the cluster in this work are (0.2 ± 0.01) mag and (13.2 ± 0.4) Gyr, respectively (Monty *et al.* 2018). NGC 2298 is also known for hosting MSPs along the MS and the RGB (Piotto *et al.* 2015; Milone *et al.* 2017). The helium difference between 1G and 2G stars along RGB sequence in GCs is determined by Milone *et al.* (2018), and it is found to be 0.011 in NGC 2298. This cluster is widely studied in optical, but the UV studies of this cluster are sparse.

As this cluster is metal-poor, its HB mainly comprises BHB and a few EHB stars

[†]Results of this work are published in Rani *et al.* (2021a).

and hence is ideal for studying the UV properties of the very hot HB population. In our quest to understand the formation and evolution of hot HB stars, here we present, for the first time, an FUV photometric study of hot HB stars in NGC 2298.

This chapter mainly aims to: a) examine the HB morphology, b) probe the helium abundance difference among the HB population in order to check the existence of MSPs, 3) characterise the hot HB stars to shed light on their properties and find their formation mechanisms in comparison with theory.

4.2 Data and Analysis

The cluster was observed with UVIT's three FUV filters, and images were generated using CCDLAB. Subsequently, PSF photometry was carried out on these finalized, science-ready images, determining the magnitudes of the stars identified by UVIT. A detailed log of UVIT observations of NGC 2298 is reported in Table 2.1 given in Chapter 2. The colour image of NGC 2298 in the F148W filter is shown in Figure 1. In this figure, the blue colour indicates UVIT FUV detections in the F148W filter. Crowding is not a problem here, as we can effectively resolve stars even in the central part of the cluster. We show our PSF-fit errors for all filters as a function of magnitude in figure 3. For further analysis, stars detected with UVIT are considered down to $\sim$22 mag in the FUV F148W filter and $\sim$ 21 mag in the F154W and F169M filters. This sets an upper limit of $\sim$0.3 mag on our photometric errors.

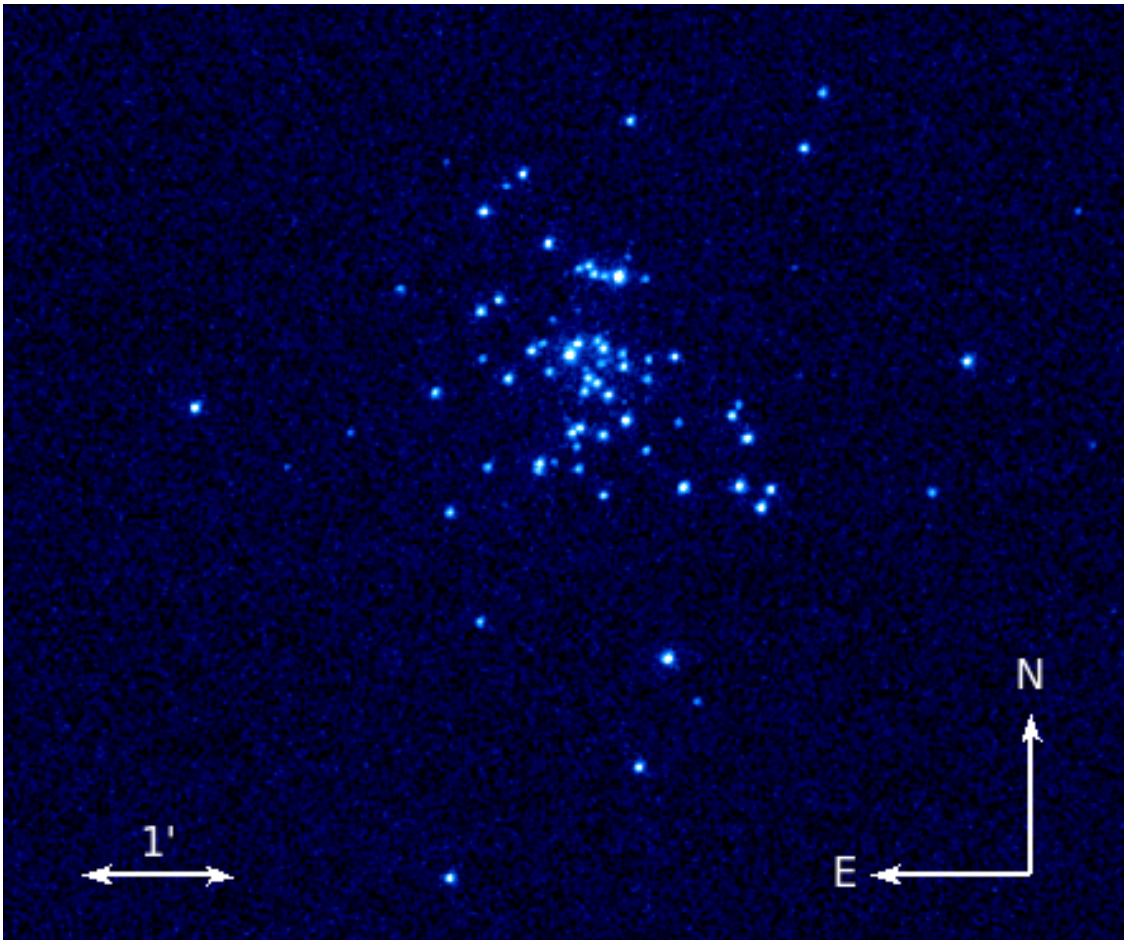

FIGURE 1: The colour image of NGC 2298 in UVIT FUV band F148W. The hot stellar populations displayed with blue colour are well resolved at the centre of the cluster.

4.3 Proper Motion Membership

To select the confirmed members of the cluster in the inner region covered by *HST*, we employed the membership probability (MP) information provided in the astro-photometric catalogue of Nardiello *et al.* (2018). To get the confirmed members of the cluster in its outer part, we have utilised *Gaia* EDR3 PM data released on December 3, 2020, (Gaia Collaboration *et al.* 2020). The *Gaia* EDR3 catalogue contains photometric and astrometric data for stars with a brightness of up to 21 mag in the Gmag band. To identify cluster members and determine the intrinsic parameters of both member and non-member star distributions, we utilised a

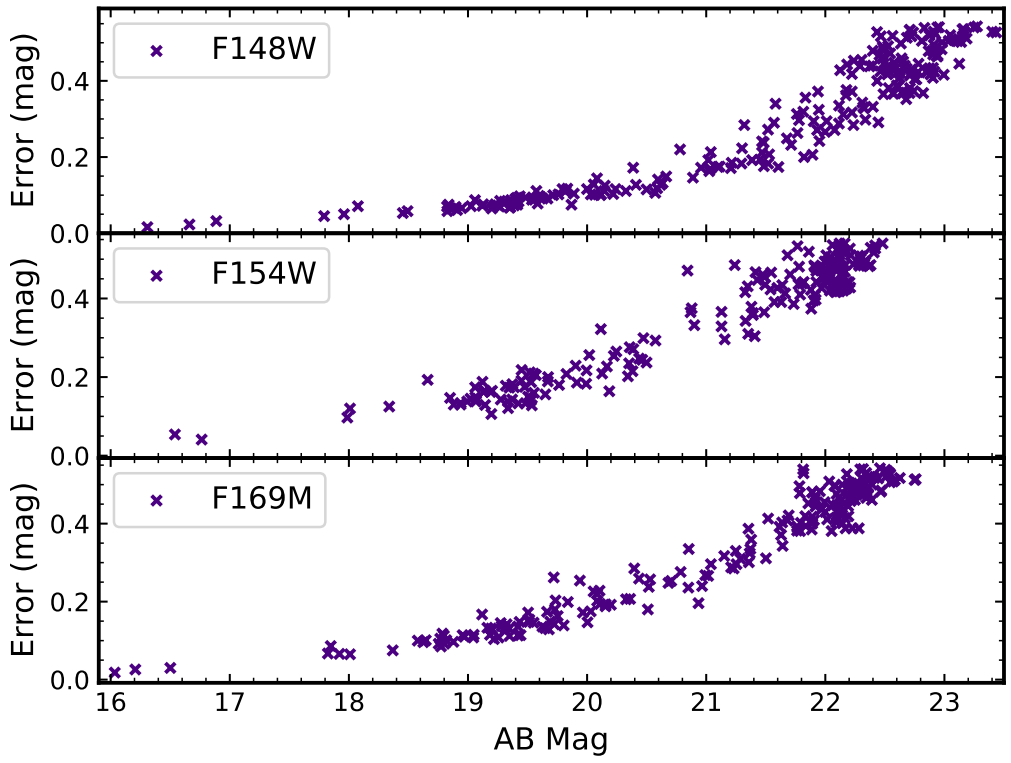

FIGURE 2: The PSF fit errors of our UVIT observations of NGC 2298 in the FUV bandpasses displayed as a function of magnitude. The panels, shown from top to bottom, present the results for the F148W, F154W, and F169M bandpasses, respectively.

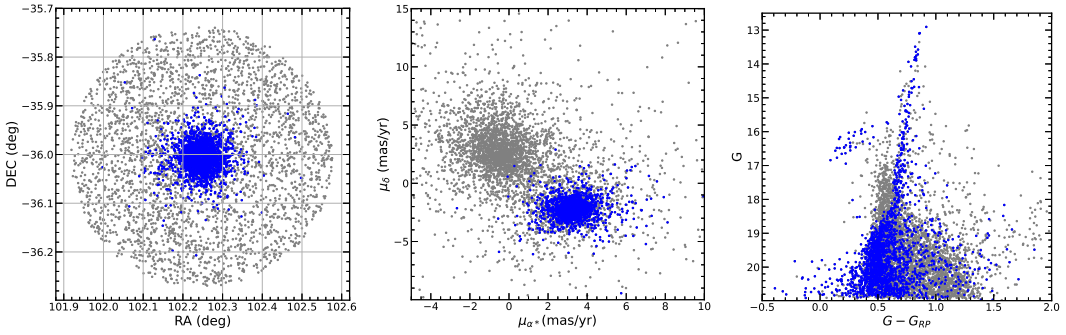

FIGURE 3: In three panels from left to right, PM members of the cluster are shown with blue dots, and the remaining *Gaia* EDR3 sample marked with grey dots represents field stars. Left Panel: position in the sky; Middle Panel: Vector Point Diagram (VPD); Right Panel: *Gaia* Optical CMD.

probabilistic GMM method. The distribution of stars in the PM space (μ_α, μ_δ) is composed of a compact cluster of member stars and a more widespread distribution of field stars. In most clusters, both distributions overlap each other, and we

can not distinguish between the two by eye. Each of the distributions follows a Gaussian distribution, and hence these two distributions are assumed to overlap two Gaussian distributions. The Gaussian probability distribution corresponding to the sum of two distributions is

$$f(\mu|\overline{\mu_i}, \sum_i) = \sum_{i=1}^{2} w_i \frac{exp\big[-1/2(\mu - \overline{\mu_i})^T \sum_i^{-1} (\mu - \overline{\mu_i})\big]}{2\pi\sqrt{det \sum_i}} \tag{4.1}$$

$$w_i \geq 0, \sum_{i=1}^{2} w_i = 1 \tag{4.2}$$

where individual PM vector is represented by μ, and μ_i represents the mean PMs for the field and cluster. $\sum$ denotes the symmetrical covariance matrix and w_i indicates the weights for the two Gaussian distributions. Full details of this method for the n-dimensional case are described in (Vasiliev 2019).

We selected *Gaia* EDR3 stars with complete astrometric data within twice the tidal radius from the cluster centre (de Marchi and Pulone 2007). In order to choose the stars with good astrometric solution, we removed those with parallaxes that deviate by more than 3σ from the expected parallax calculated using the previously known cluster's distance, where σ represents the error in parallax reported in *Gaia* EDR3 catalogue. We also removed the sources with RUWE exceeding 1.2 as larger values of this parameter might lead to an unreliable astrometric solution (Lindegren *et al.* 2018; Riello *et al.* 2021). The PM in RA and DEC of the cluster members are supposed to follow two Gaussian distributions. So, GMM is created for these two distributions, and at first, it is assumed that cluster members and field stars follow the isotropic Gaussian distributions. Initial guess for cluster PM μ_α and μ_δ values and internal velocity dispersion are taken from (Vasiliev 2019). Maximizing the total log-likelihood of the GMM and determining the mean PM and standard deviation of both Gaussian distributions was achieved

using GaiaTools*. The MPs for all chosen stars were simultaneously calculated using the same approach. The equations for maximizing the log-likelihood of the GMM and estimating the MP for the i^{th} star in the k^{th} component are presented in appendix A in Vasiliev (2019).

The cluster's mean PM and standard deviations are determined to be μ_α = 3.31 mas/yr and μ_δ = -2.176 mas/yr, with σ_c = 0.055 mas/yr. Figure 4 shows the position of stars in the sky, in the PM space known as VPD, and in an optical CMD created using *Gaia* filters. In this figure, blue dots indicate the member stars belonging to the cluster, and grey dots represent the field stars. The stars with an MP of more than 90% are selected as confirmed cluster members. The PM members in the cluster's outer part are found to be ∼1240 and considered for further analysis.

4.4 Colour Magnitude Diagrams

4.4.1 Selection of HB and BS stars

We have data in three FUV filters of UVIT, and only very hot and bright stars are expected to be detected. It is not easy to classify the stars belonging to different evolutionary sequences from the FUV CMDs. Therefore, optical CMDs are needed to identify different evolutionary sequences. Thanks to UVIT's large FOV as it covers the outer parts of the cluster. As the GCs are very dense and massive objects, *HST* is an ideal telescope to resolve and study the central region of the clusters in all available bandpasses.

*https://github.com/GalacticDynamics-Oxford/GaiaTools

To categorise the stars detected by UVIT into various stages of evolution, we cross-matched our stars within a central region with the *HST* catalogue (Nardiello *et al.* 2018) and utilised ground-based photometric data for regions beyond *HST* coverage. Nardiello *et al.* (2018) estimated the PM MPs of sources detected in the central part of the cluster using *HST* data and suggested that most likely members have a PM probability of more than 90%. Therefore, we have selected stars with a membership probability of more than 90% in the inner as well as outer regions using the *HST* and *Gaia* EDR3 catalogues, respectively. However, four stars residing in the central region have an MP of more than 80%, which are bright in UV images and found to lie along the HB locus. We have also included these stars in our study. In order to identify members in the outer part of the cluster, we first cross-matched ground-based photometric data taken from Stetson *et al.* (2019) with *Gaia* EDR3 PM membership data. For the purpose of plotting stars identified in both the inner and outer regions on the same (V-I, I) CMD, the photometric system of the *HST* ACS/WFC has been transformed to the standard Johnson-Cousins photometric system through the use of transformation equations outlined in Sirianni *et al.* (2005).

The optical CMD, created using member stars detected with the *HST* and the ground-based observations, is shown in Figure 4, where filled and open symbols indicate the stars detected in the central and outer parts, respectively. The magnitude system adopted for the Johnson-Cousin filters is Vega; hence, V-I colour and I magnitude shown in Figure 4 is in the Vega magnitude system.

The HB stars were selected by giving a specific colour and magnitude cut-off ($-0.2<$V$-$I<1.0, $14.5<$I<20.1) in an optical CMD and displayed with the filled and open red-coloured symbols in Figure 4. Since this is a metal-poor cluster, the HB is populated mainly with BHB and hot HB stars. However, there are also one or two RHB stars present along HB. Because of its low metallicity, very few variable stars, such as RR Lyrae, were detected in the cluster. Until now, only

four RR Lyrae are known in this cluster (Clement *et al.* 2001). The ground-based and *HST* photometric data have been cross-matched with the available variable star catalogue to identify the cluster's previously known RR Lyrae stars. The green inverted triangles correspond to the variable stars in Figure 4. In order to select the BSSs in the inner region, we have employed the same approach used by Raso *et al.* (2017). Their study highlighted the importance of using UV CMDs over optical CMDs to properly select BSSs in GCs. The BSSs are selected from the UV CMD created using *HST* F275W and F336W passbands and are shown with filled blue symbols in Figure 4. BSSs are selected from an optical CMD in the outer region and are displayed with open blue symbols.

4.4.2 UV and UV-optical CMDs

This section presents the FUV-optical CMDs generated by cross-identifying common stars between optical and our FUV detections. As only hot and bright stars have detectable emission in the FUV, we have cross-matched FUV-detected sources with the above-selected sample of HB and BSSs in the cluster's inner and outer regions using optical passbands. The Vega magnitude system used in the standard Johnson-Cousins photometric system is converted into the AB magnitude system to bring it in line with the UVIT magnitude system.

In Figure 5, three panels display the FUV-optical CMDs created using all three FUV filters, where filled and open markers represent the detections in the inner and outer regions, respectively. The photometric error bars shown in all panels of Figure 5 are the median of the photometric errors of stars at a selected magnitude. We have also recovered already known RR Lyrae variables displayed with filled and open green inverted triangles in all FUV-optical CMDs (See Figure 5). In our FUV images, the variable stars are basically sampled at random phases. Out of four previously known RR Lyrae stars, we found 3 in F148W, 1 in F154W,

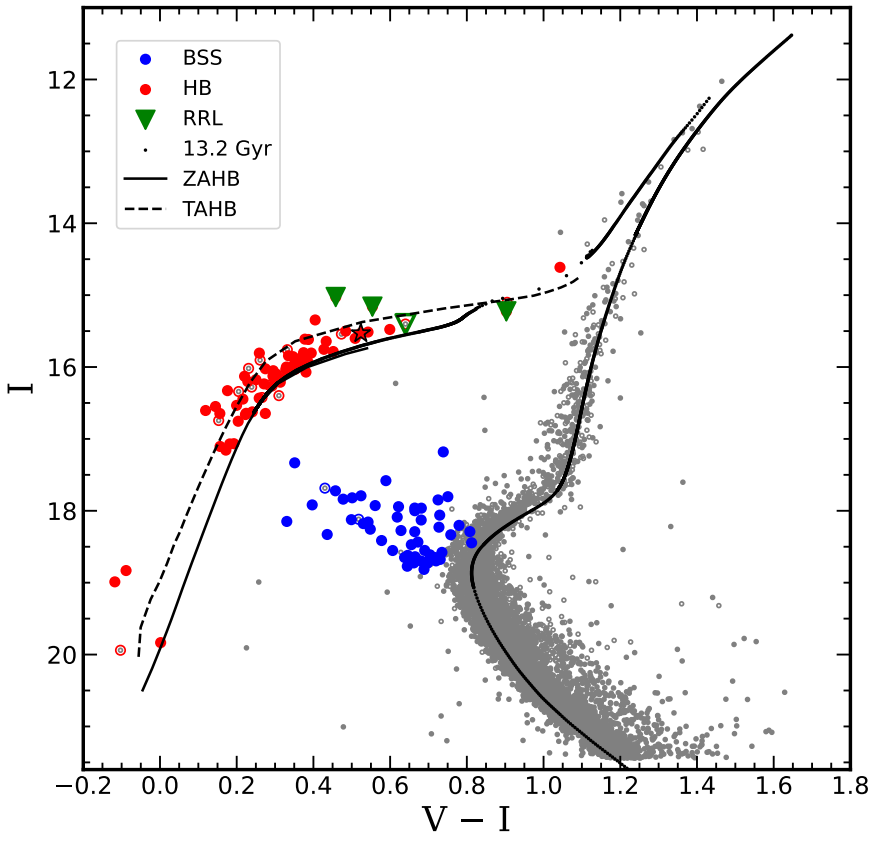

FIGURE 4: Optical CMD of NGC 2298, where Grey and coloured filled symbols represent the *HST* detected stars, whereas stars shown with grey and coloured open symbols are cross-identified using ground-based data and *Gaia* EDR3 data. All coloured symbols represent the HB and BS stars selected for further cross-match with UVIT data. All the stars in the diagram have been confirmed as PM members of the cluster. Known RR Lyrae stars are marked with green inverted triangles. For comparison with theoretical models, an updated BaSTI-IAC isochrone with an age of 13.2 Gyr and metallicity $[\mathrm{Fe/H}] = -1.92$ dex has been overlaid and depicted as black dots. The solid and dashed black lines along the HB locus indicate the ZAHB and TAHB, respectively, which signify the completion of 99% of the star's core He-burning lifetime.

and 2 in the F169M filter. Their positions in the optical and FUV-optical CMDs are shown in Figures 4 and 5, respectively. We notice that fewer HB stars are detected in the outer region of the cluster when compared to the inner region.

In all CMDs, we detect four stars at the extreme blue end of the HB. These stars are quite separated from the observed HB sequence and are likely to be very hot, as suggested by their FUV-optical colour. Out of the four stars, three are found

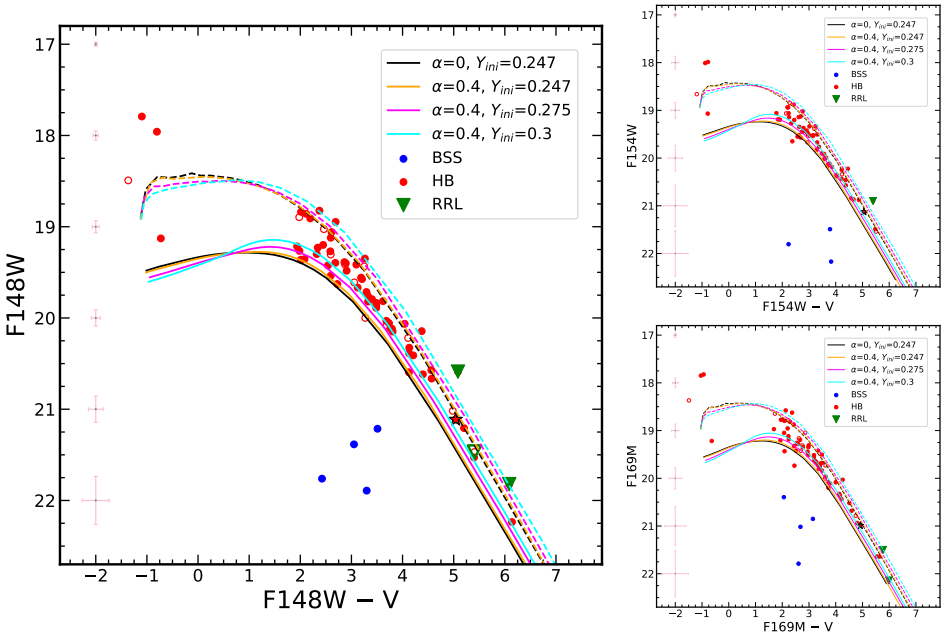

FIGURE 5: FUV-optical CMDs of NGC 2298. The red-filled and open symbols indicate the HB stars detected with UVIT in the inner and outer regions of the cluster, respectively. The meaning of different colours and symbols is displayed in the panels. The photometric errors in magnitude and colour are also shown in each panel. The solid black line on the HB locus is the ZAHB, and the dashed one represents the TAHB for $[\alpha/\mathrm{Fe}] = 0$ and normal helium abundance. The solid and dashed lines, shown with orange, magenta and cyan colour, correspond to alpha-enhanced and helium-enhanced ZAHB and TAHB tracks.

TABLE 4.1: HB and BS stars detected in different UVIT filters are listed in this table. Here N_{HB} and N_{BSS} indicate a number of detected HB and BS stars, respectively. Column 2 displays the sub-populations of HB where N_{BHB}, N_{Hot-HB} and N_{RRL} denote the number of BHB, hot HB and RRL identified with UVIT. The total number of selected HB and RRL stars from an optical CMD are shown in parentheses.

Filter	N_{HB}			N_{BSS}
	N_{BHB}	N_{Hot-HB}	N_{RRL}	
F148W	63(68)	4(4)	3(4)	4
F154W	60(68)	4(4)	1(4)	3
F169M	63(68)	4(4)	2(4)	4

to be brighter and bluer than normal BHB and EHB stars. The three bluer stars might be pHB stars, as evident from their FUV magnitudes in all FUV bands.

These hot HB stars are confirmed PM members of the cluster and are well resolved in all FUV images, as shown in Figure 6. The total number of detected BHB, hot HB, BSSs, and variable stars in all the UVIT filters are tabulated in Table 6.1. In the FUV-optical CMDs, we observe that the HB stars no longer lie along the horizontal sequence as found in the optical CMDs; instead, they follow a diagonal sequence with a significant spread. In all FUV CMDs, we also detect a few (up to 4) FUV bright BSSs.

The optical and FUV-optical CMDs overlaid with updated BaSTI-IAC isochrones and HB tracks are shown in Figures 4 and 5, respectively (Hidalgo *et al.* 2018). The updated BaSTI-IAC[†] isochrones are considered for an age 13.2 Gyr (Monty *et al.* 2018), a distance modulus of 15.75 mag (Monty *et al.* 2018), and a metallicity $[\mathrm{Fe/H}] = -1.92$ dex (Carretta *et al.* 2009) with helium abundance $Y_{ini} = 0.247$, $[\alpha/\mathrm{Fe}] = 0$, encompassing diffusion, overshooting, and mass loss efficiency parameter $\eta = 0.3$. The BaSTI-IAC model also provides the HB model, which comprises ZAHB, post-ZAHB tracks, and TAHB with or without diffusion for a particular mass range. The ZAHB and TAHB tracks have been obtained for a metallicity $[\mathrm{Fe/H}] = -1.92$ dex, including diffusion happening in the sub-atmospheric regions of these stars.

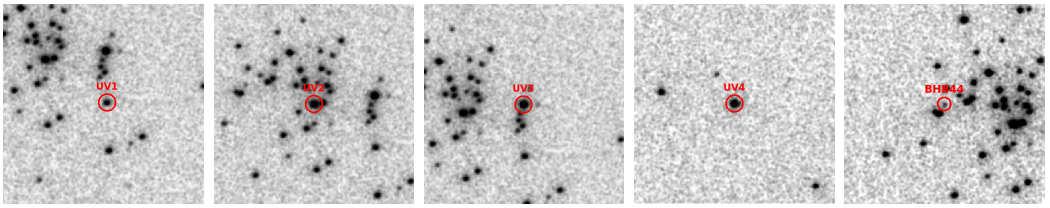

FIGURE 6: Location of hot HB and BHB44 stars on FUV F148W image of UVIT. The FOV of each image is 2′ x 2′.

The overlaid HB tracks in FUV CMDs help define the location of HB stars, which span an extensive range in colour and magnitude compared to optical CMDs. The

[†]http://basti-iac.oa-abruzzo.inaf.it/

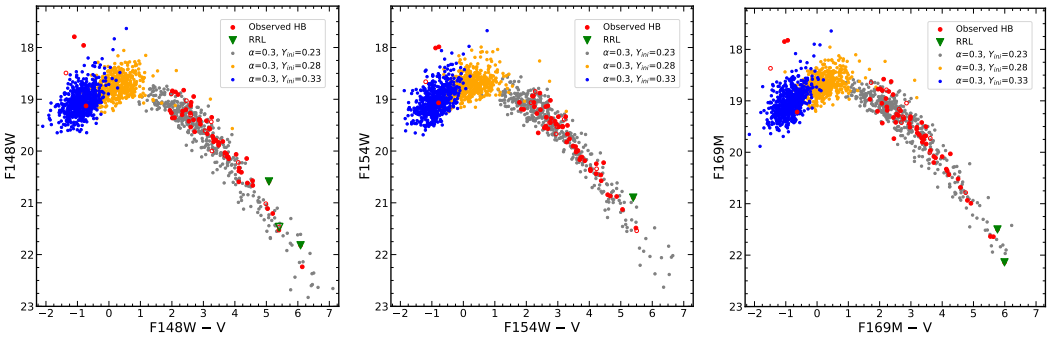

FIGURE 7: FUV-optical CMDs showing the comparison of the observed HB with synthetic HB models. The meaning of red and green symbols is the same as in Figure 5. The simulated HB populations for initial helium abundance Y_{ini} = 0.23, 0.28 and 0.33 are marked with grey, orange and blue dots, respectively.

theoretical HB models with normal helium abundance (Yini = 0.247 dex), depicted with black solid and dashed lines, do not provide a good fit for the HB sequence at the brighter end (above 20 mag). The colour/magnitude spread at brighter FUV magnitudes might be related to chemical composition differences among BHB stars, the evolutionary effects of ZAHB or photometric errors. In order to probe the cause of this spread, we have compared observations with theoretical HB models generated for enhanced $[\alpha/\mathrm{Fe}]$=0.4 dex and different initial helium abundances available in the updated BaSTI-IAC database, i.e. Y_{ini} = 0.247, 0.275, and 0.3. The ZAHB and TAHB track corresponding to these initial helium abundances are indicated with different colour solid and dashed lines in Figure 5, respectively. We find that ZAHB tracks with different initial helium abundances are not producing the colour/magnitude spread observed along the BHB sequence in all FUV-optical CMDs. We also notice that HB stars are located between the ZAHB and TAHB tracks, suggesting that some may be evolving from the HB. Three of four hotter HB stars were found to exhibit greater brightness than the TAHB tracks, indicating that they are in the pHB phase, whereas one is lying within the ZAHB and TAHB tracks implying that it is an EHB star. In order to confirm the nature of these stars, effective temperatures and bolometric luminosities are measured using the SED fitting technique described in Section 6.5.

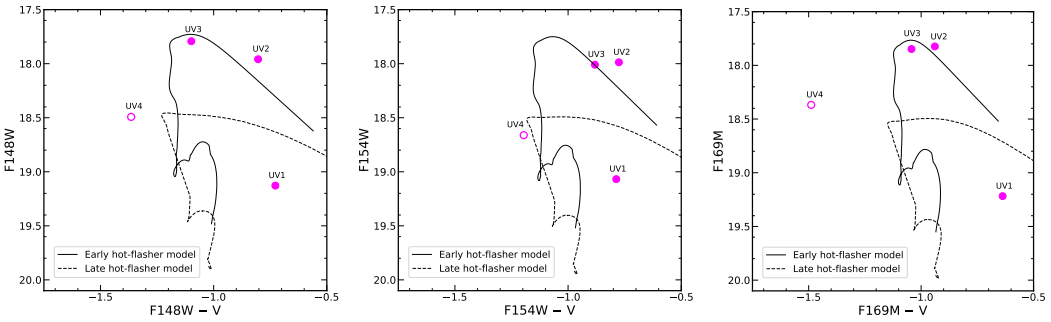

FIGURE 8: FUV-optical CMDs overplotted with hot-flasher models where solid and dashed black lines correspond to the early and late hot-flasher models, respectively. The four hot HB stars are displayed with magenta symbols. The filled symbols represent stars within the *HST* FOV, and the open symbol for the star in the outer region.

4.5 Comparison with Models

4.5.1 Synthetic Helium HB Models

We constructed the synthetic HB stellar populations for enhanced $[\alpha/\mathrm{Fe}]$=0.3 and different initial helium abundances to check for the spread in helium abundance as well as evolution. Chung *et al.* (2017) investigated the significance and potentials of populations enriched with helium in relation to second-generation populations present in the Milky Way GCs through the utilization of the YEPS model. The synthetic HB models demonstrated here utilise Yonsei-Yale (Y^2) stellar evolutionary tracks featuring elevated initial helium content (Lee *et al.* 2015). Three values are selected for Y_{ini} as 0.23, 0.28, and 0.33, at fixed Z value of 0.0002 ($[\mathrm{Fe/H}]$=-1.9 dex) and age of 13 Gyr (close to the cluster age of 13.2 Gyr). Evolutionary effects from ZAHB and observational photometric errors are taken into account. In Figure 7, the simulated CMDs for three different Y_{ini} values (0.23 in grey, 0.28 in orange, and 0.33 in blue) are shown, plotted over the observed FUV-optical CMDs, with observed HB stars displayed in red. We notice that observations match well with synthetic HB models, especially in the case of BHB stars. It is clear from the comparison of synthetic HB models with observations that all BHB

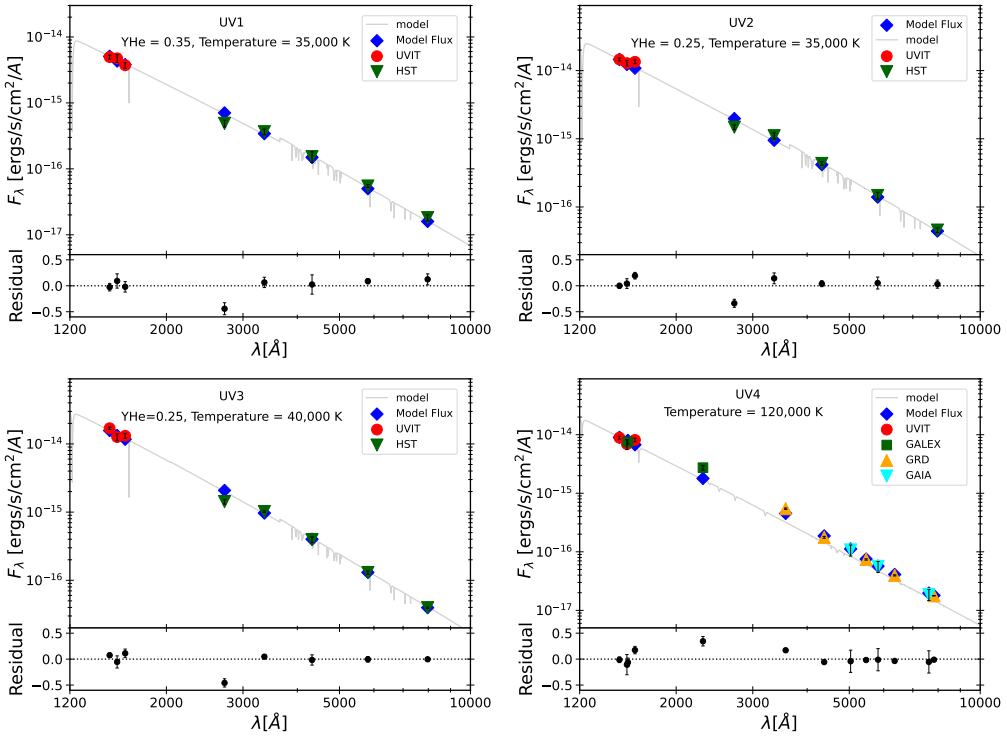

FIGURE 9: SEDs of four hot HB stars detected with UVIT after correcting for extinction. The stars, denoted with UV1, UV2 and UV3, are observed in the inner region of the cluster and UVIT (Red) and *HST* (Green) photometric data points are used to create and fit the SED, whereas for UV4, apart from UVIT, *GALEX*, *Gaia* EDR3 and ground-based photometric data points are utilised as it is identified in the outer region. Blue diamonds represent the synthetic flux from the helium-rich Husfeld model used to fit the observed SED of UV1, UV2 and UV3 stars, whereas, in UV4, they correspond to the TMAP (Grid4) model. The best-fit atmospheric parameters are mentioned in the figure. In UV1, UV2, and UV3 stars, the light grey solid line represents the theoretical helium-rich Husfeld model spectra and TMAP (Grid4) model spectra in UV4. The residuals of the SED fit are presented in the bottom panel of all plots.

stars have the same helium abundance, implying that BHBs consist of a single Y_{ini}=0.23. Therefore, we suggest that colour/magnitude spread among BHB stars is not caused by helium variation. Out of four hot HB stars, one star is found to have Y_{ini}=0.33, and another at the brighter the extension appears to be the product of enhanced helium, which, in turn, implies that these stars are originated from helium-enhanced populations. The other two hot HB stars are brighter than the simulated stars for Y_{ini}=0.33, suggesting that they are in an evolved stage, might be the progeny of helium-enhanced EHBs in this cluster. Therefore, using

synthetic HB models, we estimate a Y_{ini}=0.23 for BHB stars and four hot BHB stars are likely to have Y_{ini}=0.33. Thus, helium enrichment appears to contribute significantly to the formation of hot HB stars in this cluster.

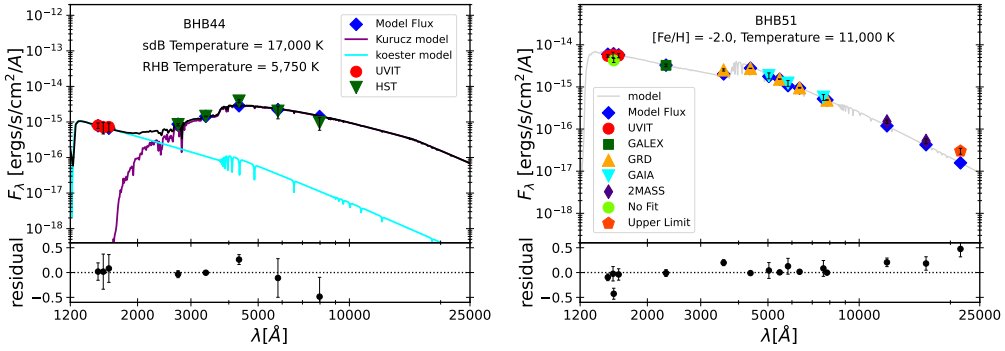

FIGURE 10: SEDs of BHB stars detected with UVIT in central (Left Panel) and outer (Right Panel) region after correcting for extinction. The left panel shows the composite SED fit of the BHB44 star where purple and cyan colour spectra indicate Kurucz and Koester model spectra as displayed in legend, respectively. The black colour represents the composite spectra. The best-fit parameters are displayed in the figure. The rest of the details are the same as in Figure 9.

4.5.2 Hot Flasher Models

The location of the very hot HB sub-population known as BHk stars in FUV-optical CMDs is not reproduced by the canonical HB models; this sub-population is hotter than the hottest point along the ZAHBs (See Figure 8 in Dalessandro *et al.* (2011)). The proposed formation scenarios for these stars are extreme mass loss on RGB, helium enrichment and mixing, and hot-flasher. A hot-flasher scenario envisions stars undergoing substantial mass loss during the RGB phase and departing from the branch before the helium core flash. These stars then rapidly transition to the cooling track of helium-core WDs and experience a helium flash due to strong electron degeneracy in their core (Castellani and Castellani 1993).

Further, depending upon the location of ignition of helium flash along the WD cooling sequence, hot-flasher models are classified into two types: EHF and LHF. These scenarios are described in detail in Brown *et al.* (2001). The progeny of hot-flashers ends up on the hotter and bluer side of the normal BHB stars. The stars, which are products of the EHF scenario, are expected to be hotter and of similar UV magnitudes compared to BHB stars in UV CMDs, known as EHB stars, whereas the stars that are hotter and fainter than normal EHB stars in UV CMDs are expected to be late hot flashers. Although we did not detect any BHk star in this cluster, there are three hot HB stars that are brighter than synthetic HB populations, and their location is not reproduced by ZAHB and TAHB tracks. In order to check whether the hot HB stars are the product of strong mass loss, we have compared observations with hot-flasher models, i.e., EHF and LHF models. The hot-flasher models were generated in UVIT and *Gaia* EDR3 filters (Cassisi *et al.* 2003)(Cassisi 2021, private comm.). The hot-flasher models superimposed on the observed hot HB stars are presented in Figure 8. These four stars are marked with the names UV1, UV2, UV3, and UV4 in this study, as shown in Figure 8. Two stars, namely UV2 and UV3, are found to lie close to the EHF model in all three FUV-optical CMDs, suggesting that they are the offspring of EHB stars originated via an EHF scenario. We notice that UV2 is slightly brighter than the hot-flasher model. UV4 is lying close to the LHF model (Dashed black line), only in (F154W, F154W−V) CMD, suggesting that it may be an evolved product of a BHk star. However, in the rest of the FUV-optical CMDs, its location is not reproduced by hot-flasher models. From this comparison, the nature of the UV4 star is not very clear. Any of the hot-flasher models do not reproduce the position of one EHB star designated with UV1, but it is well produced by helium-enhanced synthetic HB models, suggesting that it could be a result of helium enrichment in the cluster. As the stars tend to shift location among the CMDs, locating them in the H-R diagram will be ideal for evaluating their evolutionary status. Further estimation of atmospheric parameters and comparison with theoretical models in the H-R diagram is required to probe these stars' evolutionary status in detail and

shed more light on their nature.

4.6 Spectral Energy Distribution fitting

The Kurucz stellar atmospheric models are employed to construct SEDs (Castelli and Kurucz 2003; Castelli *et al.* 1997) for HB stars, which have photometry ranging from UV to IR wavelengths. We fixed the value of metallicity $[\mathrm{Fe/H}] = -2.0$, close to the cluster metallicity, and gave the range of T_{eff} from 5,000-50,000 K and $\log g$ from 3.5-5 dex in the these models to fit the SED of HB stars. The locus of ZAHB reflected in the T_{eff} versus $\log g$ plane is used to constrain the range of $\log g$ for HB stars.

We combined 3 FUV UVIT photometric data points with 5 *HST* photometric data points from Nardiello *et al.* (2018) to create SED for HB stars detected cluster's inner region. For those detected in cluster's outer region, we combined the photometric data points of UVIT (3 passbands) with *Gaia* EDR3 (3 passbands) (Gaia Collaboration *et al.* 2018), ground-based photometry (5 passbands) (Stetson *et al.* 2019), *GALEX* (2 passbands) and 2MASS (3 passbands). VOSA makes use of Fitzpatrick reddening law (Fitzpatrick 1999; Indebetouw *et al.* 2005) to correct for extinction in observed data points.

It is a well-known fact that HB stars with T_{eff} more than 11,500 K are influenced by atmospheric diffusion, which increases the atmospheric abundances of heavy elements like iron and reduces the atmospheric abundances of light elements. To take this effect into account, we fitted the SEDs of BHB stars with $T_{eff} > 11{,}500$ K with solar metallicity models and determine their atmospheric parameters. As the LHF scenario predicts enrichment in helium, the non-LTE helium-rich Husfeld

TABLE 4.2: Atmospheric parameters derived from SED fitting of four hot HB stars detected with UVIT in NGC 2298. Column 1 lists the star ID used in this work. Columns 2 and 3 display the RA and DEC of all the stars considered for fitting, respectively. Column 4 presents the different models used for the SED fit of these stars. Columns 5 and 6 lists the obtained helium mass fraction and T_{eff} from SED fitting using different theoretical models. The luminosities and radii of these stars, along with errors, are tabulated in columns 7 and 8, respectively. Columns 9 and 10 lists the reduced χ^2 value corresponding to the best fit and ratio of the number of photometric data points ($\frac{N_{fit}}{N_{tot}}$) used for the fit to the total number of available data points.

Star ID	RA (deg)	DEC (deg)	Model Used	Y_{ini} (dex)	T_{eff} (K)	$\frac{L}{L_\odot}$	$\frac{R}{R_\odot}$	χ^2_{red}	$\frac{N_{fit}}{N_{tot}}$
UV1*	102.2541	-35.99134	Husfeld	0.35	35,000 (35,000-40,000)	36.14 ± 0.12	0.17 ± 0.003	5.1	8/8
			Kurucz		$29,000 \pm 2,000$	27.58 ± 0.12	0.2 ± 0.004	2.8	8/8
UV2*	102.2512	-36.00361	Husfeld	0.25	35,000 (35,000-40,000)	103.9 ± 0.24	0.28 ± 0.005	7.8	8/8
			Kurucz		$32{,}000^{+4,000}_{-2,000}$	86.39 ± 1.01	0.3 ± 0.006	5.7	8/8
UV3	102.2446	-35.99501	Husfeld	0.25	40,000 (40,000-60,000)	128.3 ± 0.26	0.24 ± 0.004	10.4	8/8
			Kurucz		$50{,}000_{-7,000}$	235.7 ± 1.06	0.2 ± 0.004	8.7	8/8
UV4*	102.2379	-36.03683	TMAP (Grid4)		120,000 (120,000-150,000)	1148 ± 303.4	0.08 ± 0.002	7.8	13/13
	102.2379	-36.03683	Husfeld	0.35	80,000 (75,000-80,000)	469.2 ± 17.9	0.11 ± 0.002	10.7	13/13
			Kurucz		$50{,}000_{-9,000}$	108.5 ± 5.05	0.14 ± 0.003	17.4	11/13

Note that stars marked with * symbols have their estimated temperature corresponding to the best-fit SEDs and equal to the helium-rich model's lower or upper limit. The range of temperatures for the ten best fits is also mentioned in parentheses. The other atmospheric parameters are listed according to the best-fit model.

models (Husfeld *et al.* 1989) are used to fit the observed SEDs of four hot HB stars. The grid of this model have the range of stellar parameters typical of extremely helium-rich sdO stars: $35,000K \leq T_{eff} \leq 80,000K$, $4.0 \leq logg \leq 7.0$, and $0.01 \leq Y_{He} \leq 0.7$. In the case of UV4 star, we have noticed that T_{eff} derived using the Kurucz and helium-rich Husfeld model fits the observed SED corresponds to their upper limit, which indicates that this star is likely to be hotter than the estimated temperature from these models. In order to compute the accurate T_{eff} of this star, we have fitted its SED with the TMAP (Grid4) model used for hot stars (Werner *et al.* 2003; Rauch and Deetjen 2003). This model grid spans a range of atmospheric parameters.

We carried out SED fitting analysis for 63 BHB and four hot HB stars. Figures 9 and 10 show the SED fit for four hot HB and two BHB stars overplotted with the

TABLE 4.3: Atmospheric parameters derived from SED fit of BHB stellar populations detected with UVIT in NGC 2298. The notation of all columns is the same as in Table 6.2.

Star ID	RA (deg)	DEC (deg)	T_{eff} (K)	$\frac{L}{L_\odot}$	$\frac{R}{R_\odot}$	χ^2_{red}	$\frac{N_{fit}}{N_{tot}}$
BHB1	102.2435	-36.01081	$10,750 \pm 250$	70.15 ± 1.25	2.38 ± 0.04	3.8	7/8
BHB2	102.2357	-36.01813	$12,500 \pm 500$	43.64 ± 0.59	1.3 ± 0.03	12.7	8/8
BHB3	102.2252	-36.02032	$11,500 \pm 250$	50.83 ± 0.39	1.78 ± 0.03	14.3	8/8
BHB4	102.2281	-36.01802	$12,250 \pm 500$	48.67 ± 1.08	1.5 ± 0.03	4.7	8/8
BHB5	102.2501	-36.00238	$10,250 \pm 250$	73.27 ± 2.46	2.78 ± 0.05	9.2	8/8
BHB6	102.2629	-35.98792	$10,500 \pm 250$	57.85 ± 2.0	2.3 ± 0.04	4.9	8/8
BHB7	102.2271	-36.01273	$10,500 \pm 250$	54.65 ± 1.92	2.23 ± 0.04	8.4	8/8
BHB8	102.2475	-36.00676	$10,250 \pm 250$	44.37 ± 1.59	2.04 ± 0.04	14.1	8/8
BHB9	102.2552	-36.01549	$12,000 \pm 500$	30.79 ± 0.39	1.2 ± 0.02	11.4	8/8
BHB10	102.2459	-36.00806	$11,000 \pm 250$	42.73 ± 1.51	1.79 ± 0.03	6.1	8/8
BHB11	102.2508	-36.0122	$12,250 \pm 500$	33.13 ± 0.47	1.23 ± 0.02	8.9	8/8
BHB12	102.2564	-36.00318	$9,750^{+250}_{-500}$	43.34 ± 1.95	2.26 ± 0.04	35.1	8/8
BHB13	102.2595	-36.0062	$11,000 \pm 250$	39.01 ± 1.63	1.69 ± 0.03	7.4	8/8
BHB14	102.2239	-36.01842	$10,250 \pm 500$	56.95 ± 4.86	2.14 ± 0.04	7.6	8/8
BHB15	102.2633	-35.99884	$12,000^{+250}_{-500}$	32.35 ± 0.51	1.31 ± 0.03	3.6	8/8
BHB16	102.2467	-36.00291	$12,500^{+250}_{-500}$	33.43 ± 0.37	1.23 ± 0.02	7.1	8/8
BHB17	102.2439	-36.00493	$9,750^{+500}_{-250}$	48.07 ± 1.44	2.42 ± 0.05	13.2	8/8
BHB18	102.2486	-36.00619	$10,250^{+500}_{-250}$	42.13 ± 2.43	1.99 ± 0.04	5.4	8/8
BHB19	102.2498	-36.01167	$9,250^{+500}_{-250}$	45.49 ± 1.46	2.53 ± 0.05	16.7	8/8
BHB20	102.2576	-35.98383	$9,500^{+500}_{-250}$	53.68 ± 2.26	2.64 ± 0.05	12.1	8/8
BHB21	102.2608	-35.99758	$10,500^{+500}_{-250}$	37.39 ± 1.78	1.79 ± 0.03	6.7	8/8
BHB22	102.2467	-36.01245	$10,000^{+500}_{-250}$	46.03 ± 1.82	2.23 ± 0.04	3.2	8/8
BHB23	102.2292	-36.01033	$9,500 \pm 250$	51.97 ± 2.09	2.66 ± 0.05	5.5	8/8
BHB24	102.237	-36.00386	$9,250 \pm 500$	49.44 ± 2.62	2.68 ± 0.05	10.8	8/8
BHB25	102.2694	-36.00772	$10,250^{+500}_{-250}$	33.76 ± 1.81	1.72 ± 0.03	6.9	8/8
BHB26	102.2431	-35.97799	$9,500^{+500}_{-250}$	46.76 ± 3.05	2.49 ± 0.05	1.5	8/8
BHB27	102.2673	-36.02095	$9,750^{+500}_{-250}$	42.58 ± 3.83	2.09 ± 0.04	2.7	8/8
BHB28	102.2465	-36.01901	$9,000 \pm 500$	54.19 ± 2.11	2.95 ± 0.06	8.0	8/8
BHB29	102.248	-35.99478	$9,500^{+250}_{-500}$	44.69 ± 2.14	2.41 ± 0.05	5.2	8/8
BHB30	102.2554	-36.01623	$9,250^{+750}_{-250}$	41.46 ± 3.01	2.24 ± 0.04	7.9	8/8

TABLE 4.4: Continued.

Star ID	RA (deg)	DEC (deg)	T_{eff} (K)	$\frac{L}{L_\odot}$	$\frac{R}{R_\odot}$	χ^2_{red}	$\frac{N_{fit}}{N_{tot}}$
BHB31	102.2475	-36.00208	$9,250^{+500}_{-250}$	45.92 ± 2.18	2.52 ± 0.05	8.6	8/8
BHB32	102.2441	-36.00356	$9,250^{+1000}_{-250}$	38.76 ± 2.55	2.08 ± 0.04	12.5	8/8
BHB33	102.25	-36.01609	$9,000^{+500}_{-250}$	46.43 ± 3.92	2.75 ± 0.05	2.7	8/8
BHB34	102.2466	-35.99503	$9,000^{+750}_{-250}$	41.83 ± 3.11	2.36 ± 0.04	6.1	8/8
BHB35	102.2407	-36.00629	$8,750^{+500}_{-750}$	58.94 ± 4.15	3.19 ± 0.06	9.5	8/8
BHB36	102.2623	-36.01596	$9,000 \pm 500$	43.43 ± 2.52	2.53 ± 0.05	7.5	8/8
BHB37	102.2406	-36.0042	$8,750^{+500}_{-250}$	48.16 ± 2.15	2.97 ± 0.06	12.2	8/8
BHB38	102.2408	-36.01402	$8,500^{+500}_{-1000}$	77.59 ± 3.12	4.03 ± 0.08	1.8	7/8
BHB39	102.2499	-35.99423	$8,750^{+500}_{-750}$	44.66 ± 2.54	2.81 ± 0.05	11.7	8/8
BHB40	102.2469	-36.00461	$8,500 \pm 500$	46.42 ± 6.17	2.97 ± 0.06	9.9	8/8
BHB41	102.2284	-36.00907	$8,500 \pm 500$	52.18 ± 6.35	3.01 ± 0.06	5.1	8/8
BHB42	102.2741	-35.99637	$8,750^{+250}_{-500}$	40.41 ± 2.48	2.73 ± 0.05	2.0	8/8
BHB43	102.2631	-36.00405	$8,250^{+500}_{-750}$	48.52 ± 3.31	3.34 ± 0.06	10.6	8/8
BHB45	102.2548	-36.00226	$8,500^{+500}_{-1000}$	49.53 ± 3.74	3.15 ± 0.06	12.4	8/8
BHB46	102.241	-35.99525	$8,250^{+500}_{-750}$	54.8 ± 3.61	3.52 ± 0.07	5.3	8/8
BHB47	102.2486	-35.99375	$9,500^{+500}_{-250}$	41.89 ± 2.25	2.27 ± 0.04	8.6	8/8
BHB48	102.2521	-36.01067	$7,750 \pm 500$	51.41 ± 2.84	3.8 ± 0.07	14.0	6/6
BHB49	102.2503	-36.01369	$8,000 \pm 125$	51.16 ± 4.78	3.65 ± 0.07	32.9	8/8
BHB50	102.1974	-36.0043	$12,250 \pm 250$	53.02 ± 2.62	1.59 ± 0.03	1.2	15/16
BHB51	102.302	-36.00933	$11,000^{+250}_{-500}$	62.62 ± 3.29	2.15 ± 0.04	2.0	15/16
BHB52	102.2673	-36.06088	$10,000^{+250}_{-500}$	46.22 ± 6.76	2.22 ± 0.04	3.9	15/16
BHB53	102.2418	-36.04874	$10,250^{+250}_{-500}$	54.08 ± 8.19	2.32 ± 0.04	3.9	15/16
BHB54	102.1568	-36.10535	$9,500 \pm 250$	66.63 ± 4.47	2.99 ± 0.06	0.74	15/16
BHB55	102.2196	-35.98094	$10,000 \pm 500$	52.23 ± 6.51	2.39 ± 0.05	2.6	15/16
BHB56	102.2171	-35.97486	$9,750^{+250}_{-750}$	43.27 ± 6.56	2.27 ± 0.04	1.4	15/16
BHB57	102.2633	-36.03276	$8,750^{+250}_{-500}$	50.34 ± 10.56	3.01 ± 0.06	1.7	15/16
BHB58	102.2021	-36.01866	$8,750^{+250}_{-500}$	64.73 ± 11.11	3.44 ± 0.06	1.8	15/16
BHB59	102.2339	-36.04152	$8,000^{+250}_{-500}$	65.59 ± 5.47	4.16 ± 0.08	3.5	11/11
BHB60	102.2492	-36.00759	$10,750^{+250}_{-500}$	35.41 ± 2.0	1.62 ± 0.03	7.9	8/8
BHB61	102.2539	-36.00547	$9,250^{+500}_{-250}$	47.15 ± 2.99	2.61 ± 0.05	3.5	8/8
BHB62	102.2809	-36.01208	$8,250 \pm 500$	54.26 ± 4.36	3.36 ± 0.06	2.7	6/6
BHB63	102.2535	-35.99972	$8,000 \pm 500$	49.49 ± 3.77	3.48 ± 0.07	3.0	7/7

corresponding best-fit models (smallest value of χ^2_{red}) shown with light grey colour. Each plot's lower panel present the residuals, which are the differences between the observed SED and the best-fit model. The star ID used in this work, the metallicity value of the fitted model spectrum, and the estimated temperature are displayed in all the SED plots. As mentioned above in section 6.4.2, variables such as RR Lyrae are observed at random phases, so we have not considered them for SED analysis. The estimated parameters of four hot HB stars using the Kurucz, Husfeld, and TMAP (Grid4) models are tabulated in Table 6.2. The Husfeld model fits find UV1 and UV4 to be much hotter when compared to the estimates from Kurucz model fits and also suggests these stars to be helium-rich. On the other hand, the Husfeld model fits the SEDs of UV2, and UV3 provides normal helium values along with T_{eff} similar to those obtained from the Kurucz model fits (within errors). The T_{eff} (120,000 K) and luminosity ($1148 L_{\odot}$) of UV4 obtained using the TMAP (Grid4) model are much higher than estimated from the other two models. The derived values of parameters T_{eff}, $\frac{R}{R_{\odot}}$, and $\frac{L}{L_{\odot}}$ corresponding to the best-fit Kurucz model spectrum along with the errors for BHB stars are listed in Table 6.3. As errors estimated through VOSA are not realistic, we have reported the range in T_{eff} as found from the 10 best-fit values. While the $\log g$ values for these stars are also estimated using this technique, these values are not reliable as SED fits are not sensitive to this parameter.

In Figure 9, it can be seen from the residuals that the observed data points are well-fitted with the model spectrum. However, in most of the SED fits, *HST* F275W data point does not fit with the model flux. The observed flux at F275W is found to be less than the expected flux from the model, which, in turn, gives a negative residual. We note the presence of strong absorption lines, such as Fe II and Mg II, in the wavelength range covered by this filter. It might be possible that there is a mismatch in the strength of these spectral lines between the observations and the models. From the comparison of synthetic Kurucz spectra at different T_{eff}, we notice that these lines contribute to the integrated flux of F275W is more at cooler

temperatures than the hotter ones, which results in a larger deviation from the expected flux for cooler stars than the hotter stars. In order to establish the best fit to the observed SED, we have only considered the data points which fit well to the model spectra. The high temperatures of UV1 (35,000 K) and UV2 (35,000 K) suggest that they may belong to the class of EHB stars as they have temperatures around 30,000 K (Heber 1986). The other two hot HB stars, UV3 and UV4, with very high temperatures of 40,000 and 120,000 K, might belong to the pHB phase. Also, note that SEDs of all hot HB stars are well fitted with a single spectrum with minimum residual across wavelength, which, in turn, indicates that these stars could be single stars.

The SEDs of all BHB stars are presented in Appendix 4.10. The T_{eff} range of BHB stars varies from 8,000-12,250 K. For one BHB star, namely BHB44, observed SED is not fitted with a single spectrum as shown in the left panel of Figure 10. Compared to Kurucz's model spectrum and synthetic flux, there seems to be a large amount of excess flux in FUV filters. We checked whether the star is well-resolved in all FUV images (See Figure 6) and also ensured that the cross-identification with the *HST* catalogue is correct. This star is found to lie at a distance of 0.′68 from the centre of the cluster. It is possible that this star might be a binary star or variable star. If we check the position of this star, marked with a black outlined star symbol in Figures 4 and 5, in optical as well as in UV CMDs, it is lying close to or in the variable region. In the literature, it is not reported as a variable star. The temperature derived from the single fit of BHB44 corresponds to that of an RHB star which shows significant FUV excess due to a possible hot companion, as RHB stars are too cool to be seen in FUV. In order to check what type of hot companion is present, we fitted the SED with a combination of hot and cool theoretical spectra. To fit the FUV region of the observed SED of this star, we selected a Koester WD model (Tremblay and Bergeron 2009; Koester 2010). This model's free parameters are $\log g$ and T_{eff}. The value for the T_{eff} for this model ranges from 5,000-80,000 K and $\log g$ from 6.5-9.5 dex. We utilised VOSA

to obtain the binary fit of this star. In the left panel of Figure 10, we present the composite SED fit of this star where it can be seen that the hotter part of SED is well fitted with a Koester model corresponding to a temperature of 17,000 K, and the cooler part is fitted with Kurucz model of temperature 5,750 K. The detailed parameters of both companions are listed in Table 4.5. The T_{eff} and radius obtained for the cooler part from the best Kurucz model fit correspond to an RHB star. From the T_{eff} and radius, we suggest that the hot companion might belong to the class of sub-luminous sdB stars (Heber *et al.* 2003).

Further, to confirm the nature of four hot HB stars, the comparison of the obtained parameters from the SED fit with theoretical evolutionary tracks is needed and discussed in the following section.

4.7 Evolutionary Status of hot HB and BHB stars

The derived atmospheric parameters of hot HB and BHB stars from SED fit are compared with theoretical evolutionary tracks in order to check their evolutionary status. We plotted the theoretical evolutionary tracks employing the models presented by Moehler *et al.* (2019). The evolutionary track from the MS to the RGB was obtained utilising the updated BaSTI-IAC models from Hidalgo *et al.* (2018). The model chosen was based on a metallicity similar to that of the cluster. The tracks, starting from the MSTO to the point late in the pHB evolution or on the pAGB cooling sequence, are displayed in Figure 12. The tracks with varying masses beginning from the ZAHB represent the evolution during the pHB stage. The ZAHB and TAHB are shown with a dashed and dash-dotted line in Figure 12. We also have plotted the EHF and LHF tracks shown with magenta and black solid lines. The parameters estimated from the best SED fit for hot HB and BHB stars are plotted in the H-R diagram and shown with different symbols

and colours. We can see in Figure 12 that most of the BHB stars marked with red cross symbols are lying along the BHB tracks shown with blue lines. Nevertheless, there are a few BHB stars, displayed with purple cross symbols, lying above the TAHB, indicating that these stars' cores have already run out of helium and they have started evolving towards the pHB or peAGB phase.

To compare the estimated parameters of hot HB stars computed using different models, we plotted hot HB stars' location in the H-R diagram as illustrated in Figure 12. As the hot HB star, UV1 was found to be helium-rich by the synthetic HB models; we have shown only its position in the H-R diagram as found from the helium-rich Husfeld model. UV1 is found to be located between the ZAHB and TAHB and slightly hotter than the EHB track for 0.502 $M_{\odot}$. Thus, UV1 is still in the HB evolutionary phase, which implies that it is an EHB star, as also seen from Figures 5 and 7. Figure 12 shows that the hot HB star UV2 is found along the AGBM evolutionary stage, corresponding to the initial EHB mass range 0.506-0.51 $M_{\odot}$, which is likely to evolve from the EHB phase. Stars UV3 and UV4 are found to be much hotter and brighter than the EHB tracks. UV3 is found to be located close to the evolutionary track, corresponding to an EHF. We infer from here that UV3 is the progeny of an EHB star (with $\sim$0.502 $M_{\odot}$) formed through an EHF scenario. The position of the UV4 star indicates that it might have traversed the peAGB phase and is about to enter the WD cooling phase. TMAP (Grid4) model parameter estimates for UV4 star suggest that it is a product of BHB star with the mass of $\sim$0.7 $M_{\odot}$. From the model, the mass of EHB star UV1 turns out to be 0.502 $M_{\odot}$. The rest of the hot stars are likely to be evolved from the EHB stars with a ZAHB mass of $\sim$0.5 $M_{\odot}$. In comparison, the masses of BHB stars vary in the range 0.6 - 0.75 $M_{\odot}$. This suggests that the hot HB stars have lost $\sim$0.1 - 0.2 $M_{\odot}$ more envelope mass due to mass loss in the RGB. The reason for this enhanced mass loss could be many, including enhanced helium due to mixing, binary interactions, high rotation, etc. In the case of the BHB44

TABLE 4.5: Derived parameters of BHB44 star from composite SED fit.

Star ID	RA (deg)	Dec (deg)	Type	Model Used	T_{eff} (K)	$\frac{L}{L_\odot}$	$\frac{R}{R_\odot}$	χ^2_{red}	$\frac{N_{fit}}{N_{tot}}$
BHB44	102.2532	-36.01526	sdB	Koester	17000 ± 1000	4.46 ± 0.23	0.24 ± 0.005	2.9	8/8
			RHB	Kurucz	5750 ± 125	63.38 ± 5.7	8.17 ± 0.15		

star, a comparison of the L and T_{eff} of the hot companion with the theoretical evolutionary sequences for ELM WDs computed by (Althaus *et al.* 2013) suggests that it has a low mass of ∼0.187 $M_\odot$. As the mass of the sdB is too low to support the core helium burning, it might be evolving into a helium core WD and is likely to be an ELM WD candidate. Therefore, this binary is most likely to be a post-mass-transfer system consisting of an ELM-WD candidate and an RHB star.

The predicted number of stars in the pHB phase within the cluster is estimated based on the fact that the number of stars in two post-MS phases, in general, will be proportional to the ratio of the duration of these stages (Knigge *et al.* 2002). The following relation is used to calculate the expected number of pHB stars:

$$N_{pHB} = N_{HB} \left(\frac{\tau_{pHB}}{\tau_{HB}} \right)$$

Where N_{pHB} and N_{HB} correspond to the expected number of stars in pHB and HB phase in the cluster, respectively; τ_{pHB} and τ_{HB} represents the lifetimes of pHB and HB evolutionary phases of a low mass star, respectively. We have taken the duration of the HB phase as $\tau_{HB} = \sim 10^8$ years (Dorman 1992), and that of pHB phase as $\sim 10^7$ years from BaSTI pHB tracks. We, therefore, estimate the number of expected pHB stars to be ∼7. The observed number of pHB stars are six in this cluster, which matches well with the theoretically expected number.

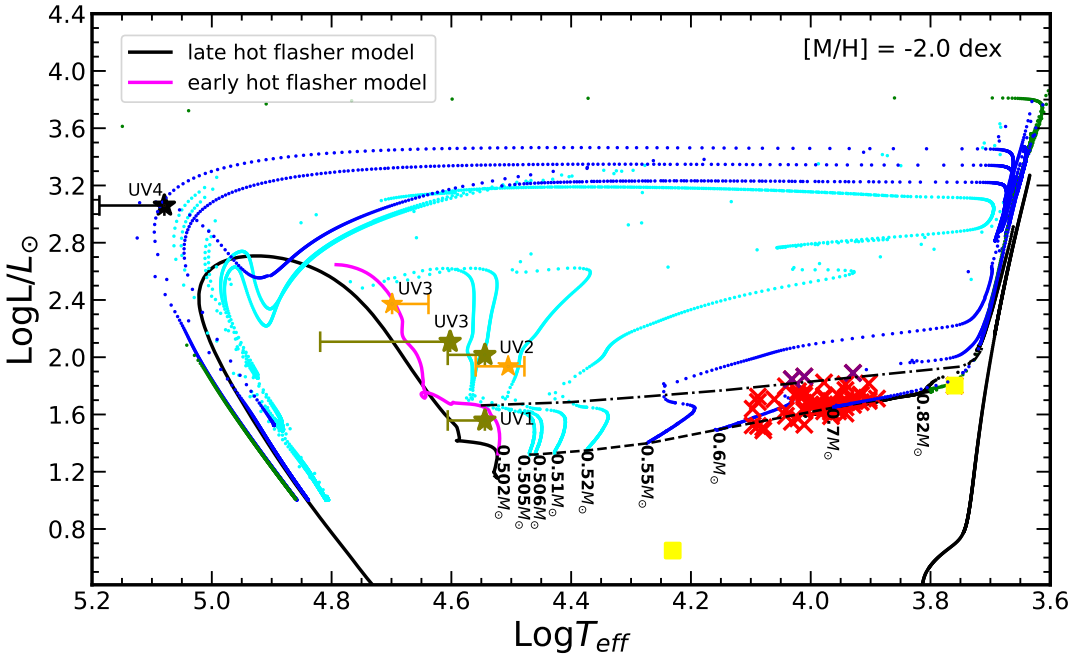

FIGURE 11: Position of hot HB and BHB stars identified with UVIT in NGC 2298 in the H-R diagram along with theoretical evolutionary tracks. The evolutionary tracks starting from MSTO to the moment when a star has entered to the WD cooling phase (Hidalgo *et al.* 2018) are presented in this plot. Along the HB phase, Post-ZAHB tracks span a mass range from $0.502 - 0.82 M_{\odot}$. In the plot, cyan, blue and green colours correspond to the sequences populating the extreme, blue and red parts of the HB. The Black dashed, and dash-dotted lines show the position of the canonical ZAHB and TAHB, respectively. The black and magenta solid lines indicate the late and early hot-flasher models. The SED fit parameters obtained from the Kucurz model fit to the observed SEDs of hot HB and BHB stars are shown with orange star and red cross symbols, respectively. The olive and black-filled star symbols present the location of hot HB stars corresponding to the helium-rich Husfeld and TMAP (Grid4) model fit, respectively. Yellow square symbols present the location of the hot and cool companion of a BHB44 star. The purple cross symbols show several BHB stars evolving towards the peAGB phase.

4.8 Discussion

We have analysed the UVIT data aboard the *AstroSat* satellite covering the GC NGC 2298 to characterise the hot HB population in order to gain insight into their formation and evolution. To date, this cluster has been studied in UV, only as a part of the group, for comparative studies of HB morphology. A focused study on the HB population of this cluster has not been done so far. This is the

first time hot HB stars are characterised in this cluster using FUV photometric data combined with the *HST* and ground-based data. We have combined FUV photometric data with optical photometry to generate the FUV-optical CMD in each FUV filter (F148W, F154W, F169M) and detected the BHB, four hot HB and a few bright BS stars.

Brown *et al.* (2016a) analysed the 53 GGCs using *HST* UV and blue photometric data to explore the HB morphology, including NGC 2298. They created colour-colour plots for all selected clusters and found two hot HB stars bluer than the gap between EHB and BHk stars in NGC 2298. They classified these two hot HB stars as BHk stars based on their location in the colour-colour plot. In our FUV images, we detected three hot HB stars in cluster's central region and one in its outer region. In FUV CMDs, three of four hot HB stars are brighter than canonical EHB stars and classified as pHB stars.

Schiavon *et al.* (2012) presented the UV CMDs for 44 GGCs using *GALEX* photometric data in NUV and FUV passbands, including NGC 2298. They had detected HB and BS stars in NGC 2298, but the sample had issues because of its limited spatial resolution and lack of membership analysis for detected stars. Our study detected more than 90 % of HB stars compared to the *HST* and ground-based catalogues, and the PM membership is also confirmed. The stars which are not detected in the FUV images are fainter than the limiting magnitude of UVIT, and the exposure times in all filters are not deep enough to detect them.

Further, we compared the observed HB sequence with theoretical ZAHB and TAHB sequences for standard and enhanced initial helium abundances. The theoretical ZAHB tracks with distinct initial helium abundances could not reproduce the observed colour spread along the BHB sequence. Milone *et al.* (2018) conducted a study of 57 GGCs and found the average difference in helium content

between 2G and 1G stars along the RGB, as well as the maximum variation of helium within each cluster. The maximum helium variation was found to be 0.011 dex in NGC 2298. Our study does not support a large spread in helium along the BHB sequence, based on a comparison of observed HB with theoretical tracks and synthetic HB, though we detect a possible helium difference of 0.1 dex between the BHB stars and the hot HB stars, as suggested by the synthetic HB simulations.

Wenderoth *et al.* (1994) presented a spectroscopic study of an extremely blue star in NGC 2298, classifying it as a helium-rich sdO star, but they could not confirm the membership of this star. In their optical CMD shown in Figure 1, the position of this star coincides with that of EHB or BHk stars. The RA and DEC information of this star is not provided in the above paper. Therefore, we could not check whether this star is detected in our FUV images or not.

It is well established from the photometric as well as from spectroscopic studies that most of the GCs like NGC 2808 and ω Cen, with well-populated HBs, contain helium-rich populations showing discrete HBs, which indicate discrete helium abundances (Dalessandro *et al.* 2011; Moehler *et al.* 2011; Marino *et al.* 2014). The four hot HB stars in NGC 2298 are found to be helium-rich with respect to BHB stars with a standard helium abundance. This may suggest that these stars are products of helium-rich second-generation stars in this cluster. However, the helium-rich population will be hard to be detected due to their small number fraction compared to the normal- or slightly enhanced initial helium abundance in the MS to RGB stages of NGC 2298.

Our T_{eff} estimation for three hot HB stars covers a range from 35,000-40,000 K, whereas T_{eff} of BHB stars ranges from 7,500-12,250 K. We could not accurately estimate the T_{eff} of UV4 star, but the temperature of this star can be around ∼100,000 K. Comparing both T_{eff} and luminosity of hot HB stars with evolutionary tracks implies that three stars have evolved away from the HB, and one is

still in the EHB phase. The hot HB stars also have lost more mass in the RGB (∼0.1-0.2 $M_{\odot}$ than the BHB stars).

Many authors put forward several formation scenarios to account for the existence of EHB and BHk stars in GCs, apart from helium enhancement. Lei *et al.* (2015) proposed that BHk stars could be the result of binary interactions. They suggested that the tidal enhancement of the stellar wind during binary evolution might cause substantial mass loss on the RGB, resulting in the formation of BHk stars. Nevertheless, our SED fits of hot HB stars do not show the signature of binarity, hence, could not support the origin through the binary interaction scenario. The other formation channel suggested for EHB and BHk stars, such as the hot-flasher scenario, is described in detail in Section 4.5.2. Sweigart (1997) demonstrated that when stars experience a late helium-core flash on the WD cooling curve, it leads to flash mixing of the hydrogen envelope with the helium core, resulting in a significant increase in the helium and carbon abundance of the envelope. However, this type of mixing is not possible in the EHF scenario, because the presence of a strong hydrogen-burning shell creates a large entropy barrier that prevents the core helium-burning products from being mixed with the surface.

Brown *et al.* (2012) presented *HST* FUV spectroscopy of hot HB stars including one pHB, five BHB and three unclassified stars with blue UV colours in GC NGC 2808. They also found enhanced helium and carbon abundances in their BHk sample, which could be the result of flash-mixing in the LHF mechanism, whereas EHB stars in their sample exhibit carbon abundances much lower than the cluster value and helium abundances at or below the solar value, that could be the effect of diffusion. The two hot HB stars in our study, UV2 and UV3, are found close to EHF tracks, whereas UV4 is located above the post-BHB track, indicating that UV2 and UV3 could be off-springs of EHB stars, and UV4 is a plausible progeny of BHB star. Therefore, the surface abundances of three stars except UV4 are expected to remain the same if they are products of the early hot-flasher scenario.

Nevertheless, these stars could have helium enrichment, as evident from a comparison with simulations. Further spectroscopic follow-up observations are necessary to confirm the nature of the evolutionary process these stars have gone through.

4.9 Summary and Conclusions

The key findings from this work can be summarised as:

- In this study, we employed UVIT observations in combination with *HST*, *Gaia* EDR3, and ground-based photometric data to examine the HB morphology of the GC NGC 2298. *Gaia* EDR3 data is utilised to obtain the PM members of the cluster in its outer region.

- We constructed optical and FUV-optical CMDs for the member stars. Only BHB and four hot HB stars are identified in all FUV images. Very few BSSs, which are hot and bright, are detected in FUV CMDs.

- Optical and FUV-optical CMDs are overlaid with updated BaSTI-IAC isochrones generated for respective filters to compare the observations with theoretical predictions. The theoretical HB tracks with enhanced alpha and helium abundances could not reproduce the observed colour/magnitude spread among BHB stars in FUV-optical CMDs.

- From the comparison of observed HB with synthetic HB simulations, we found a helium abundance difference between BHB and hot HB stars (Helium enhanced) in this cluster. However, BHB stars have a single initial helium abundance ($Y_{ini} = 0.23$), with probably a very small scatter.

- We estimated T_{eff}, luminosities, and radii of 63 BHB and four hot HB stars by generating SED using multi-wavelength data. The T_{eff} of BHB stars

ranges from 7,500-12,250 K, whereas three hot HB stars span T_{eff} from 35,000-40,000 K. The temperature of the UV4 star is found to be around ∼100,000 K.

- The evolutionary status of HB stars is probed by comparing derived parameters with theoretical evolutionary post-ZAHB tracks. Many BHB stars are found to be located between the ZAHB and TAHB, suggesting that they are evolving off the HB into the pHB phase. These stars have mass in the range of 0.6-0.75 $M_{\odot}$. Some of the BHB stars are found to be evolving towards the peAGB phase.

- We found a sub-luminous sdB companion to an RHB star in the cluster. From the comparison with the ELM WD evolutionary tracks, the mass of the sdB turns out to be ∼0.187 $M_{\odot}$, and likely to be evolving into a helium core WD. We suggest that it is probably an ELM WD candidate formed from mass transfer in this binary system.

- Out of four hot HB stars, we find that two have already evolved off the EHB phase, and they are in the AGBM phase. One star is located between the ZAHB and TAHB tracks, and hence it is a confirmed EHB star, likely to be helium enriched. One star is found to match with the theoretical prediction of the early hot-flasher scenario (and maybe one more), whereas another star has evolved off the peAGB phase and is probably evolving towards the WD cooling stage. The theoretically expected number of pHB stars matches well with the actual number observed.

- As the late and early hot-flashers are supposed to have different chemical signatures; the pHB stars are targets for further spectroscopic studies in order to explore their nature to constrain their formation pathways.

4.10 Additional plots:

The details of the SED fitting technique are described in Section 6.5. The SEDs for 61 BHB stars are shown in Figure 12.

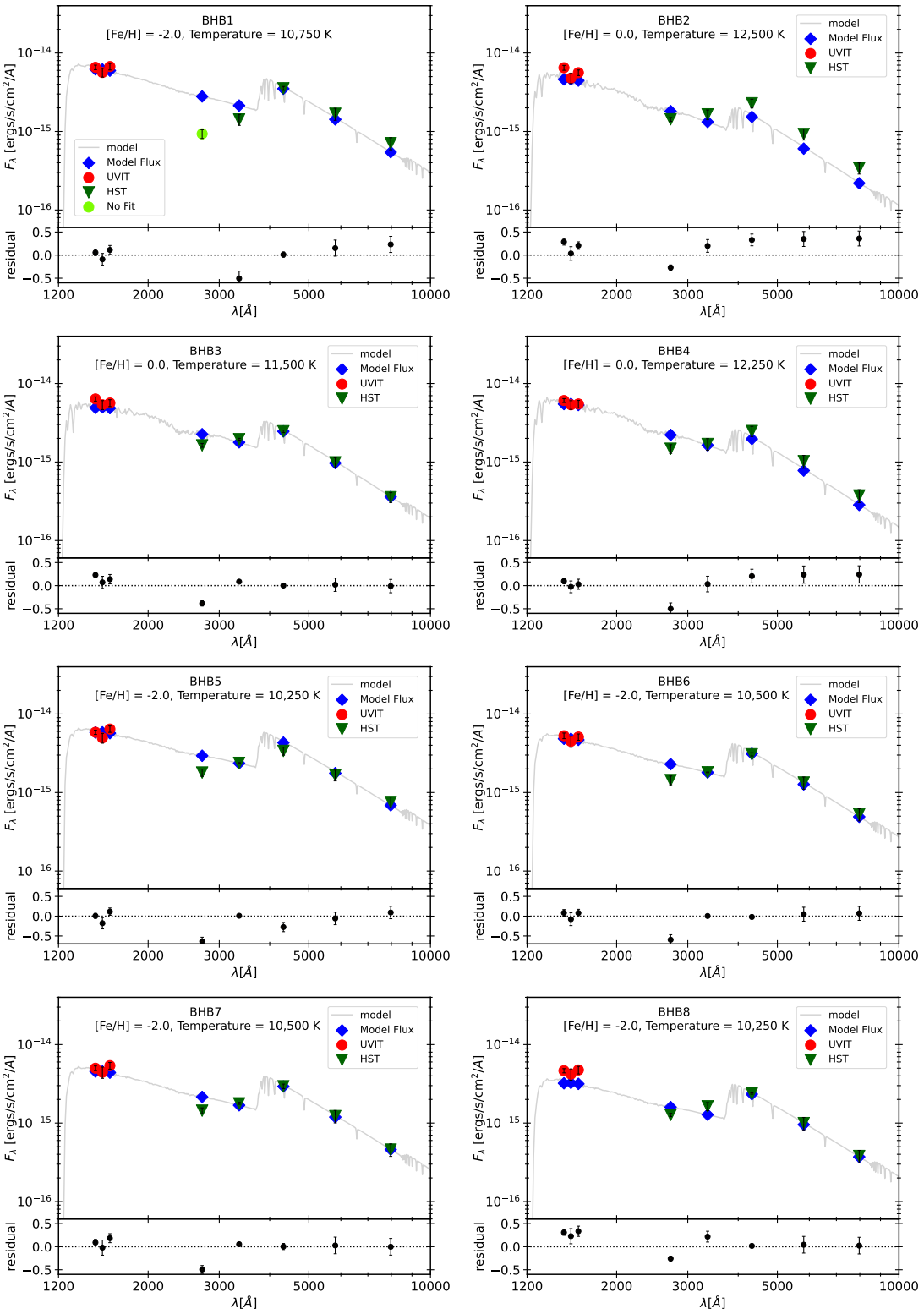

FIGURE 12: SEDs of rest of the BHB stars. The best-fit parameters are mentioned in the figure. The UVIT, *HST* data points used to create SEDs for stars lying in the inner region are shown with red circles and green inverted triangles, respectively. For the stars lying in the outer region, UVIT, *GALEX*, Ground-based photometric, *Gaia* EDR3, and 2MASS data points are shown with red circles, green squares, orange triangles, cyan inverted triangles, and purple diamonds, respectively.

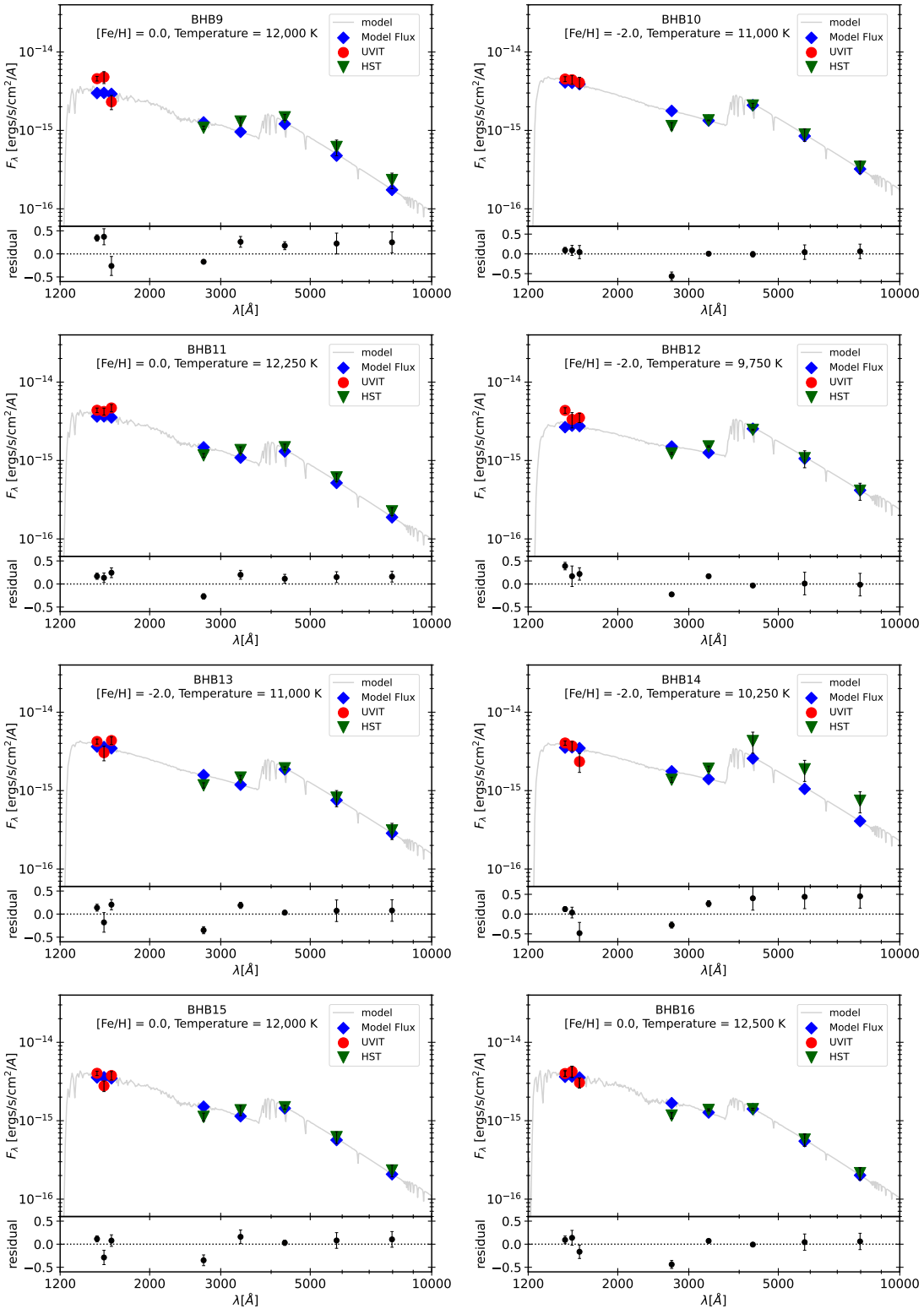

FIGURE 12: Continued.

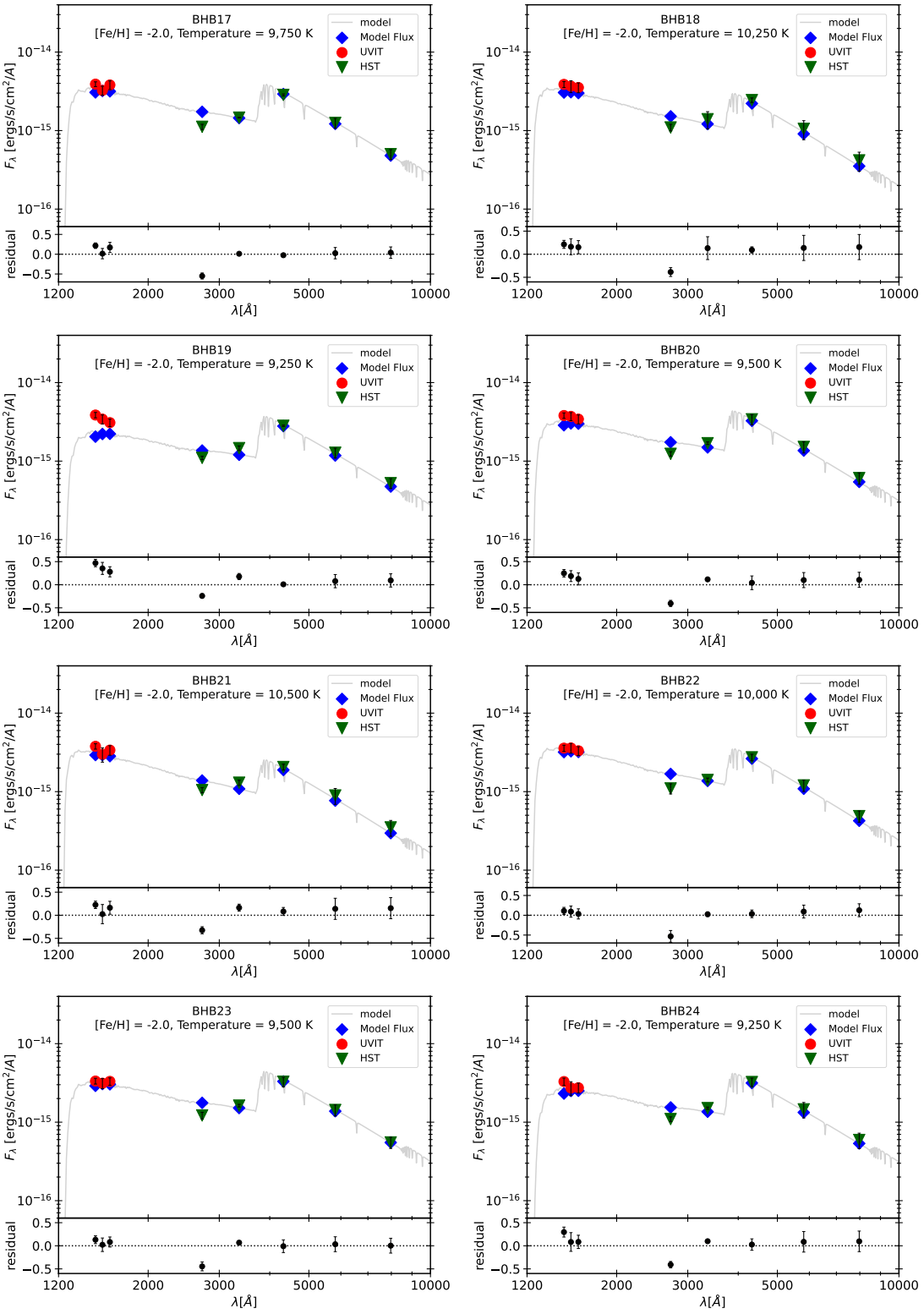

FIGURE 12: Continued.

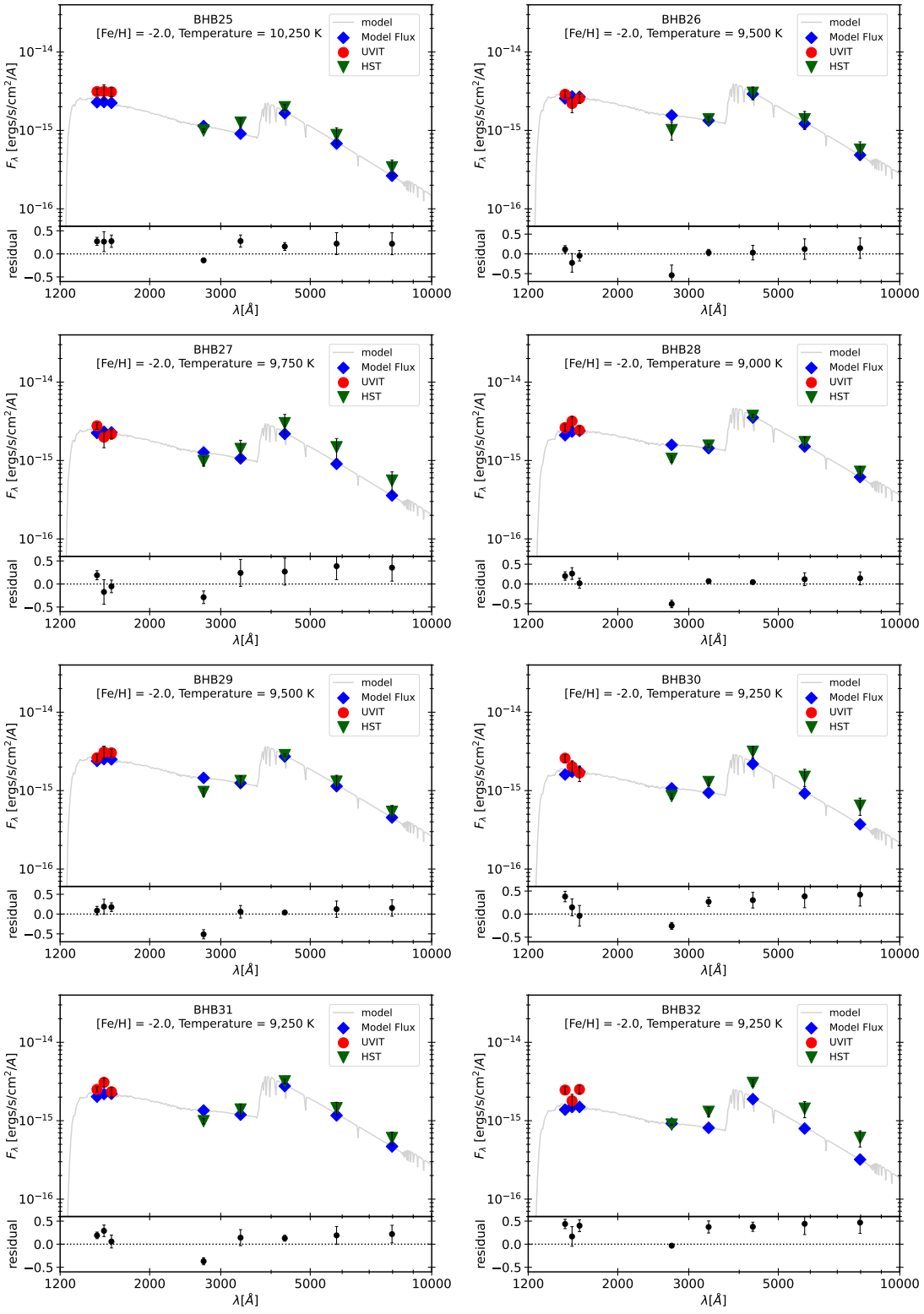

FIGURE 12: Continued.

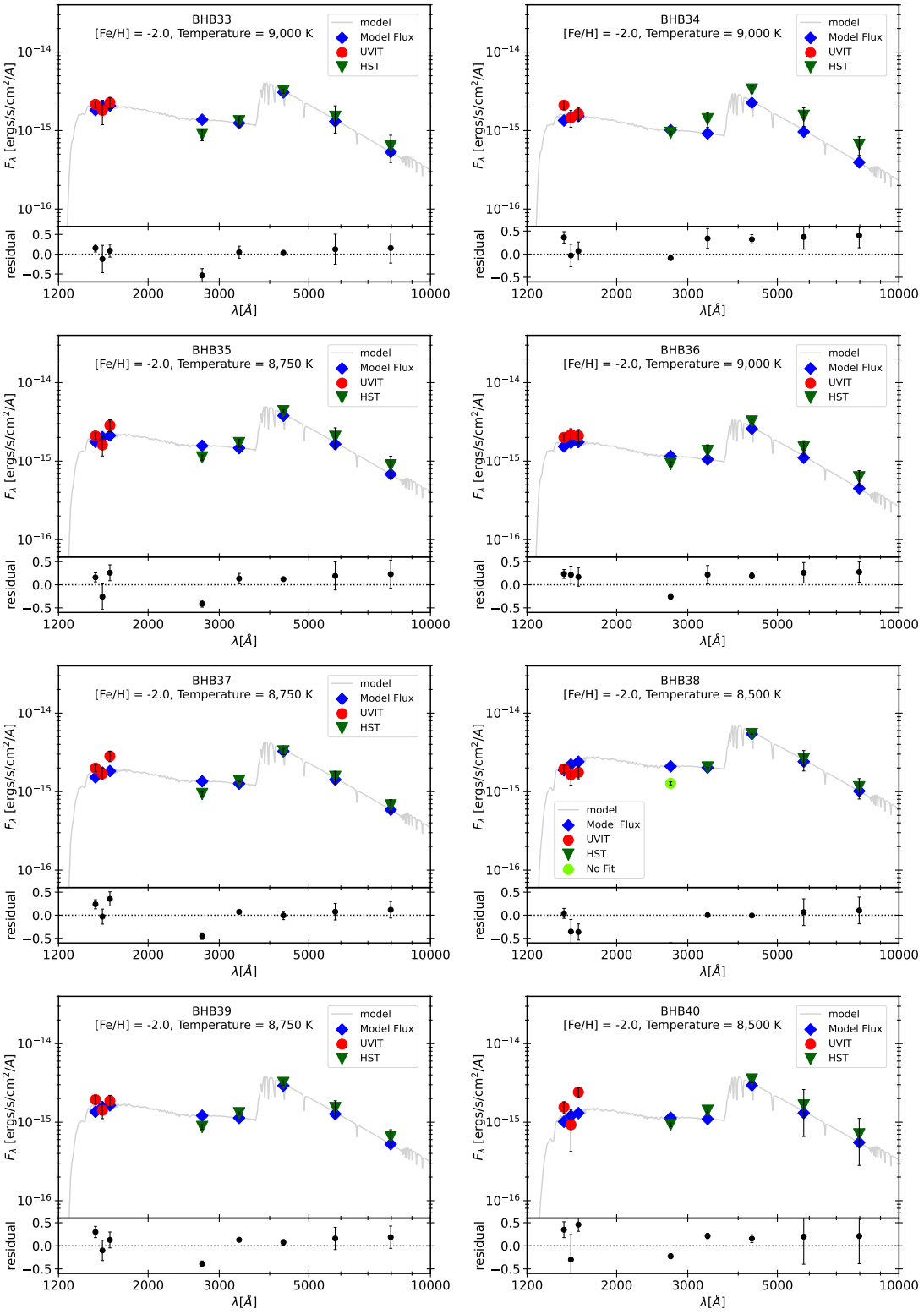

FIGURE 12: Continued.

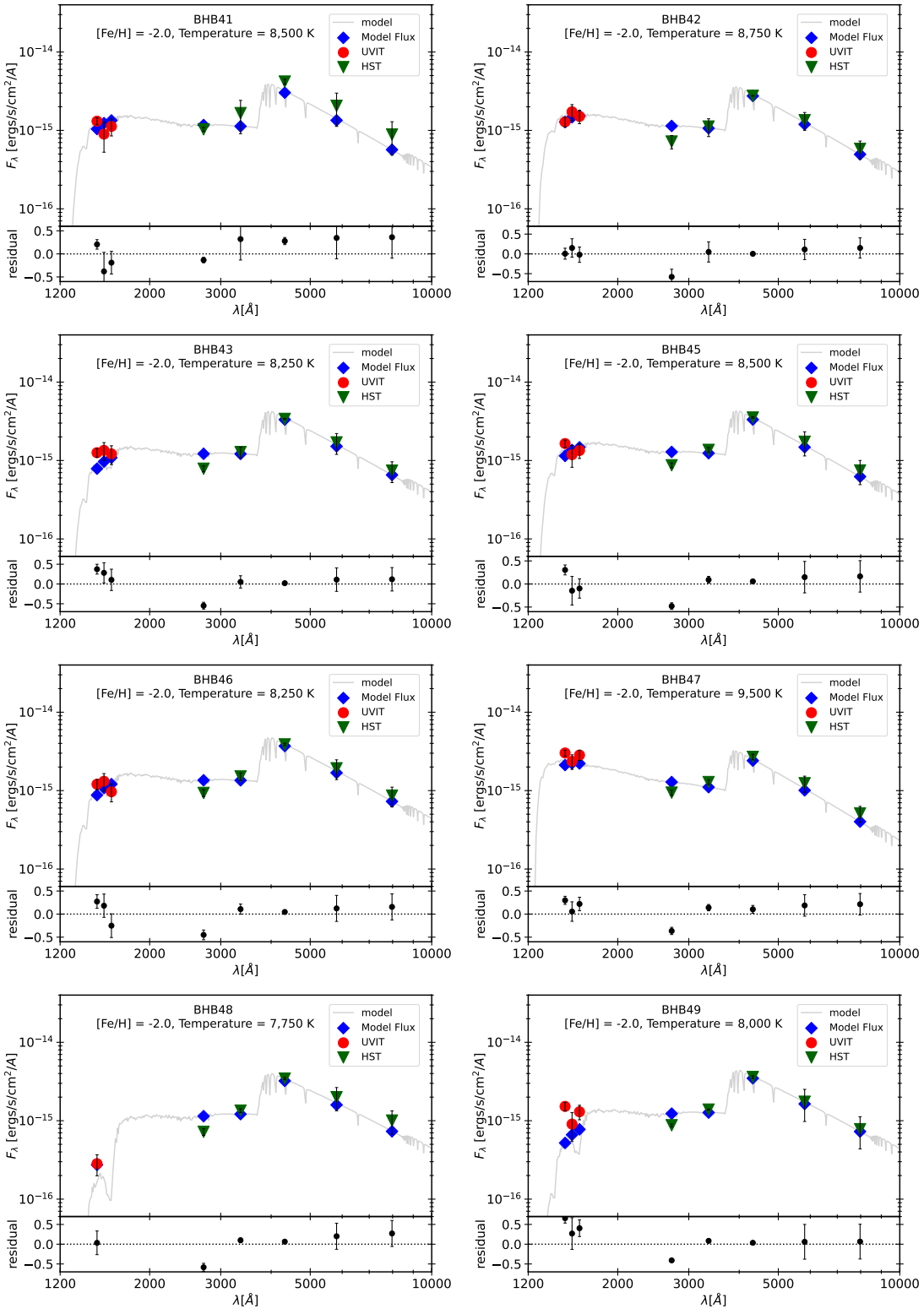

FIGURE 12: Continued.

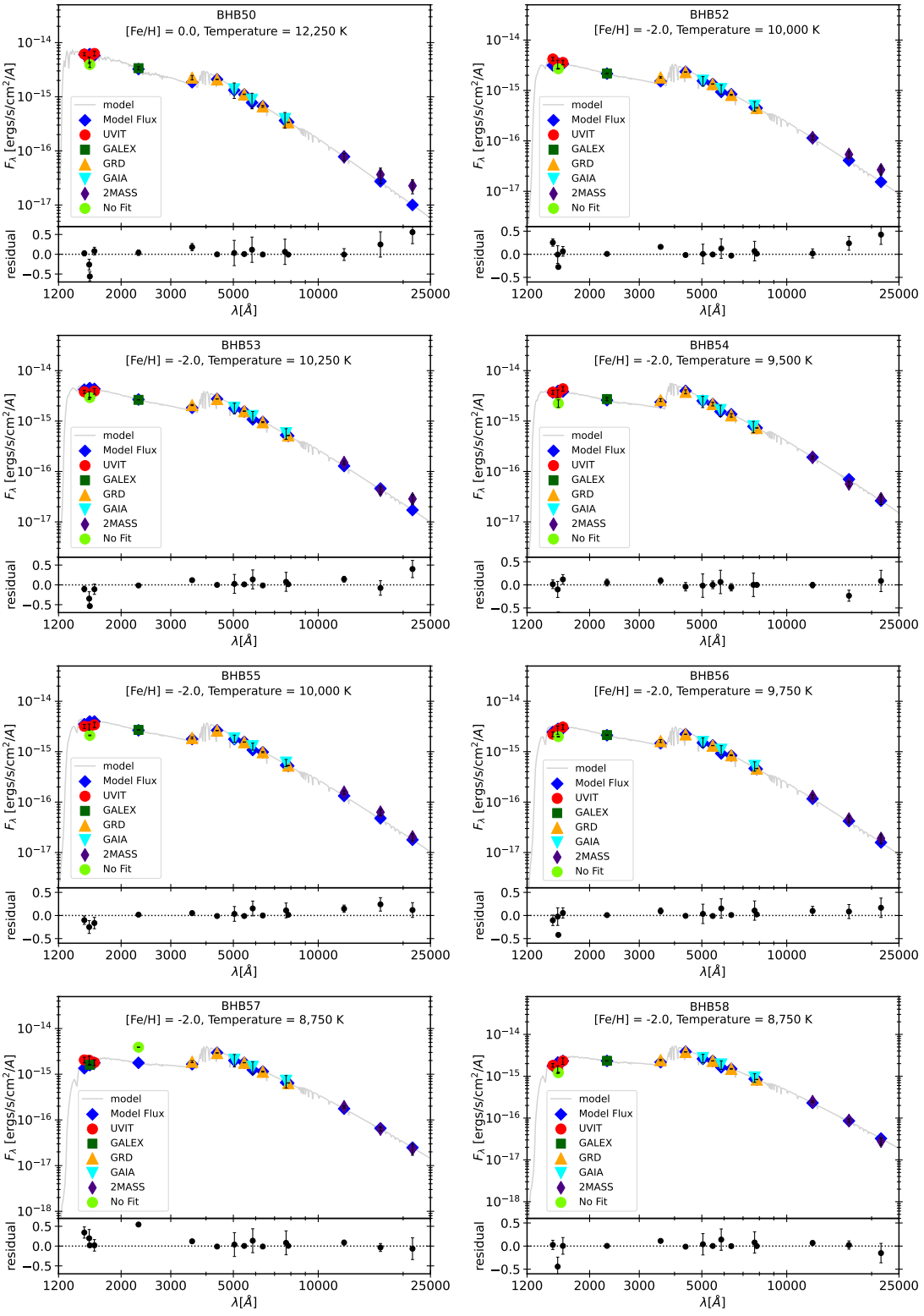

FIGURE 12: Continued.

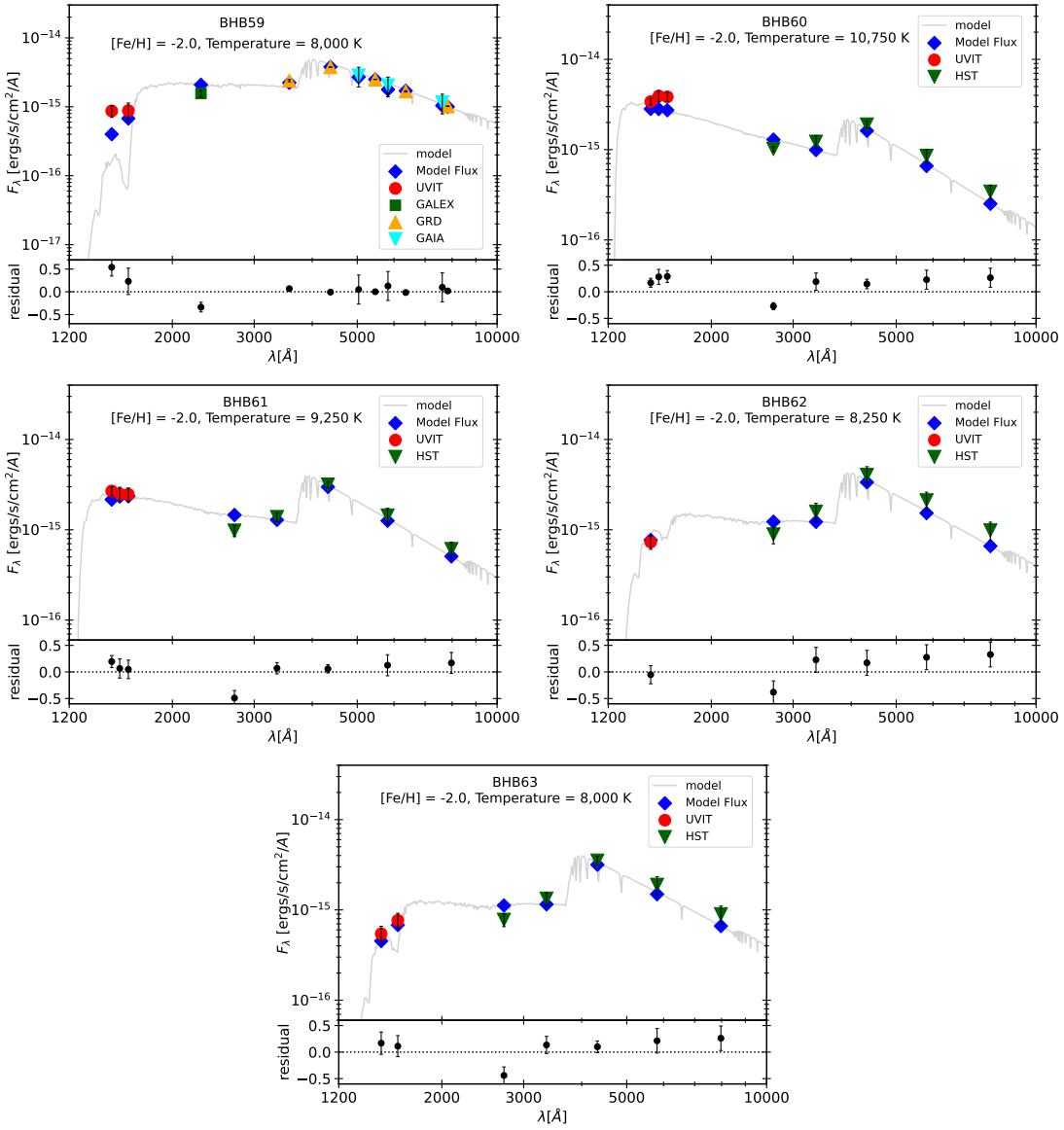

FIGURE 12: Continued.

Chapter 5

Investigation of UV bright stellar populations in NGC 188[†]

5.1 Introduction

In this chapter, we analyse one of the oldest and most well-studied OC, i.e., NGC 188 in our Galaxy. The cluster is studied widely due to its richness, metallicity, age, and its location in the Galactic plane ($\alpha_{2000} = 0^h47^m12^s.5$, $\delta_{2000} = +85°$ 14′ 49″, $l = 122.^\circ85$, $b = +22.^\circ38$). The age of this cluster is determined to be 7 Gyr (Sarajedini *et al.* 1999), and the reddening of the cluster is 0.036 ± 0.01 mag (Wang *et al.* 2015). This cluster is located at a distance of 1866 pc (Gao 2018), and the metallicity is found to be solar (Sarajedini *et al.* 1999).

Till now, a few hot subdwarfs and HB stars have been detected in two metal-rich and old OCs, i.e., NGC 6791 and NGC 188 (Kaluzny and Udalski 1992; Liebert *et al.* 1994; Green *et al.* 1997). Only one sdB star is found in NGC 188, whereas

[†]Results of this work are published in Rani *et al.* (2021c).

NGC 6791 hosts five sdB stars. Schindler *et al.* (2015) investigated 15 OCs to understand the formation of EHB stars by taking NGC 188 and NGC 6791 as template clusters. They identified only red giant clump stars, but no EHB stars were detected. The results of the UV imaging of the NGC 188 using three different filters of UVIT (Two FUV & one NUV) are presented in this study. The cluster's basic parameters adopted in this work are listed in Table 5.1.

This chapter's main objectives are 1) to identify the UV bright stars in the cluster by comparing their location in observed UV/optical CMDs to theoretically expected ones from isochrones and 2) to characterise them by analysing SEDs to throw light on their formation and evolution.

5.2 Data and Analysis

All data used in the analysis were taken in three filters: one NUV (N279N) and two FUV (F148W and F172M). The observational details of the NGC 188 UV images are tabulated in Table 2.1 presented in Chapter 2. The science-ready images of the cluster in different filters were generated using CCDLAB. The image of the cluster acquired with UVIT using the F148W FUV and N279N NUV filter is depicted in Figure 1, with blue representing the FUV detections and yellow representing the NUV detections.

Aperture photometry was carried out on the FUV F172M image to get the estimate of counts. We performed PSF photometry on one FUV F148W and NUV N279N image as described in chapter 2. The PSF-fit errors in estimated magnitudes are presented in Figure 2 as a function of magnitude for FUV and NUV filters. The stars as faint as 22 mag are detected both in FUV and NUV images with typical errors of 0.2 mag and 0.3 mag, respectively.

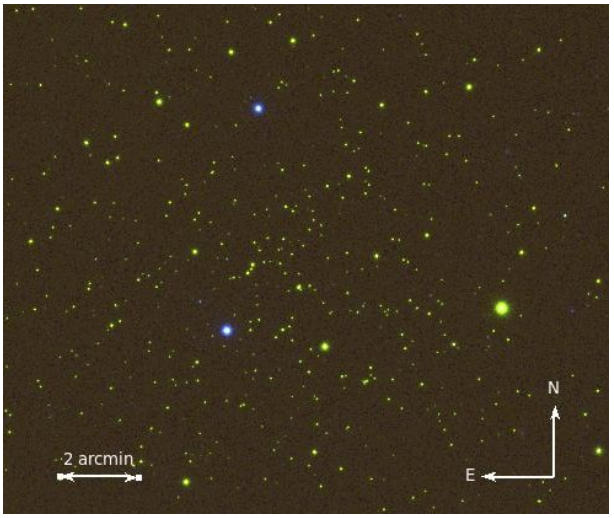

FIGURE 1: UVIT image of NGC 188 obtained by combining images in NUV (N279N) and FUV (F148W) channels. Yellow and blue colour corresponds to NUV and FUV detections, respectively.

TABLE 5.1: NGC 188 basic parameters utilised in this work.

Parameters	Values	References
Metallicity (Z)	0.02 dex	Wang *et al.* (2015)
Age	7 ± 0.5 Gyr	Sarajedini *et al.* (1999)
Distance modulus, $(m - M)_V$	11.44 mag ± 0.08 mag	Sarajedini *et al.* (1999)
Reddening, $E(B-V)$	0.036 ± 0.01 mag	Wang *et al.* (2015)

5.3 Results

5.3.1 UV and Optical Colour Magnitude Diagrams

To categorise the stars detected by UVIT into different evolutionary stages, we have employed ground-based optical photometric data (Sarajedini *et al.* 1999) of NGC 188 to cross-identify with the UVIT-detected stellar sources. First, we have selected stars with PM membership probability of more than 50% as the most likely members of the cluster from the catalogue given by Platais *et al.* (2003),

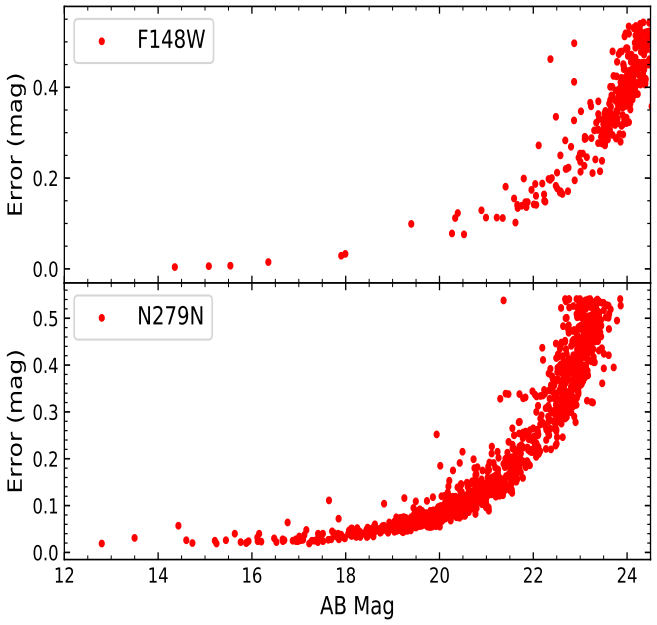

FIGURE 2: PSF fit errors as a function of magnitude for the UVIT observations of NGC 188. The top panel shows the errors for the FUV F148W filter, whereas the bottom panel shows the NUV N279N filter.

which gives us 562 member stars. Then we have cross-matched optical photometric data taken from Sarajedini *et al.* (1999) with the PM catalogue. Geller *et al.* (2008) presented the results of the RV survey of NGC 188 using WIYN data. They measured the radial velocities for 1046 stars in the direction of NGC 188 and further calculated the RV membership probability for all the stars. Out of 1046 stars, 473 stars are found to be likely cluster members. Further, we cross-matched optical data with the RV catalogue to check for the RV membership probability. After choosing all the cluster's PM and RV members, we cross-matched with UVIT-detected stars in all three filters. We have also included the stars for which PM membership probability is given, but RV membership is unknown. We identified 356 stars of NGC 188 as members of the cluster in the NUV passband, and 10 cluster members in both FUV passbands. The accuracy of this cross-match is within 1.″5. 24 BSS candidates have been catalogued by Ahumada and Lapasset (2007). According to Geller *et al.* (2008), 20 BSSs were confirmed to be members

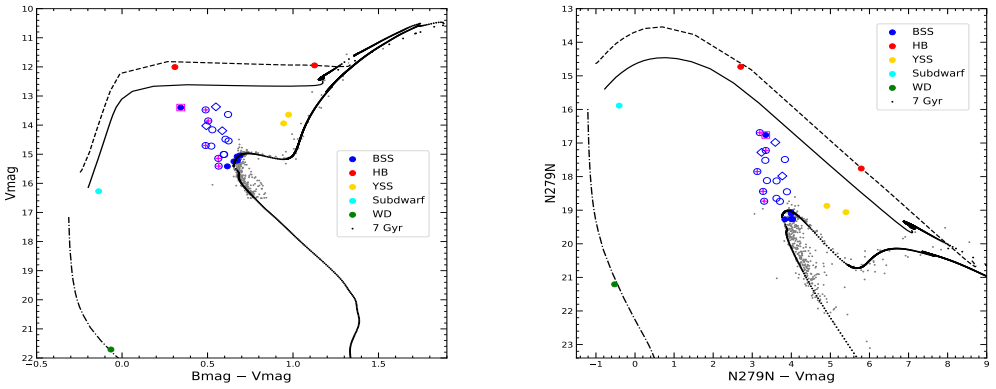

FIGURE 3: (Left panel) Optical CMD of NGC 188 of all member stars co-detected with UVIT N279N filter and optical photometric data. (Right panel) NUV-optical CMD of NGC 188 of member stars cross-identified using UVIT N279N data with optical photometric data. The meaning of all the symbols is marked in the figures. Previously known binary and single BSSs are shown as open blue circles and open blue diamonds, respectively. The BSSs with WD detections are shown with a magenta plus symbol. The BSS outlined with a magenta square symbol is bright in both NUV and FUV CMDs. The over-plotted black colour dots represent updated BaSTI-IAC model isochrones generated for an age 7 Gyr and solar metallicity. The solid and dashed lines shown along the HB track correspond to ZAHB and TAHB, respectively. The dashed-dotted black line indicates the WD cooling sequence for a WD with mass $0.5M_{\odot}$.

of the cluster based on their RV membership.

As there are many stars detected in the NUV, the detected members are segregated based on their detection in the NUV. In the NUV filter, we detect the MS, turn-off, SGB, RGB, BS, and YS stars, whereas in FUV images, only hot and bright stars are detected. We have detected 21 BSSs previously known in the literature, out of which sixteen are RV members, and five are PM members. One previously known hot subdwarf is also detected in both FUV and NUV images, but RV membership for this star is not known as it is fainter than 16 mag in optical CMD. Two YSSs are selected on the basis of their position in the optical CMD. We have also detected one very bright and hot star in NUV and one FUV image, probably a WD candidate. Both PM and RV memberships are unknown for this star. The optical and UV-optical CMDs, as illustrated in Figures 3 and 6, were created using

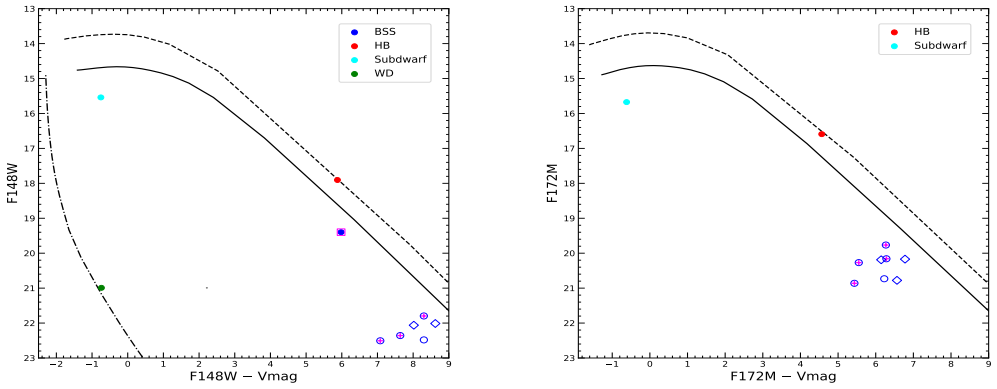

FIGURE 4: FUV-optical CMDs of NGC 188 of member stars cross-identified using UVIT FUV and ground-based optical photometric data. Other details are the same as in Figure 3.

only the stars that have been confirmed as members. The optical and UV-optical CMDs are over-plotted with updated BaSTI-IAC isochrones (Hidalgo *et al.* 2018). The updated BaSTI-IAC* isochrones are obtained for an age of 7 Gyr, a distance modulus of 11.44 mag (Sarajedini *et al.* 1999), and a solar metallicity with helium abundance of Y = 0.247, $[\alpha/\mathrm{H}] = 0$, including diffusion, overshooting, and mass loss efficiency parameter $\eta = 0.3$. The BaSTI-IAC model also provides the HB tracks, which incorporate ZAHB, post-ZAHB tracks and TAHB with or without diffusion for a selective mass range. We created the ZAHB and TAHB tracks for solar metallicity, including diffusion.

The overlaid BaSTI-IAC isochrones fit well with the observations in both optical and NUV-optical CMDs, as shown in Figure 3. This is probably the first UV CMD for this well-studied cluster in the NUV; the overlaid isochrones match the observed sequence more or less satisfactorily. The CMDs shown in figure 3 suggest that this cluster probably has an HB population with stars in the HB. Two stars marked with red colour are lying along HB tracks, implying that these stars may belong to the HB evolutionary phase. In fact, they are lying close to the TAHB track, indicating that they are about to evolve off the HB phase. The previously

*http://basti-iac.oa-abruzzo.inaf.it/

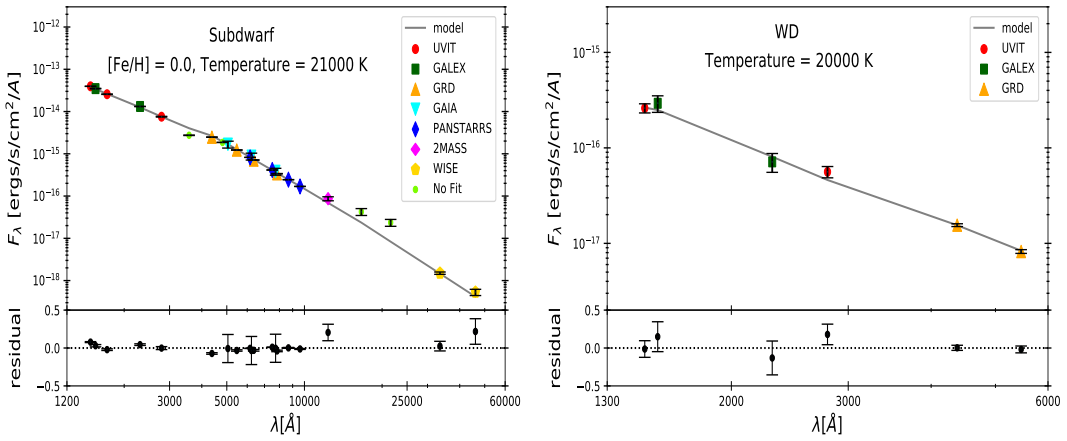

FIGURE 5: SED of a hot subdwarf and WD candidate detected with UVIT after applying corrections for extinction. The optimal fit parameters are also displayed.

known subdwarf is found close to the blue part of the ZAHB track in an optical CMD and fainter than the blue end in UV CMDs. We also plotted a WD cooling track for a 0.5 $M_\odot$ WD with hydrogen envelope with a dashed-dotted black line in Figures 3, and 6 provided by Tremblay *et al.* (2011) to define the location of WDs in all CMDs (P. Bergeron, private communication). Note that the star marked with green colour in all CMDs is lying along the WD cooling track, indicating that the star is a possible WD candidate, although its membership is uncertain. We have also detected two stars that are bright in NUV CMD with respect to other giants shown with yellow colour in the optical as well as in NUV-optical CMD (See Figure 3). In the optical CMD, these two stars are bluer than the RGB and brighter than the SGB track; hence, they are classified as YSSs.

5.3.2 SEDs of UV bright stars

In this section, our main goal is to check the evolutionary status of stars, which appear bright in NUV and FUV CMDs, by determining their stellar parameters using the SED fit technique. We constructed the SEDs to estimate the stellar parameters of stars which appear bright and hot in the UV CMDs.

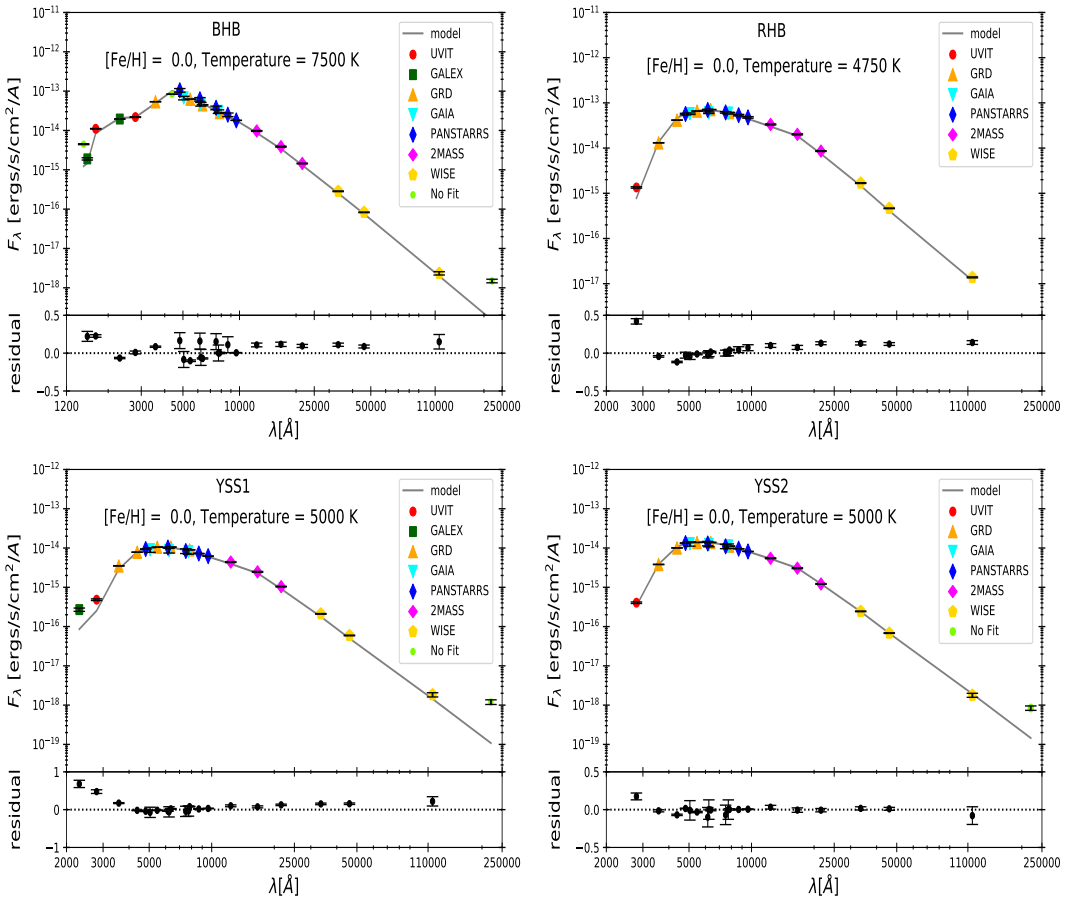

FIGURE 6: SED of two HB stars (upper panels) and two YSSs (lower panels) detected with UVIT after correcting for extinction. The best-fit parameters are displayed in the figure.

Kurucz stellar atmospheric models (Castelli *et al.* 1997; Castelli and Kurucz 2003) are used to construct SEDs for two HB, one subdwarf, and two YS stars which are bright in the NUV band when compared to RGB stars. The model provides the temperatures ranging from 5,000-50,000 K, log g from 0-5 dex, and metallicity from -2.5-0.5 dex. Since this cluster has solar metallicity, we selected the metallicity $[\mathrm{Fe/H}]$=0 dex, nearly the same as the cluster metallicity. We have given a T_{eff} and log g range from 5,000-50,000 K and 2-5 dex, respectively, for the adopted Kurucz models to fit the SEDs of the above-mentioned stars. We have combined three UVIT photometric data points with two *GALEX*, five ground photometry, three *Gaia*, five PANSTARRS, three 2MASS, and four *WISE* photometric data points to generate SEDs for UV bright stars. The actual number of data points

TABLE 5.2: SED fit parameters of bright stars detected with UVIT in this cluster. Column 1 lists the star ID used in this work. Column 2 represents the identification number (WOCS ID) according to Platais *et al.* (2003). Columns 3 to 5 show the RA, DEC, and model used for SED fit, respectively. The rest of the columns give the estimated values of various parameters along with errors. The last column contains the ratio of the number of photometric data points used for SED fitting and the number of total data points available for fitting.

Star ID	PKM ID	RA (deg)	DEC (deg)	Model	T_{eff} (K)	$\frac{L}{L_\odot}$	$\frac{R}{R_\odot}$	χ^2_{red}	$\frac{N_{fit}}{N_{tot}}$
Subdwarf	WOCS 4918	11.96753	85.31897	Kurucz	21000 ± 500	6.71 ± 0.22	0.19 ± 10^{-3}	14.23	19/23
WD	WOCS 4073	10.32108	85.23638	Koester	20000 ± 312	0.039 ± 0.003	0.02 ± 10^{-4}	0.95	6/6
BHB	WOCS 3856	9.77341	85.15604	Kurucz	7500 ± 125	49.13 ± 7.49	4.13 ± 0.01	32.92	22/25
RHB	WOCS 5027	11.98741	85.24889	Kurucz	4750 ± 125	73.83 ± 3.97	12.56 ± 0.03	30.85	20/20
YSS1	WOCS 4705	11.34416	85.21065	Kurucz	5000 ± 125	10.28 ± 1.33	4.26 ± 0.01	38.99	21/22
YSS2	WOCS 4346	10.64712	85.22385	Kurucz	5000 ± 125	13.63 ± 1.95	4.94 ± 0.01	5.6	20/21

used for fitting will be equal to or less than the above-mentioned data points, as not all stars are detected in all filters. The data points, which were not fitting well to the theoretical model, are also excluded from the fit. We have also constructed SED for a possible WD detected with UVIT in both FUV and NUV images using a Koester WD model (Tremblay and Bergeron 2009; Koester 2010). The free parameters of the Koester model are T_{eff} and $\log g$. The T_{eff} value for the Koester model ranges from 5,000-80,000 K, and $\log g$ value from 6.5-9.5 dex. We have used two UVIT photometric data points along with two *GALEX* and two Ground photometric data points to fit the SED of the WD. VOSA makes use of Fitzpatrick reddening relation (Fitzpatrick 1999; Indebetouw *et al.* 2005) to correct for extinction in observed data points.

Best SED fits are obtained for six stars, out of which two are HB, two are YSSs, one is Subdwarf, and one is WD. All star's SEDs are illustrated in Figures 5 and 6. We can notice in Figures 5 and 6 that all the data points are fitted well with the models. The estimated values of stellar parameters from the SED fit, along with errors, are tabulated in Table 5.2. The high temperature of the subdwarf (21,000 K) suggests that it belongs to the category of sdB stars (Heber 1986). The T_{eff} of the WD turns out to be 20,000 K with a radius 0.02 $R_\odot$, which confirms the

star to a possible WD candidate.

To assign the evolutionary stage to the HB stars identified with UVIT, we have plotted the theoretical evolutionary tracks utilising the updated BaSTI-IAC models presented by Hidalgo *et al.* (2018). The models are selected with metallicity close to the cluster metallicity. The evolutionary tracks from MSTO to the moment a star has entered the pHB phase are shown in the H-R diagram in Figure 7. We used DA-type WD models for 0.4 and 0.5 $M_{\odot}$ from Tremblay *et al.* (2011) to show the WD cooling tracks. The ZAHB and post-ZAHB tracks are shown for a mass range from 0.475$M_{\odot}$ to 0.8$M_{\odot}$. The TAHB is shown with a dash-dotted line in Figure 7. For WDs, the cooling sequences for 0.4 and 0.5 $M_{\odot}$ DA-type WDs are shown with a dash-dotted and solid grey line, respectively. The parameters obtained from the SED fit for six stars are depicted on the H-R diagram. The stars are marked with the same colour as in Figure 3. We can see in Figure 7 that HB stars are lying along the HB tracks suggesting that these two stars belong to the HB evolutionary phase. It can be noted that two YSSs are lying near the theoretical RGB sequence on the H-R diagram. It indicates that these two stars might belong to a giant evolutionary stage. The WD on the H-R diagram is located near the theoretical WD cooling sequence, implying that the star is likely to be a WD candidate.

5.4 Discussion

In the NUV passband, we have detected 2 HB, 21 BSSs, 2 YSSs, one hot Subdwarf, and one WD candidate along with MS, MSTO, SGB, and RGB stars, whereas, in FUV, only hot and bright BSSs, WD, Subdwarf and HB stars are detected. For comparison with theoretical predictions, we overlaid the CMDs with updated

BaSTI-IAC and WD model isochrones generated for respective UVIT and Ground-based filters. The UV magnitude distribution of all the detected member stars with UVIT is reproduced well with theoretical isochrones. Out of 21 BSSs detected with UVIT, 15 BSSs are characterised by Gosnell *et al.* (2014, 2015) using SED fitting technique. They found hot and young WD companions to 7 BSSs, out of which 5 are detected in our UVIT images. 7 BSSs binaries are likely formed from the mass transfer. The other 6 BSSs are not studied in detail in literature till now. We detected one BSS, which is both FUV and NUV bright. This BSS is a PM member of the cluster, but RV membership is not known. Detailed SED analysis is required to check whether the BSS has any hot companion. We plan to characterise the hot companions of the BSSs of this cluster in a separate study and assess their nature by placing them on the H-R diagram (Figure 7).

Out of three UV-bright stars identified with UIT, one star II-91 (numbered by Sandage 1962) is detected in both NUV and FUV images, and here it is designated as a subdwarf. This star was first identified by Sandage (1962) and used for calibration. Later Dinescu *et al.* (1996) confirmed its membership based on the PM. Green *et al.* (1997) performed the spectroscopy of UV-bright stars in OCs NGC 188 and NGC 6791. They reported that the II-91 star is an sdB star and also a spectroscopic binary. In fact, it is a close binary of 2.15 days orbital period (Green *et al.* 2004). Landsman *et al.* (1998) estimated the effective temperature of II-91 about 30,000 K from its UIT magnitude and $m_{152} - V$ colour. Our study confirms this star's UV-bright nature. The T_{eff} measured from SED fitting also confirms it to be an sdB or EHB star.

The T_{eff} of one HB star derived from SED analysis is found to be 7,500 K, which is in the range of the T_{eff} of a BHB star. For the other HB star, the derived temperature is 4,750 K, hence likely to be an RHB star in the cluster. The observed UV magnitudes of HB stars match well with theoretical TAHB isochrones, which indicates that these stars are about to evolve off the HB phase, assuming that

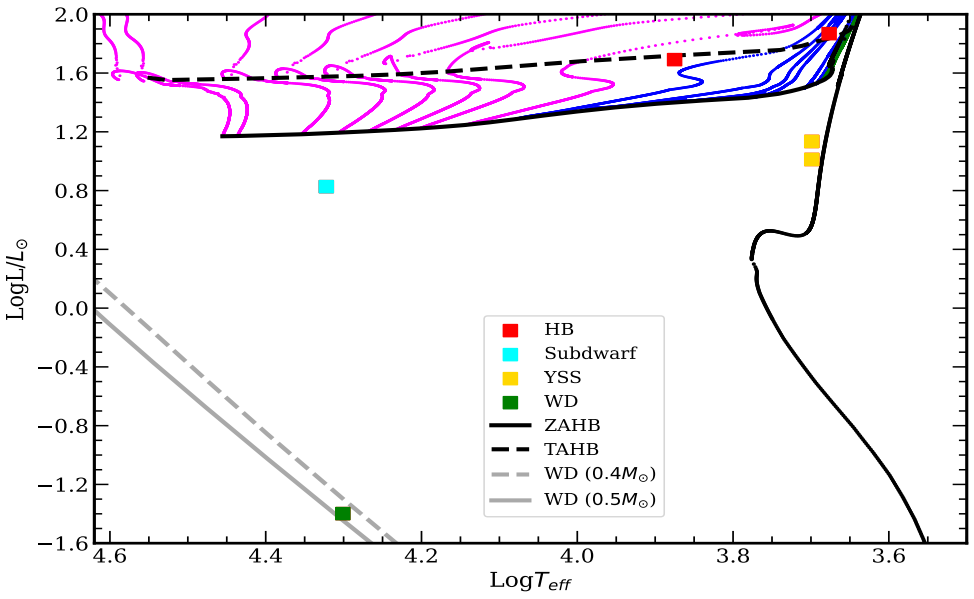

FIGURE 7: H-R diagram of UV-bright stars in NGC 188 compared to theoretical evolutionary tracks. The evolutionary tracks starting from MSTO to the moment when a star has entered the pHB phase (Hidalgo *et al.* 2018) are shown. Along the HB phase, Post-ZAHB tracks span a mass range from 0.475-0.8 $M_{\odot}$. In the plot, magenta, blue and green colours correspond to the sequences populating the extreme, blue, and red parts of the HB. The Black solid and dashed lines indicate the ZAHB and TAHB, respectively. The dash-dotted and solid grey line corresponds to the cooling tracks for 0.4 and 0.5 $M_{\odot}$ DA-type WDs. The SED fit parameters of HB stars, Subdwarf, WD, and YSSs identified with UVIT are shown with red, cyan, green, and yellow square-filled symbols, respectively.

these are, in fact, HB stars. Geller *et al.* (2008) classified BHB star as a rapid rotator (RR) and binary likely non-member (BLN) as they were unable to measure its RV because of its high rotation. Nevertheless, it is a confirmed PM member of the cluster with a membership probability of more than 80% (Platais *et al.* 2003). According to Dinescu *et al.* (1996), RHB (D719) is identified as one of the brightest giants in NGC 188.Belloni *et al.* (1998) identified X-ray sources in OCs M67 and NGC 188 using ROSAT observations. The RHB (X29) star has been identified as an X-ray source within the cluster. The spectroscopic study of this star (Harris and McClure 1985) found it to be a fast rotator with rotation velocity ~ 24 kms^{-1} and also this star exhibits emission in the Ca K and H and Hα lines. The absence of RV variations suggests that this star is a single, rapidly rotating giant, an FK

Comae-type star. Our SED fit of the RHB star also suggests that it is a single star. From V mag and B−V colour, the T_{eff} of this star was estimated to be ∼4,800 K. Our temperature measurement for the RHB star is in close agreement with previous estimations. We suggest that the chromospheric emission of this star might make it bright in the NUV region.

Two YSSs characterised in this work are also RV members, and the YSS2 star is previously identified as a giant and single member. Geller *et al.* (2008) suggested that YSS1 is a double-lined SB (SB2). Mazur and Kaluzny (1990) identified YSS1 as a variable star (V11). They also suggested that YSS1 might be an RS CVn-type binary. Gondoin (2005) studied the X-ray sources in NGC 188 using *XMM-Newton* observations, and he identified YSS1 (S18) star as an X-ray source. He also estimated the bolometric luminosity and effective temperature of this star about ∼8 $L_{\odot}$ and 5,110 K, respectively. Landsman *et al.* (1997) obtained spectra of the yellow giant S1040 in the OC M67 and found that the star is a single-lined SB (SB1). They estimated the effective temperature of a cool component as 5,150 K with a radius 5.1 $R_{\odot}$. Our estimation of luminosity (∼10 $L_{\odot}$), radius (∼5 $R_{\odot}$) and T_{eff} (5,000 K) of the YSS1 from SED fitting is close to this value. As YSS1 is an SB2, it might have two components with a similar temperature. From SED fitting, we can not separate two components with a similar temperature present in a binary system. The SED fit parameters for two YSSs indicate that these two stars may belong to the giant phase. Thus UV emission in the NUV region in the case of YSS1 is likely due to chromospheric activity, likely to be linked to its binary nature and X-ray emission.

von Hippel and Sarajedini (1998) studied the WDs in NGC 188 using the WIYN 3.5-meter telescope at KPNO. They identified 9 WD candidates, of which 3−6 are expected to be cluster members. Andreuzzi *et al.* (2002) identified 28 candidate WDs in the cluster using the data in *HST* WFPC2 F555W and F814W filters, but

their membership was not certain. We have also identified one possible WD candidate in one NUV and one FUV band. We checked with the previously available catalogue, but this star is not reported in the earlier studies.

5.5 Summary

The important results from this study are summarised below:

- In this study, we employed UVIT observations on-board *AstroSat* to identify UV-bright stars in the well-known old OC NGC 188. We further created the optical and UV-optical CMDs of member stars co-detected using UVIT and ground-based data in this cluster.
- Stars at the different evolutionary stages, namely, MS, SGB, and RGB, are detected in NUV image, but only hot stars are detected in FUV images.
- To compare the observations with theoretical predictions, optical and UV-optical CMDs are overlaid with updated BaSTI-IAC and WD models generated for respective UVIT and ground-based filters. The theoretical isochrones match the characteristics of the observed CMDs extremely well.
- This study presents the first NUV CMD for this well-studied cluster. The CMDs analysis suggests that this cluster comprises HB stars, including an RHB, a BHB, and an EHB/sdB star populating a temperature range of 4,750-21,000 K.
- We suggest two YSSs in this cluster based on their location in the CMDs. An excess of UV flux has been observed in YSS1, which could potentially be linked to its binary nature and the presence of X-ray emission.

- We detect a candidate WD from the UV images and is found to have parameters similar to that of a 0.5 $M_{\odot}$ WD.

Chapter 6

UV study of NGC 2818: BSSs, YSSs, PN, and their membership[†]

6.1 Introduction

In this chapter, we study OC NGC 2818, which has the unique distinction of being one of the Galactic OCs probably associated with a PN, and interestingly, the name NGC 2818 is assigned to both an OC and a PN. Most importantly, the membership of the PN to the OC is still debated. The age of this cluster is estimated to be ∼800 Myr, and its reddening value is E(B−V) = 0.2 mag (Sun *et al.* 2021). The distance estimated to this cluster in the most recent study is 3250 ± 300 pc, and the metallicity is found to be solar (Sun *et al.* 2021). In this work, we analyse both the cluster and the PN, NGC 2818.

NGC 2818 is one of the OCs that shows an eMSTO phenomenon (Bastian *et al.* 2018), where the cluster MSTO is extended in the CMD more than expected from

[†]Results of this work are published in Rani *et al.* (2023).

an SSP with conventional evolutionary history. It has been demonstrated that stellar rotation is the most likely explanation for this phenomenon (Bastian and de Mink 2009; Brandt and Huang 2015; Niederhofer *et al.* 2015; Cabrera-Ziri *et al.* 2016; Gossage *et al.* 2019). A spectroscopic study by Bastian *et al.* (2018) showed that, in NGC 2818, stellar rotation is indeed linked to the stars' position on the MSTO of the CMD made using the *Gaia* magnitudes (G) and colour (Gbp−Grp), such that rapidly rotating stars preferentially lie on the red side of the eMSTO. However, the colour range (Gbp−Grp) in optical CMD is relatively small. In contrast, a larger colour range is seen in UV colours, and it is expected that the rotational effects are more prominently displayed in UV colours mainly because of their sensitivity to surface (effective) temperature changes. This study also explores the correlation between the colours derived from UVIT FUV filters and stellar rotation.

This chapter presents the results of the UV imaging of NGC 2818 (both PN and OC) in four FUV filters using UVIT. Our main aims are 1) to identify and characterise the blue and yellow straggler stars in the cluster to shed light on their formation and evolution and 2) to probe the effects of stellar rotation on UV CMDs, 3) to characterise the CSPN to investigate its association with the cluster.

6.2 Data and Analysis

The observations of the cluster used in this work were made in two epochs, the first on 21st December 2018 and the second on 11th June 2020. In the first epoch, the observations were carried out in three FUV filters (F154W, F169M, and F172M), and in the second, observations were performed with deep exposures in four FUV filters (F148W, F154W, F169M, & F172M). We utilised CCDLAB software to create images of the cluster in all FUV filters. To extract the magnitudes of

detected stars in all FUV images, we have carried out PSF photometry on them. The average PSF of the stars in all FUV images is $\sim 1\farcs2$. The details of the UVIT observations of NGC 2818 used in this analysis are tabulated in Table 2.1. In Figure 1, we show the UVIT image of the cluster taken in the FUV F148W band where the orange colour depicts FUV detections. This image exhibits an extended structure displaying the beautiful PN NGC 2818, where the central star can clearly be seen in the FUV. Figure 3 displays the PSF-fit error (median) against magnitude in four FUV filters for profound observations. We have detected stellar sources down to ~ 22 mag with the most PSF-fit errors $\sim$0.3 mag in all FUV filters and considered them for further analysis.

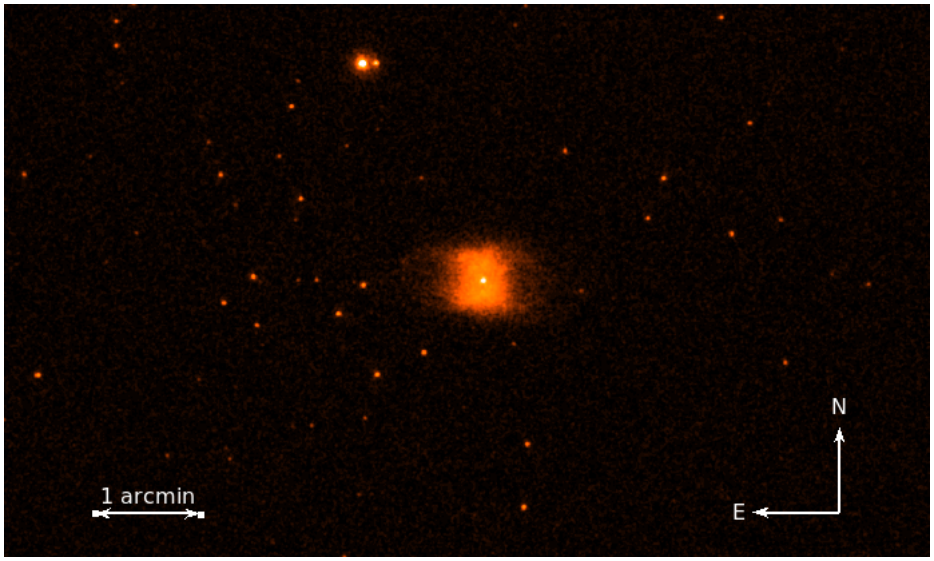

FIGURE 1: UVIT colour image of OC NGC 2818 in FUV F148W channel. Here orange colour depicts the FUV detections. The extended structure in this image represents the PN NGC 2818. North is up, and east is left in the image.

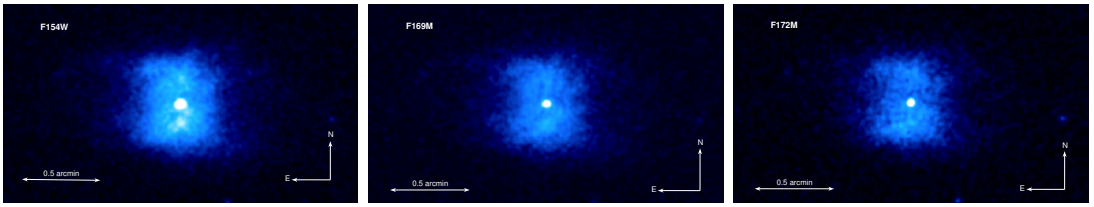

FIGURE 2: UVIT/FUV images of PN NGC 2818 in three filters: F154W, F169M, and F172M.

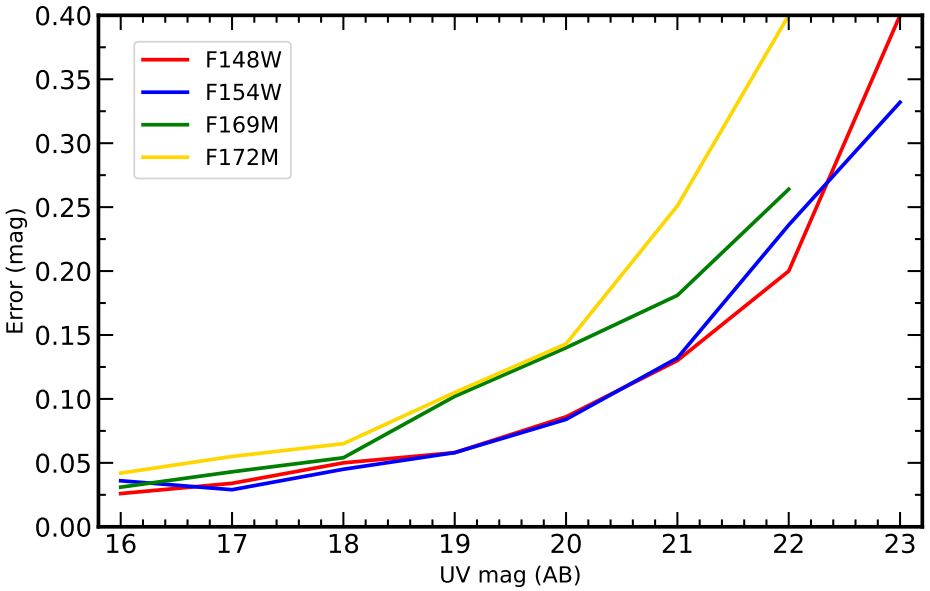

FIGURE 3: PSF-fit (median) errors versus magnitude in all FUV bandpasses of NGC,2818.

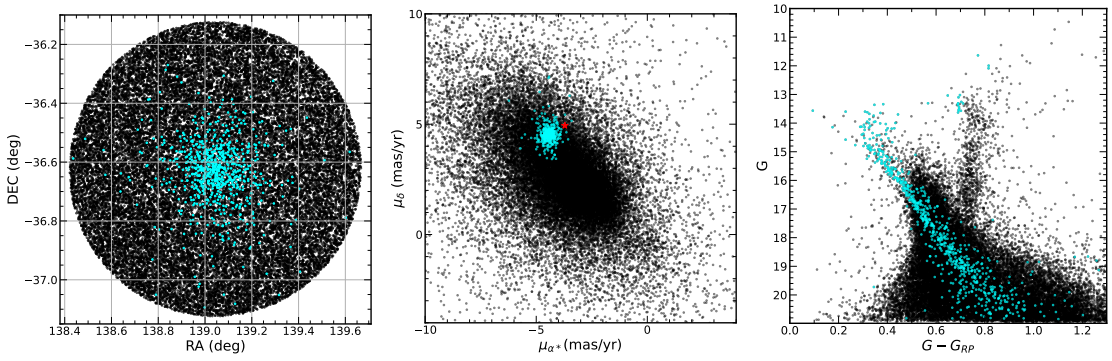

FIGURE 4: In three panels from left to right, PM members of the cluster are shown with cyan dots, and the remaining *Gaia* EDR3 sample marked with black dots represents field stars. Left Panel: position in the sky; Middle Panel: Vector Point Diagram (VPD); Right Panel: *Gaia* Optical CMD.

6.3 Membership Determination

We employed the *Gaia* EDR3 catalogue that provides data with unprecedented precision to identify the cluster members. In particular, it provides the complete 5-parameter astrometric solution (proper motions, parallaxes, and positions) and magnitudes in its three photometric bands (G_{BP}, G, and G_{RP}) with a limiting magnitude of about G$\sim$21 mag. To assign the PM membership probability (P_μ)

of all stars observed in the cluster, we first downloaded all detections located within a 30′ radius from the cluster's centre. To include all possible members of the cluster, we opted to use a radius bigger than that provided by Kharchenko *et al.* (2013) catalogue. Then, we applied the data quality criteria to select the sources with a good astrometric solution. Stars are selected as follows: (i) we removed those with parallaxes that deviate by more than 3σ from the expected parallax calculated using the previously known cluster's distance, where σ corresponds to the error in parallax given in *Gaia* EDR3 catalogue, (ii) we also removed the sources with RUWE exceeding 1.2 as larger values of this parameter might lead to an unreliable astrometric solution (Lindegren *et al.* 2018; Riello *et al.* 2021).

We made use of a probabilistic GMM method to select cluster members as described in detail in Chapter 4. We took the initial guess for cluster PM μ_α and μ_δ values and internal velocity dispersion from (Cantat-Gaudin *et al.* 2020). The mean PM values and standard deviation for the cluster were calculated to be μ_α = -4.417 mas/yr and μ_δ = 4.540 mas/yr, with σ_c = 0.045 mas/yr. In Figure 4, we show the position of stars in the sky, in the PM space known as VPD, and in an optical CMD created using *Gaia* filters. Cyan dots in all the plots depict the member stars belonging to the cluster, and black dots represent the field stars. 718 stars are identified as most likely cluster members with P_μ>50% and considered for subsequent analysis. This method works well for a distinguishable distribution of PM for the field and cluster stars in the VPD. But, in this case, the PM of cluster stars are located well within the PM distribution of the field stars, suggesting a non-trivial identification of cluster members from field stars. Therefore, it is possible that stars with a lower membership probability than the above-mentioned limit might also be members of the cluster.

6.3.1 Is the PN a member of the cluster?

The membership of the PN with OC has been debated in several studies in the past. According to Tifft *et al.* (1972), the PN NGC 2818 was found to be physically connected to the OC with the same designation. Dufour (1984) presented the results of photometric as well as spectroscopic observations of the nebula to analyse its physical properties and chemical composition. He suggested that the nebula is probably associated with the star cluster. Pedreros (1989) analysed this cluster using CCD UBV photometric data and assumed a physical association of the nebula with the cluster. Surendiranath *et al.* (1990) also suggested the association of the PN with the cluster from their CCD photometry of the cluster. Nonetheless, Mermilliod *et al.* (2001) derived accurate heliocentric RV values for 12 cluster RGB stars to obtain a mean heliocentric RV of Vhel = $+20.7 \pm 0.3$ kms^{-1}, significantly different from the estimated velocity of PN, -1 ± 3 kms^{-1} (Meatheringham *et al.* 1988), indicating that they are unrelated. (Vázquez 2012) recently used high-resolution *HST* archive imaging and high-dispersion spectroscopic data to reanalyse the complex kinematics and morphology of the nebula, determining its systemic heliocentric velocity to be $+26\pm2$ kms^{-1}, which is in greater agreement with the OC, supporting its membership. Furthermore, Frew *et al.* (2016), by analysing RV, radius, and Hα surface brightness of the PN concluded that it might be a member of the cluster.

The *Gaia* EDR3 trigonometric parallax for the CSPN is 0.0319 ± 0.21 mas, but it can be noted that the uncertainty in it is more than its value. So, it can not be used to obtain the distance to the nebula. The best estimate of the statistical distance is given by (Frew *et al.* 2016) as 3000 ± 800 pc not too far from cluster distance of 3250 ± 300 pc estimated by Sun *et al.* (2021). (Cantat-Gaudin *et al.* 2020; Cantat-Gaudin and Anders 2020) obtained the members of the several OCs, including NGC 2818, using *Gaia* DR2 PM data, and suggested that it is a non-member of the cluster.

In our membership analysis, we have obtained the membership of the CSPN using the *Gaia* EDR3 PM data. The PM in RA and DEC of the CSPN as listed in *Gaia* EDR3 catalogue is $\mu_\alpha = -3.712 \pm 0.185$ mas/yr and $\mu_\delta = 4.94 \pm 0.18$ mas/yr. Its P_μ is estimated to be ∼11%, indicating non-membership. Nevertheless, it can be noted from the location of the CSPN shown with the red star symbol in the VPD that it is lying close to the PM distribution of the cluster members (Cyan dots), implying that it is quite likely a member of the cluster. Statistically, it is lying within 3σ of the mean PM of the cluster. We expect that the future *Gaia* DR (*Gaia* DR4) might give more precise and accurate PM measurements that can re-confirm its association with the cluster. Further, assuming both cluster and nebula at the same distance, we computed their true velocity using their already available RV and PM information. We found that the true velocity of the cluster and nebula turn out to be approximately the same ($V_C = 99.7 kms^{-1}$ & $V_{PN} = 98.7 kms^{-1}$), implying that the values of the space velocity are similar.

6.3.1.1 Reddening towards the PN

Several estimates of extinction/reddening towards the cluster have been made since the initial investigation by Tifft *et al.* (1972) of E(B−V) of 0.22 mag, reconfirmed by Surendiranath *et al.* (1990) and recently refined by Sun *et al.* (2021), to 0.20 mag. However, there are a few independent estimates of extinction towards the PN NGC 2818. Dufour (1984) estimated it from the Balmer lines $H\alpha/H\beta$ ratio as 0.24±0.02 mag. Gathier and Pottasch (1988) list a value of 0.20 mag, and Frew *et al.* (2016) estimated a value of 0.17±0.08 mag. We presently estimate E(B−V) value using free-free continuum flux and the nebular $H\beta$ flux. The flux density, S_ν at 5 GHz of the entire nebula, is measured by Zhang (1995) as 33 mJy. The total $H\beta$ flux is estimated by Gathier and Pottasch (1988) as $logF(H\beta)$ as -11.40 ($ergcm^{-2}s^{-1}$). Following Pottasch (1984), the expected ratio of S_ν to $F(H\beta)$ is given as

$$\frac{S(\nu)}{F(H\beta)} = 2.51 \times 10^7 \times T_e^{0.53} \times (\nu)^{-0.1} \times Y\, Jy/ergcm^{-2}s^{-1}$$

where T_e corresponds to the electron temperature; ν represents frequency in GHz; Y = $(1 + \frac{n(He^+)}{n(H^+)})$. The value of $\frac{n(He^+)}{n(H^+)}$ is $\sim$ 0.13 assuming all He is in He^+ form. Dufour (1984) derived the $T_e[OIII]$ of 14,500±500 K. From the above relation, the $logF(H\beta)$ expected from the radio continuum is -11.07. The equation from Milne and Aller (1975) used to compute the reddening is following:

$$E(B-V) = \frac{1}{1.46} log \frac{F(H\beta)_{exp}}{F(H\beta)_{obs}}$$

Inserting the expected and observed $logF(H\beta)$ values in the above equation, we obtain the value of E(B−V) ∼0.23 mag. Thus, the reddening/extinction towards this cluster and nebula is of similar value.

From the comparison of distance, RV, PM, and extinction/reddening values of the cluster and nebula, we suggest a physical association of the PN with the OC.

6.4 Colour Magnitude Diagrams

6.4.1 Classification of Exotic sources

This section describes the classification and identification of exotic sources, such as BSSs and YSSs, expected to emit in the FUV. As mentioned in Section 6.3, we considered the probable cluster members with P_μ>50% and created the PM-cleaned optical CMD (G_{bp} - G_{rp} vs G) using the *Gaia* filters shown in Figure 5. In this CMD, stars outlined with cyan colour depict the various identified star

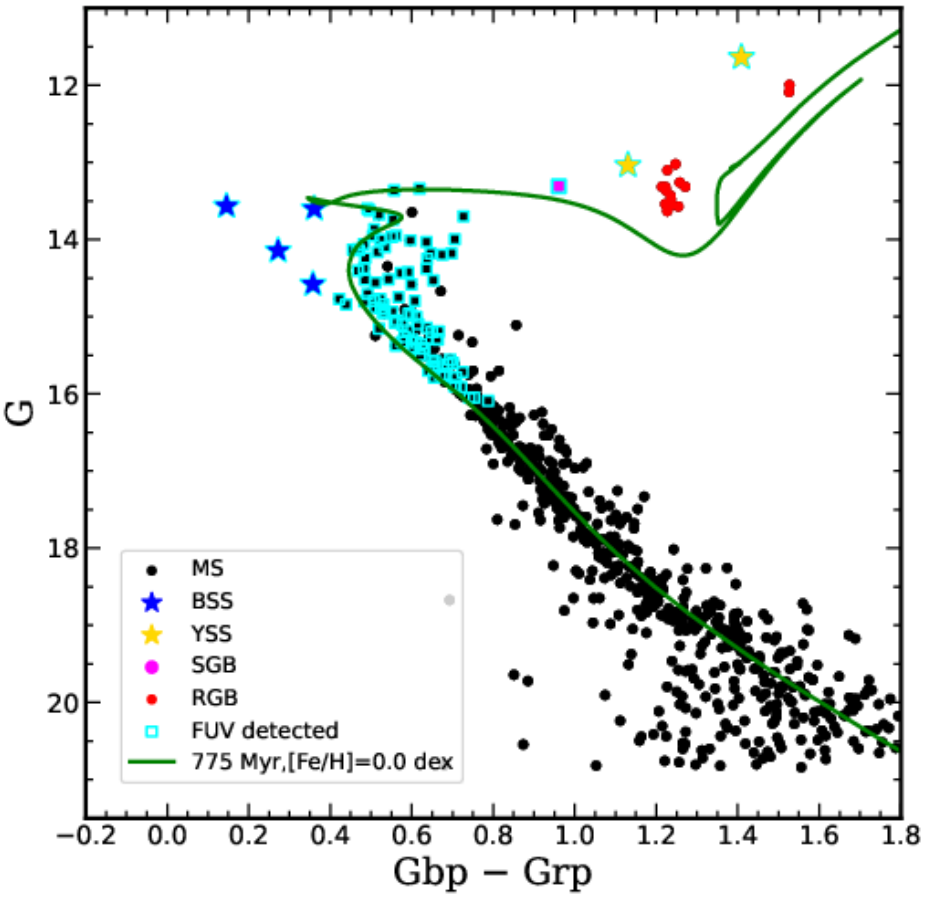

FIGURE 5: Optical CMD of the NGC 2818, created using *Gaia* EDR3 photometry. All filled symbols denote the stars with $P_\mu \geq 50\%$. Blue-filled stars and yellow-filled stars are the selected blue and yellow straggler stars used for further cross-match with UVIT data, respectively. The stars detected in all FUV images are outlined with cyan-coloured square and star symbols. The over-plotted green solid line represents the non-rotating MIST isochrone of solar metallicity and an age of 775 Myr, set at reddening, E(B−V)=0.2 mag and distance modulus, $(m-M)_V = 12.56$ mag.

populations in FUV images. Rain *et al.* (2021) presented a new proper-motion-cleaned catalogue of BSSs in Galactic OCs using *Gaia* DR2 data. We cross-matched the *Gaia* EDR3 cluster members with the BSS catalogue to classify this population in the cluster. Out of five identified BSSs in NGC 2818 by Rain *et al.* (2021), we detected four BSSs. The remaining BSS, not detected by us, is found to be a non-member of the cluster in our membership catalogue and also falls outside the FOV of NGC 2818 observed with UVIT in two epochs. Jadhav and Subramaniam (2021) also produced BSS's catalogue in OCs utilising *Gaia* DR2

data with a P_{μ}>70%, and they found two BSS candidates in this cluster. The difference in the above-mentioned catalogues could be due to the adopted age criteria, selection method, and different membership probability cut-offs used in the two studies.

We obtained the MIST isochrones for the *Gaia* EDR3 and UVIT filters from an updated MIST online database* to identify and classify distinct evolutionary sequences in the cluster (Choi *et al.* 2016; Paxton *et al.* 2018). We considered isochrones with $[\alpha/\mathrm{Fe}] = +0.0$ dex, metallicity, Z = 0.017210 (Sun *et al.* 2021), not incorporating initial rotation. Cluster parameters such as age, extinction, and distance modulus, adopted to fit the isochrone to the observed optical CMD, are 775 Myr, A_V=0.6 mag, and $(m-M)_V$=12.56, respectively (Sun *et al.* 2021). The overplotted isochrone (solid green line) over the observed optical CMD is displayed in Figure 5. We notice that the isochrone appears well-matched to the observed CMD along the MS and SGB, but it is not reproducing the observed location of the red clump. To account for this mismatch along the red clump, (Bastian *et al.* 2018) suggested that it might be due to either an incorrect calibration of the red clump models or an inaccurate transformation of theoretical isochrone properties (temperature, gravity, and luminosity) to observational data in Gaia filters.

We also selected the YSSs based on their location in the optical CMD, as they have colours in between the turn-off (TO) and RGB and appear brighter than the SGB. We have chosen two such stars marked with yellow-coloured filled symbols shown in Figure 5.

*https://waps.cfa.harvard.edu/MIST/interp_isos.html

6.4.2 FUV-optical CMDs

This section presents the FUV-optical CMDs generated by cross-identifying common stars between optical and our FUV detections. The sources detected in the UVIT FUV filters were cross-matched with those in the *Gaia* EDR3, with a maximum separation of 1.″3, which is equivalent to the UVIT filter's average PSF. To plot the FUV-optical CMDs, first, we made the magnitude system adopted by *Gaia* similar to that of UVIT. That is, we transformed the Vega magnitude system used in the *Gaia* photometric system to the AB system using the photometric zero points reported in the *Gaia* EDR3 documentation[†].

We have created and shown the FUV-optical CMDs for cluster members in Figure 6 using F148W and F169M filters. We note that a similar trend of detected stellar populations is observed in the other two filters (F154W & F172M). The error bars displayed in all FUV CMDs are estimated as the median of the stars' errors at a chosen magnitude range. The FUV-optical CMDs are also over-plotted with updated MIST isochrones (Choi *et al.* 2016) to compare the locations of the distinct sequences predicted by the theoretical models with the observed ones. In all FUV images, hot and bright stars such as BSSs, YSSs, and MS are detected. We have detected 4 BSSs out of 5 previously known in the literature (Rain *et al.* 2021). Four detected BSSs are confirmed RV and PM members. Two YSSs are also identified in all FUV images. We note that these stars are well-separated and brighter than the theoretical isochrone presenting the SGB sequence in all FUV-optical CMDs, in turn confirming their classification as YSSs. The UVIT is unable to detect RGB and Red Clump stars in the FUV region due to their faintness.
Unlike optical CMD, the FUV-optical CMDs show a large scatter along MS, as shown in Figure 6. The overlaid isochrones in all FUV-optical CMDs help to trace the MS scatter. We note that a few MS stars are brighter than theoretical MSTO not reproduced by isochrones. These might have high rotational velocities

[†]https://gea.esac.esa.int/archive/documentation

accounting for this feature. Some of them may be binaries or potential BSSs. One BSS is found to be very hot and bright in all FUV-optical CMDs compared to the other three BSSs. This BSS can be an exciting candidate to characterise, as it might have a hot WD companion. As two YSSs are detected in all FUV images and found to be bright in all FUV-optical CMDs, these stars also might have a hot companion, which leads to their detection in the FUV images. These are intriguing targets further to understand their formation and evolution in the clusters.

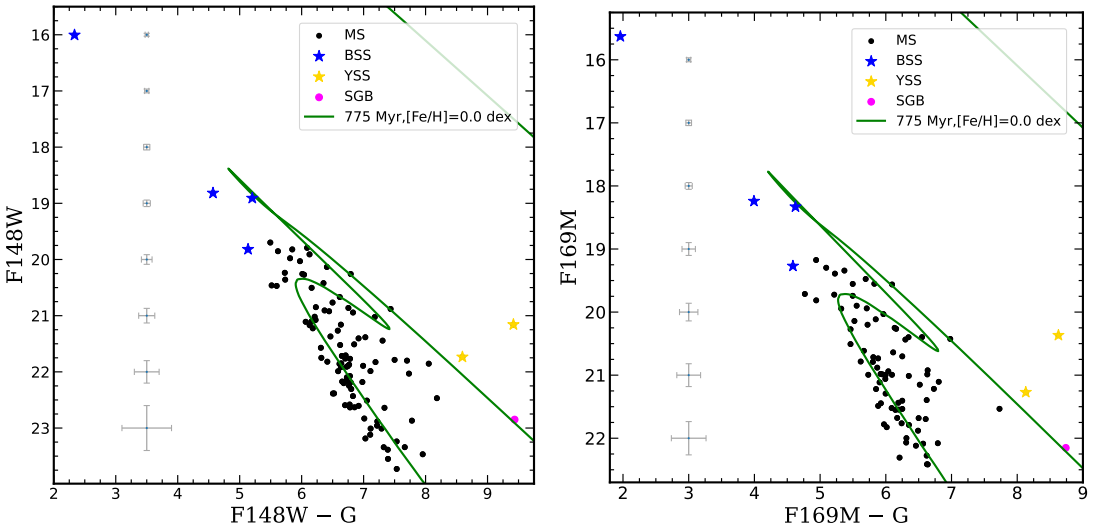

FIGURE 6: FUV-optical CMDs using F148W and F169M passbands of NGC 2818 of confirmed members cross-identified using UVIT FUV and *Gaia* EDR3 catalogue. The error bars (median) are shown in grey colour on the left side of each panel. The rest of the details are the same as in Figure 5.

6.4.3 Extended MS turn-off in FUV CMDs

In order to check the sensitivity of UVIT colours to the T_{eff} affected by the rotational velocity, we plot (Gbp−Grp) vs (F172M−G) colour as shown in Figure 7, which indicates a linear relation. The range of *Gaia* colour is only 0.4 mag whereas F172M−G spans about 3.0 mag, which makes F172M−G colour more sensitive and responsive to rotational velocity. F172M−G colour is preferred over F169M−G

because the band F172M allows only continuum light, and no chromospheric or transitional emission lines are seen in late-type stars in FUV.

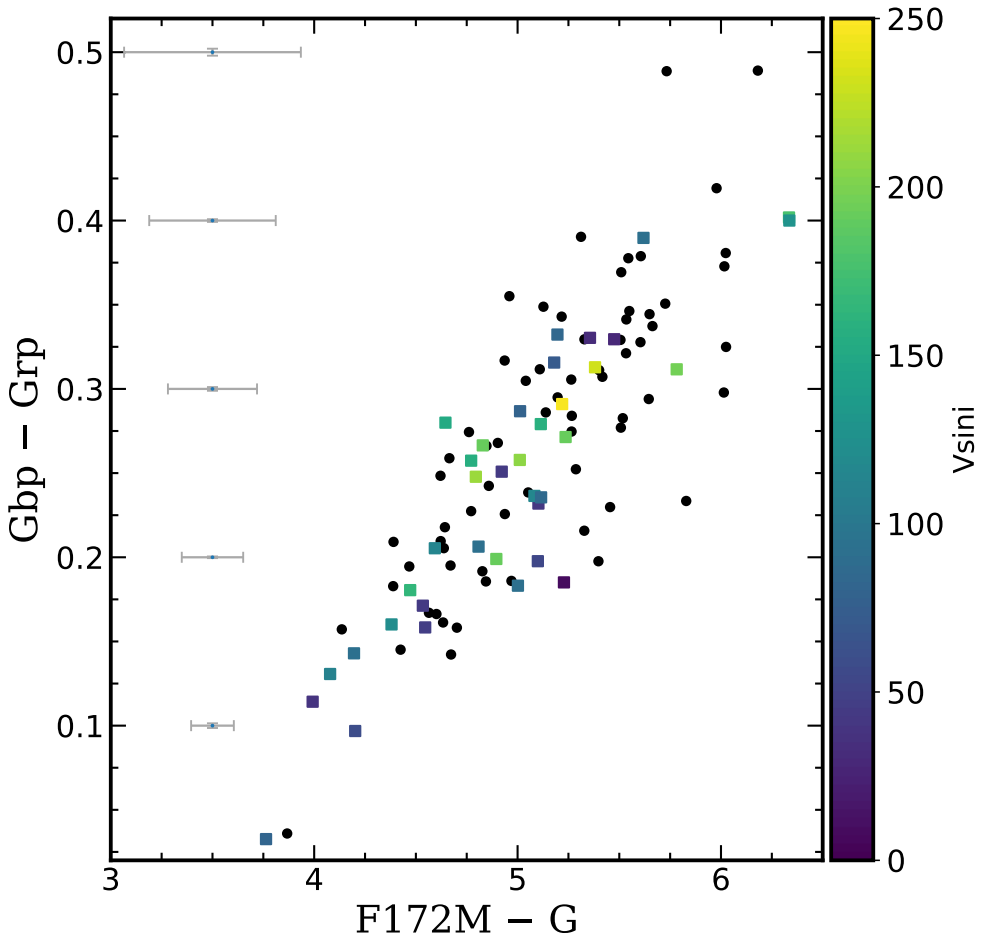

FIGURE 7: F172M−G vs Gbp−Grp colour-colour plot of all stars detected with UVIT colour-coded by their measured Vsini values. Stars with black colour symbols do not have estimated Vsini values.

Comparison of the CMD, F172M−G vs Gbp (Fig. 8 upper right) with CMD of Gbp−Grp vs Gbp (Fig. 8 upper left) shows the sensitivity of F172M−G colour. The bend in the isochrone in F172M−G vs Gbp CMD at a colour of 4.0 indicates the beginning of eMSTO prominently (unlike Fig. 8, left panel), and all the stars right of the isochrone show high rotational velocity. The MS comprises stars with both high and low rotational velocities. However, the CMD of F169M−G vs Gbp exhibits some more aspects. From the comparison of F169M−G colour with F172M−G in Fig. 8, we find that the former is redder than the latter. It can be

due to the fact that the F169M flux in late-type stars is smaller than at F172M. Moreover, the predicted colours using the theoretical isochrones are following the same trend.

It is well known that MS stars later than about F2 would possess coronal and transitional regions as evidenced in the FUV region by emission lines of C IV, He II, Si IV, N IV, N V, etc. (Linsky and Haisch 1979; Jordan and Linsky 1987). Prominent lines like C IV and He II occur in the F169M band region (unlike the F172M band). The F154W and F148W would contain a few more emission lines in addition to C IV and He II. Thus, the CMD of F169M-G vs Gbp shows that the MS stars are shifted bluewards to the isochrone, probably suggesting the presence of transitional region lines. Even in the F169M−F172M vs Gbp CMD shown in the lower right panel of Figure 8, it is evident that most stars have bluer colours than the theoretically expected ones from isochrones. It is to be noted that all stars on the blue edge of the MS in CMD of F169M−G vs Gbp (15<Gbp<16, 5<F169M−G<6) show high rotational velocity in contrast to CMD of F172M−G vs Gbp (15<Gbp<16, 4<G172M−M<5). It is fairly well established that high rotational velocities enhance the coronal and transitional line emissions (Pallavicini *et al.* 1981; Linsky *et al.* 2020). Thus, it is consistent with the suggestion that high rotation stars are on the blue side because of high emission line activity in total contrast to the MS of F172M−G vs Gbp CMD. This phenomenon sets into stars redder than (Gbp−Grp) ∼0.5 mag.

TABLE 6.1: Stellar parameters obtained from best SED fit of BSSs detected with UVIT in NGC 2818. Column 1 denotes the star ID used in the chapter. Columns 2 and 3 display the RA and DEC of all the stars considered for fitting, respectively. The T_{eff}, luminosities, and radii of all-stars, along with errors, are tabulated in columns 4, 5, and 6, respectively. The best fit's reduced χ^2 value is presented in column 7, and the ratio of the number of photometric data points used for the fit to the total number of available data points ($\frac{N_{fit}}{N_{tot}}$) can be found in column 8.

Star ID	RA (deg)	DEC (deg)	T_{eff} (K)	$\frac{L}{L_\odot}$	$\frac{R}{R_\odot}$	χ^2_{red}	Vgf	Vgf_b	$\frac{N_{fit}}{N_{tot}}$
BSS1	139.0306	-36.59184	$11,500 \pm 250$	91.55 ± 17.54	2.39 ± 0.22	12.9	12.9	1.53	11/12
BSS2	139.0279	-36.59178	$9,000 \pm 250$	32.99 ± 6.31	2.31 ± 0.21	3.1	3.1	0.88	12/12
BSS3	139.1633	-36.43083	$8,500^{+500}_{-250}$	52.28 ± 9.84	3.30 ± 0.31	4.8	4.8	1	19/19
BSS4	139.0276	-36.6423	$8,750 \pm 250$	20.97 ± 3.94	1.94 ± 0.18	4.9	4.9	0.91	19/19

TABLE 6.2: Derived parameters of YS and MS stars from the composite SED fit. The different models used to fit the cooler (A) and hotter (B) components of the SEDs are presented in column 5. The meaning of rest of the columns are consistent with those in Table 6.1.

Star ID	RA (deg)	Dec (deg)	Type	Model Used	T_{eff} (K)	$\frac{L}{L_\odot}$	$\frac{R}{R_\odot}$	χ^2_{red}	Vgf	Vgf_b	$\frac{N_{fit}}{N_{tot}}$
YSS1	139.0523	-36.57946	A	Kurucz	$4,750 \pm 125$	338.1 ± 63.25	27.01 ± 2.49	5.6	5.6	0.36	20/20
			B	Koester	$10,250 \pm 250$	$7.43^{+3.17}_{-2.36}$	$0.864^{+0.105}_{-0.083}$	4.3	4.3	0.61	
YSS2	138.9976	-36.58243	A	Kurucz	$5,000 \pm 250$	78.91 ± 15.55	10.93 ± 1	3.5	3.5	0.71	16/16
			B	Koester	$10,000 \pm 250$	$4.72^{+1.76}_{-1.51}$	$0.723^{+0.069}_{-0.069}$	2.4	2.4	0.81	
MS	139.0592	-36.60989	A	Kurucz	$6,000 \pm 125$	18.35 ± 3.47	3.98 ± 0.37	7.3	7.2	0.99	18/18
			B	Kurucz	$9,000 \pm 125$	10.79 ± 2.04	1.36 ± 0.125	7.3	7.2	0.99	

TABLE 6.3: Derived parameters of PN NGC 2818 from the best SED fit. The notation of all columns is the same as described in Table 6.1

Star ID	RA (deg)	DEC (deg)	Model Used	T_{eff} (K)	$\frac{L}{L_\odot}$	$\frac{R}{R_\odot}$	χ^2_{red}	Vgf	Vgf_b	$\frac{N_{fit}}{N_{tot}}$
PN NGC 2818	139.0061	-36.62707	TMAP(Grid3)	$190,000 \pm 8080.40$	826.75 ± 225.21	0.026 ± 0.002	8.3	8.3	4.5	6/6

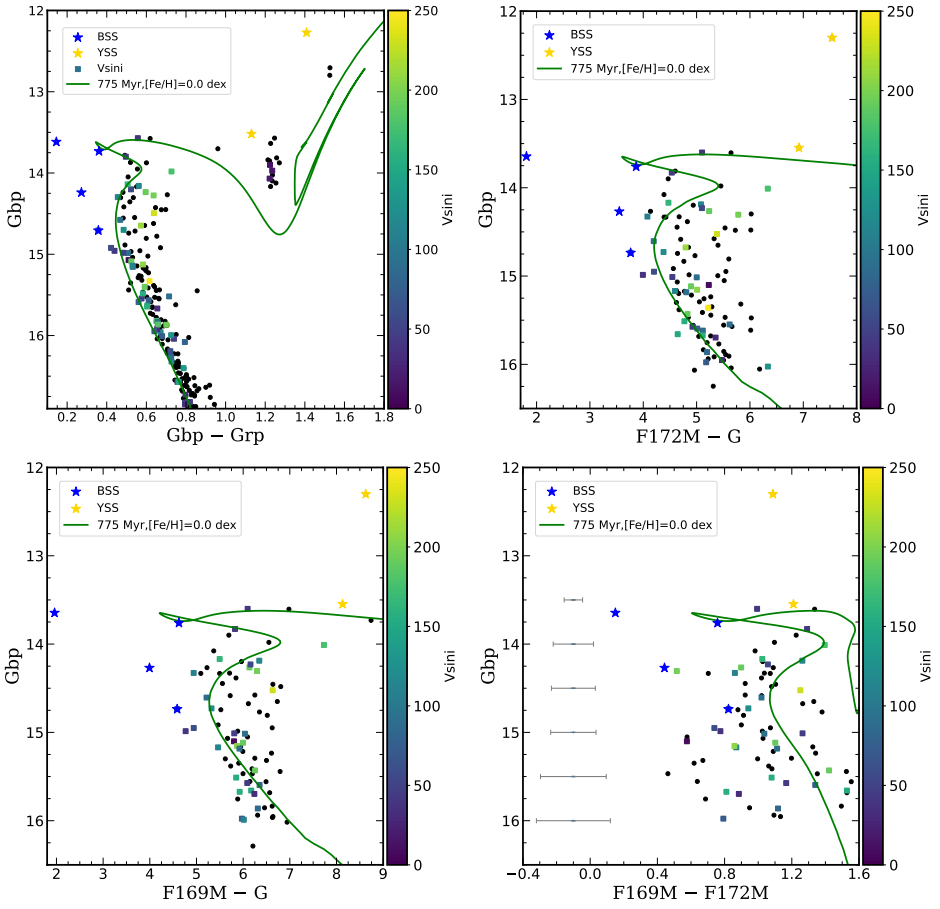

FIGURE 8: Optical (upper left), F172M-G vs Gbp (upper right), F169M-G vs Gbp (lower left), and F169M-F172M vs Gbp (lower right) CMDs of NGC 2818 members colour-coded by measured Vsini values. The rest of the details are the same as in Figure 5.

6.5 Spectral Energy Distribution Fits

It is well demonstrated in previous studies of exotic stellar populations, such as BSSs in OCs, that they are products of stellar interactions. There might be a chance of detecting a binary companion in the case of BSSs and YSSs. SEDs of such systems can be used to obtain the parameters of the multiple components. This section presents the multiwavelength SEDs constructed for the BSSs, YSSs, and CSPN identified with UVIT to derive their atmospheric parameters like T_{eff}, L ($L_{\odot}$), and R ($R_{\odot}$). We aim to probe the physical nature of these stars and probable hot companions, if present, by estimating their stellar parameters and

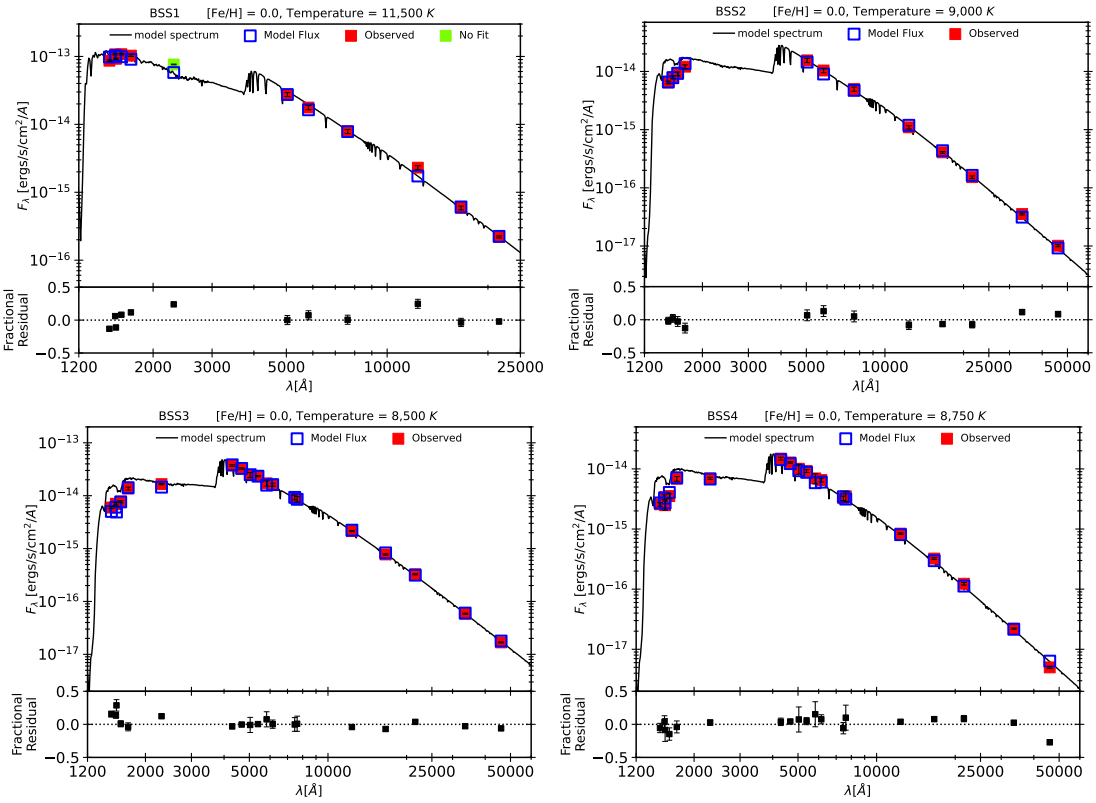

FIGURE 9: SEDs of four BSSs detected with UVIT. Extinction correction has been incorporated in all the observed photometric fluxes from UV to IR. The BSS ID adopted in this work is shown in each figure. The grey colour presents the best-fitting Kurucz model spectrum in all the plots. The data points that are excluded in the SED fit are shown with the orange colour-filled symbol. The bottom panel in all the SEDs illustrates the residual between the observed fluxes and model predictions.

placing them on the H-R diagram. SEDs are generated with the observed photometric data points spanning a wavelength range from FUV-to-IR and fitted with selected theoretical models. The details of the SED fitting technique are described in Chapter 2. In addition to χ^2_{red}, VOSA calculates two extra parameters, Vgf and Vgf_b, known as modified χ^2_{red} to estimate the goodness of fit in case the observational flux errors are too small. The value of Vgf_b should be less than 15 to achieve a reliable SED fit (Rebassa-Mansergas *et al.* 2021).

The Kurucz stellar atmospheric models are employed to create synthetic SEDs (Castelli *et al.* 1997; Castelli and Kurucz 2003) for YSSs and BSSs, which have

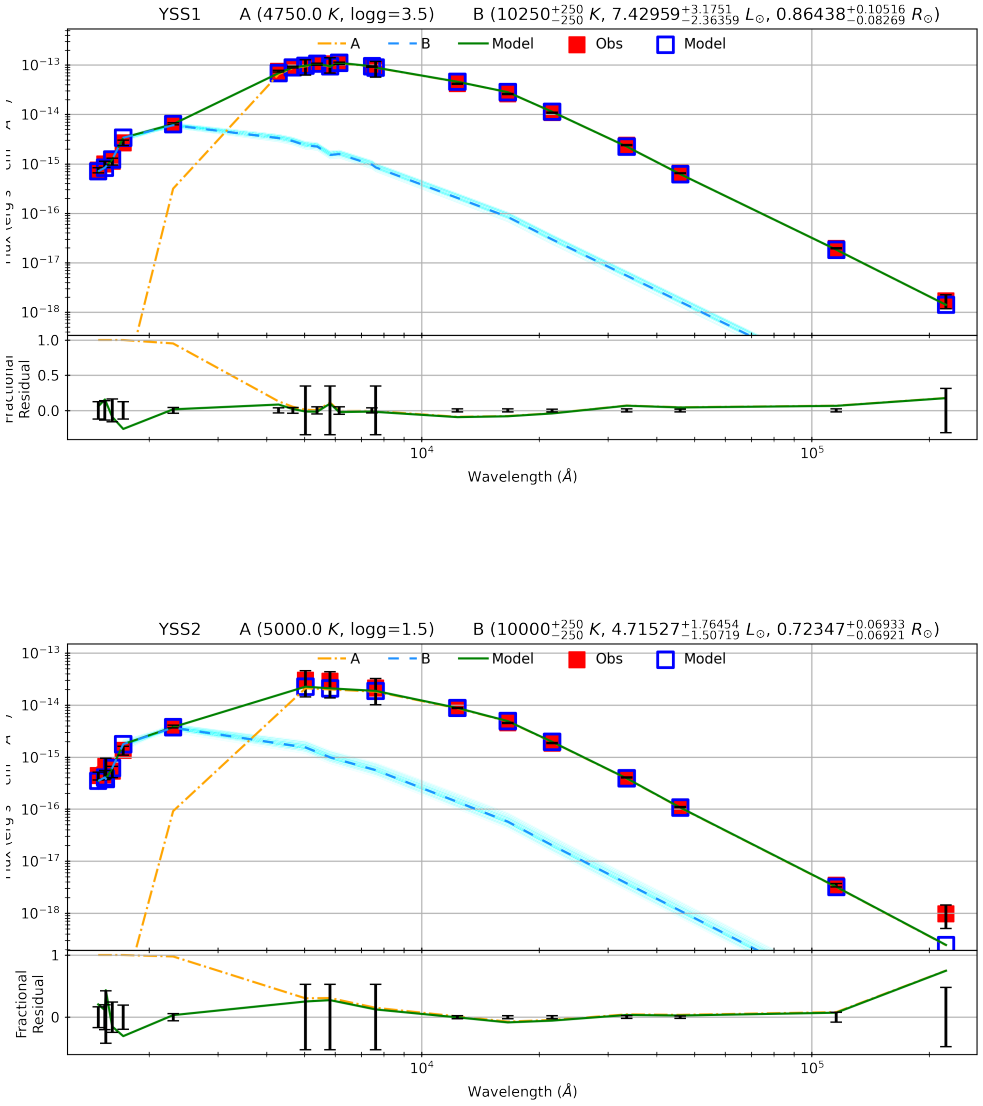

FIGURE 10: Double-fit SEDs of YSSs. The meaning of all the symbols is displayed in the legend. The star IDs and parameters of two components obtained from the fit are shown on the top of both SEDs. The green colour represents the composite model flux along with the observed fluxes marked with red symbols. Orange dotted-dash and blue dashed lines indicate Kurucz and Koester models used to fit the star's cooler and hotter components, respectively. The middle panel presents the fractional residual (Orange dashed line) corresponding to the single fit as well as the composite fit (Green solid line). The fractional observational uncertainties in the flux are also shown here. The values of χ^2_{red} and modified χ^2_{red} parameter, namely vgf_b^2 representing the best-fit are displayed in the lower panel.

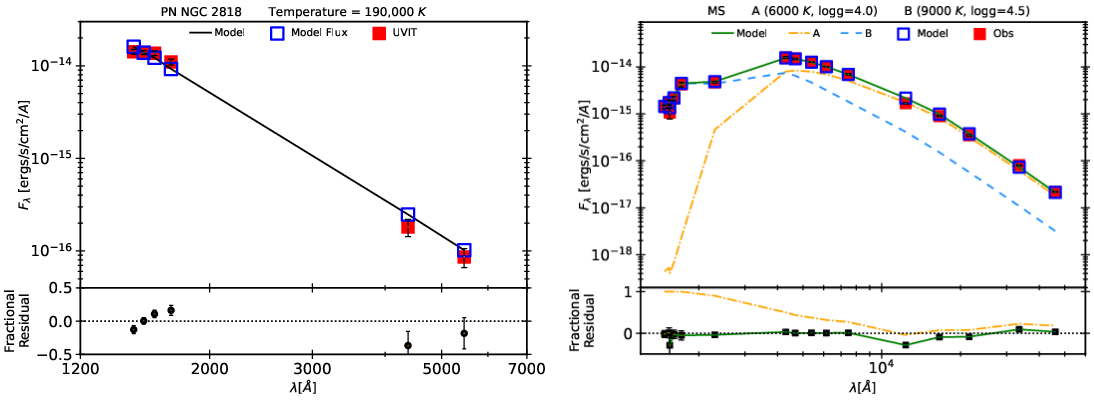

FIGURE 11: SED fit of the CSPN (left panel) and MS star (right panel) after taking into account the extinction correction. The black solid line represents the theoretical TMAP model fit to the observed fluxes shown with red symbols. The best-fit T_{eff} value is displayed in the figure. The rest of the details are the same as in Figure 9 and 10.

observed photometric data points covering a wavelength range from UV to IR. The free parameters available in the Kurucz model are T_{eff}, metallicity, and $\log g$. To fit the observed SEDs of the stars, as mentioned earlier with Kurucz models, we assumed T_{eff}, and $\log g$ as free parameters, and fixed the value of metallicity $\left[\mathrm{Fe/H}\right] = 0.0$ dex, close to the cluster metallicity. We adopted the range of T_{eff} from 5,000-50,000 K and $\log g$ from 3.5-5 dex in the Kurucz models. We combined the photometric data points of UVIT (4 passbands) with *GALEX* (2 passbands), *Gaia* EDR3 (3 passbands) (Gaia Collaboration *et al.* 2018), SDSS (3 passbands), APASS (2 passbands), 2MASS (3 passbands), and WISE (4 passbands) to generate the observed SEDs. VOSA makes use of Fitzpatrick reddening law (Fitzpatrick 1999; Indebetouw *et al.* 2005) to compute the extinction in different passbands and correct for extinction in observed fluxes for the provided A_V. VOSA utilises the Markov chain Monte Carlo (MCMC) approach to estimate the uncertainties in the stellar atmospheric parameters obtained using the SED fit.

SED fitting analysis is conducted for four BSSs, two YSSs, and PN, as described in the following subsections.

6.5.1 Blue Straggler Stars

The best-fitted SEDs for all BSSs are shown in Figure 9, where the lower panel of each SED depicts the fractional residual between the observed and predicted fluxes. The overplotted black solid line presents the synthetic Kurucz model spectrum created using the parameters corresponding to the best-fit SED. The star IDs adopted in this work are displayed on top of each SED. We observe that the SEDs of all BSSs are seemed to be well-fitted with a single model, as the residual is close to zero in all SEDs. Since the observed flux errors are very small for all the filters used, the error bars (shown in black colour) are smaller than the data points. We list their parameters corresponding to the best fit in Table 6.1. We obtain Vgf_b values for all BSSs to be around 1, indicating the good SED fits, and all the derived fundamental parameters are also reliable. The BSSs have a T_{eff} range of 8,500−11,500 K, and radii of 1.9−3.3 $R_{\odot}$. Now, here arises the two possibilities about the nature of these stars: 1) either all BSSs are single stars, 2) or they are binaries with a very faint companion, not able to detect by the UVIT observations. If these stars are single, they are likely to be formed via the merger of the component stars in a binary.

6.5.2 Yellow Straggler Stars

Figure 10 presents the SEDs of two stars classified as YSSs in this work. In this figure, the lower panel represents the fractional residual, i.e., the ratio of the difference between the observed and model flux ($F_{obs} - F_{model}$) and the observed flux at every given data point. We can see in Figure 10 that both YSSs are showing significant UV excess as a single model could not fit the entire SED. A rise in the flux in the UV wavelengths can also be seen in the fractional residual plot for a single spectrum fit (displayed as an orange dash-dotted line in the figure). To fit

the hotter component of the system, first, we gave excess for wavelength less than 3000 Å and fitted the cooler component that includes the optical and IR data points with the Kurucz model by selecting T_{eff} range from 3,500−50,000 K and log$g$ from 1.5−2.5 dex. From the single fit, the computed values of T_{eff} of the YSS1 and YSS2 are 4,750 K and 5,000 K, respectively. The radius of YSS1 and YSS2 is 27 $R_{\odot}$ and $\sim$ 11 $R_{\odot}$, respectively. From their temperature and radii, we infer that they are in the giant phase of stellar evolution. After obtaining the stellar parameters of the cooler component, then we used Binary SED Fitting[‡] code to fit the hotter part of the SED. The full details of this code are well described in Jadhav *et al.* (2021). We expect the hotter component to be compact, so we have used the Koester WD model (Tremblay and Bergeron 2009; Koester 2010). In this model, the range of free parameters T_{eff} and log$g$ is 5,000−80,000 K and 6.5−9.5, respectively. The double fit of both stars is shown in Figure 10, where the Kurucz model fit is shown with an orange dash-dotted line, and the Koester model fit with a light-blue dashed line. The composite fit is marked with a solid green line. The fractional residual in both plots is close to zero for all observed data points indicating how well the double component fit reproduces the observed SED. This is even evident from the vgf_b values (close to 1) computed from the SED fitting of both stars. The estimated parameters of both YSSs from the best binary fit are tabulated in Table 6.2. From the double fit, we estimate the T_{eff} of the hotter companion of YSS1 and YSS2 are 10,250 K and 10,000 K, respectively. The values of parameters such as T_{eff}, luminosities, and radii of the stars are mentioned on the top of each SED.

[‡]https://github.com/jikrant3/Binary_SED_Fitting

6.5.3 PN NGC 2818

As we have shown in the previous section, the PN NGC 2818 most likely has a physical association with the cluster; it will be interesting to characterise its central star to obtain information about its progenitor. We can clearly see the CSPN in the FUV image, as shown in Figure 1, implying its very high temperature. The magnitude of CSPN is a vital parameter to study its evolution as it can be used to determine the stellar parameters. The magnitude of the CSPN in optical filters was measured by Gathier and Pottasch (1988). As CSPN is well observed in all FUV images, therefore we have calculated the magnitude of the central star by doing the PSF photometry on the FUV images acquired in 1st and 2nd epoch observations. We have subtracted the nebular background in assessing the magnitude of the CSPN. The external extinction and distance to the nebula are considered to be the same as that of the cluster. Four FUV UVIT data points are combined with two optical photometric data points from Gathier and Pottasch (1988) to construct the observed SED of the nebula. As the central star seemed to be very hot, we have fitted its SED with the TMAP (Grid3) model used for hot stars (Werner *et al.* 2003; Rauch and Deetjen 2003). This model grid spans a range of atmospheric parameters such as $50,000K \leq T_{eff} \leq 190,000$ K, $5.0 \leq log\, g \leq 9.0$, and $0 \leq X_H \leq 1$. It is important to note that we took into account the external extinction while fitting its SED but did not incorporate the internal extinction in the nebula. We have noticed that T_{eff} derived using the TMAP model fit to the observed SED corresponds to their upper limit, which indicates that this star is likely to be hotter than the estimated temperature from this model. The stellar parameters computed from the best-fit SED of the nebula are summarised in Table 6.3.

6.5.4 MS stars

The SEDs are also constructed for the MS stars detected with UVIT, for which rotational velocity information was available in the literature to investigate their nature. Apart from that, we also have considered the MS stars for SED analysis for which rotational velocity was not estimated earlier, and their position in all FUV-optical CMDs was not matched with their expected one. 31 MS stars with the known rotational velocity are identified with UVIT in two epochs. Other than these stars, 6 MS stars are brighter than MS turn-off in FUV CMDs. We have used the Kurucz models to fit their observed SEDs to obtain their physical parameters and check their binarity. Out of 37 stars, we observed that only one MS star shows significant FUV excess, as illustrated in the right panel of Figure 11, whereas other stars show less or mild UV excess that could not be fitted with a double component SED. Chromospheric activity in the above star cannot account for UV excess as it is exceptionally high compared to the model. The other possibility to explain this excess is the presence of a hot companion that mainly emits at shorter wavelengths. To account for the presence of the hot companion, we fitted the entire SED with the Kurucz model using the binary fit task from VOSA. The double component fit for this star is found to be satisfactory (Right panel of Figure 11), and the best-fit parameters computed are tabulated in Table 6.2. The radii of both components suggest that they are not quite on the MS. The cooler companion is likely to be a sub-giant ($R/R_{\odot} \sim 4.0$), whereas the hot companion has a smaller radius ($R/R_{\odot} \sim 1.36$) when compared to the MS star of similar temperature ($R/R_{\odot}$ ~6.0). It might be possible that this is a post-mass transfer system where the hotter component is the donor, and the cooler component is still bloated after gaining mass. The rotational velocity (Vsini) of this star is around 39 km/s.

6.6 Evolutionary Status

Placing the stars on the H-R diagram provides information about their evolutionary stage and helps in probing the nature of the hot companions in the case of binaries. To examine the evolutionary status of exotic stars considered in this study, we have plotted the theoretical evolutionary sequences starting from the MS to the moment the star has entered the tip of the RGB stage. These tracks are taken from MIST models computed by Choi *et al.* (2016); Paxton *et al.* (2018) and selected for a known age of the cluster and metallicity close to the cluster metallicity. The stellar parameters estimated from the single SED fit for four BSSs are plotted in the H-R diagram. The meaning of the colour and symbols are marked in Figure 12. We can notice in Figure 12 that BSSs are lying bluer to the MS track, suggesting that these four stars belong to the BS evolutionary phase.

The location of two YSSs on the H-R diagram is near the theoretical RGB sequence. It indicates that their progenitors' (BSSs) have already evolved into a giant phase where the contracting helium core is surrounded by the hydrogen-burning shell. The hot companions of both YSSs seemed to be compact in nature, as indicated by their estimated radii suggesting they might belong to the WD or ELM WD or subdwarf stage of stellar evolution. In addition to the MS tracks, we have presented the DA-type WD cooling sequences with masses 0.5 $M_{\odot}$ and 0.2 $M_{\odot}$ taken from Tremblay *et al.* (2011) in Figure 12. From comparing the position of the hot companions of both YSSs with theoretical WD cooling tracks, we notice that their location is not reproduced by them, implying that they still have not entered the WD stage. While there are non-DA type WDs that are believed to result from mergers, they are not expected to be found in OCs because the merger process would take longer than the age of the cluster.

In order to find out where ELM WDs fall in the H-R diagram, we have used the field ELM WD catalogue provided by Brown *et al.* (2016b). They have estimated

the $T_{\rm eff}$ and $\log g$ values of the considered ELM WD sample in their paper. To place them on the T_{eff} vs luminosity plot, SED fitting technique is utilised to calculate the luminosity of all ELM WDs (Priv. Comm. Vikrant Jadhav). The extinction correction has been incorporated in all the stars. All field ELM WDs are marked as cyan-filled symbols in Figure 12. We note that the hot companions of the YSSs are more luminous than the field ELM WDs with a similar temperature.

As the location of the binary companions of YSSs is not reproduced by the WD tracks as well as ELM WDs, we further suspect that they might belong to the class of sdA as they are lying near the general location of subdwarfs in the H-R diagram. sdA stars are supposed to occupy the location between the dwarfs and WDs in the H-R diagram; hence, they are more compact than dwarfs, indicating a higher $\log g$ value. Brown *et al.* (2017) performed a detailed study of sdA stars to investigate their physical nature and a possible link to the ELM WDs. We used the field sdA catalogue to locate their positions on the H-R diagram. As only effective temperatures of all sdA stars were available in the catalogue, we used the SED fitting technique to determine their luminosities. The extinction in the visual band (A_V) for these stars was estimated using the reddening map provided by Schlafly and Finkbeiner (2011). We have taken care of the extinction correction in the observed fluxes in different bands of all sdA stars. The distances to these stars are available in the *Gaia* EDR3 catalogue. We have used the distances reported in Bailer-Jones *et al.* (2021), estimated using *Gaia* EDR3 catalogue, and they all fall within a range of $\sim$1.5 to 8 kpc. The sdA stars are displayed with purple-filled symbols in the H-R diagram. The hot companions of YSSs are found to be hotter than the similarly luminous field sdAs and more luminous than the similarly hot field sdAs.

From this comparison, we suggest that they are most likely to be sdA stars formed through a binary mass transfer scenario. These binaries are probably a post-mass-transfer system consisting of a sdA candidate and a YS star. We also checked the

position of the hotter and cooler components of the MS star on the H-R diagram displayed with orange-colour symbols. The hotter component occupies a location bluer than theoretical isochrone, might be evolving to the sdA type star, whereas the cooler component occupies the location expected for sub-giants. The evolution of this star might be similar to the YSS as the cooler component is evolving to the giant stage, whereas the hotter component later might end up as sdA. Thus, we speculate that this system might be a progenitor of the YSSs detected in this cluster.

Further, we have used the theoretical models of pAGB stars computed by Miller Bertolami (2016) to deduce the evolutionary state of the CSPN. We adopted the cluster metallicity (Z=$\sim$ 0.02 dex) to select the pAGB tracks. Tracks with a range of final mass as shown in Figure 12 are presented from the beginning of the pAGB phase when the H-rich envelope drops below $M_{env} = 0.01 M_*$ to the moment the star has already entered its WD cooling sequence at $L_* = L_{sun}$. The estimated parameters of the PN from the SED fit are plotted in the H-R diagram (Red filled symbol). From the comparison to these theoretical pAGB tracks, we observe that CSPN is found to be located on the track (Black dash-dotted line) corresponding to the final mass $0.657 M_{sun}$. It can be noted from here that the star has already entered the WD cooling phase.

6.7 Discussion

We have performed an observational study of OC NGC 2818 and the PN within its field using FUV medium-resolution space-based imaging data from UVIT aboard *AstroSat*. The goal of this study is to employ the most accurate and extensive *Gaia* EDR3 data on the astrometry and photometry of stars in the intermediate age OC NGC 2818 to confirm the membership of known stars and uncover the

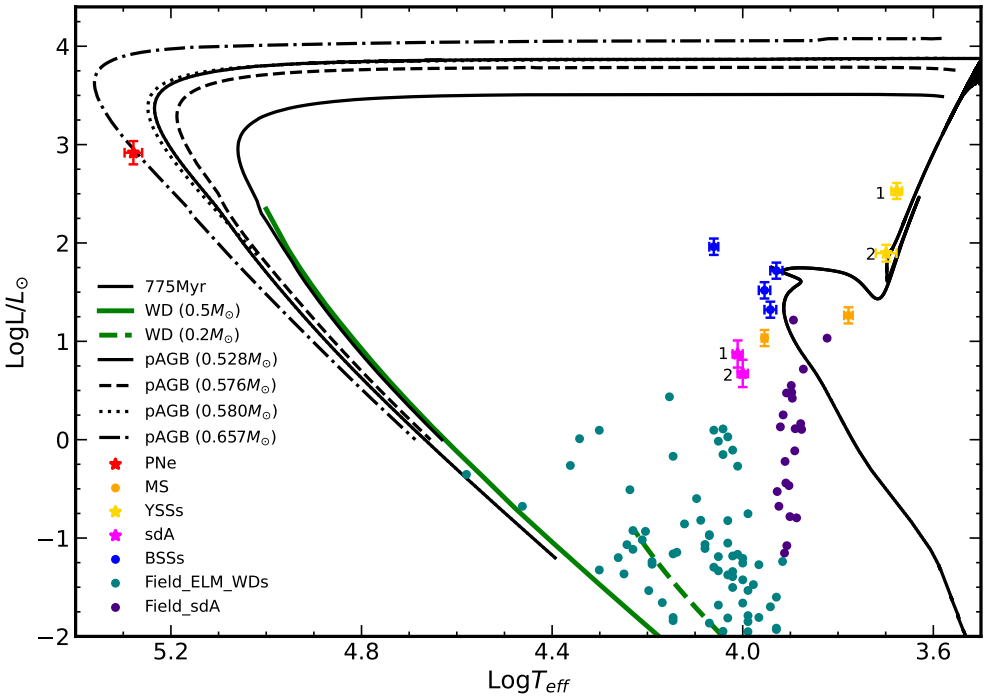

FIGURE 12: H-R diagram of the bright stars identified with UVIT. Various evolutionary tracks are presented from the beginning of the MS to the moment when a star has entered to the stage, followed by the WD cooling sequences. All these tracks are generated for cluster metallicity and age. The pAGB sequences with different final masses are shown here to compare the location of the CSPN marked with a red star symbol. BSSs and YSSs are displayed with blue-filled circles and yellow star symbols, respectively. The hotter companions of YSSs are shown with magenta star symbols. In addition, Field ELM WDs and A-type subdwarfs represented with cyan and purple symbols are also placed in the H-R diagram to compare the position of the hot companions of both YSSs. Green colour solid and dashed lines correspond to the DA-WD tracks with different masses.

evolutionary stage of exotic stars. Given that the stars are located in the central region of the cluster, we have limited our study to the inner part of the cluster with a radius of 30′, and selected 37508 stars brighter than G = 21 mag. Using the GMM method to pick out the PM members, we have chosen 718 stars as the cluster members with $P_\mu > 50\%$ and considered them further to identify their FUV counterparts with UVIT. FUV and FUV-optical CMDs were generated for the cluster members and overlaid with the MIST isochrones to compare the position of different observed evolutionary sequences with theoretically expected ones. MIST isochrones are found to match well with the observed sequences in

FUV-optical CMDs, but in FUV CMDs, especially F169M−F172M vs Gbp, most of the detected stars in both filters are lying blueward of their expected location from isochrones.

In all FUV images, we have identified four BSSs, two YSSs, and MS based on their location in the optical as well as FUV-optical CMDs. Then, we performed the SED analysis to deduce their physical properties to evaluate their nature. The T_{eff} of BSSs estimated from SED fit ranges from 8,500−11,500 K, hinting that they are quite hot, consistent with the young age (700−800 Myr) of the cluster. In the previous studies of BSSs in other OCs conducted using UVIT data, the T_{eff} range varies from cluster to cluster depending upon its age. The temperature range of BSSs in OC M67 (4 Gyr) is 6,250−9,000 K (Jadhav *et al.* 2019), in King 2 (6 Gyr) 5,750−8,500 K (Jadhav *et al.* 2021), in OC NGC 188 (7 Gyr) 6,100−6,800 K (Gosnell *et al.* 2015). In intermediate-age OCs such as NGC 7789 (1.6 Gyr) (Vaidya *et al.* 2022) and NGC 2506 (2.2 Gyr) (Panthi *et al.* 2022), BSSs span a temperature range from 7,250−10,250 K, and 7,750−9,750 K, respectively. The SEDs of all BSSs are well-fitted with a single model, and we suggest that collisions leading to the mergers might explain their formation in this cluster. Another plausible possibility is that they might have a faint WD companion undetectable with UVIT. If this is the case, then the second prominent scenario to explain their existence in star clusters, i.e., mass transfer in close binaries, will dominate over the previous one. Moreover, mass transfer in binaries will dominate in OCs as they are less dense and compact than GC systems. Further, spectroscopic analysis of these stars will help to confirm their nature.

Two YSSs, from their SED fits, are found to be binaries, and the location of YSSs and their hot components in the H-R diagram suggests that cool components are already in the RGB phase. In contrast, hot components most plausibly belong to sdA class. We infer from here that these two stars are post-mass-transfer systems

where BSS (accretor) has evolved into a giant stage and became YSS, and the donor star into a sdA. In addition, a spectroscopic study performed by Mermilliod *et al.* (2001) of RGB stars, including these two stars, found that they are spectroscopic binaries, confirming our result. Their radial velocities estimated by them also verify their membership. Hence, we suggest that these two stars are believed to have formed through a mass-transfer mechanism in this cluster.

From the comparison of the distance, extinction, RV and PM values of the PN with the cluster, it turns out that it is a most likely member of the cluster. Bohigas (2003, 2008) estimated the T_{eff} from the ionization modelling of the nebula as T_{eff} 149,000 K and log g of 7.1 (however, this might also be dependent on the distance assumed). Mata *et al.* (2016) gives the T_{eff} as 160,000 K. Gathier and Pottasch (1988) estimate the HI Zanstra temp 175,000 K and HeII Zanstra temp of 215,000 K. Kohoutek *et al.* (1986) derived the luminosity ($L_* = 851 L_\odot$) and radius ($R_* = 0.038 R_\odot$) of CSPN using optical observations, and adopting the identical distance to the nebula as that of the cluster (d=3.5 kpc). The atmospheric parameters of CSPN determined using the SED fitting technique are more or less in agreement with the previous estimations. Based on the comparison of the central star's location with the predicted ones from the theoretical models in the H-R diagram, the central star's mass turns out to be 0.66 $M_\odot$. Cummings *et al.* (2018) presented the WD IFMR for progenitor stars of $M_{initial}$ ranging from 0.85 to 7.5 $M_\odot$. In their Figure 5, they displayed the comparison of the IFMR estimated for the observed sample with the theoretical isochrones. For a given WD of mass approximately 0.66 $M_\odot$, the corresponding progenitor star's initial mass turns out to be $\sim$2.1 $M_\odot$ (From their Fig. 5). In this work, the MSTO mass of this cluster determined using isochrone fit is $\sim$2 $M_\odot$. The previously reported TO mass for this cluster and an initial mass of the nebula's progenitor are $\sim$2.1 $M_\odot$, and 2.2$\pm$0.3 $M_\odot$, respectively (Dufour 1984). Our estimations are consistent with the previous ones. From the comparison of the cluster TO mass and progenitor mass, we infer that PN is quite

likely a cluster member. Thus, this study showcases the significance of using the FUV data to study the exotic populations and end stages of intermediate-mass star's evolution in OCs.

6.8 Summary and Conclusions

The key findings from this study can be summarized as:

- In this study, we employed UVIT observations onboard *AstroSat* to identify BSSs and YSSs in the OC NGC 2818, and also characterise the CSPN. We further created the optical and UV-optical CMDs of member stars co-detected using UVIT and *Gaia* EDR3 data in this cluster.
- The PM members of the cluster are obtained using *Gaia* EDR3 data, and we found that PN NGC 2818 might be a member of this cluster, consistent with the previous studies.
- As this cluster is young, hot and bright stars such as BSSs, YSSs, and MS are detected in all FUV images.
- To compare the observations with theoretical predictions, optical and UV-optical CMDs are overlaid with non-rotating MIST isochrones generated for respective UVIT and *Gaia* filters. The theoretical isochrones reproduce the features of all CMDs quite well.
- The FUV-optical CMDs prominently show the eMSTO phenomenon already reported in this cluster, in agreement with the earlier studies.
- We characterised the four detected BSSs in the cluster, and a single model fits well to all the observed SEDs. We suggest from the single model fits that

these stars might have a faint WD companion that could not be detected with UVIT's detection limit or result from the merger of two close binaries.

- We suggest the presence of two YSSs in this cluster based on their location in the CMDs. Both YSSs were found to have excess UV flux, connected to their binary nature. They are confirmed spectroscopic binaries, and their hot companions are compact objects, likely to be sdA stars. Based on these results, we conclude that they are products of mass transfer in binary stars.

- From comparing the position of the CSPN with the theoretical pAGB evolutionary tracks, we found that it has already transitioned into the WD cooling phase with a mass of $\sim 0.66 M_{\odot}$. The progenitor star's mass is estimated to be $\sim 2.1 M_{\odot}$, similar to the cluster's turn-off mass, suggesting the possibility of its formation within the cluster.

Chapter 7

Conclusions & Future Work

In this thesis, we focussed on the identification and characterization of UV bright stellar populations in GCs as well as OCs. In GCs, HB, pHB stars, BSSs, and WDs are among the hot stellar populations that mainly emit in the UV region. However, in OCs, BSSs, YSSs, and WDs are considered hot and bright and expected to emit significant UV radiation. This thesis particularly focused on the evolved stages of low-mass stars, that include HB and pHB stars, in GCs to better understand their formation and evolution. In OCs, we did a comprehensive analysis of exotic stellar populations composed of BSSs and YSSs, which are believed to be products of non-standard stellar evolution, to better understand their nature and evolution. It is extremely rare to have PN as a member of the cluster, and in this thesis, we study a PN and the OC with the same name, NGC 2818, to derive the properties of its central star and confirm its membership to the cluster. In summary, the findings of these studies will contribute to a better understanding of theoretical models of stellar evolution. To achieve the above-stated aims, we constructed different CMDs combining UV and optical data from various sources, including the *HST*, *GALEX*, and ground-based observations, for the programme star clusters. Thanks to *Gaia* (DR2 and EDR3) for providing the accurate and precise PM data that

helped in confirming the association of the UV-detected stars to the clusters. We further did the comparison of the above-mentioned CMDs with theoretical models of stellar evolution to categorise stars in various evolutionary phases, including the classification of hot HB stars in the case GCs. Below we highlight the main results from the thesis presented in Chapters 3-6.

7.1 HB morphology

- **NGC 1261:** In FUV CMDs, only the bluest part of the HB was detected, which encompassed BHB and two EHB stars, whereas the full extent of HB consisting of RHB, BHB, RR Lyrae, and EHB were detected in the NUV CMDs. The UV-optical CMDs display a very tight sequence of HB stars that aligns well with theoretical models for these stars. The BHB stars cover a temperature range from 8,000 K to 12,750 K, with the high-temperature end approaching the G-jump temperature of 11,500 K in the HB distribution. The cluster, therefore, has an HB distribution truncating at the G-jump at the hot end and with the presence of two EHB stars. The two EHB candidates identified through UV-optical CMDs are confirmed to belong to this class from their derived temperatures using SED fitting technique and probably single stars. In summary, we constrained the origin of the EHB stars and suggested that they form via substantial mass loss along the RGB stage, which can be due to factors such as rotation or enhanced helium content or possibly through an early hot flasher scenario.

- **NGC 2298:** We detected only BHB along with four hot HB stars in each FUV image. In addition to HB, very few BSSs, which are hot and bright, are also detected in FUV CMDs. We observed a colour/magnitude spread among the blue HB stars in each FUV CMD, which could not be accounted for by the HB tracks obtained for enhanced alpha and helium abundances.

We found, by comparing the observed distribution of HB with the simulated one, that those hot HB stars are helium enhanced than BHB stars. In contrast, BHB stars have a single initial helium abundance (Y_{ini} = 0.23). The derived T_{eff} for all detected BHB stars ranges from 7,500-12,250 K. and mass in the range of 0.6-0.75 $M_{\odot}$. In the H-R diagram, some of the BHB stars are seen to be evolving towards the peAGB phase. We suggest the evolutionary effects account for the observed spread among the BHB stars. Three of four hot HB stars identified in the cluster have already evolved off the HB phase. The hottest one has evolved off the peAGB phase and is probably evolving towards the WD cooling stage. One star is a confirmed EHB star, likely to be helium enriched. We also computed the number of theoretically expected pHB stars in the cluster, which was found to match well with the observed number. In addition, we found a binary star lying along the BHB sequence that has a sub-luminous sdB companion to an RHB star in the cluster. From the comparison with the ELM WD evolutionary tracks, the mass of the sdB turns out to be $\sim 0.187 M_{\odot}$ and is likely to be evolving into a helium core WD. We suggest that it is probably an ELM WD candidate formed from mass transfer in an sdB-RHB binary system.

- **NGC 188:** We presented the UV CMDs overlaid with isochrones of this OC and reported, for the first time, the presence of HB in OC, with an RHB, a BHB, and an EHB/sdB star; a temperature range of 4,750-21,000 K is estimated from their SED analyses.

Overall, from our HB studies, we infer that UV observations play a significant role in identifying hot HB and pHB stars in GCs and old OCs, and shed more light on their origin and evolution in the clusters. The UV CMDs can also be utilised as a powerful tool to check the existence of MSPs among HB. The change in the distribution of the UV bright stars in optical and UV CMDs helps to explore their nature and evolution. The peculiarities observed in UV CMDs allow us to improve

theoretical stellar evolutionary models by further incorporating appropriate physical parameters. The hot HB stars found in both GCs are potential candidates for further spectroscopic follow-ups to probe their nature and to constrain their formation pathways. These stars most probably serve as the energy budget at short wavelengths in the old stellar systems, such as GCs and elliptical galaxies.

7.2 UV bright stars in OCs

- **NGC 188:** In each FUV image, we detect only hot and bright BSSs, a hot subdwarf, and a WD candidate. In the NUV image, we detect 21 BSSs, 2 YSSs, and one WD candidate. The theoretical isochrones well reproduce the observed UV-optical CMDs. Out of two YSSs detected in this cluster, based on their location in the CMDs, YSS1 exhibits an excess of UV flux, which may be related to its binary nature and X-ray emission. We detect a candidate WD from the UV images, found to have parameters similar to that of a 0.5 $M_{\odot}$ WD.

- **NGC 2818:** This study presents the first results of intermediate-age Galactic OC NGC 2818 observed in FUV and with a PN within its field. Our analysis of optical and FUV-optical CMDs reveals the presence of four hot and bright BSSs and two YSSs. The theoretical isochrones more or less fit the observed distribution of detected stars in all the CMDs. The parameters derived through SED analysis suggest the BSSs might have been formed through collisions or have unseen WD companions. The photometric analysis supports the binarity of the YSSs, which is in agreement with previous spectroscopic results. These YSSs are believed to have formed through a mass-transfer scenario, with their hot components potentially being sdA stars.

- **PN NGC 2818:** We explore the physical connection between the PN and the cluster using images taken from UVIT. The RV, *Gaia* EDR3 PM, and the reddening of the PN and the cluster do not contradict the possibility of PN membership. The central star's location is then compared with theoretical models for pAGB stars in the H-R diagram, which suggests that it has already transitioned into the WD cooling phase with a mass of $\sim$0.66 $M_{\odot}$. The progenitor star's mass is estimated to be $\sim$2.1 $M_{\odot}$, similar to the cluster's turn-off mass, suggesting the possibility of its formation within the cluster. We suggest that the NGC 2818 might be one of the few known clusters to host a PN, providing a unique opportunity to test stellar evolution models.

Thus, our study on the BSSs and YSSs in OCs highlights the advantage of using UVIT for observations and identifying hot companions to them if present, in turn, provides insight into their formation processes. The advantage of using UVIT data, when combined with the other multi-wavelength photometric data, to confirm the PN's membership to the cluster provides us with a remarkable opportunity to test models of stellar evolution. Finding a PN within OCs is rare, and its association with the cluster can help in constraining its age. Our study demonstrates that UVIT is well suited to explore the end stages of low-mass star evolution in both types of clusters.

7.3 Future and ongoing work

This thesis demonstrates the significance of using UV photometry in combination with optical, IR, and *Gaia* data to examine the UV bright stellar populations in star clusters. Below I present the ongoing/completed projects that I worked on

during the thesis period and the projects that I am involved in to carry out the planned future work.

- As a part of the UVIT open cluster survey (UOCS), I am analysing the BSSs in the well-studied old OC NGC 188, using the UVIT and *HST* data. From this study, we obtained exciting results about hot companions to BSSs. Our plan is to simulate the SEDs of these stars with similar parameters and confirm our results (Rani et al. under preparation).

- I am also studying the BSSs of the GC NGC 1261 by employing UVIT data along with additional archival data. As a part of the UVIT Legacy Survey of Globular clusters (GlobULeS) (Sahu *et al.* 2022), I am also interested in the multi-wavelength analyses of ω Cen (Prabhu *et al.* 2022), NGC 362, primarily focusing on the BSSs (Dattatrey *et al.* 2023), Blue Lurkers (Datatrey et al. 2023, Submitted), and HB population.

- We are also analysing the Be stars in OC NGC 663 using UVIT data in both NUV and FUV filters. This work is under preparation titled "AstroSat/UVIT study of the young open cluster NGC 663: Probe into the Be phenomena" (Nedhath et al. 2023, under preparation).

Apart from the above projects, I have a few ideas about future projects using photometric as well as spectroscopic data from telescopes worldwide.

- We plan to propose the high-resolution spectroscopic observations for the two YSSs detected with UVIT in OC NGC 2818 to confirm their binarity and derive their abundances to shed more light on their formation pathways.

- BSSs are complex systems formed via mass transfer in close binaries and mergers. There are abundant photometric studies of BSSs in star clusters

using optical and UV observations, but spectroscopic studies are still sparse. Based on the evolutionary stage of the donor, we expect the accretor star to have different or the same chemical abundances as the usual MS stars. How the stellar interactions affect the abundances in the post-interaction systems is still poorly understood. We plan to study the elemental abundances in isolated and post-interaction systems such as BSSs to evaluate the abundance patterns and their relationship with stellar age, mass, cluster metallicity and orbital parameters. To achieve the above aim, we have obtained high-resolution spectroscopic observations of two member BSSs in OC M67 with Hanle Echelle Spectrograph (HESP) mounted on a 2-m Himalayan Chandra Telescope (HCT).

- As it is well understood from the previous studies conducted in the last decade in GGCs that they consist of MSPs. While there have been a few studies that used spectroscopy to confirm the presence of MSPs in GGCs, we plan to further investigate this by analysing the high-resolution spectra of four bright giants in nearby GGCs to verify the existence of MSPs in them.

- There have been a lot of studies of variable stars in GGCs using optical data. Here arise two problems while studying the variability using optical data in GCs: 1) Crowding in the central region and 2) Small amplitude of pulsations. In this case, UV observations play an essential role as FUV images of the clusters using UVIT reveal these populations in the central region as the core of GCs is resolved, unlike in optical, and FUV light curves have the largest amplitudes of ∼3-5 mag. The UV light curves of variable stars, such as RR Lyrae, SX Phe, etc., which are abundant in GCs, provide important information regarding pulsation and the related shock mechanisms. By examining the light curves of variable stars, the basic parameters of the GCs, such as distance, metallicity, and age, can be estimated. Our plan is to study the UV light curves of the already-known variable or pulsating stars in GCs like NGC 1261, NGC 5272 and NGC 6341, which are abundant

in such stars. We acquired profound observations of GC NGC 1261 in the FUV F169M filter of UVIT (Prop. ID: A09_088, −P.I: Sharmila Rani) and also proposed the profound observations of the other two GCs (NGC 5272 and NGC 6341) (Prop. ID: A12_029, −P.I: Sharmila Rani).

Bibliography

Ahumada, J. A. and Lapasset, E., 2007, "New catalogue of blue stragglers in open clusters", *Astron. Astrophys.*, **463**(2), 789–797. [DOI], [ADS]

Althaus, Leandro G., Miller Bertolami, Marcelo M. and Córsico, Alejandro H., 2013, "New evolutionary sequences for extremely low-mass white dwarfs. Homogeneous mass and age determinations and asteroseismic prospects", *Astron. Astrophys.*, **557**, A19. [DOI], [ADS], [arXiv:1307.1882 [astro-ph.SR]]

Anderson, J., Piotto, G., King, I. R., Bedin, L. R. and Guhathakurta, P., 2009, "Mixed Populations in Globular Clusters: Et Tu, 47 Tuc?", *Astrophys. J. Lett.*, **697**(1), L58–L62. [DOI], [ADS], [arXiv:0904.1626 [astro-ph.GA]]

Andreuzzi, G., Richer, H. B., Limongi, M. and Bolte, M., 2002, "The white dwarf cooling sequence in the old open cluster NGC 188", *Astron. Astrophys.*, **390**, 961–965. [DOI], [ADS], [arXiv:astro-ph/0206186 [astro-ph]]

Arellano Ferro, A., Bustos Fierro, I. H., Calderón, J. H. and Ahumada, J. A., 2019, "NGC 1261: A Time-Series VI Study of its Variable Stars", *Revista Mexicana de Astronomía y Astrofśica*, **55**, 337–350. [DOI], [ADS], [arXiv:1908.04808 [astro-ph.SR]]

Babusiaux, C., Fabricius, C., Khanna, S., Muraveva, T., Reylé, C., Spoto, F., Vallenari, A., Luri, X., Arenou, F., Alvarez, M. A., Anders, F., Antoja, T.,

Balbinot, E., Barache, C., Bauchet, N., Bossini, D., Busonero, D., Cantat-Gaudin, T., Carrasco, J. M., Dafonte, C., Diakite, S., Figueras, F., Garcia-Gutierrez, A., Garofalo, A., Helmi, A., Jimenez-Arranz, O., Jordi, C., Kervella, P., Kostrzewa-Rutkowska, Z., Leclerc, N., Licata, E., Manteiga, M., Masip, A., Monguio, M., Ramos, P., Robichon, N., Robin, A. C., Romero-Gomez, M., Saez, A., Santovena, R., Spina, L., Torralba Elipe, G. and Weiler, M., 2022, "Gaia Data Release 3: Catalogue Validation", *arXiv e-prints*, arXiv:2206.05989. [ADS], [arXiv:2206.05989 [astro-ph.SR]]

Bailer-Jones, C. A. L., Rybizki, J., Fouesneau, M., Demleitner, M. and Andrae, R., 2021, "VizieR Online Data Catalog: Distances to 1.47 billion stars in Gaia EDR3 (Bailer-Jones+, 2021)", *VizieR Online Data Catalog*, I/352. [ADS]

Bastian, N. and de Mink, S. E., 2009, "The effect of stellar rotation on colour-magnitude diagrams: on the apparent presence of multiple populations in intermediate age stellar clusters", *Mon. Not. Roy. Astron. Soc.*, **398**(1), L11–L15. [DOI], [ADS], [arXiv:0906.1590 [astro-ph.GA]]

Bastian, N., Kamann, S., Cabrera-Ziri, I., Georgy, C., Ekström, S., Charbonnel, C., de Juan Ovelar, M. and Usher, C., 2018, "Extended main sequence turnoffs in open clusters as seen by Gaia - I. NGC 2818 and the role of stellar rotation", *Mon. Not. Roy. Astron. Soc.*, **480**(3), 3739–3746. [DOI], [ADS], [arXiv:1807.10779 [astro-ph.SR]]

Baumgardt, Holger and Makino, Junichiro, 2003, "Dynamical evolution of star clusters in tidal fields", *Mon. Not. Roy. Astron. Soc.*, **340**(1), 227–246. [DOI], [ADS], [arXiv:astro-ph/0211471 [astro-ph]]

Bayo, A., Rodrigo, C., Barrado Y Navascués, D., Solano, E., Gutiérrez, R., Morales-Calderón, M. and Allard, F., 2008, "VOSA: virtual observatory SED analyzer. An application to the Collinder 69 open cluster", *Astron. Astrophys.*, **492**(1), 277–287. [DOI], [ADS], [arXiv:0808.0270 [astro-ph]]

Bedin, L. R., Piotto, G., Anderson, J., King, I. R., Cassisi, S. and Momany, Y., 2004, "The double main sequence of Omega Centauri", *Memorie della Societa Astronomica Italiana Supplementi*, **5**, 105. [ADS], [arXiv:astro-ph/0406076 [astro-ph]]

Behr, Bradford B., 2003, "Chemical Abundances and Rotation Velocities of Blue Horizontal-Branch Stars in Six Globular Clusters", *Astrophys. J. Suppl.*, **149**(1), 67–99. [DOI], [ADS], [arXiv:astro-ph/0307178 [astro-ph]]

Bekki, Kenji, 2012, "A Possible Physical Connection between Helium-rich Stellar Populations of Massive Globular Clusters and the UV Upturn of Galactic Spheroids", *Astrophys. J.*, **747**(1), 78. [DOI], [ADS], [arXiv:1112.5240 [astro-ph.CO]]

Bellini, A., Anderson, J., Salaris, M., Cassisi, S., Bedin, L. R., Piotto, G. and Bergeron, P., 2013, "A Double White-dwarf Cooling Sequence in ω Centauri", *Astrophys. J. Lett.*, **769**(2), L32. [DOI], [ADS], [arXiv:1305.0265 [astro-ph.GA]]

Belloni, T., Verbunt, F. and Mathieu, R. D., 1998, "X-rays from old open clusters: M 67 and NGC 188", *Astron. Astrophys.*, **339**, 431–439. [ADS], [arXiv:astro-ph/9808329 [astro-ph]]

Bertelli, Gianpaolo, Nasi, Emma, Girardi, Leo, Chiosi, Cesare, Zoccali, Manuela and Gallart, Carme, 2003, "Testing Intermediate-Age Stellar Evolution Models with VLT Photometry of Large Magellanic Cloud Clusters. III. Padova Results", *Astron. J.*, **125**(2), 770–784. [DOI], [ADS], [arXiv:astro-ph/0211169 [astro-ph]]

Bertola, F., Capaccioli, M. and Oke, J. B., 1982, "IUE observations of NGC 4649, an elliptical galaxy with a strong ultraviolet flux.", *Astrophys. J.*, **254**, 494–499. [DOI], [ADS]

Bianchi, Luciana, Shiao, Bernie and Thilker, David, 2017, "Revised Catalog of GALEX Ultraviolet Sources. I. The All-Sky Survey: GUVcat_AIS", *Astrophys. J. Suppl.*, **230**(2), 24. [DOI], [ADS], [arXiv:1704.05903 [astro-ph.GA]]

Blanton, Michael R. and Roweis, Sam, 2007, "K-Corrections and Filter Transformations in the Ultraviolet, Optical, and Near-Infrared", *Astron. J.*, **133**(2), 734–754. [DOI], [ADS], [arXiv:astro-ph/0606170 [astro-ph]]

Boehm-Vitense, Erika, 1992, *Introduction to Stellar Astrophysics. Vol.3: Stellar structure and evolution*. [ADS]

Boffin, Henri M. J., Carraro, Giovanni and Beccari, Giacomo (Eds.), 2015, *Ecology of Blue Straggler Stars*, Astrophysics and Space Science Library, 413, Springer Berlin Heidelberg. [DOI], [ADS], [arXiv:1406.3909 [astro-ph.SR]]

Bohigas, J., 2003, "Infrared Imaging and Optical Imaging and Spectroscopy of (mostly) Type I Planetary Nebulae. II.", *Revista Mexicana de Astronomía y Astrofśica*, **39**, 149–170. [ADS]

Bohigas, Joaquín, 2008, "Photoionization Models Applied to Planetary Nebulae", *Astrophys. J.*, **674**(2), 954–975. [DOI], [ADS]

Brandt, Timothy D. and Huang, Chelsea X., 2015, "The Age and Age Spread of the Praesepe and Hyades Clusters: a Consistent, ~800 Myr Picture from Rotating Stellar Models", *Astrophys. J.*, **807**(1), 24. [DOI], [ADS], [arXiv:1504.00004 [astro-ph.SR]]

Brown, T. M., Cassisi, S., D'Antona, F., Salaris, M., Milone, A. P., Dalessandro, E., Piotto, G., Renzini, A., Sweigart, A. V., Bellini, A., Ortolani, S., Sarajedini, A., Aparicio, A., Bedin, L. R., Anderson, J., Pietrinferni, A. and Nardiello, D., 2016a, "The Hubble Space Telescope UV Legacy Survey of Galactic Globular Clusters. VII. Implications from the Nearly Universal Nature of Horizontal Branch Discontinuities", *Astrophys. J.*, **822**(1), 44. [DOI], [ADS], [arXiv:1603.07651 [astro-ph.SR]]

Brown, Thomas M., Ferguson, Henry C., Davidsen, Arthur F. and Dorman, Ben, 1997, "A Far-Ultraviolet Analysis of the Stellar Populations in Six Elliptical and S0 Galaxies", *Astrophys. J.*, **482**(2), 685–707. [DOI], [ADS], [arXiv:astro-ph/9701235 [astro-ph]]

Brown, Thomas M., Bowers, Charles W., Kimble, Randy A., Sweigart, Allen V. and Ferguson, Henry C., 2000, "Detection and Photometry of Hot Horizontal Branch Stars in the Core of M32", *Astrophys. J.*, **532**(1), 308–322. [DOI], [ADS], [arXiv:astro-ph/9909391 [astro-ph]]

Brown, Thomas M., Sweigart, Allen V., Lanz, Thierry, Land sman, Wayne B. and Hubeny, Ivan, 2001, "Flash Mixing on the White Dwarf Cooling Curve: Understanding Hot Horizontal Branch Anomalies in NGC 2808", *Astrophys. J.*, **562**(1), 368–393. [DOI], [ADS], [arXiv:astro-ph/0108040 [astro-ph]]

Brown, Thomas M., Smith, Ed, Ferguson, Henry C., Sweigart, Allen V., Kimble, Randy A. and Bowers, Charles W., 2008, "The Dearth of UV-Bright Stars in M32: Implications for Stellar Evolution Theory", *Astrophys. J.*, **682**(1), 319–335. [DOI], [ADS], [arXiv:0804.3376 [astro-ph]]

Brown, Thomas M., Sweigart, Allen V., Lanz, Thierry, Smith, Ed, Landsman, Wayne B. and Hubeny, Ivan, 2010, "The Blue Hook Populations of Massive Globular Clusters", *Astrophys. J.*, **718**(2), 1332–1344. [DOI], [ADS], [arXiv:1006.1591 [astro-ph.SR]]

Brown, Thomas M., Lanz, Thierry, Sweigart, Allen V., Cracraft, Misty, Hubeny, Ivan and Landsman, Wayne B., 2012, "Flash Mixing on the White Dwarf Cooling Curve: Spectroscopic Confirmation in NGC 2808", *Astrophys. J.*, **748**(2), 85. [DOI], [ADS], [arXiv:1201.4070 [astro-ph.SR]]

Brown, Warren R., Gianninas, A., Kilic, Mukremin, Kenyon, Scott J. and Allende Prieto, Carlos, 2016b, "The ELM Survey. VII. Orbital Properties of Low-Mass White Dwarf Binaries", *Astrophys. J.*, **818**(2), 155. [DOI], [ADS], [arXiv:1604.04268 [astro-ph.SR]]

Brown, Warren R., Kilic, Mukremin and Gianninas, A., 2017, "The Physical Nature of Subdwarf A Stars: White Dwarf Impostors", *Astrophys. J.*, **839**(1), 23. [DOI], [ADS], [arXiv:1703.07799 [astro-ph.SR]]

Browne, Stanley E., Welsh, Barry Y. and Wheatley, Jonathan, 2009, "GALEX Ultraviolet Observations of Stellar Variability in the Hyades and Pleiades Clusters", *Pub. Astron. Soc. Pac.*, **121**(879), 450. [DOI], [ADS], [arXiv:0904.0042 [astro-ph.GA]]

Busso, G., Cassisi, S., Piotto, G., Castellani, M., Romaniello, M., Catelan, M., Djorgovski, S. G., Recio Blanco, A., Renzini, A., Rich, M. R., Sweigart, A. V. and Zoccali, M., 2007, "The peculiar horizontal branch morphology of the Galactic globular clusters NGC 6388 and NGC 6441: new insights from UV observations", *Astron. Astrophys.*, **474**(1), 105–119. [DOI], [ADS], [arXiv:0708.1736 [astro-ph]]

Bustos Fierro, Iván H. and Calderón, J. H., 2019, "Extraction of globular clusters members with Gaia DR2 astrometry", *Mon. Not. Roy. Astron. Soc.*, **488**(3), 3024–3034. [DOI], [ADS], [arXiv:1907.02612 [astro-ph.IM]]

Cabrera-Ziri, I., Bastian, N., Hilker, M., Davies, B., Schweizer, F., Kruijssen, J. M. D., Mejía-Narváez, A., Niederhofer, F., Brandt, T. D., Rejkuba, M., Bruzual, G. and Magris, G., 2016, "Is the escape velocity in star clusters linked to extended star formation histories? Using NGC 7252: W3 as a test case", *Mon. Not. Roy. Astron. Soc.*, **457**(1), 809–821. [DOI], [ADS], [arXiv:1601.02024 [astro-ph.GA]]

Caloi, V., 1972, "Extended horizontal branch loci.", *Astron. Astrophys.*, **20**, 357–360. [ADS]

Cannon, Russell D., 2015, "Blue Straggler Stars: Early Observations That Failed to Solve the Problem", in *Astrophysics and Space Science Library*, (Eds.) Boffin, Henri M. J., Carraro, Giovanni, Beccari, Giacomo, Astrophysics and Space Science Library, 413, Springer. Springer. [DOI], [ADS], [arXiv:1406.3463 [astro-ph.SR]]

Cantat-Gaudin, T. and Anders, F., 2020, "Clusters and mirages: cataloguing stellar aggregates in the Milky Way", *Astron. Astrophys.*, **633**, A99. [DOI], [ADS], [arXiv:1911.07075 [astro-ph.SR]]

Cantat-Gaudin, T., Anders, F., Castro-Ginard, A., Jordi, C., Romero-Gómez, M., Soubiran, C., Casamiquela, L., Tarricq, Y., Moitinho, A., Vallenari, A., Bragaglia, A., Krone-Martins, A. and Kounkel, M., 2020, "Painting a portrait of the Galactic disc with its stellar clusters", *Astron. Astrophys.*, **640**, A1. [DOI], [ADS], [arXiv:2004.07274 [astro-ph.GA]]

Cardelli, Jason A., Clayton, Geoffrey C. and Mathis, John S., 1989, "The Relationship between Infrared, Optical, and Ultraviolet Extinction", *Astrophys. J.*, **345**, 245. [DOI], [ADS]

Carretta, E., Bragaglia, A., Gratton, R., D'Orazi, V. and Lucatello, S., 2009, "Intrinsic iron spread and a new metallicity scale for globular clusters", *Astron. Astrophys.*, **508**(2), 695–706. [DOI], [ADS], [arXiv:0910.0675 [astro-ph.GA]]

Cassisi, Santi, Schlattl, Helmut, Salaris, Maurizio and Weiss, Achim, 2003, "First Full Evolutionary Computation of the Helium Flash-induced Mixing in Population II Stars", *Astrophys. J. Lett.*, **582**(1), L43–L46. [DOI], [ADS], [arXiv:astro-ph/0211498 [astro-ph]]

Castellani, M. and Castellani, V., 1993, "Mass Loss in Globular Cluster Red Giants: an Evolutionary Investigation", *Astrophys. J.*, **407**, 649. [DOI], [ADS]

Castelli, F. and Kurucz, R. L., 2003, "New Grids of ATLAS9 Model Atmospheres", in *Modelling of Stellar Atmospheres*, (Eds.) Piskunov, N., Weiss, W. W., Gray, D. F., IAU Symposium, 210, the Astronomical Society of the Pacific (ASP). the Astronomical Society of the Pacific (ASP). [DOI], [ADS], [arXiv:astro-ph/0405087 [astro-ph]]

Castelli, F., Gratton, R. G. and Kurucz, R. L., 1997, "Notes on the convection in the ATLAS9 model atmospheres.", *Astron. Astrophys.*, **318**, 841–869. [ADS]

Catelan, M., 2009, "Horizontal branch stars: the interplay between observations and theory, and insights into the formation of the Galaxy", *Astrophys. Space Sci.*, **320**, 261–309. [DOI], [ADS], [arXiv:astro-ph/0507464 [astro-ph]]

Catelan, Márcio, 2007, "Structure and Evolution of Low-Mass Stars: An Overview and Some Open Problems", in *Graduate School in Astronomy: XI Special Courses at the National Observatory of Rio de Janeiro (XI CCE)*, (Eds.) Roig, Fernando, Lopes, Dalton, American Institute of Physics Conference Series, 930, [DOI], [ADS], [arXiv:astro-ph/0703724 [astro-ph]]

Chambers, K. C., Magnier, E. A., Metcalfe, N., Flewelling, H. A., Huber, M. E., Waters, C. Z., Denneau, L., Draper, P. W., Farrow, D., Finkbeiner, D. P., Holmberg, C., Koppenhoefer, J., Price, P. A., Rest, A., Saglia, R. P., Schlafly, E. F., Smartt, S. J., Sweeney, W., Wainscoat, R. J., Burgett, W. S., Chastel, S., Grav, T., Heasley, J. N., Hodapp, K. W., Jedicke, R., Kaiser, N., Kudritzki, R. P., Luppino, G. A., Lupton, R. H., Monet, D. G., Morgan, J. S., Onaka, P. M., Shiao, B., Stubbs, C. W., Tonry, J. L., White, R., Bañados, E., Bell, E. F., Bender, R., Bernard, E. J., Boegner, M., Boffi, F., Botticella, M. T., Calamida, A., Casertano, S., Chen, W. P., Chen, X., Cole, S., Deacon, N., Frenk, C., Fitzsimmons, A., Gezari, S., Gibbs, V., Goessl, C., Goggia, T., Gourgue, R., Goldman, B., Grant, P., Grebel, E. K., Hambly, N. C., Hasinger, G., Heavens, A. F., Heckman, T. M., Henderson, R., Henning, T., Holman, M., Hopp, U., Ip, W. H., Isani, S., Jackson, M., Keyes, C. D., Koekemoer, A. M., Kotak, R., Le, D., Liska, D., Long, K. S., Lucey, J. R., Liu, M., Martin, N. F., Masci, G., McLean, B., Mindel, E., Misra, P., Morganson, E., Murphy, D. N. A., Obaika, A., Narayan, G., Nieto-Santisteban, M. A., Norberg, P., Peacock, J. A., Pier, E. A., Postman, M., Primak, N., Rae, C., Rai, A., Riess, A., Riffeser, A., Rix, H. W., Röser, S., Russel, R., Rutz, L., Schilbach, E., Schultz, A. S. B., Scolnic, D., Strolger, L., Szalay, A., Seitz, S., Small, E., Smith, K. W., Soderblom, D. R., Taylor, P., Thomson, R., Taylor, A. N., Thakar, A. R., Thiel, J., Thilker,

D., Unger, D., Urata, Y., Valenti, J., Wagner, J., Walder, T., Walter, F., Watters, S. P., Werner, S., Wood-Vasey, W. M. and Wyse, R., 2016, "The Pan-STARRS1 Surveys", *arXiv e-prints*, arXiv:1612.05560. [ADS], [arXiv:1612.05560 [astro-ph.IM]]

Choi, Jieun, Dotter, Aaron, Conroy, Charlie, Cantiello, Matteo, Paxton, Bill and Johnson, Benjamin D., 2016, "Mesa Isochrones and Stellar Tracks (MIST). I. Solar-scaled Models", *Astrophys. J.*, **823**(2), 102. [DOI], [ADS], [arXiv:1604.08592 [astro-ph.SR]]

Chung, Chul, Yoon, Suk-Jin and Lee, Young-Wook, 2011, "The Effect of Helium-enhanced Stellar Populations on the Ultraviolet-upturn Phenomenon of Early-type Galaxies", *Astrophys. J. Lett.*, **740**(2), L45. [DOI], [ADS], [arXiv:1109.3463 [astro-ph.GA]]

Chung, Chul, Yoon, Suk-Jin and Lee, Young-Wook, 2017, "Yonsei Evolutionary Population Synthesis (YEPS). II. Spectro-photometric Evolution of Helium-enhanced Stellar Populations", *Astrophys. J.*, **842**(2), 91. [DOI], [ADS], [arXiv:1704.07382 [astro-ph.GA]]

Clement, Christine M., Muzzin, Adam, Dufton, Quentin, Ponnampalam, Thivya, Wang, John, Burford, Jay, Richardson, Alan, Rosebery, Tara, Rowe, Jason and Hogg, Helen Sawyer, 2001, "Variable Stars in Galactic Globular Clusters", *The Astronomical Journal*, **122**(5), 2587–2599. [DOI], [ADS], [arXiv:astro-ph/0108024 [astro-ph]]

Code, A. D. and Welch, G. A., 1979, "Ultraviolet photometry from the Orbiting Astronomical Observatory. XXVI. Energy distributions of seven early-type galaxies and the central bulge of M31.", *Astrophys. J.*, **228**, 95–104. [DOI], [ADS]

Conroy, Charlie and Gunn, James E., 2010, "The Propagation of Uncertainties in Stellar Population Synthesis Modeling. III. Model Calibration, Comparison, and Evaluation", *Astrophys. J.*, **712**(2), 833–857. [DOI], [ADS], [arXiv:0911.3151 [astro-ph.CO]]

Conroy, Charlie, Gunn, James E. and White, Martin, 2009, "The Propagation of Uncertainties in Stellar Population Synthesis Modeling. I. The Relevance of Uncertain Aspects of Stellar Evolution and the Initial Mass Function to the Derived Physical Properties of Galaxies", *Astrophys. J.*, **699**(1), 486–506. [DOI], [ADS], [arXiv:0809.4261 [astro-ph]]

Cummings, Jeffrey D., Kalirai, Jason S., Tremblay, P. E., Ramirez-Ruiz, Enrico and Choi, Jieun, 2018, "The White Dwarf Initial-Final Mass Relation for Progenitor Stars from 0.85 to 7.5 M $_\odot$", *Astrophys. J.*, **866**(1), 21. [DOI], [ADS], [arXiv:1809.01673 [astro-ph.SR]]

Dalessandro, E., Lanzoni, B., Ferraro, F. R., Rood, R. T., Milone, A., Piotto, G. and Valenti, E., 2008, "Blue Straggler Stars in the Unusual Globular Cluster NGC 6388", *Astrophys. J.*, **677**(2), 1069–1079. [DOI], [ADS], [arXiv:0712.4272 [astro-ph]]

Dalessandro, E., Salaris, M., Ferraro, F. R., Cassisi, S., Lanzoni, B., Rood, R. T., Fusi Pecci, F. and Sabbi, E., 2011, "The peculiar horizontal branch of NGC 2808", *Mon. Not. Roy. Astron. Soc.*, **410**(1), 694–704. [DOI], [ADS], [arXiv:1008.4478 [astro-ph.SR]]

Dalessandro, E., Salaris, M., Ferraro, F. R., Mucciarelli, A. and Cassisi, S., 2013, "The horizontal branch in the UV colour-magnitude diagrams - II. The case of M3, M13 and M79", *Mon. Not. Roy. Astron. Soc.*, **430**(1), 459–471. [DOI], [ADS], [arXiv:1212.4419 [astro-ph.SR]]

D'Antona, F., Caloi, V., Montalbán, J., Ventura, P. and Gratton, R., 2002, "Helium variation due to self-pollution among Globular Cluster stars. Consequences on the horizontal branch morphology", *Astron. Astrophys.*, **395**, 69–75. [DOI], [ADS], [arXiv:astro-ph/0209331 [astro-ph]]

D'Antona, F., Bellazzini, M., Caloi, V., Pecci, F. Fusi, Galleti, S. and Rood, R. T., 2005, "A Helium Spread among the Main-Sequence Stars in NGC 2808", *Astrophys. J.*, **631**(2), 868–878. [DOI], [ADS], [arXiv:astro-ph/0505347 [astro-ph]]

D'Antona, F., Di Criscienzo, M., Decressin, T., Milone, A. P., Vesperini, E. and Ventura, P., 2015, "The extended main-sequence turn-off cluster NGC 1856: rotational evolution in a coeval stellar ensemble", *Mon. Not. Roy. Astron. Soc.*, **453**(3), 2637–2643. [DOI], [ADS], [arXiv:1508.01932 [astro-ph.SR]]

Dattatrey, Arvind K., Yadav, R. K. S., Rani, Sharmila, Subramaniam, Annapurni, Singh, Gaurav, Sahu, Snehalata and Singh, Ravi S., 2023, "GlobULeS. IV. UVIT/AstroSat Detection of Extremely Low Mass White Dwarf Companions to Blue Straggler Stars in NGC 362", *Astrophys. J.*, **943**(2), 130. [DOI], [ADS], [arXiv:2212.11302 [astro-ph.SR]]

D'Cruz, Noella L., Dorman, Ben, Rood, Robert T. and O'Connell, Robert W., 1996, "The Origin of Extreme Horizontal Branch Stars", *Astrophys. J.*, **466**, 359. [DOI], [ADS], [arXiv:astro-ph/9511017 [astro-ph]]

D'Cruz, Noella L., O'Connell, Robert W., Rood, Robert T., Whitney, Jonathan H., Dorman, Ben, Landsman, Wayne B., Hill, Robert S., Stecher, Theodore P. and Bohlin, Ralph C., 2000, "Hubble Space Telescope Observations of New Horizontal-Branch Structures in the Globular Cluster ω Centauri", *Astrophys. J.*, **530**(1), 352–356. [DOI], [ADS], [arXiv:astro-ph/9909371 [astro-ph]]

de Boer, Klaas and Seggewiss, Wilhelm, 2008, *Stars and Stellar Evolution*. [ADS]

de Marchi, F., de Angeli, F., Piotto, G., Carraro, G. and Davies, M. B., 2006, "Search and analysis of blue straggler stars in open clusters", *Astron. Astrophys.*, **459**(2), 489–497. [DOI], [ADS], [arXiv:astro-ph/0608464 [astro-ph]]

de Marchi, G. and Pulone, L., 2007, "NGC 2298: a globular cluster on its way to disruption", *Astron. Astrophys.*, **467**(1), 107–115. [DOI], [ADS], [arXiv:astro-ph/0612026 [astro-ph]]

De Martino, C., Bianchi, L., Pagano, I., Herald, J. and Thilker, D., 2008, "GALEX ultraviolet photometry of NGC 2420: searching for WDs", *Mem. Societa Astronomica Italiana*, **79**, 704. [ADS], [arXiv:0712.0755 [astro-ph]]

Denissenkov, Pavel A. and VandenBerg, Don A., 2003, "Thermal Stability of Rotating Low-Mass Subgiants and Red Giants", *Astrophys. J.*, **598**(2), 1246–1254. [DOI], [ADS]

Dieball, A., Knigge, C., Maccarone, T. J., Long, K. S., Hannikainen, D. C., Zurek, D. and Shara, M., 2009, "Blue hook stars in globular clusters", *Mon. Not. Roy. Astron. Soc.*, **394**(1), L56–L60. [DOI], [ADS], [arXiv:0901.1309 [astro-ph.GA]]

Dieball, A., Rasekh, A., Knigge, C., Shara, M. and Zurek, D., 2017, "Far-ultraviolet observation of the globular cluster NGC 6397", *Mon. Not. Roy. Astron. Soc.*, **469**(1), 267–277. [DOI], [ADS], [arXiv:1705.08770 [astro-ph.SR]]

Dieball, Andrea, Long, Knox S., Knigge, Christian, Thomson, Grace S. and Zurek, David R., 2010, "A Far-ultraviolet Survey of M80: X-Ray Source Counterparts, Strange Blue Stragglers, and the Recovery of Nova T Sco", *Astrophys. J.*, **710**(1), 332–345. [DOI], [ADS], [arXiv:1001.1161 [astro-ph.SR]]

Dinescu, Dana I., Girard, Terrence M., van Altena, William F., Yang, Ting-Gao and Lee, Young-Wook, 1996, "A Proper-Motion Membership Study of the Old Open Cluster NGC 188", *Astron. J.*, **111**, 1205. [DOI], [ADS]

Dondoglio, E., Milone, A. P., Lagioia, E. P., Marino, A. F., Tailo, M., Cordoni, G., Jang, S. and Carlos, M., 2021, "Multiple Stellar Populations along the Red Horizontal Branch and Red Clump of Globular Clusters", *Astrophys. J.*, **906**(2), 76. [DOI], [ADS], [arXiv:2011.03283 [astro-ph.GA]]

Dorman, Ben, 1992, "Oxygen-enhanced Models for Globular Cluster Stars. III. Horizontal-Branch Sequences", *Astrophys. J. Suppl.*, **81**, 221. [DOI], [ADS]

Dorman, Ben, O'Connell, Robert W. and Rood, Robert T., 1995, "Ultraviolet Radiation from Evolved Stellar Populations. II. The Ultraviolet Upturn Phenomenon in Elliptical Galaxies", *Astrophys. J.*, **442**, 105. [DOI], [ADS], [arXiv:astro-ph/9405030 [astro-ph]]

Dotter, Aaron, Sarajedini, Ata, Anderson, Jay, Aparicio, Antonio, Bedin, Luigi R., Chaboyer, Brian, Majewski, Steven, Marín-Franch, A., Milone, Antonino, Paust, Nathaniel, Piotto, Giampaolo, Reid, I. Neill, Rosenberg, Alfred and Siegel, Michael, 2010, "The ACS Survey of Galactic Globular Clusters. IX. Horizontal Branch Morphology and the Second Parameter Phenomenon", *Astrophys. J.*, **708**(1), 698–716. [DOI], [ADS], [arXiv:0911.2469 [astro-ph.SR]]

Dotter, Aaron, Sarajedini, Ata and Anderson, Jay, 2011, "Globular Clusters in the Outer Galactic Halo: New Hubble Space Telescope/Advanced Camera for Surveys Imaging of Six Globular Clusters and the Galactic Globular Cluster Age-metallicity Relation", *Astrophys. J.*, **738**(1), 74. [DOI], [ADS], [arXiv:1106.4307 [astro-ph.GA]]

Dufour, R. J., 1984, "The unique planetary nebula NGC 2818.", *Astrophys. J.*, **287**, 341–352. [DOI], [ADS]

Ferraro, F. R., Lanzoni, B., Dalessandro, E., Beccari, G., Pasquato, M., Miocchi, P., Rood, R. T., Sigurdsson, S., Sills, A., Vesperini, E., Mapelli, M., Contreras, R., Sanna, N. and Mucciarelli, A., 2012, "Dynamical age differences among coeval star clusters as revealed by blue stragglers", *Nature*, **492**(7429), 393–395. [DOI], [ADS], [arXiv:1212.5071 [astro-ph.SR]]

Ferraro, Francesco R., Paltrinieri, Barbara, Fusi Pecci, Flavio, Rood, Robert T. and Dorman, Ben, 1998, "Multimodal Distributions along the Horizontal Branch", *Astrophys. J.*, **500**(1), 311–319. [DOI], [ADS], [arXiv:astro-ph/9708210 [astro-ph]]

Ferraro, Francesco R., Sills, Alison, Rood, Robert T., Paltrinieri, Barbara and Buonanno, Roberto, 2003, "Blue Straggler Stars: A Direct Comparison of Star Counts and Population Ratios in Six Galactic Globular Clusters", *Astrophys. J.*, **588**(1), 464–477. [DOI], [ADS], [arXiv:astro-ph/0301261 [astro-ph]]

Fitzpatrick, Edward L., 1999, "Correcting for the Effects of Interstellar Extinction", *Pub. Astron. Soc. Pac.*, **111**(755), 63–75. [DOI], [ADS], [arXiv:astro-ph/9809387 [astro-ph]]

Frew, David J., Parker, Q. A. and Bojičić, I. S., 2016, "The Hα surface brightness-radius relation: a robust statistical distance indicator for planetary nebulae", *Mon. Not. Roy. Astron. Soc.*, **455**(2), 1459–1488. [DOI], [ADS], [arXiv:1504.01534 [astro-ph.SR]]

Friel, E. D., 1995, "The Old Open Clusters Of The Milky Way", *Ann. Rev. Astron. Astrophys.*, **33**, 381–414. [DOI], [ADS]

Gaia Collaboration, Prusti, T., de Bruijne, J. H. J., Brown, A. G. A., Vallenari, A., Babusiaux, C., Bailer-Jones, C. A. L., Bastian, U., Biermann, M., Evans, D. W., Eyer, L., Jansen, F., Jordi, C., Klioner, S. A., Lammers, U., Lindegren, L., Luri, X., Mignard, F., Milligan, D. J., Panem, C., Poinsignon, V., Pourbaix, D., Randich, S., Sarri, G., Sartoretti, P., Siddiqui, H. I., Soubiran, C., Valette, V., van Leeuwen, F., Walton, N. A., Aerts, C., Arenou, F., Cropper, M., Drimmel, R., Høg, E., Katz, D., Lattanzi, M. G., O'Mullane, W., Grebel, E. K., Holland, A. D., Huc, C., Passot, X., Bramante, L., Cacciari, C., Castañeda, J., Chaoul, L., Cheek, N., De Angeli, F., Fabricius, C., Guerra, R., Hernández, J., Jean-Antoine-Piccolo, A., Masana, E., Messineo, R., Mowlavi, N., Nienartowicz, K., Ordóñez-Blanco, D., Panuzzo, P., Portell, J., Richards, P. J., Riello, M., Seabroke, G. M., Tanga, P., Thévenin, F., Torra, J., Els, S. G., Gracia-Abril, G., Comoretto, G., Garcia-Reinaldos, M., Lock, T., Mercier, E., Altmann, M., Andrae, R., Astraatmadja, T. L., Bellas-Velidis, I., Benson, K., Berthier, J., Blomme, R., Busso, G., Carry, B., Cellino, A., Clementini, G., Cowell, S., Creevey, O., Cuypers, J., Davidson, M., De Ridder, J., de Torres, A., Delchambre, L., Dell'Oro, A., Ducourant, C., Frémat, Y., García-Torres, M., Gosset, E., Halbwachs, J. L., Hambly, N. C., Harrison, D. L., Hauser, M., Hestroffer, D., Hodgkin, S. T., Huckle, H. E., Hutton, A., Jasniewicz, G., Jordan, S., Kontizas, M., Korn, A. J., Lanzafame, A. C., Manteiga, M., Moitinho,

A., Muinonen, K., Osinde, J., Pancino, E., Pauwels, T., Petit, J. M., Recio-Blanco, A., Robin, A. C., Sarro, L. M., Siopis, C., Smith, M., Smith, K. W., Sozzetti, A., Thuillot, W., van Reeven, W., Viala, Y., Abbas, U., Abreu Aramburu, A., Accart, S., Aguado, J. J., Allan, P. M., Allasia, W., Altavilla, G., Álvarez, M. A., Alves, J., Anderson, R. I., Andrei, A. H., Anglada Varela, E., Antiche, E., Antoja, T., Antón, S., Arcay, B., Atzei, A., Ayache, L., Bach, N., Baker, S. G., Balaguer-Núñez, L., Barache, C., Barata, C., Barbier, A., Barblan, F., Baroni, M., Barrado y Navascués, D., Barros, M., Barstow, M. A., Becciani, U., Bellazzini, M., Bellei, G., Bello García, A., Belokurov, V., Bendjoya, P., Berihuete, A., Bianchi, L., Bienaymé, O., Billebaud, F., Blagorodnova, N., Blanco-Cuaresma, S., Boch, T., Bombrun, A., Borrachero, R., Bouquillon, S., Bourda, G., Bouy, H., Bragaglia, A., Breddels, M. A., Brouillet, N., Brüsemeister, T., Bucciarelli, B., Budnik, F., Burgess, P., Burgon, R., Burlacu, A., Busonero, D., Buzzi, R., Caffau, E., Cambras, J., Campbell, H., Cancelliere, R., Cantat-Gaudin, T., Carlucci, T., Carrasco, J. M., Castellani, M., Charlot, P., Charnas, J., Charvet, P., Chassat, F., Chiavassa, A., Clotet, M., Cocozza, G., Collins, R. S., Collins, P., Costigan, G., Crifo, F., Cross, N. J. G., Crosta, M., Crowley, C., Dafonte, C., Damerdji, Y., Dapergolas, A., David, P., David, M., De Cat, P., de Felice, F., de Laverny, P., De Luise, F., De March, R., de Martino, D., de Souza, R., Debosscher, J., del Pozo, E., Delbo, M., Delgado, A., Delgado, H. E., di Marco, F., Di Matteo, P., Diakite, S., Distefano, E., Dolding, C., Dos Anjos, S., Drazinos, P., Durán, J., Dzigan, Y., Ecale, E., Edvardsson, B., Enke, H., Erdmann, M., Escolar, D., Espina, M., Evans, N. W., Eynard Bontemps, G., Fabre, C., Fabrizio, M., Faigler, S., Falcão, A. J., Farràs Casas, M., Faye, F., Federici, L., Fedorets, G., Fernández-Hernández, J., Fernique, P., Fienga, A., Figueras, F., Filippi, F., Findeisen, K., Fonti, A., Fouesneau, M., Fraile, E., Fraser, M., Fuchs, J., Furnell, R., Gai, M., Galleti, S., Galluccio, L., Garabato, D., García-Sedano, F., Garé, P., Garofalo, A., Garralda, N., Gavras, P., Gerssen, J., Geyer, R., Gilmore, G., Girona, S., Giuffrida, G., Gomes, M., González-Marcos, A., González-Núñez, J., González-Vidal, J. J., Granvik, M.,

Guerrier, A., Guillout, P., Guiraud, J., Gúrpide, A., Gutiérrez-Sánchez, R., Guy, L. P., Haigron, R., Hatzidimitriou, D., Haywood, M., Heiter, U., Helmi, A., Hobbs, D., Hofmann, W., Holl, B., Holland, G., Hunt, J. A. S., Hypki, A., Icardi, V., Irwin, M., Jevardat de Fombelle, G., Jofré, P., Jonker, P. G., Jorissen, A., Julbe, F., Karampelas, A., Kochoska, A., Kohley, R., Kolenberg, K., Kontizas, E., Koposov, S. E., Kordopatis, G., Koubsky, P., Kowalczyk, A., Krone-Martins, A., Kudryashova, M., Kull, I., Bachchan, R. K., Lacoste-Seris, F., Lanza, A. F., Lavigne, J. B., Le Poncin-Lafitte, C., Lebreton, Y., Lebzelter, T., Leccia, S., Leclerc, N., Lecoeur-Taibi, I., Lemaitre, V., Lenhardt, H., Leroux, F., Liao, S., Licata, E., Lindstrøm, H. E. P., Lister, T. A., Livanou, E., Lobel, A., Löffler, W., López, M., Lopez-Lozano, A., Lorenz, D., Loureiro, T., MacDonald, I., Magalhães Fernandes, T., Managau, S., Mann, R. G., Mantelet, G., Marchal, O., Marchant, J. M., Marconi, M., Marie, J., Marinoni, S., Marrese, P. M., Marschalkó, G., Marshall, D. J., Martín-Fleitas, J. M., Martino, M., Mary, N., Matijevič, G., Mazeh, T., McMillan, P. J., Messina, S., Mestre, A., Michalik, D., Millar, N. R., Miranda, B. M. H., Molina, D., Molinaro, R., Molinaro, M., Molnár, L., Moniez, M., Montegriffo, P., Monteiro, D., Mor, R., Mora, A., Morbidelli, R., Morel, T., Morgenthaler, S., Morley, T., Morris, D., Mulone, A. F., Muraveva, T., Musella, I., Narbonne, J., Nelemans, G., Nicastro, L., Noval, L., Ordénovic, C., Ordieres-Meré, J., Osborne, P., Pagani, C., Pagano, I., Pailler, F., Palacin, H., Palaversa, L., Parsons, P., Paulsen, T., Pecoraro, M., Pedrosa, R., Pentikäinen, H., Pereira, J., Pichon, B., Piersimoni, A. M., Pineau, F. X., Plachy, E., Plum, G., Poujoulet, E., Prša, A., Pulone, L., Ragaini, S., Rago, S., Rambaux, N., Ramos-Lerate, M., Ranalli, P., Rauw, G., Read, A., Regibo, S., Renk, F., Reylé, C., Ribeiro, R. A., Rimoldini, L., Ripepi, V., Riva, A., Rixon, G., Roelens, M., Romero-Gómez, M., Rowell, N., Royer, F., Rudolph, A., Ruiz-Dern, L., Sadowski, G., Sagristà Sellés, T., Sahlmann, J., Salgado, J., Salguero, E., Sarasso, M., Savietto, H., Schnorhk, A., Schultheis, M., Sciacca, E., Segol, M., Segovia, J. C., Segransan, D., Serpell, E., Shih, I. C., Smareglia, R., Smart, R. L., Smith, C., Solano, E., Solitro, F., Sordo, R., Soria

Nieto, S., Souchay, J., Spagna, A., Spoto, F., Stampa, U., Steele, I. A., Steidelmüller, H., Stephenson, C. A., Stoev, H., Suess, F. F., Süveges, M., Surdej, J., Szabados, L., Szegedi-Elek, E., Tapiador, D., Taris, F., Tauran, G., Taylor, M. B., Teixeira, R., Terrett, D., Tingley, B., Trager, S. C., Turon, C., Ulla, A., Utrilla, E., Valentini, G., van Elteren, A., Van Hemelryck, E., van Leeuwen, M., Varadi, M., Vecchiato, A., Veljanoski, J., Via, T., Vicente, D., Vogt, S., Voss, H., Votruba, V., Voutsinas, S., Walmsley, G., Weiler, M., Weingrill, K., Werner, D., Wevers, T., Whitehead, G., Wyrzykowski, Ł., Yoldas, A., Žerjal, M., Zucker, S., Zurbach, C., Zwitter, T., Alecu, A., Allen, M., Allende Prieto, C., Amorim, A., Anglada-Escudé, G., Arsenijevic, V., Azaz, S., Balm, P., Beck, M., Bernstein, H. H., Bigot, L., Bijaoui, A., Blasco, C., Bonfigli, M., Bono, G., Boudreault, S., Bressan, A., Brown, S., Brunet, P. M., Bunclark, P., Buonanno, R., Butkevich, A. G., Carret, C., Carrion, C., Chemin, L., Chéreau, F., Corcione, L., Darmigny, E., de Boer, K. S., de Teodoro, P., de Zeeuw, P. T., Delle Luche, C., Domingues, C. D., Dubath, P., Fodor, F., Frézouls, B., Fries, A., Fustes, D., Fyfe, D., Gallardo, E., Gallegos, J., Gardiol, D., Gebran, M., Gomboc, A., Gómez, A., Grux, E., Gueguen, A., Heyrovsky, A., Hoar, J., Iannicola, G., Isasi Parache, Y., Janotto, A. M., Joliet, E., Jonckheere, A., Keil, R., Kim, D. W., Klagyivik, P., Klar, J., Knude, J., Kochukhov, O., Kolka, I., Kos, J., Kutka, A., Lainey, V., LeBouquin, D., Liu, C., Loreggia, D., Makarov, V. V., Marseille, M. G., Martayan, C., Martinez-Rubi, O., Massart, B., Meynadier, F., Mignot, S., Munari, U., Nguyen, A. T., Nordlander, T., Ocvirk, P., O'Flaherty, K. S., Olias Sanz, A., Ortiz, P., Osorio, J., Oszkiewicz, D., Ouzounis, A., Palmer, M., Park, P., Pasquato, E., Peltzer, C., Peralta, J., Péturaud, F., Pieniluoma, T., Pigozzi, E., Poels, J., Prat, G., Prod'homme, T., Raison, F., Rebordao, J. M., Risquez, D., Rocca-Volmerange, B., Rosen, S., Ruiz-Fuertes, M. I., Russo, F., Sembay, S., Serraller Vizcaino, I., Short, A., Siebert, A., Silva, H., Sinachopoulos, D., Slezak, E., Soffel, M., Sosnowska, D., Straižys, V., ter Linden, M., Terrell, D., Theil, S., Tiede, C., Troisi, L., Tsalmantza, P., Tur, D., Vaccari, M., Vachier, F., Valles, P., Van Hamme, W., Veltz, L., Virtanen, J., Wallut,

J. M., Wichmann, R., Wilkinson, M. I., Ziaeepour, H. and Zschocke, S., 2016, "The Gaia mission", *Astron. Astrophys.*, **595**, A1. [DOI], [ADS], [arXiv:1609.04153 [astro-ph.IM]]

Gaia Collaboration, Helmi, A., van Leeuwen, F., McMillan, P. J., Massari, D., Antoja, T., Robin, A. C., Lindegren, L., Bastian, U., Arenou, F., Babusiaux, C., Biermann, M., Breddels, M. A., Hobbs, D., Jordi, C., Pancino, E., Reylé, C., Veljanoski, J., Brown, A. G. A., Vallenari, A., Prusti, T., de Bruijne, J. H. J., Bailer-Jones, C. A. L., Evans, D. W., Eyer, L., Jansen, F., Klioner, S. A., Lammers, U., Luri, X., Mignard, F., Panem, C., Pourbaix, D., Randich, S., Sartoretti, P., Siddiqui, H. I., Soubiran, C., Walton, N. A., Cropper, M., Drimmel, R., Katz, D., Lattanzi, M. G., Bakker, J., Cacciari, C., Castañeda, J., Chaoul, L., Cheek, N., De Angeli, F., Fabricius, C., Guerra, R., Holl, B., Masana, E., Messineo, R., Mowlavi, N., Nienartowicz, K., Panuzzo, P., Portell, J., Riello, M., Seabroke, G. M., Tanga, P., Thévenin, F., Gracia-Abril, G., Comoretto, G., Garcia-Reinaldos, M., Teyssier, D., Altmann, M., Andrae, R., Audard, M., Bellas-Velidis, I., Benson, K., Berthier, J., Blomme, R., Burgess, P., Busso, G., Carry, B., Cellino, A., Clementini, G., Clotet, M., Creevey, O., Davidson, M., De Ridder, J., Delchambre, L., Dell'Oro, A., Ducourant, C., Fernández-Hernández, J., Fouesneau, M., Frémat, Y., Galluccio, L., García-Torres, M., González-Núñez, J., González-Vidal, J. J., Gosset, E., Guy, L. P., Halbwachs, J. L., Hambly, N. C., Harrison, D. L., Hernández, J., Hestroffer, D., Hodgkin, S. T., Hutton, A., Jasniewicz, G., Jean-Antoine-Piccolo, A., Jordan, S., Korn, A. J., Krone-Martins, A., Lanzafame, A. C., Lebzelter, T., Löffler, W., Manteiga, M., Marrese, P. M., Martín-Fleitas, J. M., Moitinho, A., Mora, A., Muinonen, K., Osinde, J., Pauwels, T., Petit, J. M., Recio-Blanco, A., Richards, P. J., Rimoldini, L., Sarro, L. M., Siopis, C., Smith, M., Sozzetti, A., Süveges, M., Torra, J., van Reeven, W., Abbas, U., Abreu Aramburu, A., Accart, S., Aerts, C., Altavilla, G., Álvarez, M. A., Alvarez, R., Alves, J., Anderson, R. I., Andrei, A. H., Anglada Varela, E., Antiche, E., Arcay, B., Astraatmadja, T. L., Bach, N., Baker, S. G., Balaguer-Núñez, L., Balm, P., Barache, C., Barata, C.,

Barbato, D., Barblan, F., Barklem, P. S., Barrado, D., Barros, M., Barstow, M. A., Bartholomé Muñoz, S., Bassilana, J. L., Becciani, U., Bellazzini, M., Berihuete, A., Bertone, S., Bianchi, L., Bienaymé, O., Blanco-Cuaresma, S., Boch, T., Boeche, C., Bombrun, A., Borrachero, R., Bossini, D., Bouquillon, S., Bourda, G., Bragaglia, A., Bramante, L., Bressan, A., Brouillet, N., Brüsemeister, T., Brugaletta, E., Bucciarelli, B., Burlacu, A., Busonero, D., Butkevich, A. G., Buzzi, R., Caffau, E., Cancelliere, R., Cannizzaro, G., Cantat-Gaudin, T., Carballo, R., Carlucci, T., Carrasco, J. M., Casamiquela, L., Castellani, M., Castro-Ginard, A., Charlot, P., Chemin, L., Chiavassa, A., Cocozza, G., Costigan, G., Cowell, S., Crifo, F., Crosta, M., Crowley, C., Cuypers, J., Dafonte, C., Damerdji, Y., Dapergolas, A., David, P., David, M., de Laverny, P., De Luise, F., De March, R., de Martino, D., de Souza, R., de Torres, A., Debosscher, J., del Pozo, E., Delbo, M., Delgado, A., Delgado, H. E., Di Matteo, P., Diakite, S., Diener, C., Distefano, E., Dolding, C., Drazinos, P., Durán, J., Edvardsson, B., Enke, H., Eriksson, K., Esquej, P., Eynard Bontemps, G., Fabre, C., Fabrizio, M., Faigler, S., Falcão, A. J., Farràs Casas, M., Federici, L., Fedorets, G., Fernique, P., Figueras, F., Filippi, F., Findeisen, K., Fonti, A., Fraile, E., Fraser, M., Frézouls, B., Gai, M., Galleti, S., Garabato, D., García-Sedano, F., Garofalo, A., Garralda, N., Gavel, A., Gavras, P., Gerssen, J., Geyer, R., Giacobbe, P., Gilmore, G., Girona, S., Giuffrida, G., Glass, F., Gomes, M., Granvik, M., Gueguen, A., Guerrier, A., Guiraud, J., Gutiérrez-Sánchez, R., Hofmann, W., Holland, G., Huckle, H. E., Hypki, A., Icardi, V., Janßen, K., Jevardat de Fombelle, G., Jonker, P. G., Juhász, Á. L., Julbe, F., Karampelas, A., Kewley, A., Klar, J., Kochoska, A., Kohley, R., Kolenberg, K., Kontizas, M., Kontizas, E., Koposov, S. E., Kordopatis, G., Kostrzewa-Rutkowska, Z., Koubsky, P., Lambert, S., Lanza, A. F., Lasne, Y., Lavigne, J. B., Le Fustec, Y., Le Poncin-Lafitte, C., Lebreton, Y., Leccia, S., Leclerc, N., Lecoeur-Taibi, I., Lenhardt, H., Leroux, F., Liao, S., Licata, E., Lindstrøm, H. E. P., Lister, T. A., Livanou, E., Lobel, A., López, M., Managau, S., Mann, R. G., Mantelet, G., Marchal, O., Marchant, J. M., Marconi, M., Marinoni, S.,

Marschalkó, G., Marshall, D. J., Martino, M., Marton, G., Mary, N., Matijevič, G., Mazeh, T., Messina, S., Michalik, D., Millar, N. R., Molina, D., Molinaro, R., Molnár, L., Montegriffo, P., Mor, R., Morbidelli, R., Morel, T., Morris, D., Mulone, A. F., Muraveva, T., Musella, I., Nelemans, G., Nicastro, L., Noval, L., O'Mullane, W., Ordénovic, C., Ordóñez-Blanco, D., Osborne, P., Pagani, C., Pagano, I., Pailler, F., Palacin, H., Palaversa, L., Panahi, A., Pawlak, M., Piersimoni, A. M., Pineau, F. X., Plachy, E., Plum, G., Poggio, E., Poujoulet, E., Prša, A., Pulone, L., Racero, E., Ragaini, S., Rambaux, N., Ramos-Lerate, M., Regibo, S., Riclet, F., Ripepi, V., Riva, A., Rivard, A., Rixon, G., Roegiers, T., Roelens, M., Romero-Gómez, M., Rowell, N., Royer, F., Ruiz-Dern, L., Sadowski, G., Sagristà Sellés, T., Sahlmann, J., Salgado, J., Salguero, E., Sanna, N., Santana-Ros, T., Sarasso, M., Savietto, H., Schultheis, M., Sciacca, E., Segol, M., Segovia, J. C., Ségransan, D., Shih, I. C., Siltala, L., Silva, A. F., Smart, R. L., Smith, K. W., Solano, E., Solitro, F., Sordo, R., Soria Nieto, S., Souchay, J., Spagna, A., Spoto, F., Stampa, U., Steele, I. A., Steidelmüller, H., Stephenson, C. A., Stoev, H., Suess, F. F., Surdej, J., Szabados, L., Szegedi-Elek, E., Tapiador, D., Taris, F., Tauran, G., Taylor, M. B., Teixeira, R., Terrett, D., Teyssand ier, P., Thuillot, W., Titarenko, A., Torra Clotet, F., Turon, C., Ulla, A., Utrilla, E., Uzzi, S., Vaillant, M., Valentini, G., Valette, V., van Elteren, A., Van Hemelryck, E., van Leeuwen, M., Vaschetto, M., Vecchiato, A., Viala, Y., Vicente, D., Vogt, S., von Essen, C., Voss, H., Votruba, V., Voutsinas, S., Walmsley, G., Weiler, M., Wertz, O., Wevems, T., Wyrzykowski, Ł., Yoldas, A., Žerjal, M., Ziaeepour, H., Zorec, J., Zschocke, S., Zucker, S., Zurbach, C. and Zwitter, T., 2018, "Gaia Data Release 2. Kinematics of globular clusters and dwarf galaxies around the Milky Way", *Astron. Astrophys.*, **616**, A12. [DOI], [ADS], [arXiv:1804.09381 [astro-ph.GA]]

Gaia Collaboration, Brown, A. G. A., Vallenari, A., Prusti, T., de Bruijne, J. H. J., Babusiaux, C. and Biermann, M., 2020, "Gaia Early Data Release 3: Summary of the contents and survey properties", *arXiv e-prints*, arXiv:2012.01533. [ADS], [arXiv:2012.01533 [astro-ph.GA]]

Gaia Collaboration, Brown, A. G. A., Vallenari, A., Prusti, T., de Bruijne, J. H. J., Babusiaux, C., Biermann, M., Creevey, O. L., Evans, D. W., Eyer, L., Hutton, A., Jansen, F., Jordi, C., Klioner, S. A., Lammers, U., Lindegren, L., Luri, X., Mignard, F., Panem, C., Pourbaix, D., Randich, S., Sartoretti, P., Soubiran, C., Walton, N. A., Arenou, F., Bailer-Jones, C. A. L., Bastian, U., Cropper, M., Drimmel, R., Katz, D., Lattanzi, M. G., van Leeuwen, F., Bakker, J., Cacciari, C., Castañeda, J., De Angeli, F., Ducourant, C., Fabricius, C., Fouesneau, M., Frémat, Y., Guerra, R., Guerrier, A., Guiraud, J., Jean-Antoine Piccolo, A., Masana, E., Messineo, R., Mowlavi, N., Nicolas, C., Nienartowicz, K., Pailler, F., Panuzzo, P., Riclet, F., Roux, W., Seabroke, G. M., Sordo, R., Tanga, P., Thévenin, F., Gracia-Abril, G., Portell, J., Teyssier, D., Altmann, M., Andrae, R., Bellas-Velidis, I., Benson, K., Berthier, J., Blomme, R., Brugaletta, E., Burgess, P. W., Busso, G., Carry, B., Cellino, A., Cheek, N., Clementini, G., Damerdji, Y., Davidson, M., Delchambre, L., Dell'Oro, A., Fernández-Hernández, J., Galluccio, L., García-Lario, P., Garcia-Reinaldos, M., González-Núñez, J., Gosset, E., Haigron, R., Halbwachs, J. L., Hambly, N. C., Harrison, D. L., Hatzidimitriou, D., Heiter, U., Hernández, J., Hestroffer, D., Hodgkin, S. T., Holl, B., Janßen, K., Jevardat de Fombelle, G., Jordan, S., Krone-Martins, A., Lanzafame, A. C., Löffler, W., Lorca, A., Manteiga, M., Marchal, O., Marrese, P. M., Moitinho, A., Mora, A., Muinonen, K., Osborne, P., Pancino, E., Pauwels, T., Petit, J. M., Recio-Blanco, A., Richards, P. J., Riello, M., Rimoldini, L., Robin, A. C., Roegiers, T., Rybizki, J., Sarro, L. M., Siopis, C., Smith, M., Sozzetti, A., Ulla, A., Utrilla, E., van Leeuwen, M., van Reeven, W., Abbas, U., Abreu Aramburu, A., Accart, S., Aerts, C., Aguado, J. J., Ajaj, M., Altavilla, G., Álvarez, M. A., Álvarez Cid-Fuentes, J., Alves, J., Anderson, R. I., Anglada Varela, E., Antoja, T., Audard, M., Baines, D., Baker, S. G., Balaguer-Núñez, L., Balbinot, E., Balog, Z., Barache, C., Barbato, D., Barros, M., Barstow, M. A., Bartolomé, S., Bassilana, J. L., Bauchet, N., Baudesson-Stella, A., Becciani, U., Bellazzini, M., Bernet, M., Bertone, S.,

Bianchi, L., Blanco-Cuaresma, S., Boch, T., Bombrun, A., Bossini, D., Bouquillon, S., Bragaglia, A., Bramante, L., Breedt, E., Bressan, A., Brouillet, N., Bucciarelli, B., Burlacu, A., Busonero, D., Butkevich, A. G., Buzzi, R., Caffau, E., Cancelliere, R., Cánovas, H., Cantat-Gaudin, T., Carballo, R., Carlucci, T., Carnerero, M. I., Carrasco, J. M., Casamiquela, L., Castellani, M., Castro-Ginard, A., Castro Sampol, P., Chaoul, L., Charlot, P., Chemin, L., Chiavassa, A., Cioni, M. R. L., Comoretto, G., Cooper, W. J., Cornez, T., Cowell, S., Crifo, F., Crosta, M., Crowley, C., Dafonte, C., Dapergolas, A., David, M., David, P., de Laverny, P., De Luise, F., De March, R., De Ridder, J., de Souza, R., de Teodoro, P., de Torres, A., del Peloso, E. F., del Pozo, E., Delbo, M., Delgado, A., Delgado, H. E., Delisle, J. B., Di Matteo, P., Diakite, S., Diener, C., Distefano, E., Dolding, C., Eappachen, D., Edvardsson, B., Enke, H., Esquej, P., Fabre, C., Fabrizio, M., Faigler, S., Fedorets, G., Fernique, P., Fienga, A., Figueras, F., Fouron, C., Fragkoudi, F., Fraile, E., Franke, F., Gai, M., Garabato, D., Garcia-Gutierrez, A., García-Torres, M., Garofalo, A., Gavras, P., Gerlach, E., Geyer, R., Giacobbe, P., Gilmore, G., Girona, S., Giuffrida, G., Gomel, R., Gomez, A., Gonzalez-Santamaria, I., González-Vidal, J. J., Granvik, M., Gutiérrez-Sánchez, R., Guy, L. P., Hauser, M., Haywood, M., Helmi, A., Hidalgo, S. L., Hilger, T., Hładczuk, N., Hobbs, D., Holland, G., Huckle, H. E., Jasniewicz, G., Jonker, P. G., Juaristi Campillo, J., Julbe, F., Karbevska, L., Kervella, P., Khanna, S., Kochoska, A., Kontizas, M., Kordopatis, G., Korn, A. J., Kostrzewa-Rutkowska, Z., Kruszyńska, K., Lambert, S., Lanza, A. F., Lasne, Y., Le Campion, J. F., Le Fustec, Y., Lebreton, Y., Lebzelter, T., Leccia, S., Leclerc, N., Lecoeur-Taibi, I., Liao, S., Licata, E., Lindstrøm, E. P., Lister, T. A., Livanou, E., Lobel, A., Madrero Pardo, P., Managau, S., Mann, R. G., Marchant, J. M., Marconi, M., Marcos Santos, M. M. S., Marinoni, S., Marocco, F., Marshall, D. J., Martin Polo, L., Martín-Fleitas, J. M., Masip, A., Massari, D., Mastrobuono-Battisti, A., Mazeh, T., McMillan, P. J., Messina, S., Michalik, D., Millar, N. R., Mints, A., Molina, D., Molinaro, R., Molnár, L., Montegriffo, P., Mor, R., Morbidelli, R., Morel, T., Morris, D., Mulone, A. F.,

Munoz, D., Muraveva, T., Murphy, C. P., Musella, I., Noval, L., Ordénovic, C., Orrù, G., Osinde, J., Pagani, C., Pagano, I., Palaversa, L., Palicio, P. A., Panahi, A., Pawlak, M., Peñalosa Esteller, X., Penttilä, A., Piersimoni, A. M., Pineau, F. X., Plachy, E., Plum, G., Poggio, E., Poretti, E., Poujoulet, E., Prša, A., Pulone, L., Racero, E., Ragaini, S., Rainer, M., Raiteri, C. M., Rambaux, N., Ramos, P., Ramos-Lerate, M., Re Fiorentin, P., Regibo, S., Reylé, C., Ripepi, V., Riva, A., Rixon, G., Robichon, N., Robin, C., Roelens, M., Rohrbasser, L., Romero-Gómez, M., Rowell, N., Royer, F., Rybicki, K. A., Sadowski, G., Sagristà Sellés, A., Sahlmann, J., Salgado, J., Salguero, E., Samaras, N., Sanchez Gimenez, V., Sanna, N., Santoveña, R., Sarasso, M., Schultheis, M., Sciacca, E., Segol, M., Segovia, J. C., Ségransan, D., Semeux, D., Shahaf, S., Siddiqui, H. I., Siebert, A., Siltala, L., Slezak, E., Smart, R. L., Solano, E., Solitro, F., Souami, D., Souchay, J., Spagna, A., Spoto, F., Steele, I. A., Steidelmüller, H., Stephenson, C. A., Süveges, M., Szabados, L., Szegedi-Elek, E., Taris, F., Tauran, G., Taylor, M. B., Teixeira, R., Thuillot, W., Tonello, N., Torra, F., Torra, J., Turon, C., Unger, N., Vaillant, M., van Dillen, E., Vanel, O., Vecchiato, A., Viala, Y., Vicente, D., Voutsinas, S., Weiler, M., Wevers, T., Wyrzykowski, Ł., Yoldas, A., Yvard, P., Zhao, H., Zorec, J., Zucker, S., Zurbach, C. and Zwitter, T., 2021, "Gaia Early Data Release 3. Summary of the contents and survey properties", *Astron. Astrophys.*, **649**, A1. [DOI], [ADS], [arXiv:2012.01533 [astro-ph.GA]]

Gaia Collaboration, Vallenari, A., Brown, A. G. A., Prusti, T., de Bruijne, J. H. J., Arenou, F., Babusiaux, C., Biermann, M., Creevey, O. L., Ducourant, C., Evans, D. W., Eyer, L., Guerra, R., Hutton, A., Jordi, C., Klioner, S. A., Lammers, U. L., Lindegren, L., Luri, X., Mignard, F., Panem, C., Pourbaix, D., Randich, S., Sartoretti, P., Soubiran, C., Tanga, P., Walton, N. A., Bailer-Jones, C. A. L., Bastian, U., Drimmel, R., Jansen, F., Katz, D., Lattanzi, M. G., van Leeuwen,

F., Bakker, J., Cacciari, C., Castañeda, J., De Angeli, F., Fabricius, C., Fouesneau, M., Frémat, Y., Galluccio, L., Guerrier, A., Heiter, U., Masana, E., Messineo, R., Mowlavi, N., Nicolas, C., Nienartowicz, K., Pailler, F., Panuzzo, P., Riclet, F., Roux, W., Seabroke, G. M., Sordoørcit, R., Thévenin, F., Gracia-Abril, G., Portell, J., Teyssier, D., Altmann, M., Andrae, R., Audard, M., Bellas-Velidis, I., Benson, K., Berthier, J., Blomme, R., Burgess, P. W., Busonero, D., Busso, G., Cánovas, H., Carry, B., Cellino, A., Cheek, N., Clementini, G., Damerdji, Y., Davidson, M., de Teodoro, P., Nuñez Campos, M., Delchambre, L., Dell'Oro, A., Esquej, P., Fernández-Hernández, J., Fraile, E., Garabato, D., García-Lario, P., Gosset, E., Haigron, R., Halbwachs, J. L., Hambly, N. C., Harrison, D. L., Hernández, J., Hestroffer, D., Hodgkin, S. T., Holl, B., Janßen, K., Jevardat de Fombelle, G., Jordan, S., Krone-Martins, A., Lanzafame, A. C., Löffler, W., Marchal, O., Marrese, P. M., Moitinho, A., Muinonen, K., Osborne, P., Pancino, E., Pauwels, T., Recio-Blanco, A., Reylé, C., Riello, M., Rimoldini, L., Roegiers, T., Rybizki, J., Sarro, L. M., Siopis, C., Smith, M., Sozzetti, A., Utrilla, E., van Leeuwen, M., Abbas, U., Ábrahám, P., Abreu Aramburu, A., Aerts, C., Aguado, J. J., Ajaj, M., Aldea-Montero, F., Altavilla, G., Álvarez, M. A., Alves, J., Anders, F., Anderson, R. I., Anglada Varela, E., Antoja, T., Baines, D., Baker, S. G., Balaguer-Núñez, L., Balbinot, E., Balog, Z., Barache, C., Barbato, D., Barros, M., Barstow, M. A., Bartolomé, S., Bassilana, J. L., Bauchet, N., Becciani, U., Bellazzini, M., Berihuete, A., Bernet, M., Bertone, S., Bianchi, L., Binnenfeld, A., Blanco-Cuaresma, S., Blazere, A., Boch, T., Bombrun, A., Bossini, D., Bouquillon, S., Bragaglia, A., Bramante, L., Breedt, E., Bressan, A., Brouillet, N., Brugaletta, E., Bucciarelli, B., Burlacu, A., Butkevich, A. G., Buzzi, R., Caffau, E., Cancelliere, R., Cantat-Gaudin, T., Carballo, R., Carlucci, T., Carnerero, M. I., Carrasco, J. M., Casamiquela, L., Castellani, M., Castro-Ginard, A., Chaoul, L., Charlot, P., Chemin, L., Chiaramida, V., Chiavassa, A., Chornay, N., Comoretto, G., Contursi, G., Cooper, W. J., Cornez, T., Cowell, S., Crifo, F., Cropper, M., Crosta, M., Crowley, C., Dafonte, C., Dapergolas, A., David, M., David, P., de Laverny, P., De Luise, F.,

De March, R., De Ridder, J., de Souza, R., de Torres, A., del Peloso, E. F., del Pozo, E., Delbo, M., Delgado, A., Delisle, J. B., Demouchy, C., Dharmawardena, T. E., Di Matteo, P., Diakite, S., Diener, C., Distefano, E., Dolding, C., Edvardsson, B., Enke, H., Fabre, C., Fabrizio, M., Faigler, S., Fedorets, G., Fernique, P., Fienga, A., Figueras, F., Fournier, Y., Fouron, C., Fragkoudi, F., Gai, M., Garcia-Gutierrez, A., Garcia-Reinaldos, M., García-Torres, M., Garofalo, A., Gavel, A., Gavras, P., Gerlach, E., Geyer, R., Giacobbe, P., Gilmore, G., Girona, S., Giuffrida, G., Gomel, R., Gomez, A., González-Núñez, J., González-Santamaría, I., González-Vidal, J. J., Granvik, M., Guillout, P., Guiraud, J., Gutiérrez-Sánchez, R., Guy, L. P., Hatzidimitriou, D., Hauser, M., Haywood, M., Helmer, A., Helmi, A., Sarmiento, M. H., Hidalgo, S. L., Hilger, T., Hładczuk, N., Hobbs, D., Holland, G., Huckle, H. E., Jardine, K., Jasniewicz, G., Jean-Antoine Piccolo, A., Jiménez-Arranz, Ó., Jorissen, A., Juaristi Campillo, J., Julbe, F., Karbevska, L., Kervella, P., Khanna, S., Kontizas, M., Kordopatis, G., Korn, A. J., Kóspál, Á, Kostrzewa-Rutkowska, Z., Kruszyńska, K., Kun, M., Laizeau, P., Lambert, S., Lanza, A. F., Lasne, Y., Le Campion, J. F., Lebreton, Y., Lebzelter, T., Leccia, S., Leclerc, N., Lecoeur-Taibi, I., Liao, S., Licata, E. L., Lindstrøm, H. E. P., Lister, T. A., Livanou, E., Lobel, A., Lorca, A., Loup, C., Madrero Pardo, P., Magdaleno Romeo, A., Managau, S., Mann, R. G., Manteiga, M., Marchant, J. M., Marconi, M., Marcos, J., Marcos Santos, M. M. S., Marín Pina, D., Marinoni, S., Marocco, F., Marshall, D. J., Polo, L. Martin, Martín-Fleitas, J. M., Marton, G., Mary, N., Masip, A., Massari, D., Mastrobuono-Battisti, A., Mazeh, T., McMillan, P. J., Messina, S., Michalik, D., Millar, N. R., Mints, A., Molina, D., Molinaro, R., Molnár, L., Monari, G., Monguió, M., Montegriffo, P., Montero, A., Mor, R., Mora, A., Morbidelli, R., Morel, T., Morris, D., Muraveva, T., Murphy, C. P., Musella, I., Nagy, Z., Noval, L., Ocaña, F., Ogden, A., Ordenovic, C., Osinde, J. O., Pagani, C., Pagano, I., Palaversa, L., Palicio, P. A., Pallas-Quintela, L., Panahi, A., Payne-Wardenaar, S., Peñalosa Esteller, X., Penttilä, A., Pichon, B., Piersimoni, A. M., Pineau,

F. X., Plachy, E., Plum, G., Poggio, E., Prša, A., Pulone, L., Racero, E., Ragaini, S., Rainer, M., Raiteri, C. M., Rambaux, N., Ramos, P., Ramos-Lerate, M., Re Fiorentin, P., Regibo, S., Richards, P. J., Rios Diaz, C., Ripepi, V., Riva, A., Rix, H. W., Rixon, G., Robichon, N., Robin, A. C., Robin, C., Roelens, M., Rogues, H. R. O., Rohrbasser, L., Romero-Gómez, M., Rowell, N., Royer, F., Ruz Mieres, D., Rybicki, K. A., Sadowski, G., Sáez Núñez, A., Sagristà Sellés, A., Sahlmann, J., Salguero, E., Samaras, N., Sanchez Gimenez, V., Sanna, N., Santoveña, R., Sarasso, M., Schultheis, M., Sciacca, E., Segol, M., Segovia, J. C., Ségransan, D., Semeux, D., Shahaf, S., Siddiqui, H. I., Siebert, A., Siltala, L., Silvelo, A., Slezak, E., Slezak, I., Smart, R. L., Snaith, O. N., Solano, E., Solitro, F., Souami, D., Souchay, J., Spagna, A., Spina, L., Spoto, F., Steele, I. A., Steidelmüller, H., Stephenson, C. A., Süveges, M., Surdej, J., Szabados, L., Szegedi-Elek, E., Taris, F., Taylo, M. B., Teixeira, R., Tolomei, L., Tonello, N., Torra, F., Torra, J., Torralba Elipe, G., Trabucchi, M., Tsounis, A. T., Turon, C., Ulla, A., Unger, N., Vaillant, M. V., van Dillen, E., van Reeven, W., Vanel, O., Vecchiato, A., Viala, Y., Vicente, D., Voutsinas, S., Weiler, M., Wevers, T., Wyrzykowski, L., Yoldas, A., Yvard, P., Zhao, H., Zorec, J., Zucker, S. and Zwitter, T., 2022, "Gaia Data Release 3: Summary of the content and survey properties", *arXiv e-prints*, arXiv:2208.00211. [ADS], [arXiv:2208.00211 [astro-ph.GA]]

Gao, Xin-Hua, 2018, "Memberships, distance and proper-motion of the open cluster NGC 188 based on a machine learning method", *Astrophys. Space Sci.*, **363**(11), 232. [DOI], [ADS]

Gathier, R. and Pottasch, S. R., 1988, "Magnitudes of central stars of planetary nebulae.", *Astron. Astrophys.*, **197**, 266–270. [ADS]

Geller, Aaron M., Mathieu, Robert D., Harris, Hugh C. and McClure, Robert D., 2008, "WIYN Open Cluster Study. XXXII. Stellar Radial Velocities in the Old Open Cluster NGC 188", *Astron. J.*, **135**(6), 2264–2278. [DOI], [ADS], [arXiv:1512.04983 [astro-ph.SR]]

Georgy, C., Charbonnel, C., Amard, L., Bastian, N., Ekström, S., Lardo, C., Palacios, A., Eggenberger, P., Cabrera-Ziri, I., Gallet, F. and Lagarde, N., 2019, "Disappearance of the extended main sequence turn-off in intermediate-age clusters as a consequence of magnetic braking", *Astron. Astrophys.*, **622**, A66. [DOI], [ADS], [arXiv:1812.05544 [astro-ph.SR]]

Gingold, R. A., 1976, "The evolutionary status of population II cepheids.", *Astrophys. J.*, **204**, 116–130. [DOI], [ADS]

Gondoin, P., 2005, "X-ray observations of the old open stellar cluster NGC 188", *Astron. Astrophys.*, **438**(1), 291–300. [DOI], [ADS]

Gosnell, Natalie M., Mathieu, Robert D., Geller, Aaron M., Sills, Alison, Leigh, Nathan and Knigge, Christian, 2014, "Detection of White Dwarf Companions to Blue Stragglers in the Open Cluster NGC 188: Direct Evidence for Recent Mass Transfer", *Astrophys. J. Lett.*, **783**(1), L8. [DOI], [ADS], [arXiv:1401.7670 [astro-ph.SR]]

Gosnell, Natalie M., Mathieu, Robert D., Geller, Aaron M., Sills, Alison, Leigh, Nathan and Knigge, Christian, 2015, "Implications for the Formation of Blue Straggler Stars from HST Ultraviolet Observations of NGC 188", *Astrophys. J.*, **814**(2), 163. [DOI], [ADS], [arXiv:1510.04290 [astro-ph.SR]]

Gossage, Seth, Conroy, Charlie, Dotter, Aaron, Cabrera-Ziri, Ivan, Dolphin, Andrew E., Bastian, Nate, Dalcanton, Julianne J., Goudfrooij, Paul, Johnson, L. Clifton, Williams, Benjamin F., Rosenfield, Philip, Kalirai, Jason and Fouesneau, Morgan, 2019, "Combined Effects of Rotation and Age Spreads on Extended Main-Sequence Turn Offs", *Astrophys. J.*, **887**(2), 199. [DOI], [ADS], [arXiv:1907.11251 [astro-ph.SR]]

Goudfrooij, Paul, Puzia, Thomas H., Chandar, Rupali and Kozhurina-Platais, Vera, 2011, "Population Parameters of Intermediate-age Star Clusters in the Large Magellanic Cloud. III. Dynamical Evidence for a Range of Ages Being

Responsible for Extended Main-sequence Turnoffs", *Astrophys. J.*, **737**(1), 4. [DOI], [ADS], [arXiv:1105.1317 [astro-ph.SR]]

Gratton, R. G., Carretta, E., Bragaglia, A., Lucatello, S. and D'Orazi, V., 2010, "The second and third parameters of the horizontal branch in globular clusters", *Astron. Astrophys.*, **517**, A81. [DOI], [ADS], [arXiv:1004.3862 [astro-ph.SR]]

Green, Elizabeth M., Liebert, James W., Peterson, Ruth C. and Saffer, Rex A., 1997, "Bhb/ehb Stars in Old Open Clusters", in *The Third Conference on Faint Blue Stars*, (Eds.) Philip, A. G. D., Liebert, J., Saffer, R., Hayes, D. S., L. Davis Press. L. Davis Press. [ADS]

Green, Elizabeth M., For, Biqing, Hyde, Elaina A., Seitenzahl, Ivo R., Callerame, Keith, White, Brooke A., Young, Corryn N., Huff, Christopher S., Mills, Jay and Steinfadt, Justin D. R., 2004, "Companions of Post-Common Envelope sdB Binaries", *Astrophys. Space Sci.*, **291**(3), 267–274. [DOI], [ADS]

Greenstein, J. L., 1971, "New Spectroscopic Results on Subluminous Stars, V", in *White Dwarfs*, (Ed.) Luyten, Willem Jacob, 42, [ADS]

Greggio, Laura and Renzini, Alvio, 1990, "Clues on the Hot Star Content and the Ultraviolet Output of Elliptical Galaxies", *Astrophys. J.*, **364**, 35. [DOI], [ADS]

Grundahl, F., Catelan, M., Landsman, W. B., Stetson, P. B. and Andersen, M. I., 1999, "Hot Horizontal-Branch Stars: The Ubiquitous Nature of the "Jump" in Strömgren u, Low Gravities, and the Role of Radiative Levitation of Metals", *Astrophys. J.*, **524**(1), 242–261. [DOI], [ADS], [arXiv:astro-ph/9903120 [astro-ph]]

Gunn, James E., Siegmund, Walter A., Mannery, Edward J., Owen, Russell E., Hull, Charles L., Leger, R. French, Carey, Larry N., Knapp, Gillian R., York, Donald G., Boroski, William N., Kent, Stephen M., Lupton, Robert H., Rockosi, Constance M., Evans, Michael L., Waddell, Patrick, Anderson, John E., Annis, James, Barentine, John C., Bartoszek, Larry M., Bastian, Steven, Bracker, Stephen B., Brewington, Howard J., Briegel, Charles I., Brinkmann, Jon,

Brown, Yorke J., Carr, Michael A., Czarapata, Paul C., Drennan, Craig C., Dombeck, Thomas, Federwitz, Glenn R., Gillespie, Bruce A., Gonzales, Carlos, Hansen, Sten U., Harvanek, Michael, Hayes, Jeffrey, Jordan, Wendell, Kinney, Ellyne, Klaene, Mark, Kleinman, S. J., Kron, Richard G., Kresinski, Jurek, Lee, Glenn, Limmongkol, Siriluk, Lindenmeyer, Carl W., Long, Daniel C., Loomis, Craig L., McGehee, Peregrine M., Mantsch, Paul M., Neilsen, Eric H., Jr., Neswold, Richard M., Newman, Peter R., Nitta, Atsuko, Peoples, John, Jr., Pier, Jeffrey R., Prieto, Peter S., Prosapio, Angela, Rivetta, Claudio, Schneider, Donald P., Snedden, Stephanie and Wang, Shu-i., 2006, "The 2.5 m Telescope of the Sloan Digital Sky Survey", *Astron. J.*, **131**(4), 2332–2359. [DOI], [ADS], [arXiv:astro-ph/0602326 [astro-ph]]

Habing, Harm J. and Olofsson, Hans, 2004, *Asymptotic Giant Branch Stars*. [DOI], [ADS]

Harris, H. C. and McClure, R. D., 1985, "An FK Comae-like star in NGC 188.", *Pub. Astron. Soc. Pac.*, **97**, 261–263. [DOI], [ADS]

Harris, H. C., Nemec, J. M. and Hesser, J. E., 1983, "Radial velocities of stars in M 12 (NGC 6218) and M 56 (NGC 6779) andUV-bright stars in globular clusters.", *Pub. Astron. Soc. Pac.*, **95**, 256–263. [DOI], [ADS]

Harris, William E., 2010, "A New Catalog of Globular Clusters in the Milky Way", *arXiv e-prints*, arXiv:1012.3224. [ADS], [arXiv:1012.3224 [astro-ph.GA]]

Haurberg, Nathalie C., Lubell, Gabriel M. G., Cohn, Haldan N., Lugger, Phyllis M., Anderson, Jay, Cool, Adrienne M. and Serenelli, Aldo M., 2010, "Ultraviolet-bright Stellar Populations and Their Evolutionary Implications in the Collapsed-core Cluster M15", *Astrophys. J.*, **722**(1), 158–177. [DOI], [ADS], [arXiv:1009.5694 [astro-ph.SR]]

Hayashi, Chushiro, 1966, "Evolution of Protostars", *Ann. Rev. Astron. Astrophys.*, **4**, 171. [DOI], [ADS]

Heber, U., 1986, "The atmosphere of subluminous B stars. II. Analysis of 10 helium poor subdwarfs and the birthrate of sdB stars.", *Astron. Astrophys.*, **155**, 33–45. [ADS]

Heber, U., 2016, "Hot Subluminous Stars", *Pub. Astron. Soc. Pac.*, **128**(966), 082 001. [DOI], [ADS], [arXiv:1604.07749 [astro-ph.SR]]

Heber, U., Edelmann, H., Lisker, T. and Napiwotzki, R., 2003, "Discovery of a helium-core white dwarf progenitor", *Astron. Astrophys.*, **411**, L477–L480. [DOI], [ADS]

Hema, B. P., Pandey, Gajendra, Kurucz, R. L. and Allende Prieto, C., 2020, "Helium Enhancement in the Metal-rich Red Giants of ω Centauri", *Astrophys. J.*, **897**(1), 32. [DOI], [ADS], [arXiv:2005.06807 [astro-ph.SR]]

Herwig, Falk, 2005, "Evolution of Asymptotic Giant Branch Stars", *Ann. Rev. Astron. Astrophys.*, **43**(1), 435–479. [DOI], [ADS]

Hidalgo, Sebastian L., Pietrinferni, Adriano, Cassisi, Santi, Salaris, Maurizio, Mucciarelli, Alessio, Savino, Alessandro, Aparicio, Antonio, Silva Aguirre, Victor and Verma, Kuldeep, 2018, "The Updated BaSTI Stellar Evolution Models and Isochrones. I. Solar-scaled Calculations", *Astrophys. J.*, **856**(2), 125. [DOI], [ADS], [arXiv:1802.07319 [astro-ph.GA]]

Hills, J. G. and Day, C. A., 1976, "Stellar Collisions in Globular Clusters", *Astrophysics Letters*, **17**, 87. [ADS]

Hoyle, F. and Schwarzschild, M., 1955, "On the Evolution of Type II Stars.", *Astrophys. J.*, **121**, 776–778. [DOI], [ADS]

Husfeld, D., Butler, K., Heber, U. and Drilling, J. S., 1989, "Non-LTE analysis of extremly helium-rich stars. I. The hot sdO stars LSE 153, 259 and 263.", *Astron. Astrophys.*, **222**, 150–170. [ADS]

Hutchings, J. B., Postma, J., Asquin, D. and Leahy, D., 2007, "Photon Event Centroiding with UV Photon-counting Detectors", *Pub. Astron. Soc. Pac.*, **119**(860), 1152–1162. [DOI], [ADS]

Iben, Icko, 1995, "Planetary nebulae and their central stars — origin and evolution", *Physics Reports*, **250**(1), 1–94. [DOI], [ADS]

Iben, I., Jr., 1974, "Post main sequence evolution of single stars.", *Ann. Rev. Astron. Astrophys.*, **12**, 215–256. [DOI], [ADS]

Iben, I., Jr. and Renzini, A., 1983, "Asymptotic giant branch evolution and beyond.", *Ann. Rev. Astron. Astrophys.*, **21**, 271–342. [DOI], [ADS]

Iben, I., Jr. and Tutukov, A. V., 1999, "On the production by triple stars of binary blue stragglers and cataclysmic variables", in *11th European Workshop on White Dwarfs*, (Eds.) Solheim, S. E., Meistas, E. G., Astronomical Society of the Pacific Conference Series, 169, [ADS]

Iben, Icko, Jr., 1967, "Stellar Evolution Within and off the Main Sequence", *Ann. Rev. Astron. Astrophys.*, **5**, 571. [DOI], [ADS]

Iben, Icko, Jr., 1991, "Single and Binary Star Evolution", *Astrophys. J. Suppl.*, **76**, 55. [DOI], [ADS]

Iben, Icko, Jr. and Rood, Robert T., 1970, "Metal-Poor Stars. III. on the Evolution of Horizontal-Branch Stars", *Astrophys. J.*, **161**, 587. [DOI], [ADS]

Indebetouw, R., Mathis, J. S., Babler, B. L., Meade, M. R., Watson, C., Whitney, B. A., Wolff, M. J., Wolfire, M. G., Cohen, M., Bania, T. M., Benjamin, R. A., Clemens, D. P., Dickey, J. M., Jackson, J. M., Kobulnicky, H. A., Marston, A. P., Mercer, E. P., Stauffer, J. R., Stolovy, S. R. and Churchwell, E., 2005, "The Wavelength Dependence of Interstellar Extinction from 1.25 to 8.0 μm Using GLIMPSE Data", *Astrophys. J.*, **619**(2), 931–938. [DOI], [ADS], [arXiv:astro-ph/0406403 [astro-ph]]

Jadhav, Vikrant V. and Subramaniam, Annapurni, 2021, "Blue straggler stars in open clusters using Gaia: dependence on cluster parameters and possible formation pathways", *Mon. Not. Roy. Astron. Soc.*, **507**(2), 1699–1709. [DOI], [ADS], [arXiv:2108.01396 [astro-ph.SR]]

Jadhav, Vikrant V., Sindhu, N. and Subramaniam, Annapurni, 2019, "UVIT Open Cluster Study. II. Detection of Extremely Low Mass White Dwarfs and Post-Mass Transfer Binaries in M67", *Astrophys. J.*, **886**(1), 13. [DOI], [ADS], [arXiv:1910.01819 [astro-ph.SR]]

Jadhav, Vikrant V., Pandey, Sindhu, Subramaniam, Annapurni and Sagar, Ram, 2021, "UOCS. IV. Discovery of diverse hot companions to blue stragglers in the old open cluster King 2", *Journal of Astrophysics and Astronomy*, **42**(2), 89. [DOI], [ADS], [arXiv:2102.13375 [astro-ph.SR]]

Janes, K. and Adler, D., 1982, "Open clusters and galactic structure.", *Astrophys. J. Suppl.*, **49**, 425–446. [DOI], [ADS]

Jordan, Carole and Linsky, Jeffrey L., 1987, "Chromospheres and Transition Regions", in *Exploring the Universe with the IUE Satellite*, (Eds.) Kondo, Y., Wamsteker, W., Astrophysics and Space Science Library, 129, Springer, Dordrecht. Springer, Dordrecht. [DOI], [ADS]

Kaluzny, J. and Udalski, A., 1992, "Photometric Study of the Old Open Cluster NGC 6791", *Acta Astronomica*, **42**, 29–47. [ADS]

Keller, Stefan C., Mackey, A. Dougal and Da Costa, Gary S., 2011, "The Extended Main-sequence Turnoff Clusters of the Large Magellanic Cloud—Missing Links in Globular Cluster Evolution", *Astrophys. J.*, **731**(1), 22. [DOI], [ADS], [arXiv:1102.1723 [astro-ph.GA]]

Kharchenko, N. V., Piskunov, A. E., Schilbach, E., Röser, S. and Scholz, R. D., 2013, "Global survey of star clusters in the Milky Way. II. The catalogue of basic parameters", *Astron. Astrophys.*, **558**, A53. [DOI], [ADS], [arXiv:1308.5822 [astro-ph.GA]]

Kippenhahn, Rudolf, Weigert, Alfred and Weiss, Achim, 2013, *Stellar Structure and Evolution*. [DOI], [ADS]

Knigge, Christian, Zurek, David R., Shara, Michael M. and Long, Knox S., 2002, "A Far-Ultraviolet Survey of 47 Tucanae. I. Imaging", *Astrophys. J.*, **579**(2), 752–759. [DOI], [ADS], [arXiv:astro-ph/0207060 [astro-ph]]

Koester, D., 2010, "White dwarf spectra and atmosphere models", *Mem. Societa Astronomica Italiana*, **81**, 921–931. [ADS]

Kohoutek, L., Roth-Hoeppner, M. L. and Laustsen, S., 1986, "Study of the planetary nebula NGC 2818. I. Photometry of the central star.", *Astron. Astrophys.*, **162**, 232–234. [ADS]

Krause, Martin G. H., Offner, Stella S. R., Charbonnel, Corinne, Gieles, Mark, Klessen, Ralf S., Vázquez-Semadeni, Enrique, Ballesteros-Paredes, Javier, Girichidis, Philipp, Kruijssen, J. M. Diederik, Ward, Jacob L. and Zinnecker, Hans, 2020, "The Physics of Star Cluster Formation and Evolution", *Space Sci. Rev.*, **216**(4), 64. [DOI], [ADS], [arXiv:2005.00801 [astro-ph.GA]]

Kravtsov, V., Alcaíno, G., Marconi, G. and Alvarado, F., 2010, "Wide-field multicolor photometry of the Galactic globular cluster NGC 1261", *Astron. Astrophys.*, **516**, A23. [DOI], [ADS], [arXiv:1005.0007 [astro-ph.GA]]

Krumholz, Mark R., McKee, Christopher F. and Bland-Hawthorn, Joss, 2019, "Star Clusters Across Cosmic Time", *Ann. Rev. Astron. Astrophys.*, **57**, 227–303. [DOI], [ADS], [arXiv:1812.01615 [astro-ph.GA]]

Kumar, Amit, Ghosh, S. K., Hutchings, J., Kamath, P. U., Kathiravan, S., Mahesh, P. K., Murthy, J., Nagbhushana, S., Pati, A. K., Rao, M. N., Rao, N. K., Sriram, S. and Tandon, S. N., 2012, "Ultra Violet Imaging Telescope (UVIT) on ASTROSAT", in *Space Telescopes and Instrumentation 2012: Ultraviolet to Gamma Ray*, (Eds.) Takahashi, Tadayuki, Murray, Stephen S., den Herder, Jan-Willem A., Society of Photo-Optical Instrumentation Engineers (SPIE) Conference Series, 8443, SPIE. SPIE. [DOI], [ADS], [arXiv:1208.4670 [astro-ph.IM]]

Kurucz, Robert, 1993, "ATLAS9 Stellar Atmosphere Programs and 2 km/s grid.", *ATLAS9 Stellar Atmosphere Programs and 2 km/s grid. Kurucz CD-ROM No. 13. Cambridge*, **13**. [ADS]

Kwitter, K. B., Méndez, R. H., Peña, M., Stanghellini, L., Corradi, R. L. M., De Marco, O., Fang, X., Henry, R. B. C., Karakas, A. I., Liu, X. W., López, J. A., Manchado, A. and Parker, Q. A., 2014, "The Present and Future of Planetary Nebula Research. A White Paper by the IAU Planetary Nebula Working Group", *Revista Mexicana de Astronomía y Astrofśica*, **50**, 203–223. [ADS], [arXiv:1403.2246 [astro-ph.SR]]

Kwok, Sun, 2000, *The Origin and Evolution of Planetary Nebulae*. [ADS]

Lagioia, E. P., Milone, A. P., Marino, A. F., Tailo, M., Renzini, A., Carlos, M., Cordoni, G., Dondoglio, E., Jang, S., Karakas, A. and Dotter, A., 2021, "Multiple Stellar Populations in Asymptotic Giant Branch Stars of Galactic Globular Clusters", *Astrophys. J.*, **910**(1), 6. [DOI], [ADS], [arXiv:2101.09843 [astro-ph.SR]]

Landsman, W., Aparicio, J., Bergeron, P., Di Stefano, R. and Stecher, T. P., 1997, "S1040 in M67: A Post–Mass Transfer Binary with a Helium Core White Dwarf", *Astrophys. J. Lett.*, **481**(2), L93–L96. [DOI], [ADS], [arXiv:astro-ph/9703053 [astro-ph]]

Landsman, Wayne, Bohlin, Ralph C., Neff, Susan G., O'Connell, Robert W., Roberts, Morton S., Smith, Andrew M. and Stecher, Theodore P., 1998, "The Hot Stars of Old Open Clusters: M67, NGC 188, and NGC 6791", *Astron. J.*, **116**(2), 789–800. [DOI], [ADS], [arXiv:astro-ph/9804164 [astro-ph]]

Lee, Jae-Woo, Kang, Young-Woon, Lee, Jina and Lee, Young-Wook, 2009, "Enrichment by supernovae in globular clusters with multiple populations", *Nature*, **462**(7272), 480–482. [DOI], [ADS], [arXiv:0911.4798 [astro-ph.GA]]

Lee, Young-Wook, Joo, Seok-Joo, Han, Sang-Il, Chung, Chul, Ree, Chang H., Sohn, Young-Jong, Kim, Yong-Cheol, Yoon, Suk-Jin, Yi, Sukyoung K. and

Demarque, Pierre, 2005, "Super-Helium-rich Populations and the Origin of Extreme Horizontal-Branch Stars in Globular Clusters", *Astrophys. J. Lett.*, **621**(1), L57–L60. [DOI], [ADS], [arXiv:astro-ph/0501500 [astro-ph]]

Lee, Young-Wook, Joo, Seok-Joo, Han, Sang-Il, Na, Chongsam, Lim, Dongwook and Roh, Dong-Goo, 2015, "Population Models for Massive Globular Clusters", *Highlights of Astronomy*, **16**, 247–248. [DOI], [ADS]

Lei, Zhenxin, Chen, Xuemei, Zhang, Fenghui and Han, Zhanwen, 2015, "A possible formation channel for blue hook stars in globular clusters", *Mon. Not. Roy. Astron. Soc.*, **449**(3), 2741–2749. [DOI], [ADS], [arXiv:1503.08885 [astro-ph.SR]]

Leiner, Emily, Mathieu, Robert D., Stello, Dennis, Vanderburg, Andrew and Sandquist, Eric, 2016, "The K2 M67 Study: An Evolved Blue Straggler in M67 from K2 Mission Asteroseismology", *Astrophys. J. Lett.*, **832**(1), L13. [DOI], [ADS], [arXiv:1611.01158 [astro-ph.SR]]

Li, Chengyuan, Wang, Yue, Tang, Baitian, Milone, Antonino P., Yang, Yujiao and Ji, Xin, 2020, "When Does the Onset of Multiple Stellar Populations in Star Clusters Occur? III. No Evidence of Significant Chemical Variations in Main-sequence Stars of NGC 419", *Astrophys. J.*, **893**(1), 17. [DOI], [ADS], [arXiv:2003.00159 [astro-ph.SR]]

Liebert, James, Saffer, Rex A. and Green, Elizabeth M., 1994, "The Evolved Hot Stars of The Old, Metal-Rich Galactic Cluster NGC 6791", *Astron. J.*, **107**, 1408. [DOI], [ADS]

Lindegren, L., Hernández, J., Bombrun, A., Klioner, S., Bastian, U., Ramos-Lerate, M., de Torres, A., Steidelmüller, H., Stephenson, C., Hobbs, D., Lammers, U., Biermann, M., Geyer, R., Hilger, T., Michalik, D., Stampa, U., McMillan, P. J., Castañeda, J., Clotet, M., Comoretto, G., Davidson, M., Fabricius, C., Gracia, G., Hambly, N. C., Hutton, A., Mora, A., Portell, J., van Leeuwen, F., Abbas, U., Abreu, A., Altmann, M., Andrei, A., Anglada, E., Balaguer-Núñez, L., Barache, C., Becciani, U., Bertone, S., Bianchi, L., Bouquillon, S.,

Bourda, G., Brüsemeister, T., Bucciarelli, B., Busonero, D., Buzzi, R., Cancelliere, R., Carlucci, T., Charlot, P., Cheek, N., Crosta, M., Crowley, C., de Bruijne, J., de Felice, F., Drimmel, R., Esquej, P., Fienga, A., Fraile, E., Gai, M., Garralda, N., González-Vidal, J. J., Guerra, R., Hauser, M., Hofmann, W., Holl, B., Jordan, S., Lattanzi, M. G., Lenhardt, H., Liao, S., Licata, E., Lister, T., Löffler, W., Marchant, J., Martin-Fleitas, J. M., Messineo, R., Mignard, F., Morbidelli, R., Poggio, E., Riva, A., Rowell, N., Salguero, E., Sarasso, M., Sciacca, E., Siddiqui, H., Smart, R. L., Spagna, A., Steele, I., Taris, F., Torra, J., van Elteren, A., van Reeven, W. and Vecchiato, A., 2018, "Gaia Data Release 2. The astrometric solution", *Astron. Astrophys.*, **616**, A2. [DOI], [ADS], [arXiv:1804.09366 [astro-ph.IM]]

Linsky, J. L. and Haisch, B. M., 1979, "Outer atmospheres of cool stars. I. The sharp division into solar-type and non-solar-type stars.", *Astrophys. J. Lett.*, **229**, L27–L32. [DOI], [ADS]

Linsky, Jeffrey L., Wood, Brian E., Youngblood, Allison, Brown, Alexander, Froning, Cynthia S., France, Kevin, Buccino, Andrea P., Cranmer, Steven R., Mauas, Pablo, Miguel, Yamila, Pineda, J. Sebastian, Rugheimer, Sarah, Vieytes, Mariela, Wheatley, Peter J. and Wilson, David J., 2020, "The Relative Emission from Chromospheres and Coronae: Dependence on Spectral Type and Age", *Astrophys. J.*, **902**(1), 3. [DOI], [ADS], [arXiv:2009.01958 [astro-ph.SR]]

Mackey, A. D. and Broby Nielsen, P., 2007, "A double main-sequence turn-off in the rich star cluster NGC 1846 in the Large Magellanic Cloud", *Mon. Not. Roy. Astron. Soc.*, **379**(1), 151–158. [DOI], [ADS], [arXiv:0704.3360 [astro-ph]]

Marino, A. F., Villanova, S., Piotto, G., Milone, A. P., Momany, Y., Bedin, L. R. and Medling, A. M., 2008, "Spectroscopic and photometric evidence of two stellar populations in the Galactic globular cluster NGC 6121 (M 4)", *Astron. Astrophys.*, **490**(2), 625–640. [DOI], [ADS], [arXiv:0808.1414 [astro-ph]]

Marino, A. F., Milone, A. P., Przybilla, N., Bergemann, M., Lind, K., Asplund, M., Cassisi, S., Catelan, M., Casagrande, L., Valcarce, A. A. R., Bedin, L. R., Cortés, C., D'Antona, F., Jerjen, H., Piotto, G., Schlesinger, K., Zoccali, M. and Angeloni, R., 2014, "Helium enhanced stars and multiple populations along the horizontal branch of NGC 2808: direct spectroscopic measurements", *Mon. Not. Roy. Astron. Soc.*, **437**(2), 1609–1627. [DOI], [ADS], [arXiv:1310.4527 [astro-ph.SR]]

Martin, Christopher, Barlow, Thomas, Barnhart, William, Bianchi, Luciana, Blakkolb, Brian K., Bruno, Dominique, Bushman, Joseph, Byun, Yong-Ik, Chiville, Michael, Conrow, Timothy, Cooke, Brian, Donas, Jose, Fanson, James L., Forster, Karl, Friedman, Peter G., Grange, Robert, Griffiths, David, Heckman, Timothy, Lee, James, Jelinsky, Patrick N., Kim, Sug-Whan, Lee, Siu-Chun, Lee, Young-Wook, Liu, Dankai, Madore, Barry F., Malina, Roger, Mazer, Alan, McLean, Ryan, Milliard, Bruno, Mitchell, William, Morais, Marco, Morrissey, Patrick F., Neff, Susan G., Raison, Frederic, Randall, David, Rich, Michael, Schiminovich, David, Schmitigal, Wes, Sen, Amit, Siegmund, Oswald H. W., Small, Todd, Stock, Joseph M., Surber, Frank, Szalay, Alexander, Vaughan, Arthur H., Weigand, Timothy, Welsh, Barry Y., Wu, Patrick, Wyder, Ted, Xu, C. Kevin and Zsoldas, Jennifer, 2003, "The Galaxy Evolution Explorer", in *Future EUV/UV and Visible Space Astrophysics Missions and Instrumentation.*, (Eds.) Blades, J. Chris, Siegmund, Oswald H. W., Society of Photo-Optical Instrumentation Engineers (SPIE) Conference Series, 4854, [DOI], [ADS]

Martocchia, S., Bastian, N., Usher, C., Kozhurina-Platais, V., Niederhofer, F., Cabrera-Ziri, I., Dalessandro, E., Hollyhead, K., Kacharov, N., Lardo, C., Larsen, S., Mucciarelli, A., Platais, I., Salaris, M., Cordero, M., Geisler, D., Hilker, M., Li, C. and Mackey, D., 2017, "The search for multiple populations in Magellanic Cloud Clusters - III. No evidence for multiple populations in the

SMC cluster NGC 419", *Mon. Not. Roy. Astron. Soc.*, **468**(3), 3150–3158. [DOI], [ADS], [arXiv:1703.04631 [astro-ph.GA]]

Mata, H., Ramos-Larios, G., Guerrero, M. A., Nigoche-Netro, A., Toalá, J. A., Fang, X., Rubio, G., Kemp, S. N., Navarro, S. G. and Corral, L. J., 2016, "Spitzer mid-infrared spectroscopic observations of planetary nebulae", *Mon. Not. Roy. Astron. Soc.*, **459**(1), 841–853. [DOI], [ADS], [arXiv:1603.06667 [astro-ph.SR]]

Mathieu, Robert D., Latham, David W. and Griffin, R. F., 1990, "Orbits of 22 Spectroscopic Binaries in the Open Cluster M67", *Astron. J.*, **100**, 1859. [DOI], [ADS]

Mazur, Beata and Kaluzny, Janusz, 1990, "BV photometry of two evolved variables in NGC 188.", *Acta Astronomica*, **40**, 361. [ADS]

McCrea, W. H., 1964, "Extended main-sequence of some stellar clusters", *Mon. Not. Roy. Astron. Soc.*, **128**, 147. [DOI], [ADS]

Meatheringham, Stephen J., Wood, P. R. and Faulkner, D. J., 1988, "A Study of Some Southern Planetary Nebulae", *Astrophys. J.*, **334**, 862. [DOI], [ADS]

Mengel, John G., Norris, John and Gross, Peter G., 1976, "Binary Hypothesis for the Subdwarf B Stars", *Astrophys. J.*, **204**, 488–492. [DOI], [ADS]

Mermilliod, J. C., Clariá, J. J., Andersen, J., Piatti, A. E. and Mayor, M., 2001, "Red giants in open clusters. IX. NGC 2324, 2818, 3960 and 6259", *Astron. Astrophys.*, **375**, 30–39. [DOI], [ADS]

Miller Bertolami, Marcelo Miguel, 2016, "New models for the evolution of post-asymptotic giant branch stars and central stars of planetary nebulae", *Astron. Astrophys.*, **588**, A25. [DOI], [ADS], [arXiv:1512.04129 [astro-ph.SR]]

Milne, D. K. and Aller, L. H., 1975, "Radio observations at 5 GHz of southern planetary nebulae.", *Astron. Astrophys.*, **38**, 183–196. [ADS]

Milone, A. P., Bedin, L. R., Piotto, G., Anderson, J., King, I. R., Sarajedini, A., Dotter, A., Chaboyer, B., Marín-Franch, A., Majewski, S., Aparicio, A., Hempel, M., Paust, N. E. Q., Reid, I. N., Rosenberg, A. and Siegel, M., 2008, "The ACS Survey of Galactic Globular Clusters. III. The Double Subgiant Branch of NGC 1851", *Astrophys. J.*, **673**(1), 241–250. [DOI], [ADS], [arXiv:0709.3762 [astro-ph]]

Milone, A. P., Bedin, L. R., Piotto, G. and Anderson, J., 2009, "Multiple stellar populations in Magellanic Cloud clusters. I. An ordinary feature for intermediate age globulars in the LMC?", *Astron. Astrophys.*, **497**(3), 755–771. [DOI], [ADS], [arXiv:0810.2558 [astro-ph]]

Milone, A. P., Marino, A. F., Dotter, A., Norris, J. E., Jerjen, H., Piotto, G., Cassisi, S., Bedin, L. R., Recio Blanco, A., Sarajedini, A., Asplund, M., Monelli, M. and Aparicio, A., 2014, "Global and Nonglobal Parameters of Horizontal-branch Morphology of Globular Clusters", *Astrophys. J.*, **785**(1), 21. [DOI], [ADS], [arXiv:1312.4169 [astro-ph.SR]]

Milone, A. P., Marino, A. F., D'Antona, F., Bedin, L. R., Da Costa, G. S., Jerjen, H. and Mackey, A. D., 2016, "Multiple stellar populations in Magellanic Cloud clusters - IV. The double main sequence of the young cluster NGC 1755", *Mon. Not. Roy. Astron. Soc.*, **458**(4), 4368–4382. [DOI], [ADS], [arXiv:1603.03493 [astro-ph.SR]]

Milone, A. P., Piotto, G., Renzini, A., Marino, A. F., Bedin, L. R., Vesperini, E., D'Antona, F., Nardiello, D., Anderson, J., King, I. R., Yong, D., Bellini, A., Aparicio, A., Barbuy, B., Brown, T. M., Cassisi, S., Ortolani, S., Salaris, M., Sarajedini, A. and van der Marel, R. P., 2017, "The Hubble Space Telescope UV Legacy Survey of Galactic globular clusters - IX. The Atlas of multiple stellar populations", *Mon. Not. Roy. Astron. Soc.*, **464**(3), 3636–3656. [DOI], [ADS], [arXiv:1610.00451 [astro-ph.SR]]

Milone, A. P., Marino, A. F., Renzini, A., D'Antona, F., Anderson, J., Barbuy, B., Bedin, L. R., Bellini, A., Brown, T. M., Cassisi, S., Cordoni, G., Lagioia, E. P., Nardiello, D., Ortolani, S., Piotto, G., Sarajedini, A., Tailo, M., van der Marel, R. P. and Vesperini, E., 2018, "The Hubble Space Telescope UV legacy survey of galactic globular clusters - XVI. The helium abundance of multiple populations", *Mon. Not. Roy. Astron. Soc.*, **481**(4), 5098–5122. [DOI], [ADS], [arXiv:1809.05006 [astro-ph.SR]]

Milone, Antonino P. and Marino, Anna F., 2022, "Multiple Populations in Star Clusters", *Universe*, **8**(7), 359. [DOI], [ADS], [arXiv:2206.10564 [astro-ph.GA]]

Moehler, S., 2001, "Hot Stars in Globular Clusters: A Spectroscopist's View", *Pub. Astron. Soc. Pac.*, **113**(788), 1162–1177. [DOI], [ADS], [arXiv:astro-ph/0105145 [astro-ph]]

Moehler, S., Sweigart, A. V., Landsman, W. B., Heber, U. and Catelan, M., 1999, "Physical parameters of hot horizontal-branch stars in NGC 6752: deep mixing and radiative levitation", *Astron. Astrophys.*, **346**, L1–L4. [ADS], [arXiv:astro-ph/9904377 [astro-ph]]

Moehler, S., Sweigart, A. V., Landsman, W. B. and Heber, U., 2000, "Hot HB stars in globular clusters - Physical parameters and consequences for theory — V. Radiative levitation versus helium mixing", *Astron. Astrophys.*, **360**, 120–132. [ADS], [arXiv:astro-ph/0006182 [astro-ph]]

Moehler, S., Koester, D., Zoccali, M., Ferraro, F. R., Heber, U., Napiwotzki, R. and Renzini, A., 2004a, "Spectral types and masses of white dwarfs in globular clusters", *Astron. Astrophys.*, **420**, 515–525. [DOI], [ADS], [arXiv:astro-ph/0403245 [astro-ph]]

Moehler, S., Sweigart, A. V., Landsman, W. B., Hammer, N. J. and Dreizler, S., 2004b, "Spectroscopic analyses of the blue hook stars in NGC 2808: A more stringent test of the late hot flasher scenario", *Astron. Astrophys.*, **415**, 313–323. [DOI], [ADS], [arXiv:astro-ph/0311215 [astro-ph]]

Moehler, S., Dreizler, S., Lanz, T., Bono, G., Sweigart, A. V., Calamida, A. and Nonino, M., 2011, "The hot horizontal-branch stars in ω Centauri", *Astron. Astrophys.*, **526**, A136. [DOI], [ADS], [arXiv:1009.3191 [astro-ph.SR]]

Moehler, S., Landsman, W. B., Lanz, T. and Miller Bertolami, M. M., 2019, "Hot UV-bright stars of galactic globular clusters", *Astron. Astrophys.*, **627**, A34. [DOI], [ADS], [arXiv:1905.06718 [astro-ph.SR]]

Moffat, A. F. J. and Vogt, N., 1973, "An up-to-date picture of galactic spiral features based on young open star clusters.", *Astron. Astrophys.*, **23**, 317. [ADS]

Moitinho, André, 2010, "Observational properties of the open cluster system of the Milky Way and what they tell us about our Galaxy", in *Star Clusters: Basic Galactic Building Blocks Throughout Time and Space*, (Eds.) de Grijs, Richard, Lépine, Jacques R. D., 266, [DOI], [ADS], [arXiv:0911.1459 [astro-ph.GA]]

Momany, Y., Bedin, L. R., Cassisi, S., Piotto, G., Ortolani, S., Recio-Blanco, A., De Angeli, F. and Castelli, F., 2004, "The ubiquitous nature of the horizontal branch second U-jump. A link with the Blue Hook scenario?", *Astron. Astrophys.*, **420**, 605–617. [DOI], [ADS], [arXiv:astro-ph/0402594 [astro-ph]]

Momany, Yazan, Piotto, Giampaolo, Recio-Blanco, Alejandra, Bedin, Luigi R., Cassisi, Santi and Bono, Giuseppe, 2002, "A New Feature along the Extended Blue Horizontal Branch of NGC 6752", *Astrophys. J. Lett.*, **576**(1), L65–L68. [DOI], [ADS], [arXiv:astro-ph/0207580 [astro-ph]]

Moni Bidin, C., Moehler, S., Piotto, G., Recio-Blanco, A., Momany, Y. and Méndez, R. A., 2006, "The lack of close binaries among hot horizontal branch stars in <ASTROBJ>NGC 6752</ASTROBJ>", *Astron. Astrophys.*, **451**(2), 499–513. [DOI], [ADS], [arXiv:astro-ph/0602075 [astro-ph]]

Moni Bidin, C., Moehler, S., Piotto, G., Momany, Y. and Recio-Blanco, A., 2009, "A lack of close binaries among hot horizontal branch stars in globular clusters. M 80 and NGC 5986", *Astron. Astrophys.*, **498**(3), 737–751. [DOI], [ADS], [arXiv:0903.2072 [astro-ph.GA]]

Moni Bidin, C., Villanova, S., Piotto, G. and Momany, Y., 2011, "A lack of close binaries among hot horizontal branch stars in globular clusters. II. NGC 2808", *Astron. Astrophys.*, **528**, A127. [DOI], [ADS], [arXiv:1102.1699 [astro-ph.SR]]

Monty, Stephanie, Puzia, Thomas H., Miller, Bryan W., Carrasco, Eleazar R., Simunovic, Mirko, Schirmer, Mischa, Stetson, Peter B., Cassisi, Santi, Venn, Kim A., Dotter, Aaron, Goudfrooij, Paul, Perina, Sibilla, Pessev, Peter, Sarajedini, Ata and Taylor, Matthew A., 2018, "The GeMS/GSAOI Galactic Globular Cluster Survey (G4CS). I. A Pilot Study of the Stellar Populations in NGC 2298 and NGC 3201", *Astrophys. J.*, **865**(2), 160. [DOI], [ADS], [arXiv:1808.05271 [astro-ph.GA]]

Moraux, E., 2016, "Open clusters and associations in the Gaia era", in *EAS Publications Series*, EAS Publications Series, 80-81, [DOI], [ADS], [arXiv:1607.00027 [astro-ph.SR]]

Mucciarelli, A., Dalessandro, E., Ferraro, F. R., Origlia, L. and Lanzoni, B., 2014, "No Evidence of Chemical Anomalies in the Bimodal Turnoff Cluster NGC 1806 in the Large Magellanic Cloud", *Astrophys. J. Lett.*, **793**(1), L6. [DOI], [ADS], [arXiv:1409.0259 [astro-ph.SR]]

Myers, P. C. and Benson, P. J., 1983, "Dense cores in dark clouds. II. NH3 observations and star formation.", *Astrophys. J.*, **266**, 309–320. [DOI], [ADS]

Naoz, Smadar and Fabrycky, Daniel C., 2014, "Mergers and Obliquities in Stellar Triples", *Astrophys. J.*, **793**(2), 137. [DOI], [ADS], [arXiv:1405.5223 [astro-ph.SR]]

Nardiello, D., Libralato, M., Piotto, G., Anderson, J., Bellini, A., Aparicio, A., Bedin, L. R., Cassisi, S., Granata, V., King, I. R., Lucertini, F., Marino, A. F., Milone, A. P., Ortolani, S., Platais, I. and van der Marel, R. P., 2018, "The Hubble Space Telescope UV Legacy Survey of Galactic Globular Clusters - XVII. Public Catalogue Release", *Mon. Not. Roy. Astron. Soc.*, **481**(3), 3382–3393. [DOI], [ADS], [arXiv:1809.04300 [astro-ph.SR]]

Niederhofer, F., Georgy, C., Bastian, N. and Ekström, S., 2015, "Apparent age spreads in clusters and the role of stellar rotation", *Mon. Not. Roy. Astron. Soc.*, **453**(2), 2070–2074. [DOI], [ADS], [arXiv:1507.07561 [astro-ph.SR]]

Pace, G., Recio-Blanco, A., Piotto, G. and Momany, Y., 2006, "Abundance anomalies in hot horizontal branch stars of the Galactic globular cluster NGC 2808", *Astron. Astrophys.*, **452**(2), 493–501. [DOI], [ADS]

Pallavicini, R., Golub, L., Rosner, R., Vaiana, G. S., Ayres, T. and Linsky, J. L., 1981, "Relations among stellar X-ray emission observed from Einstein, stellar rotation and bolometric luminosity.", *Astrophys. J.*, **248**, 279–290. [DOI], [ADS]

Pandey, Gajendra, Kameswara Rao, N., Lambert, David L., Jeffery, C. Simon and Asplund, Martin, 2001, "Abundance analyses of cool extreme helium stars", *Mon. Not. Roy. Astron. Soc.*, **324**(4), 937–959. [DOI], [ADS], [arXiv:astro-ph/0101518 [astro-ph]]

Panthi, Anju, Vaidya, Kaushar, Jadhav, Vikrant, Rao, Khushboo K., Subramaniam, Annapurni, Agarwal, Manan and Pandey, Sindhu, 2022, "UOCS -VIII. UV study of the open cluster NGC 2506 using ASTROSAT-", *Mon. Not. Roy. Astron. Soc.*, **516**(4), 5318–5330. [DOI], [ADS], [arXiv:2209.00880 [astro-ph.GA]]

Parada, Javiera, Richer, Harvey, Heyl, Jeremy, Kalirai, Jason and Goldsbury, Ryan, 2016, "Formation and Evolution of Blue Stragglers in 47 Tucanae", *Astrophys. J.*, **830**(2), 139. [DOI], [ADS], [arXiv:1609.02115 [astro-ph.SR]]

Paxton, Bill, Schwab, Josiah, Bauer, Evan B., Bildsten, Lars, Blinnikov, Sergei, Duffell, Paul, Farmer, R., Goldberg, Jared A., Marchant, Pablo, Sorokina, Elena, Thoul, Anne, Townsend, Richard H. D. and Timmes, F. X., 2018, "Modules for Experiments in Stellar Astrophysics (MESA): Convective Boundaries, Element Diffusion, and Massive Star Explosions", *Astrophys. J. Suppl.*, **234**(2), 34. [DOI], [ADS], [arXiv:1710.08424 [astro-ph.SR]]

Pedreros, Mario, 1989, "The Open Cluster NGC 2818 and Its Associated Planetary Nebula", *Astron. J.*, **98**, 2146. [DOI], [ADS]

Perets, Hagai B. and Fabrycky, Daniel C., 2009, "On the Triple Origin of Blue Stragglers", *Astrophys. J.*, **697**(2), 1048–1056. [DOI], [ADS], [arXiv:0901.4328 [astro-ph.SR]]

Pietrinferni, Adriano, Cassisi, Santi, Salaris, Maurizio and Castelli, Fiorella, 2004, "A Large Stellar Evolution Database for Population Synthesis Studies. I. Scaled Solar Models and Isochrones", *Astrophys. J.*, **612**(1), 168–190. [DOI], [ADS], [arXiv:astro-ph/0405193 [astro-ph]]

Pietrinferni, Adriano, Hidalgo, Sebastian, Cassisi, Santi, Salaris, Maurizio, Savino, Alessandro, Mucciarelli, Alessio, Verma, Kuldeep, Silva Aguirre, Victor, Aparicio, Antonio and Ferguson, Jason W., 2021, "Updated BaSTI Stellar Evolution Models and Isochrones. II. α-enhanced Calculations", *Astrophys. J.*, **908**(1), 102. [DOI], [ADS], [arXiv:2012.10085 [astro-ph.SR]]

Piotto, G., Zoccali, M., King, I. R., Djorgovski, S. G., Sosin, C., Rich, R. M. and Meylan, G., 1999, "HUBBLE SPACE TELESCOPE Observations of Galactic Globular Cluster Cores. II. NGC 6273 and the Problem of Horizontal-Branch Gaps", *Astron. J.*, **118**(4), 1727–1737. [DOI], [ADS], [arXiv:astro-ph/9906269 [astro-ph]]

Piotto, G., Bedin, L. R., Anderson, J., King, I. R., Cassisi, S., Milone, A. P., Villanova, S., Pietrinferni, A. and Renzini, A., 2007, "A Triple Main Sequence in the Globular Cluster NGC 2808", *Astrophys. J. Lett.*, **661**(1), L53–L56. [DOI], [ADS], [arXiv:astro-ph/0703767 [astro-ph]]

Piotto, G., Milone, A. P., Anderson, J., Bedin, L. R., Bellini, A., Cassisi, S., Marino, A. F., Aparicio, A. and Nascimbeni, V., 2012, "Hubble Space Telescope Reveals Multiple Sub-giant Branch in Eight Globular Clusters", *Astrophys. J.*, **760**(1), 39. [DOI], [ADS], [arXiv:1208.1873 [astro-ph.SR]]

Piotto, G., Milone, A. P., Bedin, L. R., Anderson, J., King, I. R., Marino, A. F., Nardiello, D., Aparicio, A., Barbuy, B., Bellini, A., Brown, T. M., Cassisi, S., Cool, A. M., Cunial, A., Dalessandro, E., D'Antona, F., Ferraro, F. R., Hidalgo,

S., Lanzoni, B., Monelli, M., Ortolani, S., Renzini, A., Salaris, M., Sarajedini, A., van der Marel, R. P., Vesperini, E. and Zoccali, M., 2015, "The Hubble Space Telescope UV Legacy Survey of Galactic Globular Clusters. I. Overview of the Project and Detection of Multiple Stellar Populations", *Astron. J.*, **149**(3), 91. [DOI], [ADS], [arXiv:1410.4564 [astro-ph.SR]]

Piotto, Giampaolo, Villanova, Sandro, Bedin, Luigi R., Gratton, Raffaele, Cassisi, Santi, Momany, Yazan, Recio-Blanco, Alejandra, Lucatello, Sara, Anderson, Jay, King, Ivan R., Pietrinferni, Adriano and Carraro, Giovanni, 2005, "Metallicities on the Double Main Sequence of ω Centauri Imply Large Helium Enhancement", *Astrophys. J.*, **621**(2), 777–784. [DOI], [ADS], [arXiv:astro-ph/0412016 [astro-ph]]

Platais, Imants, Kozhurina-Platais, Vera, Mathieu, Robert D., Girard, Terrence M. and van Altena, William F., 2003, "WIYN Open Cluster Study. XVII. Astrometry and Membership to V=21 in NGC 188", *Astron. J.*, **126**(6), 2922–2935. [DOI], [ADS], [arXiv:astro-ph/0309749 [astro-ph]]

Portegies Zwart, Simon F., McMillan, Stephen L. W. and Gieles, Mark, 2010, "Young Massive Star Clusters", *Ann. Rev. Astron. Astrophys.*, **48**, 431–493. [DOI], [ADS], [arXiv:1002.1961 [astro-ph.GA]]

Postma, J., Hutchings, J. B. and Leahy, D., 2011, "Calibration and Performance of the Photon-counting Detectors for the Ultraviolet Imaging Telescope (UVIT) of the Astrosat Observatory", *Pub. Astron. Soc. Pac.*, **123**(905), 833. [DOI], [ADS], [arXiv:1105.5361 [astro-ph.IM]]

Postma, Joseph E. and Leahy, Denis, 2017, "CCDLAB: A Graphical User Interface FITS Image Data Reducer, Viewer, and Canadian UVIT Data Pipeline", *Pub. Astron. Soc. Pac.*, **129**(981), 115 002. [DOI], [ADS]

Postma, Joseph E. and Leahy, Denis, 2020, "An Algorithm for Coordinate Matching in World Coordinate Solutions", *Pub. Astron. Soc. Pac.*, **132**(1011), 054503. [DOI], [ADS]

Postma, Joseph E. and Leahy, Denis, 2021, "UVIT data reduction pipeline: A CCDLAB and UVIT tutorial", *Journal of Astrophysics and Astronomy*, **42**(2), 30. [DOI], [ADS]

Pottasch, S. R., 1984, *Planetary nebulae. A study of late stages of stellar evolution*, 107, Springer Dordrecht. [DOI], [ADS]

Prabhu, Deepthi S., Subramaniam, Annapurni and Sahu, Snehalata, 2021, "The First Extensive Exploration of UV-bright Stars in the Globular Cluster NGC 2808", *Astrophys. J.*, **908**(1), 66. [DOI], [ADS], [arXiv:2012.05732 [astro-ph.SR]]

Prabhu, Deepthi S., Subramaniam, Annapurni, Sahu, Snehalata, Chung, Chul, Leigh, Nathan W. C., Dalessandro, Emanuele, Chatterjee, Sourav, Rao, N. Kameswara, Shara, Michael, Côté, Patrick, Choudhury, Samyaday, Pandey, Gajendra, Valcarce, Aldo A. R., Singh, Gaurav, Postma, Joesph E., Rani, Sharmila, Bandyopadhyay, Avrajit, Geller, Aaron M., Hutchings, John, Puzia, Thomas, Simunovic, Mirko, Sohn, Young-Jong, Thirupathi, Sivarani and Yadav, Ramakant Singh, 2022, "Globular Cluster UVIT Legacy Survey (GlobULeS). III. Omega Centauri in Far-ultraviolet", *Astrophys. J. Lett.*, **939**(2), L20. [DOI], [ADS], [arXiv:2210.05160 [astro-ph.SR]]

Prialnik, Dina, 2009, *An Introduction to the Theory of Stellar Structure and Evolution*. [ADS]

Quijada, M. A., Boucarut, R., Telfer, R., Baggett, S., Kim Quijano, J., Allen, George and Arsenovic, Peter, 2006, "Spectral and imaging performance of WFC3 interference filters", in *Society of Photo-Optical Instrumentation Engineers (SPIE) Conference Series*, (Eds.) Mather, John C., MacEwen, Howard A., de Graauw, Mattheus W. M., Society of Photo-Optical Instrumentation Engineers (SPIE) Conference Series, 6265, [DOI], [ADS]

Rain, M. J., Ahumada, J. A. and Carraro, G., 2021, "A new, Gaia-based, catalogue of blue straggler stars in open clusters", *Astron. Astrophys.*, **650**, A67. [DOI], [ADS], [arXiv:2103.06004 [astro-ph.SR]]

Rani, Sharmila, Pandey, Gajendra, Subramaniam, Annapurni, Sahu, Snehalala and Rao, N. Kameswara, 2020, "The horizontal branch morphology of the globular cluster NGC 1261 using AstroSat", *Journal of Astrophysics and Astronomy*, **41**(1), 35. [DOI], [ADS], [arXiv:2010.00569 [astro-ph.SR]]

Rani, Sharmila, Pandey, Gajendra, Subramaniam, Annapurni, Chung, Chul, Sahu, Snehalata and Kameswara Rao, N., 2021a, "AstroSat Study of the Globular Cluster NGC 2298: Probable Evolutionary Scenarios of Hot Horizontal Branch Stars", *Astrophys. J.*, **923**(2), 162. [DOI], [ADS], [arXiv:2110.04528 [astro-ph.SR]]

Rani, Sharmila, Pandey, Gajendra, Subramaniam, Annapurni, Sahu, Snehalata and Rao, N. Kameswara, 2021b, "Study of UV-bright stellar populations in the globular cluster NGC 1261 using Astrosat", *Mon. Not. Roy. Astron. Soc.*, **501**(2), 2140–2155. [DOI], [ADS], [arXiv:2012.01213 [astro-ph.SR]]

Rani, Sharmila, Subramaniam, Annapurni, Pandey, Sindhu, Sahu, Snehalata, Mondal, Chayan and Pandey, Gajendra, 2021c, "UOCS. V. UV study of the old open cluster NGC 188 using AstroSat", *Journal of Astrophysics and Astronomy*, **42**(2), 47. [DOI], [ADS], [arXiv:2012.00510 [astro-ph.SR]]

Rani, Sharmila, Pandey, Gajendra, Subramaniam, Annapurni and Rao, N. Kameswara, 2023, "UOCS-IX. AstroSat/UVIT Study of the Open Cluster NGC 2818: Blue Stragglers, Yellow Stragglers, Planetary Nebula, and their Membership", *Astrophys. J.*, **945**(1), 11. [DOI], [ADS], [arXiv:2301.01943 [astro-ph.SR]]

Raso, S., Ferraro, F. R., Dalessandro, E., Lanzoni, B., Nardiello, D., Bellini, A. and Vesperini, E., 2017, "The "UV-route" to Search for Blue Straggler Stars in Globular Clusters: First Results from the HST UV Legacy Survey", *Astrophys. J.*, **839**(1), 64. [DOI], [ADS], [arXiv:1704.01453 [astro-ph.SR]]

Rauch, T. and Deetjen, J. L., 2003, "Handling of Atomic Data", in *Stellar Atmosphere Modeling*, (Eds.) Hubeny, Ivan, Mihalas, Dimitri, Werner, Klaus, Astronomical Society of the Pacific Conference Series, 288, The ASP. The ASP. [ADS], [arXiv:astro-ph/0403239 [astro-ph]]

Rebassa-Mansergas, A., Solano, E., Jiménez-Esteban, F. M., Torres, S., Rodrigo, C., Ferrer-Burjachs, A., Calcaferro, L. M., Althaus, L. G. and Córsico, A. H., 2021, "White dwarf-main-sequence binaries from Gaia EDR3: the unresolved 100 pc volume-limited sample", *Mon. Not. Roy. Astron. Soc.*, **506**(4), 5201–5211. [DOI], [ADS], [arXiv:2107.06303 [astro-ph.SR]]

Rich, R. Michael, Sosin, Craig, Djorgovski, S. George, Piotto, Giampaolo, King, Ivan R., Renzini, Alvio, Phinney, E. Sterl, Dorman, Ben, Liebert, James and Meylan, Georges, 1997, "Discovery of Extended Blue Horizontal Branches in Two Metal-rich Globular Clusters", *Astrophys. J. Lett.*, **484**(1), L25–L28. [DOI], [ADS], [arXiv:astro-ph/9705039 [astro-ph]]

Riello, M., De Angeli, F., Evans, D. W., Montegriffo, P., Carrasco, J. M., Busso, G., Palaversa, L., Burgess, P. W., Diener, C., Davidson, M., Rowell, N., Fabricius, C., Jordi, C., Bellazzini, M., Pancino, E., Harrison, D. L., Cacciari, C., van Leeuwen, F., Hambly, N. C., Hodgkin, S. T., Osborne, P. J., Altavilla, G., Barstow, M. A., Brown, A. G. A., Castellani, M., Cowell, S., De Luise, F., Gilmore, G., Giuffrida, G., Hidalgo, S., Holland, G., Marinoni, S., Pagani, C., Piersimoni, A. M., Pulone, L., Ragaini, S., Rainer, M., Richards, P. J., Sanna, N., Walton, N. A., Weiler, M. and Yoldas, A., 2021, "Gaia Early Data Release 3. Photometric content and validation", *Astron. Astrophys.*, **649**, A3. [DOI], [ADS], [arXiv:2012.01916 [astro-ph.IM]]

Rosenberg, Alfred, Recio-Blanco, Alejandra and García-Marín, Macarena, 2004, "Discovery of Blue Hook Stars in the Massive Globular Cluster M54", *Astrophys. J.*, **603**(1), 135–138. [DOI], [ADS], [arXiv:astro-ph/0310746 [astro-ph]]

Sahu, Snehalata, Subramaniam, Annapurni, Côté, Patrick, Rao, N. Kameswara and Stetson, Peter B., 2019, "UVIT-HST-GAIA view of NGC 288: a census of the hot stellar population and its properties from UV", *Mon. Not. Roy. Astron. Soc.*, **482**(1), 1080–1095. [DOI], [ADS], [arXiv:1810.01846 [astro-ph.SR]]

Sahu, Snehalata, Subramaniam, Annapurni, Singh, Gaurav, Yadav, Ramakant, Valcarce, Aldo R., Choudhury, Samyaday, Rani, Sharmila, Prabhu, Deepthi S., Chung, Chul, Côté, Patrick, Leigh, Nathan, Geller, Aaron M., Chatterjee, Sourav, Kameswara Rao, N., Bandyopadhyay, Avrajit, Shara, Michael, Dalessandro, Emanuele, Pandey, Gajendra, Postma, Joesph E., Hutchings, John, Simunovic, Mirko, Stetson, Peter B., Thirupathi, Sivarani, Puzia, Thomas and Sohn, Young-Jong, 2022, "Globular Cluster UVIT Legacy Survey (GlobULeS) - I. FUV-optical colour-magnitude diagrams for eight globular clusters", *Mon. Not. Roy. Astron. Soc.*, **514**(1), 1122–1139. [DOI], [ADS], [arXiv:2204.12886 [astro-ph.GA]]

Saio, Hideyuki and Jeffery, C. Simon, 2000, "The evolution of a rapidly accreting helium white dwarf to become a low-luminosity helium star", *Mon. Not. Roy. Astron. Soc.*, **313**(4), 671–677. [DOI], [ADS]

Salinas, R., Contreras Ramos, R., Strader, J., Hakala, P., Catelan, M., Peacock, M. B. and Simunovic, M., 2016, "An AO-assisted Variability Study of Four Globular Clusters", *Astron. J.*, **152**(3), 55. [DOI], [ADS], [arXiv:1605.06517 [astro-ph.SR]]

Sandage, A. R., 1953, "The color-magnitude diagram for the globular cluster M 3.", *Astron. J.*, **58**, 61–75. [DOI], [ADS]

Sandage, Allan, 1962, "Photometric Data for the Old Galactic Cluster NGC 188.", *Astrophys. J.*, **135**, 333. [DOI], [ADS]

Sandage, Allan and Wallerstein, George, 1960, "Color-Magnitude Diagram for Disk Globular Cluster NGC 6356 Compared with Halo Clusters.", *Astrophys. J.*, **131**, 598. [DOI], [ADS]

Sandage, Allan and Wildey, Robert, 1967, "The Anomalous Color-Magnitude Diagram of the Remote Globular Cluster NGC 7006", *Astrophys. J.*, **150**, 469. [DOI], [ADS]

Santana, F. A., Muñoz, R. R., Geha, M., Coté, P., Stetson, P., Simon, J. and Djorgovski, S. G., 2012, "Blue Stragglers in Milky Way Satellites", in *Galactic Archaeology: Near-Field Cosmology and the Formation of the Milky Way*, (Eds.) Aoki, W., Ishigaki, M., Suda, T., Tsujimoto, T., Arimoto, N., Astronomical Society of the Pacific Conference Series, 458, [ADS]

Santucci, Rafael M., Placco, Vinicius M., Rossi, Silvia, Beers, Timothy C., Reggiani, Henrique M., Lee, Young Sun, Xue, Xiang-Xiang and Carollo, Daniela, 2015, "The Frequency of Field Blue-Straggler Stars in the Thick Disk and Halo System of the Galaxy", *Astrophys. J.*, **801**(2), 116. [DOI], [ADS], [arXiv:1501.03559 [astro-ph.SR]]

Sarajedini, Ata, von Hippel, Ted, Kozhurina-Platais, Vera and Demarque, Pierre, 1999, "WIYN Open Cluster Study. II. UBVRI CCD Photometry of the Open Cluster NGC 188", *Astron. J.*, **118**(6), 2894–2907. [DOI], [ADS]

Schiavon, Ricardo P., Dalessandro, Emanuele, Sohn, Sangmo T., Rood, Robert T., O'Connell, Robert W., Ferraro, Francesco R., Lanzoni, Barbara, Beccari, Giacomo, Rey, Soo-Chang, Rhee, Jaehyon, Rich, R. Michael, Yoon, Suk-Jin and Lee, Young-Wook, 2012, "Ultraviolet Properties of Galactic Globular Clusters with GALEX. I. The Color-Magnitude Diagrams", *Astron. J.*, **143**(5), 121. [DOI], [ADS], [arXiv:1201.5377 [astro-ph.GA]]

Schindler, Jan-Torge, Green, Elizabeth M. and Arnett, W. David, 2015, "Exploring Stellar Evolution Models of sdB Stars using MESA", *Astrophys. J.*, **806**(2), 178. [DOI], [ADS], [arXiv:1410.8204 [astro-ph.SR]]

Schlafly, Edward F. and Finkbeiner, Douglas P., 2011, "Measuring Reddening with Sloan Digital Sky Survey Stellar Spectra and Recalibrating SFD", *Astrophys. J.*, **737**(2), 103. [DOI], [ADS], [arXiv:1012.4804 [astro-ph.GA]]

Schonberner, D. and Drilling, J. S., 1984, "Effective temperatures and luminosities of very hot O type subdwarfs.", *Astrophys. J.*, **278**, 702–710. [DOI], [ADS]

Schwarzschild, M. and Härm, R., 1962, "Red Giants of Population II. II.", *Astrophys. J.*, **136**, 158. [DOI], [ADS]

Siegel, Michael H., Porterfield, Blair L., Linevsky, Jacquelyn S., Bond, Howard E., Holland, Stephen T., Hoversten, Erik A., Berrier, Joshua L., Breeveld, Alice A., Brown, Peter J. and Gronwall, Caryl A., 2014, "The Swift UVOT Stars Survey. I. Methods and Test Clusters", *Astron. J.*, **148**(6), 131. [DOI], [ADS], [arXiv:1408.4676 [astro-ph.SR]]

Sindhu, N., Subramaniam, Annapurni and Radha, C. Anu, 2018, "Ultraviolet stellar population of the old open cluster M67 (NGC 2682)", *Mon. Not. Roy. Astron. Soc.*, **481**(1), 226–243. [DOI], [ADS], [arXiv:1808.06814 [astro-ph.SR]]

Singh, Gaurav, Sahu, Snehalata, Subramaniam, Annapurni and Yadav, R. K. S., 2020, "Peculiarities in the Horizontal Branch Stars of Globular Cluster NGC 1851: Discovery of a Blue Straggler Companion to an EHB Star", *Astrophys. J.*, **905**(1), 44. [DOI], [ADS], [arXiv:2010.06979 [astro-ph.SR]]

Singh, Kulinder Pal, 2022, "The AstroSat Observatory", *arXiv e-prints*, arXiv:2203.04610. [ADS], [arXiv:2203.04610 [astro-ph.IM]]

Singh, Kulinder Pal, Tandon, S. N., Agrawal, P. C., Antia, H. M., Manchanda, R. K., Yadav, J. S., Seetha, S., Ramadevi, M. C., Rao, A. R., Bhattacharya, D., Paul, B., Sreekumar, P., Bhattacharyya, S., Stewart, G. C., Hutchings, J., Annapurni, S. A., Ghosh, S. K., Murthy, J., Pati, A., Rao, N. K., Stalin, C. S., Girish, V., Sankarasubramanian, K., Vadawale, S., Bhalerao, V. B., Dewangan, G. C., Dedhia, D. K., Hingar, M. K., Katoch, T. B., Kothare, A. T., Mirza, I., Mukerjee, K., Shah, H., Shah, P., Mohan, R., Sangal, A. K., Nagabhusana, S., Sriram, S., Malkar, J. P., Sreekumar, S., Abbey, A. F., Hansford, G. M., Beardmore, A. P., Sharma, M. R., Murthy, S., Kulkarni, R., Meena, G., Babu, V. C.

and Postma, J., 2014, "ASTROSAT mission", in *Space Telescopes and Instrumentation 2014: Ultraviolet to Gamma Ray*, (Eds.) Takahashi, Tadayuki, den Herder, Jan-Willem A., Bautz, Mark, Society of Photo-Optical Instrumentation Engineers (SPIE) Conference Series, 9144, [DOI], [ADS]

Sirianni, M., Jee, M. J., Benítez, N., Blakeslee, J. P., Martel, A. R., Meurer, G., Clampin, M., De Marchi, G., Ford, H. C., Gilliland, R., Hartig, G. F., Illingworth, G. D., Mack, J. and McCann, W. J., 2005, "The Photometric Performance and Calibration of the Hubble Space Telescope Advanced Camera for Surveys", *Pub. Astron. Soc. Pac.*, **117**(836), 1049–1112. [DOI], [ADS], [arXiv:astro-ph/0507614 [astro-ph]]

Skrutskie, M. F., Cutri, R. M., Stiening, R., Weinberg, M. D., Schneider, S., Carpenter, J. M., Beichman, C., Capps, R., Chester, T., Elias, J., Huchra, J., Liebert, J., Lonsdale, C., Monet, D. G., Price, S., Seitzer, P., Jarrett, T., Kirkpatrick, J. D., Gizis, J. E., Howard, E., Evans, T., Fowler, J., Fullmer, L., Hurt, R., Light, R., Kopan, E. L., Marsh, K. A., McCallon, H. L., Tam, R., Van Dyk, S. and Wheelock, S., 2006, "The Two Micron All Sky Survey (2MASS)", *Astron. J.*, **131**(2), 1163–1183. [DOI], [ADS]

Soker, Noam, 1998, "Can Planets Influence the Horizontal Branch Morphology?", *Astron. J.*, **116**(3), 1308–1313. [DOI], [ADS], [arXiv:astro-ph/9803223 [astro-ph]]

Stetson, P. B., Pancino, E., Zocchi, A., Sanna, N. and Monelli, M., 2019, "Homogeneous photometry - VII. Globular clusters in the Gaia era", *Mon. Not. Roy. Astron. Soc.*, **485**(3), 3042–3063. [DOI], [ADS], [arXiv:1902.09925 [astro-ph.SR]]

Stetson, Peter B., 1987, "DAOPHOT: A Computer Program for Crowded-Field Stellar Photometry", *Pub. Astron. Soc. Pac.*, **99**, 191. [DOI], [ADS]

Subramaniam, Annapurni, Sahu, Snehalata, Postma, Joseph E., Côté, Patrick, Hutchings, J. B., Darukhanawalla, N., Chung, Chul, Tandon, S. N., Rao, N. Kameswara, George, K., Ghosh, S. K., Girish, V., Mohan, R., Murthy, J., Pati, A. K., Sankarasubramanian, K., Stalin, C. S. and Choudhury, S.,

2017, "The Horizontal Branch Population of NGC 1851 as Revealed by the Ultraviolet Imaging Telescope (UVIT)", *Astron. J.*, **154**(6), 233. [DOI], [ADS], [arXiv:1710.03730 [astro-ph.SR]]

Sun, Weijia, de Grijs, Richard, Deng, Licai and Albrow, Michael D., 2021, "Binary-driven stellar rotation evolution at the main-sequence turn-off in star clusters", *Mon. Not. Roy. Astron. Soc.*, **502**(3), 4350–4358. [DOI], [ADS], [arXiv:2102.02352 [astro-ph.SR]]

Surendiranath, R., Kameswara Rao, N., Sagar, Ram, Nathan, J. S. and Ghosh, K. K., 1990, "CCD photometry in VRI bands ofthe galactic cluster NGC 2818", *Journal of Astrophysics and Astronomy*, **11**, 151. [DOI], [ADS]

Sweigart, A. V. and Mengel, J. G., 1979, "Meridional circulation and CNO anomalies in red giant stars.", *Astrophys. J.*, **229**, 624–641. [DOI], [ADS]

Sweigart, A. V., Mengel, J. G. and Demarque, P., 1974, "On the Origin of the Blue Halo Stars", *Astron. Astrophys.*, **30**, 13. [ADS]

Sweigart, Allen V., 1997, "Effects of Helium Mixing on the Evolution of Globular Cluster Stars", *Astrophys. J. Lett.*, **474**(1), L23–L26. [DOI], [ADS]

Sweigart, Allen V., 2002, "Horizontal branch models as a test of mixing on the RGB", *Highlights of Astronomy*, **12**, 292–294. [ADS], [arXiv:astro-ph/0103133 [astro-ph]]

Tailo, M., Milone, A. P., Lagioia, E. P., D'Antona, F., Marino, A. F., Vesperini, E., Caloi, V., Ventura, P., Dondoglio, E. and Cordoni, G., 2020, "Mass-loss along the red giant branch in 46 globular clusters and their multiple populations", *Mon. Not. Roy. Astron. Soc.*, **498**(4), 5745–5771. [DOI], [ADS], [arXiv:2009.01080 [astro-ph.SR]]

Tandon, S. N., Hutchings, J. B., Ghosh, S. K., Subramaniam, A., Koshy, G., Girish, V., Kamath, P. U., Kathiravan, S., Kumar, A., Lancelot, J. P., Mahesh, P. K., Mohan, R., Murthy, J., Nagabhushana, S., Pati, A. K., Postma, J., Rao,

N. Kameswara, Sankarasubramanian, K., Sreekumar, P., Sriram, S., Stalin, C. S., Sutaria, F., Sreedhar, Y. H., Barve, I. V., Mondal, C. and Sahu, S., 2017a, "In-orbit Performance of UVIT and First Results", *Journal of Astrophysics and Astronomy*, **38**(2), 28. [DOI], [ADS], [arXiv:1612.00612 [astro-ph.IM]]

Tandon, S. N., Subramaniam, Annapurni, Girish, V., Postma, J., Sankarasubramanian, K., Sriram, S., Stalin, C. S., Mondal, C., Sahu, S., Joseph, P., Hutchings, J., Ghosh, S. K., Barve, I. V., George, K., Kamath, P. U., Kathiravan, S., Kumar, A., Lancelot, J. P., Leahy, D., Mahesh, P. K., Mohan, R., Nagabhushana, S., Pati, A. K., Kameswara Rao, N., Sreedhar, Y. H. and Sreekumar, P., 2017b, "In-orbit Calibrations of the Ultraviolet Imaging Telescope", *Astron. J.*, **154**(3), 128. [DOI], [ADS], [arXiv:1705.03715 [astro-ph.IM]]

Tandon, S. N., Postma, J., Joseph, P., Devaraj, A., Subramaniam, A., Barve, I. V., George, K., Ghosh, S. K., Girish, V., Hutchings, J. B., Kamath, P. U., Kathiravan, S., Kumar, A., Lancelot, J. P., Leahy, D., Mahesh, P. K., Mohan, R., Nagabhushana, S., Pati, A. K., Rao, N. Kameswara, Sankarasubramanian, K., Sriram, S. and Stalin, C. S., 2020, "Additional Calibration of the Ultraviolet Imaging Telescope on Board AstroSat", *Astron. J.*, **159**(4), 158. [DOI], [ADS], [arXiv:2002.01159 [astro-ph.IM]]

Taylor, Mark, 2011, "TOPCAT: Tool for OPerations on Catalogues And Tables", [ADS]

Tifft, W. G., Connolly, L. P. and Webb, D. F., 1972, "NGC 2818.", *Mon. Not. Roy. Astron. Soc.*, **158**, 47. [DOI], [ADS]

Tonry, J. L., Stubbs, C. W., Lykke, K. R., Doherty, P., Shivvers, I. S., Burgett, W. S., Chambers, K. C., Hodapp, K. W., Kaiser, N., Kudritzki, R. P., Magnier, E. A., Morgan, J. S., Price, P. A. and Wainscoat, R. J., 2012, "The Pan-STARRS1 Photometric System", *Astrophys. J.*, **750**(2), 99. [DOI], [ADS], [arXiv:1203.0297 [astro-ph.IM]]

Tremblay, P. E. and Bergeron, P., 2009, "Spectroscopic Analysis of DA White Dwarfs: Stark Broadening of Hydrogen Lines Including Nonideal Effects", *Astrophys. J.*, **696**(2), 1755–1770. [DOI], [ADS], [arXiv:0902.4182 [astro-ph.SR]]

Tremblay, P. E., Bergeron, P. and Gianninas, A., 2011, "An Improved Spectroscopic Analysis of DA White Dwarfs from the Sloan Digital Sky Survey Data Release 4", *Astrophys. J.*, **730**(2), 128. [DOI], [ADS], [arXiv:1102.0056 [astro-ph.SR]]

Tsukamoto, Yusuke, Maury, Anaëlle, Commerçon, Benoît, Alves, Felipe O., Cox, Erin G., Sakai, Nami, Ray, Tom, Zhao, Bo and Machida, Masahiro N., 2022, "The role of magnetic fields in the formation of protostars, disks, and outflows", *arXiv e-prints*, arXiv:2209.13765. [ADS], [arXiv:2209.13765 [astro-ph.SR]]

Tutukov, A. and Iungelson, L., 1987, "On the origin of faint blue stars.", in *IAU Colloq. 95: Second Conference on Faint Blue Stars*, (Eds.) Philip, A. G. Davis, Hayes, D. S., Liebert, James W., [ADS]

Vaidya, Kaushar, Panthi, Anju, Agarwal, Manan, Pandey, Sindhu, Rao, Khushboo K., Jadhav, Vikrant and Subramaniam, Annapurni, 2022, "UOCS - VII. Blue straggler populations of open cluster NGC 7789 with UVIT/AstroSat", *Mon. Not. Roy. Astron. Soc.*, **511**(2), 2274–2284. [DOI], [ADS], [arXiv:2201.08773 [astro-ph.SR]]

van den Bergh, S., 1967, "UBV photometry of globular clusters.", *Astron. J.*, **72**, 70–81. [DOI], [ADS]

VandenBerg, Don A., Brogaard, K., Leaman, R. and Casagrand e, L., 2013, "The Ages of 55 Globular Clusters as Determined Using an Improved VHB_TO Method along with Color-Magnitude Diagram Constraints, and Their Implications for Broader Issues", *Astrophys. J.*, **775**(2), 134. [DOI], [ADS], [arXiv:1308.2257 [astro-ph.GA]]

Vanderbeke, Joachim, De Propris, Roberto, De Rijcke, Sven, Baes, Maarten, West, Michael, Alonso-García, Javier and Kunder, Andrea, 2015, "G2C2 - IV. A novel

approach to study the radial distributions of multiple populations in Galactic globular clusters", *Mon. Not. Roy. Astron. Soc.*, **451**(1), 275–281. [DOI], [ADS], [arXiv:1504.06509 [astro-ph.GA]]

Vasiliev, Eugene, 2019, "Proper motions and dynamics of the Milky Way globular cluster system from Gaia DR2", *Mon. Not. Roy. Astron. Soc.*, **484**(2), 2832–2850. [DOI], [ADS], [arXiv:1807.09775 [astro-ph.GA]]

Vázquez, Roberto, 2012, "Bubbles and Knots in the Kinematical Structure of the Bipolar Planetary Nebula NGC 2818", *Astrophys. J.*, **751**(2), 116. [DOI], [ADS], [arXiv:1203.6048 [astro-ph.SR]]

von Hippel, Ted and Sarajedini, Ata, 1998, "WIYN Open Cluster Study. I. Deep Photometry of NGC 188", *Astron. J.*, **116**(4), 1789–1800. [DOI], [ADS], [arXiv:astro-ph/9806100 [astro-ph]]

von Rudloff, I. R., Vandenberg, Don A. and Hartwick, F. D. A., 1988, "Thermal Instabilities in Low-Mass Subgiants?", *Astrophys. J.*, **324**, 840. [DOI], [ADS]

Walker, Christopher K., 1994, "The Early Stages of Protostellar Evolution", in *American Astronomical Society Meeting Abstracts*, American Astronomical Society Meeting Abstracts, 185, [ADS]

Wang, Chen, Langer, Norbert, Schootemeijer, Abel, Milone, Antonino, Hastings, Ben, Xu, Xiao-Tian, Bodensteiner, Julia, Sana, Hugues, Castro, Norberto, Lennon, D. J., Marchant, Pablo, de Koter, A. and de Mink, Selma E., 2022, "Stellar mergers as the origin of the blue main-sequence band in young star clusters", *Nature Astronomy*, **6**, 480–487. [DOI], [ADS], [arXiv:2202.05552 [astro-ph.SR]]

Wang, Jiaxin, Ma, Jun, Wu, Zhenyu, Wang, Song and Zhou, Xu, 2015, "BATC 15 Band Photometry of the Open Cluster NGC 188", *Astron. J.*, **150**(2), 61. [DOI], [ADS], [arXiv:1506.07402 [astro-ph.GA]]

Webbink, R. F., 1984, "Double white dwarfs as progenitors of R Coronae Borealis stars and type I supernovae.", *Astrophys. J.*, **277**, 355–360. [DOI], [ADS]

Weidemann, V., 2000, "Revision of the initial-to-final mass relation", *Astron. Astrophys.*, **363**, 647–656. [ADS]

Weidemann, Volker, 1990, "Mases and evolutionary status of white dwarfs and their progenitors.", *Ann. Rev. Astron. Astrophys.*, **28**, 103–137. [DOI], [ADS]

Wenderoth, Erich, Alvarado, Franklin, Liller, William and Phillips, Mark M., 1994, "Spectroscopy of an Extremely Blue Star in the Globular Cluster NGC 2298", *Pub. Astron. Soc. Pac.*, **106**, 718. [DOI], [ADS]

Werner, K., Deetjen, J. L., Dreizler, S., Nagel, T., Rauch, T. and Schuh, S. L., 2003, "Model Photospheres with Accelerated Lambda Iteration", in *Stellar Atmosphere Modeling*, (Eds.) Hubeny, Ivan, Mihalas, Dimitri, Werner, Klaus, Astronomical Society of the Pacific Conference Series, 288, The ASP. The ASP. [ADS], [arXiv:astro-ph/0209535 [astro-ph]]

Whitford, A. E., 1958, "The law of interstellar reddening.", *Astron. J.*, **63**, 201–207. [DOI], [ADS]

Windhorst, Rogier A., Cohen, Seth H., Hathi, Nimish P., McCarthy, Patrick J., Ryan, Russell E., Jr., Yan, Haojing, Baldry, Ivan K., Driver, Simon P., Frogel, Jay A., Hill, David T., Kelvin, Lee S., Koekemoer, Anton M., Mechtley, Matt, O'Connell, Robert W., Robotham, Aaron S. G., Rutkowski, Michael J., Seibert, Mark, Straughn, Amber N., Tuffs, Richard J., Balick, Bruce, Bond, Howard E., Bushouse, Howard, Calzetti, Daniela, Crockett, Mark, Disney, Michael J., Dopita, Michael A., Hall, Donald N. B., Holtzman, Jon A., Kaviraj, Sugata, Kimble, Randy A., MacKenty, John W., Mutchler, Max, Paresce, Francesco, Saha, Abihit, Silk, Joseph I., Trauger, John T., Walker, Alistair R., Whitmore, Bradley C. and Young, Erick T., 2011, "The Hubble Space Telescope Wide Field Camera 3 Early Release Science Data: Panchromatic Faint Object

Counts for 0.2-2 μm Wavelength", *Astrophys. J. Suppl.*, **193**(2), 27. [DOI], [ADS], [arXiv:1005.2776 [astro-ph.CO]]

Wright, Edward L., Eisenhardt, Peter R. M., Mainzer, Amy K., Ressler, Michael E., Cutri, Roc M., Jarrett, Thomas, Kirkpatrick, J. Davy, Padgett, Deborah, McMillan, Robert S., Skrutskie, Michael, Stanford, S. A., Cohen, Martin, Walker, Russell G., Mather, John C., Leisawitz, David, Gautier, Thomas N., III, McLean, Ian, Benford, Dominic, Lonsdale, Carol J., Blain, Andrew, Mendez, Bryan, Irace, William R., Duval, Valerie, Liu, Fengchuan, Royer, Don, Heinrichsen, Ingolf, Howard, Joan, Shannon, Mark, Kendall, Martha, Walsh, Amy L., Larsen, Mark, Cardon, Joel G., Schick, Scott, Schwalm, Mark, Abid, Mohamed, Fabinsky, Beth, Naes, Larry and Tsai, Chao-Wei, 2010, "The Wide-field Infrared Survey Explorer (WISE): Mission Description and Initial On-orbit Performance", *Astron. J.*, **140**(6), 1868–1881. [DOI], [ADS], [arXiv:1008.0031 [astro-ph.IM]]

Wurster, James and Li, Zhi-Yun, 2018, "The role of magnetic fields in the formation of protostellar discs", *Frontiers in Astronomy and Space Sciences*, **5**, 39. [DOI], [ADS], [arXiv:1812.06728 [astro-ph.SR]]

Yi, Sukyoung K., Lee, Jihye, Sheen, Yun-Kyeong, Jeong, Hyunjin, Suh, Hyewon and Oh, Kyuseok, 2011, "The Ultraviolet Upturn in Elliptical Galaxies and Environmental Effects", *Astrophys. J. Suppl.*, **195**(2), 22. [DOI], [ADS], [arXiv:1107.0005 [astro-ph.GA]]

Yong, David and Grundahl, Frank, 2008, "An Abundance Analysis of Bright Giants in the Globular Cluster NGC 1851", *Astrophys. J. Lett.*, **672**(1), L29. [DOI], [ADS], [arXiv:0711.1394 [astro-ph]]

York, Donald G., Adelman, J., Anderson, John E., Jr., Anderson, Scott F., Annis, James, Bahcall, Neta A., Bakken, J. A., Barkhouser, Robert, Bastian, Steven, Berman, Eileen, Boroski, William N., Bracker, Steve, Briegel, Charlie, Briggs, John W., Brinkmann, J., Brunner, Robert, Burles, Scott, Carey, Larry,

Carr, Michael A., Castander, Francisco J., Chen, Bing, Colestock, Patrick L., Connolly, A. J., Crocker, J. H., Csabai, István, Czarapata, Paul C., Davis, John Eric, Doi, Mamoru, Dombeck, Tom, Eisenstein, Daniel, Ellman, Nancy, Elms, Brian R., Evans, Michael L., Fan, Xiaohui, Federwitz, Glenn R., Fiscelli, Larry, Friedman, Scott, Frieman, Joshua A., Fukugita, Masataka, Gillespie, Bruce, Gunn, James E., Gurbani, Vijay K., de Haas, Ernst, Haldeman, Merle, Harris, Frederick H., Hayes, J., Heckman, Timothy M., Hennessy, G. S., Hindsley, Robert B., Holm, Scott, Holmgren, Donald J., Huang, Chi-hao, Hull, Charles, Husby, Don, Ichikawa, Shin-Ichi, Ichikawa, Takashi, Ivezić, Željko, Kent, Stephen, Kim, Rita S. J., Kinney, E., Klaene, Mark, Kleinman, A. N., Kleinman, S., Knapp, G. R., Korienek, John, Kron, Richard G., Kunszt, Peter Z., Lamb, D. Q., Lee, B., Leger, R. French, Limmongkol, Siriluk, Lindenmeyer, Carl, Long, Daniel C., Loomis, Craig, Loveday, Jon, Lucinio, Rich, Lupton, Robert H., MacKinnon, Bryan, Mannery, Edward J., Mantsch, P. M., Margon, Bruce, McGehee, Peregrine, McKay, Timothy A., Meiksin, Avery, Merelli, Aronne, Monet, David G., Munn, Jeffrey A., Narayanan, Vijay K., Nash, Thomas, Neilsen, Eric, Neswold, Rich, Newberg, Heidi Jo, Nichol, R. C., Nicinski, Tom, Nonino, Mario, Okada, Norio, Okamura, Sadanori, Ostriker, Jeremiah P., Owen, Russell, Pauls, A. George, Peoples, John, Peterson, R. L., Petravick, Donald, Pier, Jeffrey R., Pope, Adrian, Pordes, Ruth, Prosapio, Angela, Rechenmacher, Ron, Quinn, Thomas R., Richards, Gordon T., Richmond, Michael W., Rivetta, Claudio H., Rockosi, Constance M., Ruthmansdorfer, Kurt, Sandford, Dale, Schlegel, David J., Schneider, Donald P., Sekiguchi, Maki, Sergey, Gary, Shimasaku, Kazuhiro, Siegmund, Walter A., Smee, Stephen, Smith, J. Allyn, Snedden, S., Stone, R., Stoughton, Chris, Strauss, Michael A., Stubbs, Christopher, SubbaRao, Mark, Szalay, Alexander S., Szapudi, Istvan, Szokoly, Gyula P., Thakar, Anirudda R., Tremonti, Christy, Tucker, Douglas L., Uomoto, Alan, Vanden Berk, Dan, Vogeley, Michael S., Waddell, Patrick, Wang, Shu-i., Watanabe, Masaru, Weinberg, David H., Yanny, Brian, Yasuda, Naoki and SDSS Collaboration, 2000, "The Sloan Digital Sky Survey: Technical

Summary", *Astron. J.*, **120**(3), 1579–1587. [DOI], [ADS], [arXiv:astro-ph/0006396 [astro-ph]]

Zhang, C. Y., 1995, "A Statistical Distance Scale for Galactic Planetary Nebulae", *Astrophys. J. Suppl.*, **98**, 659. [DOI], [ADS]

Zinn, R. J., Newell, E. B. and Gibson, J. B., 1972, "A search for UV-bright stars in 27 globular clusters.", *Astron. Astrophys.*, **18**, 390–402. [ADS]